

DESY-THESIS-2000-030

August 2000

hep-ph/0009068

Semi-analytical calculation of QED radiative
corrections to $e^+e^- \rightarrow \bar{f}f$ with special emphasis
on kinematical cuts to the final state

Dissertation

zur Erlangung des akademischen Grades
doctor rerum naturalium
(Dr. rer. nat.)
im Fach Physik

eingereicht an der
Mathematisch-Naturwissenschaftlichen Fakultät I
der Humboldt-Universität zu Berlin

von

Mark Alexander Jack

Abstract

In this dissertation a complete calculation of QED radiative corrections is presented for total cross sections and forward-backward asymmetries for s -channel fermion pair production in e^+e^- annihilation with kinematical cuts to the final state. This includes cuts on the maximal acollinearity angle θ_{acol} and on the minimal energies E_{min} of the final state fermion pair and on the cosine of the scattering angle of one fermion $\cos\vartheta$. The applied cuts pose a realistic alternative for leptonic final states to cuts on the invariant mass squared s' of the fermion pair and on $\cos\vartheta$.

The derived QED flux functions $\rho(s'/s)$, with s as center-of-mass (c.m.) energy squared, are convoluted over s' in an improved Born approximation and were implemented into the semi-analytical Fortran program **ZFITTER**. It is used at the LEP and SLC experiments for precision tests to the Standard model and for searches of new particle physics phenomena. This calculation had become necessary due to the much higher experimental precision obtained now and the insufficient accuracy of the approximate, earlier coding.

The hard photon flux functions partly correct unpublished earlier results or constitute otherwise new, general formulae which contain known results as special cases. Very compact expressions are obtained when omitting a cut on $\cos\vartheta$.

An analysis of the updated code together with other numerical two-fermion codes yields for the acollinearity cut option an agreement of cross sections and asymmetries of better than 0.1 per mil on the Z boson resonance, and of better than 0.3 to 1 per mil at the wings ($\sqrt{s} = M_Z \pm 3 \text{ GeV}$). Deviations between the codes at LEP 2 energies up to several per cent in case of Z radiative return events are now understood due to an approximation for higher order QED effects with an acollinearity cut in **ZFITTER**. At c.m. energies up to roughly 800 GeV, **ZFITTER** and other codes deviate not more than 0.5 to 1 per cent for different s' cuts and different higher order QED corrections.

The new formulae and the analysis presented in this thesis for high energies and luminosities form an essential building block for an upgrading of two-fermion codes like **ZFITTER** for a future e^+e^- Linear Collider.

Zusammenfassung

In dieser Dissertation wird eine vollständige Berechnung der QED-Strahlungskorrekturen für totale Wirkungsquerschnitte und Vorwärts-Rückwärtsasymmetrien für s -Kanal-Fermionpaarproduktion in e^+e^- -Annihilation dargestellt, einschließlich kinematischer Schnitte am Endzustand. Diese umfassen Schnitte an dem maximalen Akollinearitätswinkel θ_{acol} und den minimalen Energien E_{min} des Fermionpaares im Endzustand und an dem Kosinus des Streuwinkels eines Fermions $\cos\vartheta$. Für leptonische Endzustände bilden diese Schnitte eine realistische Alternative zu Schnitten an der invarianten Masse s' des Fermionpaares und an $\cos\vartheta$. Die berechneten QED-Radiatorfunktionen $\rho(s'/s)$ mit s als quadrierter Schwerpunktsenergie werden über s' in einer effektiven Bornapproximation gefaltet und wurden in das semi-analytische Fortranprogramm **ZFITTER** implementiert, welches für Präzisionstests zum Standardmodell und für die Suche nach neuen Physikphänomenen bei den LEP- und SLC-Experimenten eingesetzt wird. Diese Berechnung war durch die jetzt höhere experimentelle Präzision und die unzureichende Genauigkeit der approximativen früheren Programmierung notwendig geworden. Die Radiatorfunktionen zur harten Bremsstrahlung korrigieren zum Teil ältere, unpublizierte Resultate oder bilden ansonsten neue, allgemeine Formeln, welche bekannte Resultate als Spezialfälle enthalten. Die Vernachlässigung des Schnittes an $\cos\vartheta$ liefert sehr kompakte Ausdrücke. Eine Analyse des erneuerten Programms mit anderen Zweifermionprogrammen ergibt jetzt auf der Z -Bosonresonanz für Wirkungsquerschnitte und Asymmetrien eine Übereinstimmung um besser als 0.1 Promille und um besser als 0.3 bis 1 Promille an den Flügelregionen ($\sqrt{s} = M_Z \pm 3 \text{ GeV}$). Mehrere Prozent große Abweichungen zwischen den Programmen bei LEP 2-Energien im Falle einer radiativen Rückkehr zur Z -Resonanz sind jetzt verstanden und können auf eine Näherung der höheren QED-Korrekturen mit Akollinearitätsschnitt in **ZFITTER** zurückgeführt werden. Für Schwerpunktsenergien bis ungefähr 800 GeV weichen **ZFITTER** und andere Programme um nicht mehr als 0.5 bis 1 Prozent ab, für verschiedene Schnitte an s' und für verschiedene QED-Korrekturen höherer Ordnung. Die in dieser Thesis dargestellten neuen Formeln und die Analyse im Falle hoher Energien und Luminositäten bilden eine essentielle Vorarbeit für eine Aufwertung von Zweifermionprogrammen wie **ZFITTER** für einen zukünftigen e^+e^- -Linearbeschleuniger.

Contents

Introduction	1
Motivation	1
The Z line shape around the Z boson resonance	4
Outline of this Thesis	12
1 The Electroweak Standard Model	14
2 Precision Physics on the Z Boson Resonance	21
2.1 Electroweak precision observables	22
2.2 Realistic observables and the ZFITTER approach	30
2.3 QED bremsstrahlung with <i>acollinearity cut</i>	37
2.3.1 The phase space for hard photon emission	38
2.3.2 Initial state radiation and mass singularities	41
2.3.3 Cross section formulae	47
2.4 Numerical results of ZFITTER and comparisons	57
2.4.1 Hard bremsstrahlung corrections in ZFITTER	57
2.4.2 Comparisons of ZFITTER with different numerical programs	63
2.4.3 Effects on the experimental analysis at LEP	65
2.5 Conclusions	66
3 Fermion Pair Production at LEP 2 Energies	68
3.1 Physics effects in virtual radiative corrections	69
3.2 Photonic corrections above the Z resonance	72
3.3 Comparisons with different programs	75
3.4 Conclusions	79
4 The e^+e^- Linear Collider and Fermion Pairs	81
4.1 Searches for <i>Physics beyond the Standard Model</i>	81
4.2 Higher order QED corrections	83
4.3 Conclusions	88
Summary	89
Results	89

Outlook	94
A Cross Sections and Phase Space	98
A.1 Feynman diagrams and matrix element	98
A.2 Kinematics	102
A.3 The three-particle phase space with acollinearity cut	104
B Hard bremsstrahlung corrections	112
B.1 Initial state radiation	112
B.2 Initial-final state interference	133
B.3 Final state radiation	140
C Soft and virtual photonic corrections	154
C.1 Soft photonic corrections	154
C.1.1 Initial state radiation	155
C.1.2 The complete soft photonic corrections	159
C.2 Virtual corrections	161
C.2.1 Initial state and final state virtual corrections	161
C.2.2 Virtual box corrections	168

List of Figures

1	Peak cross sections and forward-backward asymmetries	11
2.1	$\Delta\chi^2$ distribution of LEP data fit	29
2.2	Muon pair production cross sections at the Z peak	35
2.3	Muon pair and $b\bar{b}$ production cross sections and asymmetries with cuts above the Z peak	36
2.4	Phase space with acollinearity cut	39
2.5	Ratios of muon pair cross sections from ZFITTER and TOPAZO . . .	64
3.1	Ratios of improved Born cross sections for $b\bar{b}$ and $d\bar{d}$ production .	70
3.2	Comparison of electroweak box and QED corrections	71
3.3	Initial state and interference corrections for ZFITTER at LEP 2 . .	72
3.4	QED interference corrections for ZFITTER at LEP 2	73
3.5	Final state corrections for ZFITTER at LEP 2	74
3.6	Net corrections for ZFITTER at LEP 2	75
3.7	Early comparison of ALIBABA and ZFITTER above the Z peak . . .	76
3.8	Comparison of TOPAZO, ALIBABA, and ZFITTER above the Z peak .	77
3.9	Comparison of σ_T for TOPAZO and ZFITTER above the Z peak . .	78
3.10	Comparison of A_{FB} for TOPAZO and ZFITTER above the Z peak . .	79
4.1	Comparison of TOPAZO, ZFITTER, and KK2f at the Linear Collider without initial-final state interference	85
4.2	Comparison of TOPAZO, ZFITTER, and KK2f at the Linear Collider with initial-final state interference	86
A.1	Feynman diagrams for real photon emission	98
A.2	Acollinearity angle	102
A.3	Angles of phase space	103
A.4	Different cases in phase space with acollinearity cut	110
B.1	Phase space with acollinearity cut (axis rotated)	140
C.1	Photonic vertex corrections	162
C.2	Fermion self-energies and counter term diagrams	165
C.3	Direct and crossed box diagrams	168

List of Tables

2.1	High precision measurements at the Z peak	21
2.2	Minimal center-of-mass energies without radiative return to the Z peak	41
2.3	Corrections to initial state radiation and initial-final state interference in σ_T for ZFITTER at the Z peak	60
2.4	Corrections to initial state radiation and initial-final state interference in A_{FB} for ZFITTER at the Z peak	61
2.5	Corrections to final state radiation for ZFITTER at the Z peak . .	62
2.6	Net corrections for ZFITTER at the Z peak	63
2.7	Muon pair cross sections from ZFITTER and TOPAZ0 at the Z peak	65
A.1	Regions of phase space for an acollinearity cut	111

Introduction

Motivation

Up to now the phenomenology of particles and their interactions has been so successfully described by the *Standard Model* [1–7]. The fundamental particles are classified as fermions into three families consisting of leptons and quarks. Electromagnetic, weak, and strong interactions are mediated between the fermions in a quantum field theoretical picture through the exchange of spin-1 vector bosons. The underlying symmetries of these particles and interactions can be described by the semi-simple gauge group $SU_C(3) \times SU_L(2) \times U_Y(1)$, i.e. the Lagrangian \mathcal{L} of the theory has to be invariant under these local symmetry transformations applied to the fermionic and bosonic fields. Leptons and quarks are combined into left-handed doublets or described as right-handed singlets with respect to the $SU_L(2)$ gauge group, while an extra quantum number called *color* is assorted to each quark making it to a triplet of the fundamental representation of $SU_C(3)$. A key characteristic of electroweak interactions is that flavor changing neutral current transitions are not observed, in the Standard model explained by the *GIM mechanism* [8].

While *quantum chromodynamics* can be treated as an exact, non-abelian gauge symmetry $SU_C(3)$ with massless, self-interacting gauge bosons, the *gluons*, the unified description of electromagnetic and weak forces in nature is not exactly given by an $SU_L(2) \times U_Y(1)$ gauge symmetry, but the symmetry is ‘broken’: the weak charged and neutral vector bosons were discovered to be massive with different masses [9–12], while the photon is massless with an exact $U_{em}(1)$ as gauge symmetry.

The *Higgs-Kibble mechanism*, which introduces an extra complex scalar doublet to the theory with a non-vanishing vacuum expectation value, shows a possible way out to describe the electroweak ‘symmetry breakdown’ in a gauge-invariant way [13, 14]. In principal the underlying symmetry of \mathcal{L} is not really broken, but hidden: We obtain a multiplet of vacuum states which do not possess the symmetry of the Lagrangian \mathcal{L} , therefore when choosing one, the underlying gauge symmetry of \mathcal{L} is not apparent anymore in this vacuum state. Choosing a

specific gauge, the *unitary gauge*, transforms the unphysical degrees of freedom of the scalar fields into longitudinal components of the weak vector bosons, thus giving them masses while the photon remains massless. From the scalar fields one massive scalar boson, the *Higgs boson*, remains which is so extensively searched for at existing high-energy colliders as last missing building block of the mass generation mechanism in the electroweak sector.

At the high-energy e^+e^- colliders LEP 1 [15–21] and SLC [22, 23], for example, the main objective is to determine the neutral current properties of the electroweak theory: the mass M_Z and the total and partial decay widths of the Z boson into fermion pairs Γ_Z and Γ_f and the neutral current vector and axial-vector couplings v_f and a_f . For example, from the precise measurement of the shape of the Z boson resonance curve, i.e the fermionic peak cross sections, M_Z and Γ_Z were determined at LEP 1 and SLC with relative errors of roughly 2×10^{-5} , or 10^{-3} respectively [15, 16].

The calculation of quantum effects to observables in the Standard Model is in this context of course absolutely mandatory. For a perturbative expansion of the S matrix of scattering processes in the small coupling constants of the theory it was shown that all divergences arising during the calculation can be completely removed by a redefinition of bare fields and parameters in the Lagrangian [24–27]. This can be done once and for all by adding a finite number of counter terms removing all singularities to all orders of perturbation theory. A basic, finite set of parameters fixed by experiment at a certain energy scale suffices as input to calculate all other **SM** observables. Thus, the Standard Model (**SM**) as gauge-invariant field theory is renormalizable and yields finite and therefore physically meaningful results.

From virtual radiative corrections one can, for example, also determine indirectly the top quark mass m_t at LEP or SLC as test for the Tevatron results where the top quark can be directly produced [28, 29]. Even indirect upper bounds on the mass M_H of the **SM** Higgs boson [30], which has still escaped direct observation, can be obtained in this way. But finally, searching for *physics beyond the SM* at existing or future colliders is probably the main motivation for any high-energy physicist to ask for higher and higher luminosities and energies. Either one studies again virtual effects of massive new particles coupling to the **SM** ones, predicted for example by supersymmetric, grand-unifying, or string-inspired models, or one tries and produces them directly at high energies.

For this, radiative corrections to cross section observables have to be accurately dealt with. In the **SM** we have pure QED, electroweak, and QCD corrections which all influence observables like fermion pair cross sections and asymmetries. On the Z boson resonance the QED corrections dominate, but also the inclusion of the other corrections is ultimately important to correctly reproduce the experimental observations.

In this dissertation the effects of QED radiative corrections to cross sections and asymmetries are examined for the Z boson resonance region, for LEP 2 energies, and for higher energies like at a future e^+e^- Linear Collider. Real soft and hard photon emission from the initial and final state fermions is considered together with the QED interference and the virtual photonic corrections. This is done for the semi-analytical Fortran program **ZFITTER** [31–38] in comparison with other numerical codes for two-fermion production in e^+e^- annihilation. The program **ZFITTER** is used for example together with other codes e.g. at LEP in data-fitting routines. New results for hard photon radiation were derived with realistic cuts for totally integrated and differential cross sections. They constitute general analytical formulae which contain earlier results in the literature with kinematically simpler cuts as special case [34, 35] and yield very compact expressions when omitting one angular cut. The applied energy and angular cuts are experimentally especially interesting for leptonic final states like $\bar{\mu}\mu$, where they pose an alternative to a kinematically simpler cut on the final state invariant mass squared [20].

In order to illustrate the general importance of QED bremsstrahlung, a brief discussion of its influence on cross sections at the Z boson resonance shall be given in the remaining part of this Introduction. The modifications to cross sections at the Z peak by QED radiative corrections are *universal*. They arise from multiple soft or virtual photonic corrections, i.e. finite contributions due to real photon emission or virtual photon exchange for vanishing photon momenta. In first approximation they do not depend on the details of the final state phase space like kinematical cuts or final state masses. The main corrections develop from the photonic corrections to the initial state fermion pair. Exactly on the Z peak, the emission of hard photons is strongly suppressed and will therefore be neglected during most of the calculation in our introductory approximate description of cross sections and asymmetries around the Z peak. With the per mil, and partly better than per mil precision experimentally available for observables in the Z boson resonance region the hard QED bremsstrahlung will, however, have to be included for SM precision tests. This latter point will be treated in detail in Chapter 2.

Away from the Z boson resonance and for higher center-of-mass energies the importance of hard photon emission grows and its dependence on the kinematical cuts applied has to be correctly taken into account. Events with a *radiative return to the Z boson*, where the effective center-of-mass energy after initial state hard photon emission is shifted onto the Z boson mass in case of no or only loose kinematical cuts, produce a strong cross section enhancement. Also higher order QED corrections will start to play a larger role. Both issues will be discussed for center-of-mass energies typical at LEP 2 or at a future e^+e^- Linear Collider (LC) in Chapters 3 and 4.

The Z line shape around the Z boson resonance

The three major effects to the Z line shape in the Z boson resonance region, i.e. to cross sections at center-of-mass energies of roughly $88 \text{ GeV} < \sqrt{s} < 95 \text{ GeV}$, can be summarized through following three ‘rules of thumb’:

1. The peak cross section σ_{max} is lowered with respect to the Born case σ_{max}^0 approximately by a factor $(\Gamma_Z/M_Z)^{\beta_e}$ [39,40], with M_Z and Γ_Z as mass and total width of the Z boson [41–46]:

$$\sigma_{\text{max}} = \sigma(\sqrt{s} \approx M_Z) = \sigma_{\text{max}}^0 \left(\frac{\Gamma_Z}{M_Z} \right)^{\beta_e} (1 + \bar{S}), \quad (0.1)$$

$$\beta_e = \frac{2\alpha}{\pi} [L_e(M_Z^2) - 1], \quad L_e(M_Z^2) = \ln \frac{M_Z^2}{m_e^2}, \quad (\Gamma_Z/M_Z)^{\beta_e} \approx 0.7. \quad (0.2)$$

The term \bar{S} stands for the finite corrections from soft and virtual photons.

2. The peak position $\sqrt{s_{\text{max}}}$ is shifted with respect to the Z boson mass M_Z to a slightly higher value:

$$\sqrt{s_{\text{max}}} = M_Z \left[1 + \frac{\pi\beta_e}{4}\gamma - \frac{\gamma^2}{4} \right], \quad \gamma = \frac{\Gamma_Z}{M_Z}, \quad (0.3)$$

where the first term $\pi\beta_e\gamma/4$ [47–51], is due to the main bremsstrahlung corrections to the Z boson resonance described by a Breit-Wigner resonance formula, while the second term proportional to γ^2 arises also taking into account the γZ interference contribution and an s -dependence of the Z boson width in the Z boson propagator of the squared matrix element, $\Gamma_Z(s) \equiv s/M_Z^2 \cdot \Gamma_Z$ [33,42,52–54].

3. The hard photon emission enhances the cross section values $\sigma(s)$ with respect to the Born values $\sigma^0(s)$ for center-of-mass energies \sqrt{s} above the Z boson resonance region roughly by a factor $C \cdot M_Z/\Gamma_Z$, with C being a factor of $O(1)$ [53].

Corresponding effects to the forward-backward asymmetries $A_{FB}(s)$ at or above the Z boson resonance [53–56] will be briefly mentioned at the end of our presentation for total cross sections there [48–51, 53, 54].

The dominant QED corrections to the total cross section $\sigma(s)$ by initial state bremsstrahlung are given by following approximate formula:

$$\sigma(s) = \int_{s_{\text{min}}}^s \frac{ds'}{s} \sigma^0(s') R(v) \quad (0.4)$$

$$= \int_{s_{\min}}^s \frac{ds'}{s} \sigma^0(s') \cdot \left[(1 + \bar{S}) \beta_e v^{\beta_e - 1} + \bar{H}(v) \right], \quad (0.5)$$

$$\text{with } v \equiv 1 - \frac{s'}{s}. \quad (0.6)$$

The term $\sigma^0(s')$ is the effective Born cross section. The variable s' is the effective invariant mass squared after initial state radiation and v is equivalent to the normalized photon energy. The *improved Born term* $\sigma^0(s')$ contains the remaining electroweak and QCD corrections. At the Z boson resonance they decouple from the pure QED radiative corrections and can be described accurately through effective couplings, form factors, and an s -dependent Z boson width in the effective Born expressions [33, 42, 52].

For the QED description, $\sigma^0(s')$ is convoluted over s' with a flux function $R(v)$ for the QED bremsstrahlung. The integration reaches from a minimum value s_{\min} to the maximal value s . Finite corrections from soft and virtual photons or from hard photons are contained in the terms \bar{S} and \bar{H} , respectively. The factor $\beta_e v^{\beta_e - 1}$ denoted in (0.4) combines all leading logarithmic soft and virtual photonic corrections in a *soft and virtual photon exponentiation* [57–59].

In order to demonstrate the QED effects on the cross section maximum at the Z boson resonance (peak cross sections), it is instructive in a first approach to use a Breit-Wigner resonance formula with a constant width Γ_Z , where the γZ interference term $\sigma_{\gamma Z}^0$ and the pure QED part σ_γ^0 (see 0.7 to 0.10) have been omitted for simplicity. Their corrections to the peak cross sections will then be discussed afterwards.

Simple approach

So, starting with the effective Born cross section $\sigma^0(s)$ of our convolution integral (0.4) for the corrected peak cross section, we have

$$\sigma^0(s) = \sigma_Z^0(s) + \sigma_{\gamma Z}^0(s) + \sigma_\gamma^0(s) \approx \sigma_Z^0(s), \quad (0.7)$$

$$\sigma_Z^0(s) = \sigma_{\max}^0 \cdot \frac{s \Gamma_Z^2}{(s - M_Z^2)^2 + M_Z^2 \Gamma_Z^2}, \quad (0.8)$$

$$\sigma_{\gamma Z}^0(s) = \frac{4\pi\alpha^2}{3} J_f \frac{s - M_Z^2}{(s - M_Z^2)^2 + M_Z^2 \Gamma_Z^2}, \quad (0.9)$$

$$\sigma_\gamma^0(s) = \frac{4\pi\alpha^2}{3s} Q_e^2 Q_f^2 N_{cf}, \quad (0.10)$$

with the factor J_f given by SM couplings and the SM maximal Born cross section σ_{\max}^0 by

$$\sigma_{\max}^0 = \frac{12\pi\Gamma_e\Gamma_f}{M_Z^2\Gamma_Z^2}. \quad (0.11)$$

In this simple approach [48,50,51], we just consider the Breit-Wigner resonant part $\sigma_Z^0(s)$ of $\sigma^0(s)$ in (0.4) and omit the hard photon term $\bar{H}(v)$. For the integration of the soft photon part over the variable $v \equiv 1 - R$ only a negligible numerical error is introduced when one extends the integration region from $[0; 1]$ to $[0; \infty]$.

$$\sigma(s) = \int_{s_{\min}}^s \frac{ds'}{s} \sigma^0(s') (1 + \bar{S}) \beta_e v^{\beta_e-1} \quad (0.12)$$

$$\approx \sigma_{\max}^0 (1 + \bar{S}) \frac{M_Z^2 \Gamma_Z^2}{s} \beta_e \int_0^\infty dv v^{\beta_e-1} \frac{1-v}{v^2 + 2\eta \cos \zeta v + \eta^2} \quad (0.13)$$

$$\approx \sigma_{\max}^0 (1 + \bar{S}) \frac{M_Z^2 \Gamma_Z^2}{s} \cdot \left\{ \mathcal{J}_{\beta_e} \left[\eta \left(\frac{M_Z}{s}, \frac{\Gamma_Z}{s} \right), \zeta \left(\frac{M_Z}{s}, \frac{\Gamma_Z}{s} \right) \right] - \frac{\beta_e}{\beta_e + 1} \mathcal{J}_{\beta_e+1} \left[\eta \left(\frac{M_Z}{s}, \frac{\Gamma_Z}{s} \right), \zeta \left(\frac{M_Z}{s}, \frac{\Gamma_Z}{s} \right) \right] \right\}, \quad (0.14)$$

with

$$\mathcal{J}_{\beta_e}(\eta, \zeta) = \beta_e \int_0^\infty \frac{dx}{x} x^{\beta_e} \cdot \frac{1}{x^2 + 2\eta \cos \zeta \cdot x + \eta^2} \quad (0.15)$$

$$= \eta^{\beta_e-2} \cdot \Phi(\cos \zeta, \beta_e), \quad (0.16)$$

$$\Phi(\cos \zeta, \beta_e) = \frac{\pi \beta_e \sin [(1 - \beta_e) \zeta]}{\sin(\pi \beta_e) \sin \zeta}, \quad (0.17)$$

and

$$\eta^2 = a^2 + b^2, \quad \cos \zeta = \frac{a}{\eta}, \quad \sin \zeta = \frac{b}{\eta}, \quad a = M_Z^2/s - 1, \quad b = (M_Z \Gamma_Z)/s. \quad (0.18)$$

The above equation (0.14) then leads us to:

$$\begin{aligned} \sigma_{\max} = \sigma(\sqrt{s_{\max}}) &= \sigma_{\max}^0 (1 + \bar{S}) \frac{M_Z \Gamma_Z}{s} \eta^{\beta_e-1} \left\{ \frac{\pi \beta_e \sin [(1 - \beta_e) \zeta]}{\sin(\pi \beta_e)} \right. \\ &\quad \left. - \eta \frac{\beta_e}{\beta_e + 1} \frac{\pi (\beta_e + 1) \sin [(1 - (\beta_e + 1)) \zeta]}{\sin(\pi (\beta_e + 1))} \right\}. \end{aligned} \quad (0.19)$$

For the evaluation of the peak height σ_{\max} , we can safely neglect the second term proportional to η in (0.19) with $\eta = \Gamma_Z/M_Z \ll 1$ and $\zeta = \pi/2$:

$$\sigma_{\max} = \sigma_{\max}^0 (1 + \bar{S}) \frac{\pi \beta_e \sin [(1 - \beta_e)(\pi/2)]}{\sin(\pi \beta_e)} \cdot \left(\frac{\Gamma_Z}{M_Z} \right)^{\beta_e} \quad (0.20)$$

$$= \sigma_{\max}^0 \frac{\pi \beta_e/2}{\sin(\pi \beta_e/2)} (1 + \bar{S}) \cdot \left(\frac{\Gamma_Z}{M_Z} \right)^{\beta_e}. \quad (0.21)$$

With $\frac{\pi\beta_e/2}{\sin(\pi\beta_e/2)} \approx 1$, we therefore observe the decrease of the Born peak cross section by a factor $(\Gamma_Z/M_Z)^{\beta_e}$ [39,40] with a small correction term $(1+\bar{S})$ [50,51]. This effect at the Z peak is solely produced by the multiple soft and virtual photon corrections and independent of the small hard photon emission there. It is therefore a universal, i.e. completely process and cut-independent phenomenon.

In order to see the shift of the peak position $\sqrt{s_{\max}}$, we introduce the variable $y := (s - M_Z^2)/(\Gamma_Z M_Z)$ and use the fact that the shift $\sqrt{s_{\max}}$ will be negligibly small compared to the Z boson width Γ_Z . With $y \ll 1$ and $\gamma \equiv \Gamma_Z/M_Z \ll 1$, we finally get, omitting terms of $O(y^3)$ and $O(y\gamma)$:

$$\begin{aligned} \sigma(s(y)) &= \sigma_{\max}^0 \frac{\pi\beta_e}{\sin(\pi\beta_e)} (1 + \bar{S}) \left(\frac{\Gamma}{M} \right)^{\beta_e} \cdot \\ &\quad \left[\cos\left(\frac{\beta_e\pi}{2}\right) + (1 - \beta_e) \sin\left(\frac{\beta_e\pi}{2}\right) y - \frac{(1 - \beta_e)^2}{2} \cos\left(\frac{\beta_e\pi}{2}\right) y^2 \right]. \end{aligned} \quad (0.22)$$

The logarithmic term $\beta_e = \beta_e(s \approx M_Z^2)$ from (0.2) can safely be treated as constant for the small deviations y which are considered here. Setting $d\sigma/ds(s = s_{\max}) = 0$, we finally obtain the following result for the peak position $\sqrt{s_{\max}}$ which is slightly shifted with respect to M_Z through the QED effects [48–51]:

$$y = \frac{\tan(\pi\beta_e/2)}{2 - \beta_e} \approx \frac{\pi\beta_e}{4}, \quad (0.23)$$

$$\longrightarrow \sqrt{s_{\max}} \approx M_Z \left(1 + \frac{\pi\beta_e}{8} \gamma \right) \quad \text{with} \quad \gamma \equiv \frac{\Gamma_Z}{M_Z}. \quad (0.24)$$

Effects by an s dependent width $\Gamma_Z(s)$

The total Z boson decay width Γ_Z can be calculated from perturbation theory and is basically given by the imaginary part of the self-energy correction Σ_Z to the Z boson propagator [49, 52]:

$$M_Z \Gamma_Z = \frac{\Im m(\Sigma_Z(M_Z^2))}{1 + \Pi_Z(M_Z^2)}, \quad \Pi_Z(s) = \frac{\partial}{\partial s} \Re e(\Sigma_Z(s)). \quad (0.25)$$

The value Γ_Z can be calculated in different renormalization schemes, for example, with M_Z , G_μ , and $\alpha_{em}(M_Z^2)$ as input values. G_μ is the muon decay constant and can be written at tree-level as $G_\mu = \pi\alpha/(\sqrt{2}\sin^2\theta_W M_W^2)$, while $\alpha_{em}(M_Z^2)$ is the running electromagnetic coupling constant derived at $s = M_Z^2$. This introduces an s -dependency to the width Γ_Z [42–44]:

$$\Gamma_Z(s) = \frac{\sqrt{2}G_\mu M_Z s}{3\pi} \sum_f N_{cf}(v_f^2 + a_f^2) \equiv \frac{s}{M_Z^2} \Gamma_Z, \quad (0.26)$$

with N_{cf} as fermionic color factor, v_f and a_f as weak neutral current couplings, and the constant Γ_Z extracted as a factor in the way given in (0.26).

In a more realistic approach, we therefore have to replace the constant-width resonance curve in (0.7) with the following Breit-Wigner ansatz, which provides a much better description of the actual case:

$$\sigma^0(s') = \sigma_{\max}^0 \cdot \frac{s' \Gamma_Z^2}{(s' - M_Z^2)^2 + s'^2 (\Gamma_Z/M_Z)^2}. \quad (0.27)$$

It is now straightforward to show that the s -dependency of the width can be removed in the denominator by the Z boson transformation [33, 52, 54, 60]:

$$M_Z = \frac{\bar{M}_Z}{\sqrt{1 + \Gamma_Z^2}}, \quad (0.28)$$

$$\Gamma_Z = \frac{\bar{\Gamma}_Z}{\sqrt{1 + \Gamma_Z^2}}, \quad (0.29)$$

$$G_\mu = \frac{\bar{G}_\mu}{1 - i\gamma} \quad \text{with} \quad \gamma \equiv \frac{\Gamma_Z}{M_Z} = \frac{\bar{\Gamma}_Z}{\bar{M}_Z}. \quad (0.30)$$

This leads us from (0.27) to following Born expression which is to be convoluted into (0.12) with the QED radiator there:

$$\sigma^0(s') = \sigma_{\max}^0 \cdot \frac{s' \bar{\Gamma}_Z^2}{(s' - \bar{M}_Z^2)^2 + (\bar{M}_Z \bar{\Gamma}_Z)^2}. \quad (0.31)$$

This Z boson transformation in (0.28) produces an effective Z boson mass \bar{M}_Z and a new effective constant width $\bar{\Gamma}_Z$.¹ The next term in the expansion yields [50, 51]:

$$\sqrt{s_{\max}} \approx \bar{M}_Z \left(1 + \frac{\pi\beta_e}{8} \gamma + \frac{1}{4} \gamma^2 \right). \quad (0.32)$$

The peak position is now given in terms of the effective values \bar{M}_Z and $\bar{\Gamma}_Z$ and after transformation can be re-expressed in terms of the Z boson mass and width, M_Z and Γ_Z , which naturally produces a further negative shift [52–54]:

$$\sqrt{s_{\max}} \approx M_Z \left(1 + \frac{\pi\beta_e}{8} \gamma - \frac{1}{4} \gamma^2 \right). \quad (0.33)$$

The Born level shift $+\frac{1}{4}\gamma^2$ in (0.32) of the peak position with respect to M_Z is about +17 MeV. The additional shift $\Delta\sqrt{s_{\max}}$ of the peak position in (0.33)

¹ The back transformation $\bar{M}_Z, \bar{\Gamma}_Z \rightarrow M_Z, \Gamma_Z$ is absolutely symmetric with $\bar{M}_Z = M_Z/\sqrt{1 + \Gamma_Z^2}$, $\bar{\Gamma}_Z = \Gamma_Z/\sqrt{1 + \Gamma_Z^2}$, and $\gamma \equiv \frac{\Gamma_Z}{M_Z}$.

then amounts to about +112 MeV [50] for the leading logarithmic approximation of soft and virtual photons and to about +128 MeV taking into account also the $O(\alpha^2)$ QED corrections with a soft and virtual photon resummation [52]. Finally a further negative shift of -34 MeV arises from the s -dependence of the width [52]. The shift agrees nicely within a few MeV with the experimental observation [50].

Further small corrections to the height and position of the peak cross section are introduced by the γZ interference and pure QED terms $\sigma_{\gamma Z}^0(s')$ and $\sigma_\gamma^0(s')$ in the effective Born term (0.7). The QED part $\sigma_\gamma^0(s')$ especially has an effect for the muon pair final state due to logarithmic corrections proportional to $\ln(M_Z^2/m_\mu^2)$.² This slightly increases σ_{\max} for muon pairs by a few per cent with respect to the hadronic case. The QED term does not change the peak position.

The peak position is however modified by $\sigma_{\gamma Z}^0(s')$, which can also be measured with the available experimental precisions. The γ^2 -dependent term in (0.33) is replaced by [53, 54]:

$$+ \frac{1}{4} \Gamma_Z^2 \left(1 + \frac{\mathcal{J}}{\mathcal{R}} \right) - \frac{1}{2} \Gamma_Z^2, \quad (0.34)$$

with the factor \mathcal{J}/\mathcal{R} parameterizing the relative weight of the coupling factors to $\sigma_Z^0(s')$ and $\sigma_{\gamma Z}^0(s')$.

These effects can finally also be discussed in the context of ZZ' mixing when searching for extra heavy neutral gauge bosons Z' predicted in different extensions to the SM. This has been treated in a model-independent approach in [61] and produces a further shift of M_Z depending on the ZZ' mass splitting and neutral current couplings to Z and Z' which can be experimentally tested.

The radiative tail from hard photon emission

The third important effect of QED radiative corrections to the peak cross section is the radiative tail, i.e. the cross section enhancement compared to the Born situation, observed at energies above the Z boson resonance.

We want to give a quick ad-hoc computation of the tail effect. First, for the Born case, the resonance part in (0.27) develops for $\sqrt{s} > M_Z$ roughly like

$$\sigma^0(s) = \frac{C}{M_Z^2} \cdot \frac{s}{(s - M_Z^2)^2 + \Gamma_Z^2 M_Z^2} \approx \frac{C}{M_Z^2} \cdot \frac{1}{s}, \quad (0.35)$$

with a constant factor $C \approx O(1)$. For the QED convoluted case we can write generically for $\sigma(s)$:

² To see this, one has to replace the lower integration limit in (0.12) by $4m_\mu^2/s$.

$$\sigma(s) = C \cdot \int_{s_{\min}}^s \frac{ds'}{s} f\left(\frac{s'}{s}\right) \cdot \frac{1}{|s' - M_Z^2 + iM_Z\Gamma_Z|^2}, \quad (0.36)$$

with $f(s'/s)$ being the QED radiator and $1/|s' - M_Z^2 + iM_Z\Gamma_Z|^2$ the squared Z boson propagator. (0.36) can then be reexpressed in terms of the imaginary part of the propagator:

$$\sigma(s) = \frac{C}{M_Z\Gamma_Z} \cdot \int_{s_{\min}}^s \frac{ds'}{s} f\left(\frac{s'}{s}\right) \cdot \Im m \left(\frac{1}{s' - M_Z^2 + iM_Z\Gamma_Z} \right). \quad (0.37)$$

We first consider the case, $s_{\min} < M_Z < s$, taking into account QED bremsstrahlung through the flux function $f(s'/s)$. The function $f(s'/s)$ evolves slowly over most of the integration region in (0.36) and we can replace $f(s'/s)$ by some medium value $f(s_0/s)$. Its detailed structure is not important here. We have therefore following approximation:

$$\sigma(s) \approx -\frac{C}{M_Z\Gamma_Z} \cdot f\left(\frac{s_0}{s}\right) \cdot \int_{s_{\min}}^s \frac{ds'}{s} \Im m \left(\frac{1}{s' - M_Z^2 + iM_Z\Gamma_Z} \right) \quad (0.38)$$

$$= -\frac{C'}{M_Z\Gamma_Z} \cdot \int_{s_{\min}}^s \frac{ds'}{s} \Im m \left(\frac{1}{s' - M_Z^2 + iM_Z\Gamma_Z} \right). \quad (0.39)$$

With the general relation $\ln(-|R| \pm i\varepsilon) \approx \ln|R| \pm i\pi$, we can obtain the following approximation for $\sigma(s)$:

$$\begin{aligned} & \int_{s_{\min}}^s \frac{ds'}{s} \Im m \left(\frac{1}{s' - M_Z^2 + iM_Z\Gamma_Z} \right) = \frac{1}{s} \Im m \left\{ \ln \left(-\frac{s - M_Z^2 + iM_Z\Gamma_Z}{M_Z^2 - s_{\min} - iM_Z\Gamma_Z} \right) \right\} \\ &= \frac{1}{s} \Im m \left\{ \ln \left(-\frac{s - M_Z^2}{M_Z^2 - s_{\min}} - iM_Z\Gamma_Z \frac{s - s_{\min}}{(s - M_Z^2)(M_Z^2 - s_{\min})} \right) \right\} \approx -\pi \cdot \frac{1}{s}, \end{aligned} \quad (0.40)$$

$$\rightarrow \quad \sigma(s) = C''' \frac{\pi}{M_Z\Gamma_Z} \cdot \frac{1}{s}. \quad (0.41)$$

For the last step in (0.40) $\Gamma_Z/M_Z \ll 1$ was used. The factors C , C' , C'' , and C''' are all terms of $O(1)$. We finally observe a substantial cross section enhancement by roughly a factor M_Z/Γ_Z [53], comparing (0.40) with the Born case (0.35). The radiative tail effects above the Z peak can also be seen from Fig. 1.

If we had considered the case, $M_Z < s_{\min} < s$, through a sufficiently strong cut s_{\min} on s' against hard photon emission, we would have had instead: $\ln(|R| \pm i\varepsilon) \approx$

$\ln |R| \pm i\varepsilon$ and with this,

$$\begin{aligned} \int_{s_{\min}}^s \frac{ds'}{s} \Im m \left(\frac{1}{s' - M_Z^2 + iM_Z\Gamma_Z} \right) &= \frac{1}{s} \Im m \left\{ \ln \left(\frac{s - M_Z^2 + iM_Z\Gamma_Z}{s_{\min} - M_Z^2 + iM_Z\Gamma_Z} \right) \right\} \\ &= \frac{1}{s} \Im m \left\{ \ln \left(\frac{s - M_Z^2}{s_{\min} - M_Z^2} - i \frac{\Gamma_Z}{M_Z} \cdot \frac{M_Z(s - s_{\min})}{(s_{\min} - M_Z^2)^2} \right) \right\} = -O \left(\frac{\Gamma_Z}{M_Z} \right), \end{aligned} \quad (0.42)$$

and therefore no radiative tail is developed. These general considerations do not change for the more realistic case with an s -dependent width, which can be easily seen using the Z boson transformation. The changes of peak height and position have been depicted for muon and b quark pair cross sections in Fig. 1.

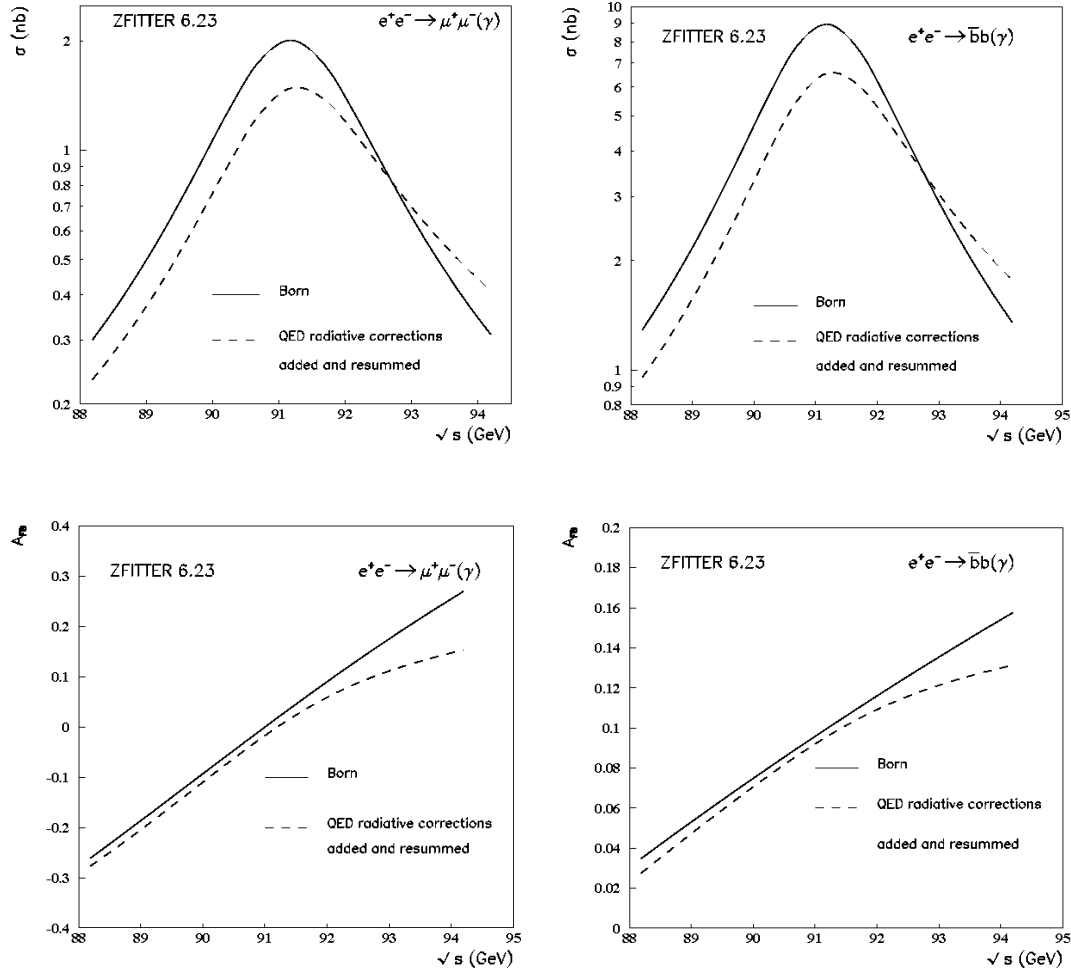


Figure 1: Born and QED corrected peak cross sections and forward-backward asymmetries for muon and b quark pair production calculated with ZFITTER v.6.23 [36, 38]. QED corrections include full $O(\alpha^2)$ and leading logarithmic $O(\alpha^3)$ corrections with soft and virtual photon exponentiation for initial state bremsstrahlung.

The above discussion can be similarly done for the shift of the zero position of A_{FB} with respect to M_Z [53, 54, 56]. The figure also shows the changes to forward-backward asymmetries A_{FB} at the Z peak and the shifts of peak positions and A_{FB} zero positions.

An overall correction factor arises from hard photons compared to the Born asymmetries A_{FB}^0 which lowers the asymmetry values for growing $s > M_Z^2$ (see Fig. 1). In order to derive this, it is crucial to take into account the γZ interference term $\sigma_{FB,\gamma Z}^0(s')$ in the Born asymmetry $\sigma_{FB}^0(s')$, which is added to the resonant part $\sigma_{FB,Z}^0(s')$ and convoluted with the QED flux function in analogy to (0.7). Further numerical analysis is also given in [33, 62, 63]. More recently some discussion has also started in this context on the importance of electroweak two-loop corrections in self-energy corrections to the Z boson propagator and on the definition of masses and widths of massive bosons like the Z and *Higgs* boson [64–68].

Summarizing, we have seen that QED radiative corrections have profound effects on cross sections and asymmetries at the Z peak. Theoretically, this can be described in a semi-analytical approach, convoluting QED bremsstrahlung flux functions with improved Born observables. The modifications to peak cross sections and asymmetries by QED are not influenced by the remaining electroweak and QCD corrections, which can be included correctly in effective parameters in the improved Born approach. For cross section predictions at the per mil level or better by theory at the Z boson resonance we will see that the exact treatment of hard photon bremsstrahlung with kinematical cuts will be absolutely mandatory.

Outline of this Thesis

The evaluation of radiative corrections to fermion pair observables now also forms the main task pursued in this dissertation:

We shall present in this work new analytical formulae for total cross sections and forward-backward asymmetries for s -channel fermion pair production $e^+e^- \rightarrow \bar{f}f$. We will focus on the dominant radiative corrections from QED bremsstrahlung and apply realistic kinematical cuts to the final state. These calculations are given for first order flux functions for the complete hard photon corrections with kinematical cuts on the acollinearity angle and the energies of the final state fermion pairs, and, optionally, on the scattering angle of one fermion. The remaining electroweak and QCD corrections can be described in effective Born observables convoluted with our derived QED flux functions, which gives a well-established and -justified approximate description of realistic observables. These results partly correct or replace so-far unpublished older results [69, 70] or are completely new and constitute especially for leptonic final states an alternative to corresponding formulae with a kinematically simpler cut on the final state

invariant mass squared s' [34, 35]. Corrections from soft and virtual photons or higher order QED effects can be straightforwardly included in our flux functions' description, in order to have physically complete and finite predictions.

The dissertation is structured as follows: In Chapter 2 a quick guide is given through the gauge theory description of the electroweak sector of the Standard Model. We will then discuss in Chapter 2 fermion pair precision observables for LEP 1 and SLC applications with radiative corrections. This is done together with a description of the implementation of fermion pair observables in the semi-analytical Fortran program **ZFITTER** [31–38]. In this context, we will discuss the importance of kinematical cuts to the hard photon phase space.

As one of the main analytical results of this thesis we will present very compact formulae for the initial state, final state, and initial-final state interference flux functions to total cross sections and forward-backward asymmetries with the above mentioned cuts, but omitting a cut on the scattering angle. These results have been published in [37] and implemented in the code **ZFITTER** recently [38]. For the initial state case also one example will be presented for the general hard photon flux functions with all angular cuts. The numerical effects at LEP 1 energies are analyzed for the program **ZFITTER** in comparison with other available numerical codes. We then expand this analysis in Chapters 3 and 4 to the LEP 2 case and the especial situation at a future e^+e^- Linear Collider. As an instructive example, we will look at muon pair production and take into account higher order QED corrections with different kinematical cuts. In the Summary, the presented results of this dissertation are briefly reviewed and an outlook on possible future applications of the program **ZFITTER** is given.

The Appendix derives a suitable parameterization of the hard photon phase space for the applied cuts and then a complete calculation of all hard photon radiator functions with all mentioned cuts for total cross sections and asymmetries. The Appendix also contains for completeness a collection of all formulae for the remaining soft and virtual photonic flux functions.

Chapter 1

The Electroweak Standard Model

The observed gauge symmetry of electroweak interactions is described in the Standard Model (SM) by the semi-simple gauge group [1–3]

$$G \equiv SU_L(2) \times U_Y(1). \quad (1.1)$$

The subscript L in (1.1) indicates that the unitary transformations of the weak isospin under $SU_L(2)$ only apply to left-handed doublet fields, while $U_Y(1)$ is the abelian gauge group of weak hypercharge. One constructs left-handed lepton or quark doublet fields $\Psi_1(x)$ and right-handed singlets $\Psi_2(x)$ under $SU_L(2)$. For the first particle generation this is:

$$\Psi_1(x) = \begin{pmatrix} \nu_e \\ e^- \end{pmatrix}_L, \quad \begin{pmatrix} u \\ d \end{pmatrix}_L, \quad \text{and} \quad \Psi_2(x) = (\nu_e)_R, e_R^-, u_R, d_R. \quad (1.2)$$

The free Lagrangian

$$\mathcal{L}_0 = \sum_{j=1}^3 i \bar{\Psi}_j(x) \gamma_\mu \partial_\mu \Psi_j(x), \quad (1.3)$$

is invariant under global $SU_L(2) \times U_Y(1)$ transformations of the fermion fields:

$$\Psi_j(x) \longrightarrow \Psi'_j(x) \equiv \exp\left(i \frac{\tau_k}{2} \alpha_k\right) \exp(i Y_j \beta) \Psi_j(x). \quad (1.4)$$

The τ_k , $k = 1, 2, 3$, are the Pauli-matrices with the commutation relation

$$[\tau_i, \tau_j] = 2 i \varepsilon_{ijk} \tau_k. \quad (1.5)$$

The index k in (1.4) is summed. The value Y_j denotes the weak hypercharge value of the field $\Psi_j(x)$, with the operator Y acting on left- and right-handed fields. For the further discussion it suffices to consider infinitesimal transformations:

$$\Psi_j(x) \longrightarrow \Psi'_j(x) \equiv \left(1 + i\frac{\tau_k}{2}\alpha_k + iY_j\beta\right) \Psi_j(x). \quad (1.6)$$

The invariance of \mathcal{L}_0 under local $SU_L(2) \times U_Y(1)$ transformations, with $\alpha_k(x)$ and $\beta(x)$ now depending on x , can be achieved by the *minimal substitution*:

$$\partial_\mu \Psi_j(x) \longrightarrow D_\mu \Psi_j(x) \equiv \left(\partial_\mu - ig\frac{\tau_k}{2}W_\mu^k(x) - ig'Y_jB_\mu(x)\right) \Psi_j(x), \quad (1.7)$$

with $D_\mu \Psi_j(x)$ now transforming like $\Psi_j(x)$. This naturally introduces the gauge fields W_μ^k and B_μ which have to transform infinitesimally like

$$B_\mu(x) \longrightarrow B'_\mu(x) \equiv B_\mu(x) + \frac{1}{g'}\partial_\mu\beta(x), \quad (1.8)$$

$$W_\mu^i(x) \longrightarrow W_\mu^{i'}(x) \equiv W_\mu^i(x) + \frac{1}{g}\partial_\mu\alpha_k(x) - \varepsilon_{ijk}\alpha_j(x)W_\mu^k(x), \quad (1.9)$$

in order to keep \mathcal{L}_0 invariant. The parameters g and g' are the couplings of the fermion-gauge field interactions. The complete Lagrangian \mathcal{L} of course also has to contain the free kinetic terms of the gauge fields. Introducing the field strength tensors

$$B_{\mu\nu} = [D_\mu B_\nu, D_\nu B_\mu], \quad W_{\mu\nu} = [D_\mu W_\nu, D_\nu W_\mu], \quad (1.10)$$

$$\longrightarrow B_{\mu\nu} = \partial_\mu B_\nu - \partial_\nu B_\mu, \quad W_{\mu\nu}^i = \partial_\mu W_\nu^i - \partial_\nu W_\mu^i + g\varepsilon_{ijk}W_\mu^jW_\nu^k, \quad (1.11)$$

with $W^\mu = \sum_i W_i^\mu \tau_i$, we can construct the electroweak Lagrangian without mass terms:

$$\mathcal{L} = \sum_{j=1}^3 i\bar{\Psi}_j(x)D_\mu\Psi_j(x) - \frac{1}{4}B_{\mu\nu}B^{\mu\nu} - \frac{1}{4}W_{\mu\nu}^k W_k^{\mu\nu}. \quad (1.12)$$

So, (1.12) produces with (1.11) for the $SU_L(2)$ gauge fields W_μ^k self-interaction terms which are trilinear and quadrilinear in the gauge fields. Such gauge-field self-interactions are a characteristic feature of a non-abelian gauge theory. The coupling of the gauge fields is provided by the same coupling constant g as for the fermion-gauge field interactions.

The charged-current interaction term can now be easily deduced from (1.12):

$$\mathcal{L}_{CC} = \frac{g}{2\sqrt{2}} \left\{ W_\mu^\dagger \cdot J^\mu + W^\mu \cdot J_\mu^\dagger \right\}, \quad (1.13)$$

with

$$W_\mu^{(\dagger)} = \frac{1}{\sqrt{2}} (W_\mu^1 \pm iW_\mu^2) \quad \text{and} \quad J^\mu \equiv \bar{u}\gamma^\mu \frac{1-\gamma_5}{2} d + \bar{\nu}_e\gamma^\mu \frac{1-\gamma_5}{2} e. \quad (1.14)$$

For the neutral current case we have to consider that the two neutral gauge fields W_μ^3 and B^μ , connected to the two diagonal generators $I_3 = \tau_3/2$ and Y , mix in order to produce the photon field A_μ and the weak neutral gauge field Z_μ . Parameterizing this transition as a rotation of the neutral fields W_μ^3 and B_μ via the weak mixing angle θ_W ,

$$\begin{pmatrix} W_\mu^3 \\ B_\mu \end{pmatrix} = \begin{pmatrix} \cos \theta_W & \sin \theta_W \\ -\sin \theta_W & \cos \theta_W \end{pmatrix} \begin{pmatrix} Z_\mu \\ A_\mu \end{pmatrix}, \quad (1.15)$$

we obtain for the neutral current Lagrangian:

$$\begin{aligned} \mathcal{L}_{NC} = \sum_j \bar{\Psi}_j \gamma^\mu \left\{ A_\mu \left[\frac{g}{2} \tau_3 \sin \theta_W + g' Y_j \cos \theta_W \right] \right. \\ \left. + Z_\mu \left[\frac{g}{2} \tau_3 \cos \theta_W - g' Y_j \sin \theta_W \right] \right\} \Psi_j. \end{aligned} \quad (1.16)$$

From (1.16) we can immediately derive a relation between the couplings and the weak mixing angle if we demand, as is observed in nature, that A_μ only couples to particles with electric charges:

$$g \sin \theta_W = g' \cos \theta_W = e. \quad (1.17)$$

For (1.17) we also had to impose that the electromagnetic charge Q , the weak isospin I_3 , and the weak hypercharge Y fulfill the relation:

$$Q = I_3 + Y. \quad (1.18)$$

The neutral current part \mathcal{L}_{NC} of the Lagrangian can also be written in terms of currents:

$$\mathcal{L}_{NC} = \mathcal{L}_{QED} + \mathcal{L}_{NC}^Z = e A_\mu J_{em}^\mu + \frac{e}{2 \sin \theta_W \cos \theta_W} Z_\mu J_Z^\mu, \quad (1.19)$$

with

$$J_Z^\mu = J_3^\mu - 2 \sin^2 \theta_W J_{em}^\mu, \quad (1.20)$$

$$J_{em}^\mu = \sum_j \bar{\Psi}_j(x) \gamma^\mu Q_j \Psi_j(x), \quad J_3^\mu = \sum_j \bar{\Psi}_j(x) \gamma^\mu \tau_3 \Psi_j(x), \quad (1.21)$$

or equivalently in terms of the vector and axial-vector couplings v_f and a_f :

$$\mathcal{L}_{NC} = eA^\mu \sum_f Q_f \bar{f} \gamma^\mu f + \frac{e}{2 \sin \theta_W \cos \theta_W} Z^\mu \sum_f \bar{f} \gamma^\mu (v_f - a_f \gamma_5) f, \quad (1.22)$$

$$v_e = -\frac{1}{2} + 2 \sin^2 \theta_W, \quad a_e = \frac{1}{2}, \quad Q_e = -1, \quad (1.23)$$

$$v_f = I_3^f - 2Q_f \sin^2 \theta_W, \quad a_f = I_3^f. \quad (1.24)$$

Inserting (1.15) into (1.12) and applying (1.17) and (1.18), one can also derive the gauge boson interaction terms between the physically observed fields W_μ^\pm , Z_μ , and A_μ .

The mere addition of mass terms of the form $M_W^2 W_\mu^+ W^{\mu-}$ or $m \bar{\Psi} \Psi$ to the Lagrangian \mathcal{L} would now introduce combinations of right-handed singlet fields with left-handed doublet fields, which is not invariant under $SU_L(2)$ transformations and therefore forbidden. A nice possibility to generate masses for both the weak gauge bosons and the fermions is the *Higgs-Kibble mechanism* [13, 14], which can be regarded as a generalization of the *Goldstone mechanism* [71] to gauge theories. The weak gauge bosons acquire masses after a spontaneous breakdown of the $SU_L(2) \times U_Y(1)$ symmetry through a coupling to a complex scalar doublet $\Phi(x)$ introduced to the theory with $Y_\Phi = 1/2$:

$$\Phi(x) \equiv \begin{pmatrix} \phi^{(+)}(x) \\ \phi^{(0)}(x) \end{pmatrix}. \quad (1.25)$$

The couplings to the gauge fields are again constructed via a minimal substitution like in (1.7) respecting the underlying gauge symmetry.

$$\mathcal{L}_H = (D_\mu \Phi)^\dagger D^\mu \Phi - \mu^2 \Phi^\dagger \Phi - h (\Phi^\dagger \Phi), \quad (1.26)$$

$$D_\mu \Phi(x) \equiv \left(\partial_\mu - ig \frac{\tau_k}{2} W_\mu^k(x) - ig' Y_\Phi B_\mu(x) \right) \Phi(x). \quad (1.27)$$

With both μ^2 and $h > 0$, the introduced complex doublet $\Phi(x)$ develops a non-vanishing vacuum-expectation value v :

$$| \langle 0 | \phi^{(0)} | 0 \rangle | = \frac{-\mu^2}{2h} \equiv \frac{v}{\sqrt{2}}. \quad (1.28)$$

That is, while the Lagrangian \mathcal{L}_H is invariant under $SU_L(2) \times U_Y(1)$ transformations, its vacuum ground state $\phi^{(0)}(x)$ is not. To be exact, one obtains a multiplet of degenerate ground states which can be transformed into each other via $SU_L(2) \times U_Y(1)$ rotations. Due to the presence of gauge fields these massless degrees of freedom can be absorbed in the longitudinal components of the weak gauge fields by choosing a suitable gauge, the *physical or unitary gauge*.

$$\Phi(x) \rightarrow \frac{1}{\sqrt{2}} \begin{pmatrix} 0 \\ v + H(x) \end{pmatrix}. \quad (1.29)$$

At the same time this generates the masses of the three weak gauge bosons W^\pm and Z^0 and of one scalar boson, the Higgs boson H :

$$\mathcal{L}_H = \frac{1}{2}\partial_\mu H \partial^\mu H + (v + H)^2 \left\{ \frac{g^2}{4} W_\mu^\dagger W^\mu + \frac{g^2}{8 \cos^2 \theta_W} Z_\mu Z^\mu \right\} + \dots, \quad (1.30)$$

with

$$M_Z \cos \theta_W = M_W = \frac{1}{2} g v. \quad (1.31)$$

The doublet $\Phi(x)$ with $Y_\Phi = 1/2$ in (1.25) has been chosen in such a way that the photon A necessarily remains massless: Only one real, charge-conserving component $\phi^0(x)$ of $\Phi(x)$ is still present after rotation. One can easily verify that the number of degrees of freedom remains the same before and after the symmetry breakdown as it should: Four massless gauge bosons with 8 and a complex scalar doublet with 4 degrees of freedom are transformed into three massive gauge fields W^\pm and Z with 9 degrees of freedom, by acquiring extra longitudinal components, one massless photon A with 2 possible spin orientations, and one massive scalar particle providing the missing degree of freedom.

For the fermionic case a similar mass generation can be obtained adding the extra complex scalar doublet $\Phi'(x)$ to the Lagrangian,

$$\Phi'(x) \equiv (i\Phi(x)\tau_2)^\dagger = \begin{pmatrix} \phi^{(0)}(x) \\ \phi^{(-)}(x) \end{pmatrix}, \quad (1.32)$$

which transforms like $\Phi(x)$ but with hypercharge $Y' = -1/2$. For the fermions one can construct Yukawa-type terms invariant under $SU_L(2) \times U_Y(1)$ of the form (here shown for the quarks):

$$\mathcal{L}_{Yukawa} = -\lambda(\bar{u} \bar{d})_L \Phi'(x) u_R - \lambda^* \bar{u}_R \Phi'^\dagger(x) \begin{pmatrix} u \\ d \end{pmatrix}_L. \quad (1.33)$$

Relation (1.33) couples the $SU_L(2)$ doublets to $SU_L(2)$ singlets with coupling λ , also preserving hypercharge Y . If we choose the coupling λ to be real we can have mass terms after spontaneous symmetry breaking, for example for the u quark:

$$\mathcal{L}_{Yukawa} = -\frac{\lambda v}{\sqrt{2}} \bar{u} u. \quad (1.34)$$

The factor $(-\lambda v/\sqrt{2})$ ($\lambda < 0$) in (1.34) can be interpreted as mass term m_u . This can be done in an equivalent manner for the d quark and the leptonic case.

In reality this picture has to be slightly modified when adding the full particle content to the theory: The number of particle families is increased to three, each family providing one left-handed lepton, one doublet of an up and down-type

quark, and the corresponding right-handed $SU_L(2)$ singlets. The six different quark flavors are (u, d, s, c, b, t) accompanied by three leptons (e, μ, τ) and the associated neutrinos $(\nu_e, \nu_\mu, \nu_\tau)$. The interactions of the additional two particle generations with the gauge fields are simply copied from the first family. The mass generation in (1.32) to (1.34) can of course also be repeated analogously for the other particle generations.

The larger particle content allows mixing between the massive quarks, which is really observed in nature, while the leptons do not mix as the neutrinos are considered massless in a minimal SM description.¹ This produces for the charged current interactions flavor changing transitions because the eigenstates of the weak interaction Hamiltonian and the mass eigenstates do not coincide anymore. In the original Lagrangian the three-dimensional unitary transformations of the weak eigenstates of the up- and down-type quark fields into their mass eigenstates are combined to one, in general complex but unitary 3×3 mixing matrix (V_{ij}) , $i, j = 1, 2, 3$. This introduces to the quark sector the *Cabbibo-Kobayashi-Maskawa mixing matrix* (CKM) (V_{ij}) [73, 74], in the charged current Lagrangian \mathcal{L}_{CC} in (1.35). Including all particle generations, it reads (over index j is summed):

$$\mathcal{L}_{CC} = \frac{g}{2\sqrt{2}} \left\{ W_\mu^\dagger \left[\sum_{ij} \bar{u}_i \gamma^\mu \frac{1 - \gamma_5}{2} V_{ij} d_j + \sum_l \bar{\nu}_l \gamma^\mu \frac{1 - \gamma_5}{2} l \right] + \text{h.c.} \right\}. \quad (1.35)$$

For massless neutrinos there is no meaning in a distinction between interaction and mass eigenstates and a corresponding mixing matrix between leptons and neutrinos can always be chosen unitary.

Furthermore, the existence of at least three particle generations allows to introduce one complex phase to the CKM mixing matrix (V_{ij}) in (1.35) while all other matrix elements can be chosen real through suitable field redefinitions. This introduces *CP violation* in the SM at the tree level.

From (1.22) one can also see that flavor changing neutral current transitions do not exist in the SM at tree-level, i.e. when replacing the Cabibbo-rotated eigenstates in (1.22) by the quark mass eigenstates, the neutral current Lagrangian \mathcal{L}_{NC} remains diagonal in the quark flavors. This *GIM mechanism* [8] predicted for example the existence of an additional fourth quark, the charm quark.

Finally, *anomalies* from quantum effects which break the original symmetry of the Lagrangian [75–77] and therefore could destroy the renormalizability of the theory do not have an effect in the SM: Such anomalies can occur in chiral gauge symmetries which contain both axial and vector currents, leading to divergent loop contributions when one axial current couples to two vector currents.

¹ This fact has changed recently since the observation of neutrino oscillations at the Super Kamiokande experiment [72] has given evidence to neutrino masses and neutrino-lepton mixing.

The number of particle flavors and quark colors, however, is balanced in such a way that the sum of these single divergent contributions exactly cancel. So, the complete $SU_c(3) \times SU_L(2) \times U_Y(1)$ gauge symmetry and lepton-quark family structure of the theory is needed in order to have a consistent and renormalizable description of electroweak interactions.

The determination of weak neutral current parameters at e^+e^- annihilation experiments like LEP or SLC now forms one key test to the **SM** description of electroweak interactions and shall be discussed in the next Chapter.

Chapter 2

Precision Physics on the Z Boson Resonance

In the past decade one of the great tasks of phenomenological particle physics was to unravel experimentally the physics of electroweak interactions, so successfully described by the Standard Model (SM). For this, especially e^+e^- colliding experiments like LEP at CERN or SLC at SLAC have provided a detailed view into the nature of electroweak interactions of the SM. During the starting phase of LEP and at SLC the main focus was on precision physics at the Z boson resonance: With center-of-mass energies on resonance, i.e. for $\sqrt{s} \approx M_Z \pm 1.8 \text{ GeV}$, the main task of both experiments was to measure the properties of the neutral, massive vector boson Z^0 with very high precision [15–23]. These are basically the mass and the total decay width of the Z boson, M_Z and Γ_Z , the partial decay widths Γ_f into different leptonic and hadronic decay channels ($f = e, \mu, \tau, \nu_e, \nu_\mu, \nu_\tau, u, d, s, c, b$), and the fermionic vector and axial-vector couplings v_f and a_f to the Z boson. The increase of precision by experiment over the last 10 years was for example summarized in [78] and is shown here in Table 2.1:

Quantity	LP 89 (233 events)	LP 99 (17×10^6 events)
M_Z (GeV)	91.17 ± 0.18	91.1871 ± 0.0021
Γ_Z (GeV)	$1.95^{+0.40}_{-0.30}$	2.4944 ± 0.0024
N_ν (light)	3.0 ± 0.9	2.9835 ± 0.0083

Table 2.1: Examples for the development of high precision measurements at the Z boson resonance [78].

2.1 Electroweak precision observables

We see from Chapter (1) that the unified description of electromagnetic and weak interactions in the SM neglecting masses and mixing in the fermionic sector is completely determined by g and g' as electroweak couplings and v as vacuum expectation value of a SM Higgs doublet. For the three couplings generally the following three up-to-now experimentally best known electroweak parameters are used as input [79]:

$$\begin{aligned}\alpha(0)^{-1} &= 137.0359895 \pm 0.0000061 && \text{the Feinstructure constant;} \\ G_\mu &= (1.16637 \pm 0.00001) \times 10^{-5} \text{ GeV}^{-2} && \text{the Muon decay constant;} \\ M_Z &= (91.1871 \pm 0.0021) \text{ GeV} && \text{the Z boson mass.}\end{aligned}$$

Further input values are the top quark mass m_t and the (still unknown) Higgs mass M_H . The Higgs mass M_H is used as free input value which leads to small logarithmic corrections to different observables, while for m_t the experimental results from direct top quark production can be plugged in.

The Feinstructure constant in the Thomson limit $\alpha(0)^{-1}$ is most precisely extracted from comparisons of the experimental and theoretical values for the electron anomalous magnetic moment a_e^γ which has now been calculated up to 4-loop order [80–82]. The muon decay constant G_μ is determined from the muon lifetime τ_μ , where the complete two-loop electromagnetic corrections have been calculated [83–87] while the remaining electroweak corrections are contained for historical reasons in the muon decay constant G_μ itself. The Z boson mass with the other neutral current properties are determined with high precision from measurements of cross sections and asymmetries at the Z peak.

As starting point for the latter point, the differential fermion pair production Born cross sections are given below in (2.1). In case of unpolarized e^+ and e^- beams with $h_f = \pm 1$ as the two helicities and $\cos \vartheta$ as the scattering angle of the produced fermion f with respect to the e^- beam, they are:

$$\frac{d\sigma}{d\Omega} = \frac{\alpha^2}{8s} N_{cf} \left\{ A(1 + \cos^2 \vartheta) + B \cos \vartheta - h_f [C(1 + \cos^2 \vartheta) + D \cos \vartheta] \right\}, \quad (2.1)$$

$$A = Q_e^2 Q_f^2 + 2Q_e Q_f v_e v_f \Re e(\chi) + (v_e^2 + a_e^2)(v_f^2 + a_f^2) |\chi|^2, \quad (2.2)$$

$$B = 2Q_e Q_f a_e a_f \Re e(\chi) + 4v_e a_e v_f a_f |\chi|^2, \quad (2.3)$$

$$C = 2Q_e Q_f v_e a_f \Re e(\chi) + 2(v_e^2 + a_e^2) v_f a_f |\chi|^2, \quad (2.4)$$

$$D = 2Q_e Q_f a_e v_f \Re e(\chi) + 4v_e a_e (v_f^2 + a_f^2) |\chi|^2, \quad (2.5)$$

with

$$\chi = \frac{G_\mu M_Z^2}{2\sqrt{2}\pi\alpha} \frac{s}{s - M_Z^2 + is\Gamma_Z/M_Z}. \quad (2.6)$$

The values N_{cf} are the fermion colour factor ($N_{cq} = 3$, $N_{cl} = 1$) and Q_e and Q_f the electric charges. The vector and axial-vector couplings were already given in (1.23) and (1.24).

In a lowest order approximation, (2.1) yields **SM** cross sections $\sigma^0(s)$,

$$\sigma^0(s) = \sigma_Z^0(s) + \sigma_{\gamma Z}^0(s) + \sigma_\gamma^0(s) = \frac{4\pi\alpha^2}{3s} N_{cf} A, \quad (2.7)$$

with

$$\sigma_Z^0(s) = \frac{12\pi}{M_Z^2} \frac{\Gamma_e \Gamma_f}{\Gamma_Z^2} \frac{s\Gamma_Z^2}{(s - M_Z^2)^2 + s^2\Gamma_Z^2/M_Z^2}, \quad (2.8)$$

$$\sigma_{\gamma Z}^0(s) = \frac{4\pi\alpha^2}{3} J_f \frac{s - M_Z^2}{(s - M_Z^2)^2 + s^2\Gamma_Z^2/M_Z^2}, \quad (2.9)$$

$$\sigma_\gamma^0(s) = \frac{4\pi\alpha^2}{3s} Q_e^2 Q_f^2 N_{cf}, \quad (2.10)$$

for s-channel processes $e^+e^- \rightarrow \bar{f}f$, $f \neq e, \nu_e$, together with the three contributions $\sigma_Z^0(s)$, $\sigma_{int}^0(s)$, and $\sigma_\gamma^0(s)$ from the Z resonance term, the γZ interference, and pure γ exchange. For a constant width description see also (0.7) to (0.10) in the Introduction. Different asymmetries $\mathcal{A}_a(s)$ calculated from (2.1) are:

$$\mathcal{A}_{FB}(s) = \frac{N_F - N_B}{N_F + N_B} = \frac{3}{8} \frac{B}{A}, \quad (2.11)$$

$$\mathcal{A}_{pol}(s) = \frac{\sigma^{(h_f=+1)} - \sigma^{(h_f=-1)}}{\sigma^{(h_f=+1)} + \sigma^{(h_f=-1)}} = -\frac{C}{A}, \quad (2.12)$$

$$\mathcal{A}_{FB,pol}(s) = \frac{N_F^{(h_f=+1)} - N_F^{(h_f=-1)} - N_B^{(h_f=+1)} + N_B^{(h_f=-1)}}{N_F^{(h_f=+1)} + N_F^{(h_f=-1)} + N_B^{(h_f=+1)} + N_B^{(h_f=-1)}} = -\frac{3}{8} \frac{D}{A}. \quad (2.13)$$

The numbers N_F and N_B are the number of particles scattered into the forward and backward hemisphere with respect to the e^- beam. The coupling combinations A , B , C , and D containing the Z propagator $\chi(s)$ are defined in (2.2) to (2.5).

The Z boson mass M_Z and the total and partial decay widths Γ_Z and Γ_f can now e.g. be extracted from **SM** fits to measured leptonic and hadronic total cross sections on the Z boson resonance (see (0.11) or apply (2.7)):

$$\sigma^{0,f} = \sigma^0(M_Z^2) \approx \frac{12\pi}{M_Z^2} \frac{\Gamma_e \Gamma_f}{\Gamma_Z^2}. \quad (2.14)$$

In (2.14) the fact was used that exactly on the Z peak the γZ interference term σ_{int}^0 (2.9) does not contribute, while the pure QED term σ_γ^0 (2.10) only yields a small correction there. In the special case of b and c quark final states, the branching ratios R_b and R_c are measured instead:

$$R_b = \frac{\Gamma_b}{\Gamma_{had}} \quad , \quad R_c = \frac{\Gamma_c}{\Gamma_{had}}. \quad (2.15)$$

The Born fermionic decay widths $\Gamma_f = \Gamma_f(s = M_Z^2)$ in (2.8) and (2.14) and the γZ interference contribution J_f in (2.9) contain the vector and axial-vector coupling dependence of the cross sections:

$$\Gamma_f = \frac{G_\mu M_Z^3}{6\sqrt{2}\pi} N_{cf}(v_f^2 + a_f^2), \quad (2.16)$$

$$J_f = \frac{G_\mu M_Z^3}{\sqrt{2}\pi\alpha} Q_e Q_f v_e v_f. \quad (2.17)$$

While Γ_l and J_l can be determined separately for each lepton flavor, tricky flavor tagging techniques are utilized in order to identify exclusive quark flavors. For the heavy b and c quarks this works fairly well, whereas for the light quark sector $q = u, d, s$ a sum is performed over the different quark flavors. Thus, Γ_{had} is defined as $\Gamma_{had} = \sum_q \Gamma_q$ with $q = u, d, c, s, b$.

When determining parameters like M_Z and Γ_Z in a model-independent approach, the strong correlation between different parameters as e.g. M_Z and the γZ interference term \mathcal{J} has to be dealt with [53, 54, 60]:

$$\sigma_T^0(s) \sim \frac{\alpha^2(M_Z)}{s} + \frac{\mathcal{R}s + \mathcal{J}(s - M_Z^2)}{|s - M_Z^2 + iM_Z\Gamma_Z(s)|^2}. \quad (2.18)$$

In the **SM** case we would have in (2.18): $\mathcal{R} = 12\pi\Gamma_e\Gamma_f/M_Z^2$ and $\mathcal{J} = J_f$. This correlation has been studied at LEP energies. The hadron production data allow to deduce from (2.18) for example for the L3 experiment [20]:

$$M_Z = 91\,188 \pm 3 \pm 2.7 \text{ MeV}. \quad (2.19)$$

When determined from Z peak data alone, the error in (2.19) is $\pm 3 \pm 13$ MeV. The **SM** fit yields $M_Z = 91187.1 \pm 2.1$ MeV [21], where the $Zf\bar{f}$ couplings and thus \mathcal{J} in (2.18) are fixed and lepton universality is assumed. The very good agreement of the two fit procedures is a valuable test of the **SM**.

Furthermore, the invisible Z decay width for neutrino pair production is defined as

$$\frac{\Gamma_{inv}}{\Gamma_l} = \frac{N_\nu \Gamma(Z \rightarrow \bar{\nu}\nu)}{\Gamma_l} = \frac{N_\nu}{2(|v_l|^2 + |a_l|^2)}, \quad (2.20)$$

from which the total number N_ν of light SM neutrinos can be extracted, together with neutrino counting measurements using the channel $e^+e^- \rightarrow \nu\bar{\nu}\gamma(\gamma)$ [88]. The value N_ν is given at the 95% C.L. in Table 2.1. On the Z boson resonance the asymmetries of (2.13) yield the fermionic asymmetries $\mathcal{A}_a^{0,f}$,

$$\mathcal{A}_{FB}^{0,f} = \mathcal{A}_{FB}(M_Z^2) = \frac{3}{4}A_e A_f, \quad (2.21)$$

$$\mathcal{A}_{pol}^{0,f} = \mathcal{A}_{pol}(M_Z^2) = A_f, \quad (2.22)$$

$$\mathcal{A}_{FB,pol}^{0,f} = \mathcal{A}_{FB,pol}(M_Z^2) = \frac{3}{4}A_e, \quad (2.23)$$

$$\text{with} \quad A_f = -\frac{2v_f a_f}{v_f^2 + a_f^2}, \quad (2.24)$$

from which together with the partial widths Γ_f (see (2.16)) the couplings v_f and a_f can now be determined for the leptonic case $f = l = e, \mu, \tau$ and for the heavy quarks $f = b, c$.

Utilizing a polarized beam, which is e.g. done for the electron beam at the SLC experiment, we can also use the left-right asymmetry \mathcal{A}_{LR}^0 to determine A_e from a simple ratio of total cross sections for left- and right-handed polarized e^- .

$$\mathcal{A}_{LR}^0 = \mathcal{A}_{LR}(M_Z^2) = \frac{\sigma_L(M_Z^2) - \sigma_R(M_Z^2)}{\sigma_L(M_Z^2) + \sigma_R(M_Z^2)} \frac{1}{P_e} = -A_e. \quad (2.25)$$

In (2.25) the dependence on the beam polarization P_e , which can be measured separately, has been divided out for this.

With the definitions of v_f and a_f in (1.24) one sees immediately that the asymmetries A_f are therefore especially sensitive to the weak mixing angle $\sin^2 \theta_W$:

$$\sin^2 \theta_W = \frac{1}{4} \left[1 - \frac{v_f}{a_f} \right]. \quad (2.26)$$

From the three precisely known values $\alpha(0)^{-1}$, G_μ , and M_Z one can also evaluate tree-level results for the W boson mass M_W and the sine squared of the weak mixing angle $\sin^2 \theta_W$:

$$M_W^2 = \frac{M_Z^2}{2} \left\{ 1 + \sqrt{1 - \frac{4A}{M_Z^2}} \right\} = 80.94 \text{ GeV}, \quad (2.27)$$

$$\sin^2 \theta_W = \frac{1}{2} \left\{ 1 - \sqrt{1 - \frac{4A}{M_Z^2}} \right\} = 0.2121, \quad (2.28)$$

$$\text{with} \quad A = \frac{\pi\alpha}{\sqrt{2}G_\mu} = [(37.2802 \pm 0.0003) \text{ GeV}]^2. \quad (2.29)$$

Up to now only relations valid at Born level between couplings, masses, widths, and different cross section observables have been presented. The outcome of the measurements performed on the Z boson resonance, however, was that tree-level relations as in (2.26), (2.27), and (2.28) do not correctly reproduce the measured values, but some large deviations from these are experimentally observed. The great success of the SM lies in the amazingly accurate prediction of measured observables when taking into account all quantum corrections, for example using perturbation theory.

One example for the importance of radiative corrections at the Z resonance is the running of the QED coupling $\alpha = \alpha(s)$ which develops an s -dependence due to vacuum polarization effects to the photon propagator. In fact, in the relations given up to now the coupling $\alpha(0)$, valid only at low momentum transfers, has to be replaced by the renormalized coupling $\alpha(M_Z)$ at the Z boson mass. There exists a measured 6% enhancement of the Feinstructure constant $\alpha(M_Z)$ with respect to the Thomson limit [89]:

$$\alpha(M_Z) = \frac{\alpha(0)}{1 - \Delta\alpha} \quad (2.30)$$

This correction $\Delta\alpha$ is a large effect, where the main contributions are proportional to logarithmic mass terms $\ln(s/m_f^2)$, arising from self-energy corrections to the photon propagator including leptons and light quarks. In (2.30) the leading logarithmic terms have been resummed. While the calculation of the corrections by the leptonic loops can be dealt with straightforwardly in perturbation theory [90], the inclusion of light quark effects is much more involved due to non-perturbative contributions at small loop momenta. In the latter case one needs to partly rely on dispersion relations utilizing low-energy data on hadronic cross sections $e^+e^- \rightarrow \text{hadrons}$ and on τ decay data [91,92].

Another example, where additionally electroweak corrections beyond the running of α have to be included, is the correct determination of the electroweak parameters Δr and $\Delta\hat{r}$. They are defined to summarize radiative corrections to the sine squared of the weak mixing angle in two different renormalization schemes [93] (A defined in (2.29)):

$$s^2 c^2 = \frac{A^2}{M_Z^2(1 - \Delta r)} \quad , \quad \hat{s}^2 \hat{c}^2 = \frac{A^2}{M_Z^2(1 - \Delta\hat{r})} \quad (2.31)$$

In (2.31) $s^2 = \sin^2 \theta_W \equiv 1 - M_W^2/M_Z^2$ and $\hat{s}^2 = \sin^2 \hat{\theta}_W(M_Z)$ introduce the renormalized effective weak mixing angles in the on-shell and $\overline{\text{MS}}$ renormalization schemes, respectively ($c^2 = 1 - s^2$, $\hat{c}^2 = 1 - \hat{s}^2$). In both cases, the measured correction factors $\Delta r - \Delta\alpha$ and $\Delta\hat{r} - \Delta\alpha$, where the contributions from running α have been removed, deviate considerably from the tree-level value zero. It is an

impressive 9.7σ effect in the first case, and 9.9σ in the latter [93]. These large deviations from the tree-level prediction can only be explained accurately if both the numerically leading fermionic contributions and the subleading corrections by vector and Higgs boson loops are taken into account.

In cross section observables, defined at Born level e.g. in (2.7), the one-loop electroweak radiative corrections consist of self-energy corrections to the vector boson propagators, virtual corrections to the $\gamma f \bar{f}$ and $Z f \bar{f}$ vertices, and weak box corrections with WW or ZZ exchange. In general, due to a non-decoupling of heavy gauge fields in a spontaneously broken gauge symmetry like the electroweak sector of the SM [94] the main corrections to observables arise from heavy fermion doublets with large mass-splitting. This stands in contrast to exact gauge symmetries like QED and QCD where the heavy degrees of freedom decouple from the low energy part. That is, the main corrections arise there from vacuum polarization effects with leptons and light quarks. In the electroweak sector, however, we obtain important, m_t^2 -dependent terms from the large $m_t^2 - m_b^2$ mass splitting in electroweak radiative corrections. Corrections from virtual Higgs bosons do not contribute quadratically, but only logarithmically due to an extra global, i.e. *custodial* $SU(2)$ symmetry of the electroweak SM with its Higgs mechanism [95].

The first complete one-loop calculation of electroweak and QED radiative corrections without a treatment of the Z boson resonance, of QCD and of higher order electroweak corrections, and of hard bremsstrahlung had been derived in [96], and later including a correct Z resonance treatment in [33, 41, 97–99]. Now also the leading and sub-leading two-loop corrections proportional to $G_\mu^2 m_t^4$ and $G_\mu^2 m_t^2 M_Z^2$ to relations between electroweak observables are known [100–104].

QCD corrections, including mixed QED \otimes QCD and non-factorizable EW \otimes QCD corrections to the vector boson self energies or $Z q \bar{q}$ vertex also play an important role and are included up to $O(G_\mu m_t^2 \alpha_S^2)$ [105, 106] for the pure QCD terms, and at $O(\alpha \alpha_S)$ and $O(\alpha \alpha_S^2)$ [107–110] for the mixed QED \otimes QCD contributions. The remaining QCD contributions from real gluon bremsstrahlung for hadronic final states have been treated up to $O(\alpha_S^3)$ and $O(\alpha \alpha_S)$ [111, 112].

In [113, 114] it has been shown, if only considering leading terms from the virtual corrections that the relations (2.27) and (2.28) can be generalized for the corrected W boson mass M_W and $\sin^2 \theta_W$ to (A defined in (2.27)):

$$M_W^2 = \frac{\rho M_Z^2}{2} \left\{ 1 + \sqrt{1 - \frac{4A^2}{\rho M_Z^2} \frac{1}{1 - \Delta\alpha}} \right\}, \quad (2.32)$$

$$\sin^2 \theta_W(M_Z^2) = 1 - \frac{M_W^2}{\rho M_Z^2} = \frac{1}{2} \left\{ 1 - \sqrt{1 - \frac{4A^2}{\rho M_Z^2} \frac{1}{1 - \Delta\alpha}} \right\}. \quad (2.33)$$

The parameter ρ relates the charged to neutral current couplings, introduced in [95] and given in [113] for the main corrections from charge renormalization

and from heavy fermion corrections to the weak gauge boson propagators. In the ρ parameter for example the dependence of electroweak radiative corrections on the top mass m_t was first examined in [115]. It can be used to indirectly determine the top mass m_t , which poses an alternative to its direct measurement performed at the Tevatron experiment [28,29]. A thorough discussion of radiative corrections and their importance for electroweak precision physics was presented in [116,117].

As illustrated in the Introduction, the dominant radiative corrections to cross sections and asymmetries arise now from QED bremsstrahlung. On resonance, for example, the hadronic peak cross section is lowered by some 30%, mainly through multiple soft and virtual photon corrections. The large numerical effect develops from logarithmic mass terms $\ln(s/m_e^2)$ due to collinear photon emission from the initial state. So, if one wants to successfully test the SM by checking the predicted EW or QCD quantum effects, experiment needs precise theoretical tools in order to accurately remove the even larger bulk of corrections introduced by QED bremsstrahlung.

On the Z resonance the interference between initial and final state radiation and the added interference from Born and $\gamma\gamma$ - and γZ -exchange box diagrams contribute few per mil changes for loose kinematical cuts, but may carry more weight with tighter cuts or at higher energies. The small final state corrections can usually be approximated by a global correction factor to cross sections [50,55,118]. With per mil level measurements performed by experiments on the Z resonance, the initial state bremsstrahlung has to be known there at $O(\alpha^2)$ exactly [62] and in leading $O(\alpha^3)$ approximation [119,120]. Also QED corrections from the creation of fermion pairs after photon emission from the initial state are known up to leading fourth order in α now [62,121–123] and will be or are already included in the experimental analysis [124].

As the full results for cross section observables including all electroweak and QCD corrections with QED bremsstrahlung are in general quite complicated and lengthy, a short and handy description of the main corrections seems quite attractive, especially when having data-fitting routines with limited CPU time in mind. Fortunately, due to a factorization of electroweak and QCD corrections on the Z boson resonance these can be treated in an *effective* or *improved Born approximation*: Vector and axial-vector couplings v_f and a_f may be replaced by effective, in general complex valued couplings \bar{v}_f and \bar{a}_f [33], while for the Z boson width [41–46] an s -dependence can be introduced, $\Gamma_Z = \Gamma_Z(s)$ [33,42,52–54]. Experimentally, the real parts of \bar{v}_f and \bar{a}_f define the effective vector and axial-vector couplings v_f^{eff} and a_f^{eff} which may be measured, while the imaginary parts are small at the Z peak and usually calculated within the SM. The weak box contributions are non-resonant near the Z peak and produce only small corrections there with their different angular dependence being neglected [114]. They are infrared-finite and added at $O(\alpha)$. QCD effects can be parameterized by effective

color factors to \bar{v}_f and \bar{a}_f , i.e. factors of the type: $N_q = N_c \left\{ 1 + \frac{\alpha_s}{\pi} + \dots \right\}$. See also [38] and references therein.

The pure QED corrections which form a gauge-invariant subset of the radiative corrections can then be described by convoluting QED *flux functions* (*radiators*) with the improved Born observables containing the effective couplings and the added weak box corrections. A common convolution integral of the initial and final state radiators can be performed with the leading logarithmic soft and virtual corrections resummed and the QED interference and box parts usually added at $O(\alpha)$. Infrared singularities from soft photon corrections cancel completely. The full QED description of such an effective Born approach to cross sections and asymmetries will be presented in detail in the next Section 2.2.

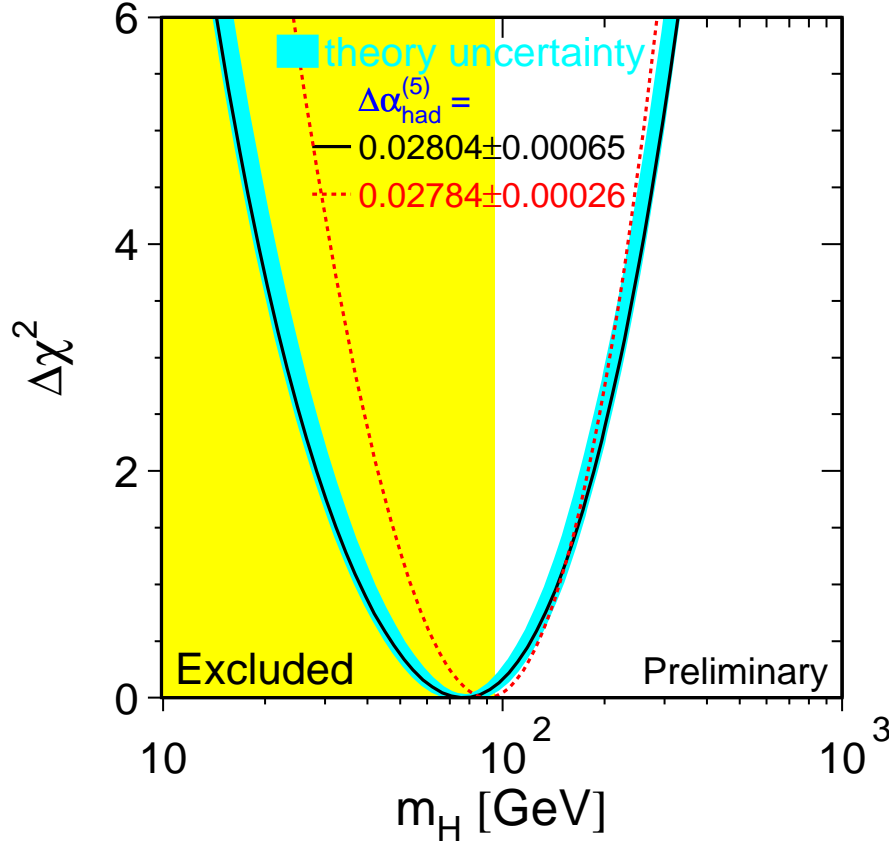


Figure 2.1: The $\Delta\chi^2$ distribution of the total LEP data fit depending on the Higgs boson mass m_H compared with program ZFITTER [16, 21].

An important application of these calculations is of course the investigation of indirect effects from a SM Higgs boson through virtual corrections: Bounds on the mass M_H of a SM Higgs boson can be derived from the logarithmic Higgs

mass dependence of different electroweak precision observables, using the directly measured value for m_t from the Tevatron. These corrections were calculated and analyzed in [125–129].

Such an indirect determination of M_H is for example illustrated in Fig. 2.1, depicting the $\Delta\chi^2$ distribution of a SM fit to LEP data on different electroweak precision observables with M_H as a free parameter. The minimum of the curve clearly indicates a low-mass SM Higgs boson. The solid and hatch-marked lines together with the shaded error band were calculated using the programs ZFITTER [31–38] and TOPAZO [130,131], which calculate SM observables at the Z peak within an effective Born approximation described above. The depicted error band is obtained changing the values of the SM input like e.g. the hadronic contributions $\Delta\alpha_{had}^{(5)}$ as main uncertainties to the running electromagnetic coupling. At the 95% C.L. one has from a recent analysis [16],

$$M_H < 262 \text{ GeV}, \quad (2.34)$$

while a lower bound of at least $M_H > 90 \text{ GeV}$ (95% C.L.) is determined from direct searches at LEP which could increase up to $M_H > \sqrt{s} - M_Z \approx 109 \text{ GeV}$ for $\sqrt{s} \approx 200 \text{ GeV}$ at the end of LEP [16].

2.2 Realistic observables and the ZFITTER approach

In the Introduction it was illustrated that the main corrections to fermion pair production cross sections and asymmetries arise from QED bremsstrahlung. While multiple soft and virtual corrections can be treated universally with a suitable resummation procedure, especially important on the Z peak, hard photon emission is strongly suppressed there. This is due to a strong decrease of the effective Born cross section or asymmetry as soon as the radiation of a hard photon from the initial state shifts the effective center-of-mass energy s' after photon emission away from the Z boson resonance. Although these hard photon effects, which are strongly cut-dependent, are small on the peak they are still important for the per mil and sub per mil level analysis of experimental data performed at LEP and SLC.

At higher energies the photonic corrections lead to the observed pronounced radiative tail for total cross sections σ_T and forward-backward asymmetries A_{FB} , with s' being shifted to M_Z^2 due to initial state hard photon emission. While σ_T is strongly enhanced, A_{FB} is decreased by a correction factor. This effect, the *radiative return to the Z*, can be removed completely or approximately by sufficiently strong kinematical cuts to the hard photon phase space. This is very

often preferred by experiment in order to probe the interesting electroweak or ‘New Physics’ sector.

Experiments at LEP 1, SLC, LEP 2, and those planned at a future e^+e^- Linear Collider aim at precisions well below a per cent and need theoretical predictions with an accuracy of the order of 0.1 % or better. A basic ingredient of the predictions is the complete $O(\alpha)$ photonic correction including initial and final state radiations and their interference:

$$\sigma(s) = \sigma^0(s) + \sigma^{ini}(s) + \sigma^{int}(s) + \sigma^{fin}(s). \quad (2.35)$$

These corrections have to be determined for two basic quantities: The total cross section $\sigma_T(s)$ and the forward-backward asymmetry $A_{FB} = \sigma_{FB}/\sigma_T$; other asymmetries may then easily be derived from them.

Basically, there are two experimental set-ups to be treated:

- (i) a lower cut on the final state fermions’ invariant mass squared, $s', s'_{\min} \geq 4m_f^2$,
- (ii) or combined cuts on the maximal *acollinearity angle* $\theta_{\text{acol}}^{\max} \leq 180^\circ$, and on the *minimal energy* of the fermions $E_{\min} \geq m_f$.

The *acollinearity angle* defines the small angular deviation from the back-to-back scattering situation in case of hard photon emission. It is discussed in more detail in Appendix A and shown in Fig. A.2 there.

Both cut settings (i) and (ii) may be combined with an acceptance cut $c, c \leq 1$, on the cosine of the fermionic production angle ϑ (*acceptance cut*). While case (i) is suitable to describe hadronic events, where due to jets from the hadronization of the final state quarks a definition of angular cuts is not easily possible, case (ii) provides an alternative to remove hard photon effects from leptonic final states instead of the kinematically simpler s' -cut.

In order to illustrate the effects of QED corrections at LEP 1 and LEP 2 energies, the semi-analytical program **ZFITTER** [31–38] is used. The semi-analytical approach of the **ZFITTER** code consists of a fast, one-dimensional numerical integration of analytical formulae for different observables like cross sections, asymmetries, and angular distributions with the inclusion of different experimentally relevant cut options. The $O(\alpha)$ soft and virtual QED terms are resummed and dominant higher order effects included. Corresponding numerical programs for fermion pair production like **TOPAZO** [130, 131], **ALIBABA** [132], or **KORALZ/KK2f** [133–136], are in this respect complementary to our approach as they can in principle treat multi-differential observables with more complex cuts to the final state phase space, but this at the expense of a clear increase in computing time.

With ZFITTER three different cut options are available [36, 38]: (i) no cuts [31, 32], (ii) cuts on s' and on the scattering angle ϑ of one fermion [34, 35], or (iii) cuts on the fermions' acollinearity angle θ_{acol} on their energies $E^f = E^{\bar{f}}$ and on $\cos \vartheta$ [37]. The effective Born cross sections $\sigma^0(s')$ may also be chosen according to following approaches: (A) SM, (B) Model Independent, (C) Others [33, 36, 38].

Without cuts, i.e. in case of complete acceptance and including all hard photon effects, total cross section formulae with the exact $O(\alpha)$ initial state radiation have been calculated in [32, 137]: In analogy to (0.4), the initial state corrected total cross section $\sigma_T^{\text{ini}}(s)$ may be written as a convolution integral of the (effective) Born cross section $\sigma^0(s')$ with a *flux function (radiator)* describing the photon-emission over the (normalized) invariant mass squared $R \equiv s'/s$ of the final state fermion pair:

$$\sigma_T^{\text{ini}}(s) = \int dR \sigma^0(s') \rho_T^{\text{ini}}(R). \quad (2.36)$$

Including a resummation of soft and virtual photonic higher order corrections [58, 59], the initial state radiator function $\rho_T^{\text{ini}}(R)$ can be written as:

$$\rho_T^{\text{ini}}(R) = (1 + \bar{S}^{\text{ini}}) \beta_e (1 - R)^{\beta_e - 1} + \bar{H}_T^{\text{ini}}(R), \quad (2.37)$$

with

$$\bar{S}^{\text{ini}} = \frac{3}{4} \beta_e + \frac{\alpha}{\pi} Q_e^2 \left(\frac{\pi^2}{3} - \frac{1}{2} \right), \quad \beta_e = \frac{2\alpha}{\pi} Q_e^2 \left(\ln \frac{s}{m_e^2} - 1 \right), \quad (2.38)$$

and

$$\bar{H}_T^{\text{ini}}(R) = \left[H_{BM}(R) - \frac{\beta_e}{1 - R} \right], \quad (2.39)$$

where

$$H_{BM}(R) = \frac{1}{2} \frac{1 + R^2}{1 - R} \beta_e \quad (2.40)$$

is the Bonneau-Martin term for the one-loop hard photon correction [137], while $(1 + \bar{S})$ are the regularized, infrared-finite soft and virtual contributions.

Historically, effects from soft and virtual photonic corrections to total cross sections are already known since [138]. The function $\rho_T^{\text{ini}}(R)$ in (2.36) and (2.37) is a regularized and infrared-finite flux function as according to [138] all infrared divergences from soft and virtual photon contributions have to cancel exactly to arbitrary perturbative order. The same holds for unphysical singularities arising for vanishing fermion masses which have to disappear in the complete scattering amplitude of a process [139, 140]. Only logarithmic mass terms of the

type $\ln(s/m^2)$ ($m = m_e, m_f$) from collinear photon-emission from the initial or final state fermions are allowed to survive. Also any unphysical distinction between soft and hard photon phase space, typically denoted with an arbitrary soft photon cut-off parameter ε , has to disappear in the final results at any given order [138–140].

That the leading logarithmic soft and virtual terms exponentiate, in (2.37) given by the term $(1 + \bar{S})\beta_e(1 - R)^{\beta_e-1}$, was first shown in [57]. The divergent contributions proportional to $(\ln \varepsilon)^n$ from the soft and hard photon radiators of course have to cancel to all orders. Technically, also other resummation procedures than a *soft photon exponentiation* [58, 59] are possible [57, 141, 142]. Analytically, they have to exactly reproduce the calculated two-loop results [62] after expansion in the coupling, and numerically the observed Z boson line shape [50, 55].

Having in mind kinematical cuts to the hard photon phase space, a generalization of the Bonneau-Martin formula in (2.39) with (2.40) with soft photon exponentiation, may be found in [32, 34]. There, all three corrections – the initial state, the final state, and the initial-final state interference – are treated for a cut on s' , without [32] or with an additional acceptance cut c [34]. The extremely compact expressions with $c = 1$ get quite involved when the acceptance cut is applied. The corresponding formulae are contained in the program **ZFITTER** [36, 38].

In the initial and final state soft and vertex corrections infrared singularities cancel each other completely; for this the necessary counter term diagrams from self-energy corrections to external fermion legs have to be included. This cancellation occurs separately for the initial and the final state radiator functions. The corresponding Feynman diagrams are shown in Fig. A.1, C.1, and C.2 in the Appendix. The QED box contributions consist in first order approximation of the interference terms between the Born diagram and the $\gamma\gamma$ and γZ exchange, direct and crossed box diagrams (see Fig. C.3 in the Appendix). They have to be combined with the initial-final state interference in order to obtain infrared-finite results.

The slightly more involved treatment of higher order soft and virtual photonic effects is given for initial or final state radiation in **ZFITTER**. Alternatively, also a common treatment of the initial and final state soft photon emission is possible [34]. The interference and QED box corrections are added exactly at $O(\alpha)$. In principle, following [58, 59], an analogous resummation procedure for soft interference and box corrections is possible [35, 143, 144].

A realistic description of total or forward-backward cross sections $\sigma_A(c)$, $A = T, FB$ ($\bar{A} = FB, T$), which is calculated by **ZFITTER** with acceptance cut, is:

$$\begin{aligned}
 \sigma_A(c) &= \left(\int_0^c \pm \int_{-c}^0 \right) d\cos\vartheta \frac{d\sigma}{d\cos\vartheta} \\
 &= \int_0^{1-4m_f^2/s} dv \left\{ \left[\sigma_A^0(s', c) \left(1 + \bar{S}^{ini} \right) \beta_e v^{\beta_e-1} + \sigma_A^0(s') \bar{H}_A^{ini}(v, c) \right] \bar{R}_A^{fin}(v) \right. \\
 &\quad \left. + \sigma_A^0(s, s') \left[H_A^{int}(v, c) - \frac{\sigma_A^0(s)}{\sigma_A^0(s, s')} H_A^{int, sing}(v, c) \right] \right\} \\
 &\quad + \sigma_A^0(s, c) \bar{S}_A^{int} + \sum_{m, n=\gamma, Z} \sigma_A^0(s, s, m, n) B_A(c, m, n). \tag{2.41}
 \end{aligned}$$

The convolution integral in (2.41) has $v \equiv 1 - R = 1 - s'/s$ as integration variable which corresponds to the normalized energy of the emitted or virtual photon. The (effective) Born expressions $\sigma_A^0(s, s')$ in (2.41) are introduced in (2.42) and (2.43):

$$\sigma_T^0(s, s') = \sum_{V_i, V_j=\gamma, Z} \sigma_T^0(s, s', i, j) = \frac{4\pi\alpha^2}{3s'} \mathcal{V}, \tag{2.42}$$

$$\sigma_{FB}^0(s, s') = \sum_{V_i, V_j=\gamma, Z} \sigma_{FB}^0(s, s', i, j) = \frac{\pi\alpha^2}{s'} \mathcal{A}, \tag{2.43}$$

with the combinations \mathcal{V} and \mathcal{A} for the neutral current couplings v_e, a_e, v_f , and a_f from (1.23) and (1.24) and the Z boson propagator, defined in (2.6):

$$\mathcal{V} = Q_e^2 Q_f^2 + Q_e Q_f v_e v_f \Re[\chi(s) + \chi(s')] + (v_e^2 + a_e^2)(v_f^2 + a_f^2) \Re[\chi(s) \chi^*(s')], \tag{2.44}$$

$$\mathcal{A} = Q_e Q_f a_e a_f \Re[\chi(s) + \chi(s')] + 4v_e a_e v_f a_f \Re[\chi(s) \chi^*(s')]. \tag{2.45}$$

The general formulae (2.42) and (2.43) hold exactly as effective Born total and forward-backward cross sections for the initial-final state interference. The corresponding initial state results $\sigma_{T, FB}^0(s')$ and final state results $\sigma_{T, FB}^0(s)$ can be obtained easily from (2.42) and (2.43) setting $s = s'$, or $s' = s$ respectively:

$$\sigma_A^{0, ini} = \sigma_A^0(s') = \sigma_A^0(s', s'), \tag{2.46}$$

$$\sigma_A^{0, fin} = \sigma_A^0(s) = \sigma_A^0(s, s). \tag{2.47}$$

In (2.41) all (regularized) hard, soft, and virtual photonic, together with the QED box corrections are contained in form of the radiator functions:

$$H(\bar{H})_A^a, \quad S(\bar{S})^a, \quad \text{and} \quad B_{\bar{A}}(c, m, n), \quad a = ini, int, \quad m, n = \gamma, Z. \tag{2.48}$$

The (un)barred radiators in (2.48) are (un)regularized functions, respectively. The corresponding final state radiator $\bar{R}_A^{fin}(v)$ is completely analogous to the initial state term in front with the necessary substitutions $s/m_e^2, Q_e \rightarrow s'/m_f^2, Q_f$. It can be convoluted together with the initial state radiator over $v = 1 - s'/s$ in a common soft photon exponentiation formula. This is done in (2.41) introducing the factor $\beta_e v^{\beta_e-1}$ for the resummed leading higher order effects to the initial state from soft and virtual photons. The $O(\alpha)$ QED interference and box corrections are regularized and added. Also note the antisymmetric angular dependence of the QED interference and box terms with respect to the initial and final state radiators which are multiplied with the effective Borns $\sigma_{FB}^0(s, c)$ in $\sigma_T(c)$ and $\sigma_T^0(s, c)$ in $\sigma_{FB}(c)$. Formula (2.41) is thus exact at first order in ZFITTER, but may include the exact two- [62] and leading three-loop [119, 120] contributions for initial state bremsstrahlung.

If the radiative return is prevented, the influence of hard photonic corrections will be much larger at higher energies than it is near the Z resonance where hard bremsstrahlung is strongly suppressed. Fig. 2.2 demonstrates that different portions of hard photon emission lead to nearly identical cross sections unless the region is reached where even soft photon emission is touched (lowest lying curve). The excellent precision of ZFITTER at the Z peak, however, does not

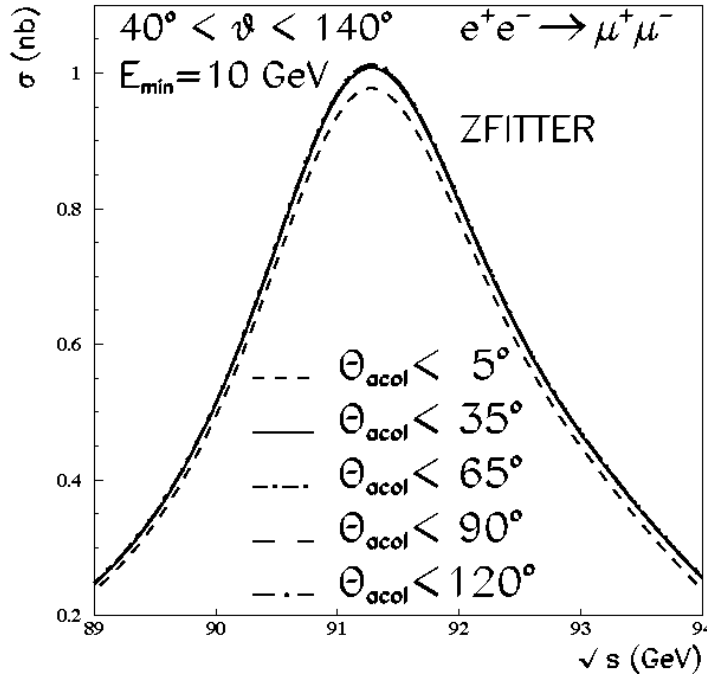


Figure 2.2: Muon pair production cross sections from ZFITTER [36, 38] with different cuts on maximal acollinearity θ_{acol} at the Z boson resonance [145].

automatically guarantee a sufficient accuracy at higher energies, especially since the hard photonic contributions including higher order corrections are no longer suppressed. For this compare Fig. 2.3 with Fig. 2.2. It is well-known that deviations up to several per cent may result from different treatments of radiative corrections.

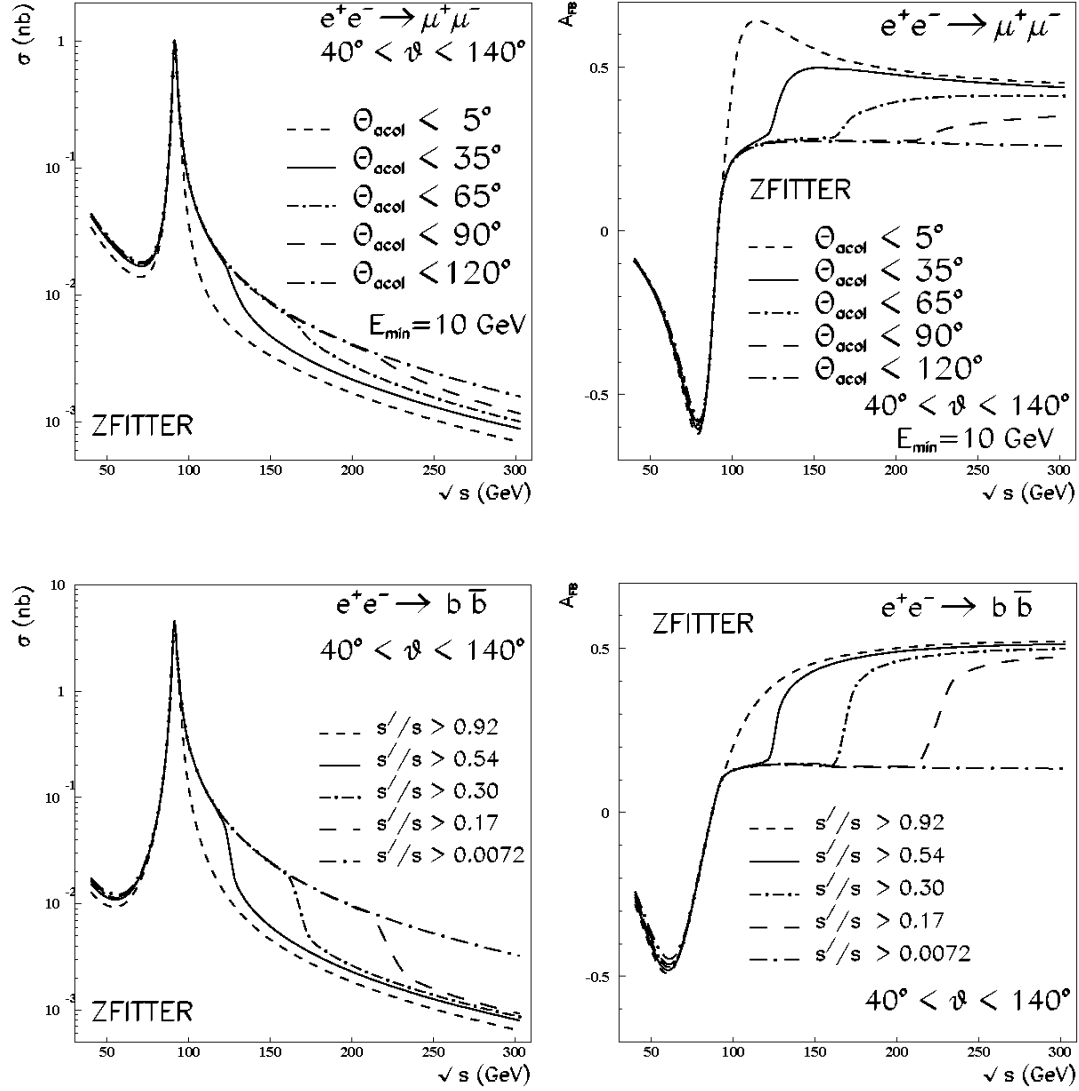


Figure 2.3: Cross sections and forward-backward asymmetries from ZFITTER [36, 38] for muon pair and $b\bar{b}$ production with different cuts on a. the maximal acollinearity angle θ_{acol} or b. minimal invariant mass squared s' [145].

Fig. 2.3 shows muon pair cross section predictions for different acollinearity cuts at LEP 1 and LEP 2 energies. The radiative return is prevented if $\sqrt{s'} > M_Z$.

Depending on the value of the hard photon cut, this implies a certain center-of-mass energy $\sqrt{s^{\min}}$ above which the radiative return is suppressed (see Section (2.3.1 and Table 2.2 for this). For comparison, the corresponding curves for $b\bar{b}$ production with s' -cut are shown as well. The s' -cut values given in the figure corresponds approximately to the acollinearity cut values in the left-hand plots.

Traditionally, an accuracy of ZFITTER at LEP 1 energies of the order of 0.5% was aimed at. The successful running of LEP 1 together with the precise knowledge of the beam energy, however, made an even higher precision necessary [146]: For the final measurements relative errors for total cross sections and absolute errors for asymmetries are expected up to 0.15% at the Z peak and of up to 0.5% at $\sqrt{s} = M_Z \pm$ several GeV. Aiming from the theoretical side ideally at a tenth of these values for the errors of single corrections, limits of 0.015%, and 0.05% respectively, can be estimated. First applications of ZFITTER at energies above the Z resonance have become relevant since data from LEP 1.5 and LEP 2 are being analyzed.

Recent studies for a cut on s' [147] claim for the Bhabha scattering process $e^+e^- \rightarrow e^+e^-(n\gamma)$ that an accuracy of 0.3% for $O(\alpha)$ corrections and of 1% for the complete corrections has been reached at LEP 2 energies as long as the radiative return to the Z peak is prevented by cuts. Similarly, a comparison of codes ALIBABA and TOPAZ0 had delivered for LEP 1 energies maximal theoretical uncertainties of 0.6 per mil [148]. These conclusions were also drawn for s -channel fermion pair production processes in [149–155].

2.3 QED bremsstrahlung with *acollinearity cut*

In the previous Section we briefly introduced the two different cut options which are semi-analytically treatable: (i) kinematical cuts on the final state invariant mass squared s' , and on the minimal scattering angle ϑ ; or (ii) cuts on the final state maximal acollinearity angle θ_{acol} , on their minimal energies $E_{\bar{f},f}$, and on the minimal scattering angle ϑ .

For the kinematically simpler s' -cut the correct $O(\alpha)$ photonic corrections with or without a cut on one scattering angle are given in [32, 34, 35]. The ZFITTER program relies on these duplicated analytical calculations, with its $O(\alpha)$ corrections basically remaining untouched since about 1989. Numerical comparisons with other two-fermion codes showed the reliability of the predictions at LEP energies; see e.g. [149, 151, 152] for the LEP 1 and [156] for the LEP 2 case.

Concerning the acollinearity cut, which is experimentally interesting for leptonic final states as alternative to an s' -cut, the situation was not so clear: There has been no independent check until recently for the acollinearity cut branch and

only little literature available on the exact $O(\alpha)$ final state corrections to the total cross section and forward-backward asymmetry [157].

The corresponding part of ZFITTER [70] was never checked independently and is not documented, except for a collection of some formulae related to the initial state corrections and its combined exponentiation with final state radiation for the angular distribution in [69]. For total cross sections only the final state corrections are analytically known [157].

Furthermore, when comparing cross section results from ZFITTER with those from program ALIBABA [132], first deviations were observed at LEP 1 energies, but especially at intermediate energies above the Z resonance where effects from a radiative return to the Z could not be prevented completely by the applied cut. These deviations were of the order of several per cent. Slightly later it was observed in [152] that the perfect agreement of many predictions of ZFITTER v.5.20 and TOPAZ0 v.4.3 at LEP 1 energies of about typically 0.01% could not be reproduced when an acollinearity cut was applied and the initial-final state interference was taken into account.

So, a recalculation and documentation of the acollinearity cut situation was absolutely mandatory with the main focus first at energies around the Z boson resonance.¹ First compact formulae and numerical comparisons were published in [146] for initial state bremsstrahlung without acceptance cut, and for all first order corrections in [37]. Before analytical results are presented, the hard photon phase space and a suitable parameterization for an acollinearity cut shall be briefly described.

2.3.1 The phase space for hard photon emission

It was already mentioned earlier that a three-, or respectively two-fold analytical integration of the squared matrix elements has to be performed in order to calculate total cross section observables like $\sigma_{T,FB}(s)$, or angular cross section distributions respectively. The final integration over $R = s'/s$ is then performed numerically. We follow the phase space parameterization presented in [158].

¹ The slightly more involved Bhabha scattering case with extra t channel contributions is kept for a later analysis.

The Dalitz plot given in Fig. 2.4 may help to understand the relation between a kinematically simple s' -cut and a more involved acollinearity cut. The variable

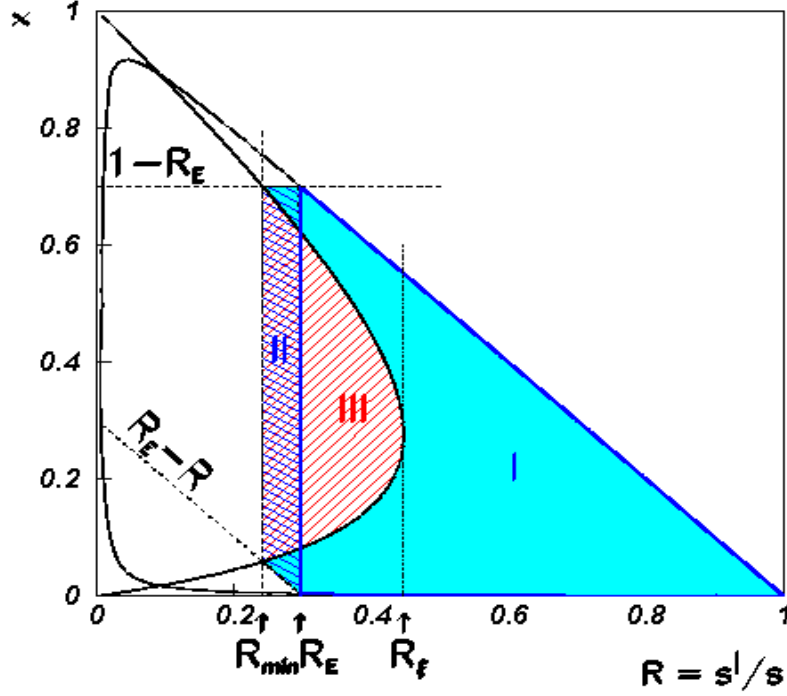


Figure 2.4: Phase space with cuts on maximal acollinearity and minimal energy of the fermions with $x \equiv 2p_\gamma p_{\bar{f}}/s$ [37, 145, 146].

shown in Fig. 2.4 besides R is x , the normalized invariant mass of the $(\bar{f} + \gamma)$ rest system. The phase space is naturally split into three separate parts due to the cuts applied, each region described by a different and only one cut:

- The main triangular region I is constrained for the variable x by the kinematical boundary approximately given by $(1 - R)$. It is equivalent to a phase space with a cut on s' ; the minimal R -value R_E is defined by the minimal fermion energy, while maximal $R \rightarrow 1 - \varepsilon$ touches the soft photon corner of phase space.
- Then a trapezoidal region II is added. The bounds for x are defined by the minimal energies cut $R_E = 2E_{\min}/s$; the minimal R -value $R_{\min} < R_E$ is given below in (2.50) with R_E as upper bound of R .
- Region III with a curved boundary from the cut on maximal acollinearity θ_{acol}^{\max} , is subtracted. The variable R ranges between R_{\min} and a maximal value $R_{\theta_{acol}}$ defined in (2.57).

Depending on the cuts applied, special cases can arise, if one uses sufficiently strong cuts on acollinearity or energies, where only regions I and II or regions I and III are kinematically allowed.

As Fig. 2.4 shows, we have to determine cross sections in three different regions of phase space with different boundary values of x with R fixed:

$$\frac{d\sigma^{hard}}{d\cos\vartheta} = \left[\int_I + \int_{II} - \int_{III} \right] dR dx \frac{d\sigma^{hard}}{dR dx d\cos\vartheta}. \quad (2.49)$$

Region I corresponds to a simple s' -cut. The integration over R extends from R_{\min} to 1 with

$$R_{\min} = R_E \left(1 - \frac{\sin^2(\theta_{\text{acol}}^{\max}/2)}{1 - R_E \cos^2(\theta_{\text{acol}}^{\max}/2)} \right). \quad (2.50)$$

The R value R_E is defined in (2.56). The soft photon corner of the phase space resides at $R = 1$. Thus, the additional contributions related to the acollinearity cut are exclusively due to hard photons. The boundaries for the integration over x are, for a given value of R :

$$x_{\max, \min}(R) = \frac{1}{2}(1 - R) [1 \pm A(R)], \quad (2.51)$$

where the value $A = A(R)$ depends in every region on only one of the cuts applied:

$$A_I(R) = \sqrt{1 - \frac{R_m}{R}} \approx 1, \quad (2.52)$$

$$A_{II}(R) = \frac{1 + R - 2R_E}{1 - R}, \quad (2.53)$$

$$A_{III}(R) = \sqrt{1 - \frac{R(1 - R_{\theta_{\text{acol}}})^2}{R_{\theta_{\text{acol}}}(1 - R)^2}}, \quad (2.54)$$

with

$$R_m = \frac{4m_f^2}{s}, \quad (2.55)$$

$$R_E = \frac{2E_{\min}}{\sqrt{s}}, \quad (2.56)$$

$$R_{\theta_{\text{acol}}} = \frac{1 - \sin(\theta_{\text{acol}}^{\max}/2)}{1 + \sin(\theta_{\text{acol}}^{\max}/2)}. \quad (2.57)$$

Here, m_f and E_{\min} are the final state fermions' mass and a cut on their individual energies in the cms. For simplicity, equal energy cuts are used for both fermions.

An acollinearity cut may act as a simple cut on invariant masses and thus it may prevent the radiative return of $\sqrt{s'}$ to the Z peak (and the development of the radiative tail) for measurements at higher \sqrt{s} . In Fig. 2.4 it may be seen that a reasonable analogue of a cut value $\sqrt{s^{\min}}$ is the upper value of s' of region III, $R_{\theta_{\text{acol}}}$, defined in (2.57):

$$\sqrt{s^{\min}} = \frac{M_Z}{\sqrt{R_{\theta_{\text{acol}}}}}.$$

The relations are also visualized in Table (2.2) and the effects of some cut values have been shown in Fig. 2.3.

θ_{acol}	$R_{\theta_{\text{acol}}}$	$\sqrt{s^{\min}}$
0.0°	1.0000	91.2 GeV
2.0°	0.9657	92.8 GeV
5.0°	0.9164	95.3 GeV
10.0°	0.8397	99.5 GeV
15.0°	0.7691	104.0 GeV
20.0°	0.7041	108.7 GeV
25.0°	0.6441	113.6 GeV
30.0°	0.5888	118.8 GeV
45.0°	0.4465	136.5 GeV
60.0°	0.3333	157.9 GeV
75.0°	0.2432	184.9 GeV
90.0°	0.1716	220.1 GeV
120.0°	0.0718	340.3 GeV
150.0°	0.0173	692.6 GeV
180.0°	0.	∞

Table 2.2: The minimal center-of-mass energy $\sqrt{s^{\min}}$ at which the radiative return to the Z peak is prevented by an acollinearity cut given as a function of this cut [145].

2.3.2 Initial state radiation and mass singularities

In the last section we saw that the Dalitz plot in Fig. 2.4 describing the hard photon phase space is independent of the scattering angle $\cos\vartheta$. Here it will be shown that the integrations in regions II and III are nevertheless crucially

influenced by $\cos \vartheta$. We will have to deal with artificially arising mass singularities when neglecting masses for analytical integration and will have to adjust our phase space treatment accordingly. The final results, however, can be shown to be finite when going to the continuous phase space limit. We want to illustrate this for the integration of the hard initial state radiation. The treatment of the QED initial-final state interference is then completely analogous, the final state is safe of these mass singularities.

First, we want to denote with k_1 , k_2 , p_1 , p_2 , and p the 4-momenta of e^- , e^+ , f^- , \bar{f} and of the hard photon, respectively. We have two photon angles φ_γ and θ_γ and one fermionic scattering angle ϑ . The variables depicted in Fig. 2.4 were $R = s'/s$ as normalized final state invariant mass squared ($s' = m_{f\bar{f}}^2$) and $x = 2p_2p/s$ as normalized invariant mass squared of the $(\bar{f} + \gamma)$ subsystem. A detailed description of the phase space and complete kinematics is given in Appendix A. The analytical integration will be performed over the three variables φ_γ , x , which is affine linear in $\cos \vartheta_\gamma$, and $\cos \vartheta$, if interested in flux functions for total cross sections and asymmetries. The final results for cross sections and their angular distributions over $\cos \vartheta$ are obtained from a numerical integration over $v \equiv 1 - R = 1 - s'/s$ (or equivalently over R) after regularization with the first order soft and virtual corrections.

Starting with the bremsstrahlung contribution from *initial state radiation*, the corresponding squared matrix element contains the electron (positron) propagator, and these terms are proportional to first and second powers of

$$\frac{1}{Z_{1(2)}} = -\frac{1}{(k_{1(2)} - p)^2 - m_e^2} = \frac{1}{2k_{1(2)}p} \quad (2.58)$$

$$= \frac{1}{A_{1(2)} \pm b \cos \varphi_\gamma}, \quad (2.59)$$

with

$$A_{1(2)} = \frac{s}{2}(1 - R)(1 \pm \beta_0 \cos \vartheta \cos \theta_\gamma), \quad (2.60)$$

$$B = \frac{s}{2}(1 - R)\beta_0 \sin \vartheta \sin \theta_\gamma, \quad (2.61)$$

and

$$\beta_0 = \sqrt{1 - 4m_e^2/s}, \quad (2.62)$$

$$\cos \theta_\gamma = \frac{\lambda_1 - \lambda_2 - \lambda_p}{2\sqrt{\lambda_2\lambda_p}}, \quad (2.63)$$

and with $\sqrt{\lambda_1} = (1 - x)s$, $\sqrt{\lambda_2} = (x + R)s$, and $\sqrt{\lambda_p} = (1 - R)s$. Final state mass effects have to be neglected for a complete analytical integration over all angles of phase space.

The first analytical integration is now performed over φ_γ , the photon production angle in the $(f + \gamma)$ rest system [158]:

$$\frac{d\sigma^{hard}}{dR dx d\cos\vartheta} = \int_0^{2\pi} d\varphi_\gamma \frac{d\sigma^{hard}}{dR dx d\cos\vartheta d\varphi_\gamma}. \quad (2.64)$$

It is important to take care of the electron mass m_e in order to regularize mass singularities from collinear initial state photon emission. This has to be done e.g. in the following contribution:

$$\int_0^{2\pi} d\varphi_\gamma \frac{1}{Z_i(R, \cos\vartheta, x, \varphi_\gamma)} = \frac{2\pi\sqrt{\lambda_2}}{\sqrt{C_i}}, \quad (2.65)$$

$$C_i = s^2 a_i x^2 - 2s b_i x + c_i, \quad (2.66)$$

$$a_i = s^2(z_i^2 - R\eta_0^2), \quad (2.67)$$

$$b_i = s^3[R z_i(1 - z_i) - \frac{1}{2}R(1 - R)\eta_0^2], \quad (2.68)$$

$$c_i = s^4 R^2 (1 - z_i)^2, \quad (2.69)$$

$$z_{1(2)} = \frac{1 \mp \beta_0 \cos\vartheta}{2} + R \frac{1 \pm \beta_0 \cos\vartheta}{2}, \quad (2.70)$$

$$\eta_0^2 = 1 - \beta_0^2; \quad \beta_0^2 = 1 - \frac{4m_e^2}{s}. \quad (2.71)$$

In the second step we integrate over x with limits given in (2.51). One of the basic integrals arising is for example:

$$\begin{aligned} I_i^0(R, \cos\vartheta) &= s \int_{x_{min}}^{x_{max}} \frac{dx}{\sqrt{C_i}} \\ &= \frac{1}{\sqrt{a_i}} \ln \left[\sqrt{a_i} C_i^{\frac{1}{2}} + (s a_i x - b_i) \right] \Big|_{x_{min}}^{x_{max}}, \end{aligned} \quad (2.72)$$

with

$$C_i^{\frac{1}{2}}|_{x_{max,min}} = \frac{1}{2} s^2 (1 - R) \sqrt{(y_i \pm A z_i)^2 + R(1 - A^2) \eta_0^2}, \quad (2.73)$$

$$(s a_i x - b_i) \Big|_{x_{min}}^{x_{max}} = (1 - R)(y_i \pm A z_i) + O(\eta_0^2), \quad (2.74)$$

and

$$y_{1(2)} = \frac{1 \mp \beta_0 \cos\vartheta}{2} - R \frac{1 \pm \beta_0 \cos\vartheta}{2}. \quad (2.75)$$

Again, in order to be able to integrate analytically over $\cos \vartheta$, we are now interested in the limit of vanishing electron mass m_e for the subsequent integrations. In this limit, there will occur zeros in arguments of logarithms like the one in (2.72) at four different locations in the remaining $\cos \vartheta$ - R phase space. These locations are defined by the conditions:

$$y_i \pm Az_i = y_i(R, \cos \vartheta) \pm A(R) z_i(R, \cos \vartheta) = 0, \quad i = 1, 2. \quad (2.76)$$

These zeros appear as functions of $\cos \vartheta$ with parameters R and $A = A(R)$ at certain values $\cos \vartheta = c_i^\pm$ ($i = 1, 2$):

$$c_1^+(R) = -\frac{1 - R + A(R)(1 + R)}{1 + R + A(R)(1 - R)} \leq 0 \quad \forall R \in [0; 1], \quad (2.77)$$

$$c_1^-(R) = -\frac{1 - R - A(R)(1 + R)}{1 + R - A(R)(1 - R)}, \quad (2.78)$$

$$c_2^+(R) = -c_1^+(R) \geq 0 \quad \forall R \in [0; 1], \quad (2.79)$$

$$c_2^-(R) = -c_1^-(R). \quad (2.80)$$

The relations $c_1^+ \leq c_1^-$ and $c_2^+ \geq c_2^-$ are also fulfilled.

In the course of integration, different analytical expressions have to be used in different kinematical regions when neglecting m_e wherever possible, except for logarithmic terms proportional to $L_e = \ln(s/m_e^2)$ and $L_\beta = \ln(1 \pm \beta_0 \cos \vartheta)$ from collinear photon emission. This results in cutting the remaining phase space for the $\cos \vartheta$ -integration, at fixed R and for given i , into three different regions. This splitting of phase space of course translates into a phase space splitting for each one of the three regions I, II, and III parameterized by $A(R)$ in (2.52) to (2.54), depending on the specific value of R and depicted in Fig. 2.4.

The differential cross section $d\sigma/(dR d\cos \vartheta)$ is a double-sum over $i = 1, 2$, but for the s' -cut-like region I the conditions (2.77) to (2.80) become trivial,

$$c_2^+(I) = -c_1^+(I) = -c_1^-(I) = -c_2^-(I) = 1, \quad (2.81)$$

only leaving one case to be studied ($-1 \leq \cos \vartheta \leq 1$). In regions II and III, however, $d\sigma/(dR d\cos \vartheta)$ will consist of different analytical expressions for each combination of the kinematical ranges defined by (2.77) to (2.80). The final result for e.g. I_i^0 after integration over x , setting $m_e = 0$, becomes ($i = 1, 2$):

(i) For $|\cos \vartheta| < |c_i^-|$ with $y_i \pm Az_i > 0$ (case $(i)^{++}$):

$$I_i^0 = \frac{1}{sz_i} \ln \left(\frac{y_i + Az_i}{y_i - Az_i} \right), \quad (2.82)$$

(ii) for $|c_i^-| < |\cos \vartheta| < |c_i^+|$ with $y_i + Az_i > 0$ and $y_i - Az_i < 0$ (case $(i)^{+-}$):

$$I_i^0 = \frac{1}{sz_i} \left\{ \ln \left[\frac{z_i^2 (y_i + Az_i)(Az_i - y_i)}{R^2 (1 - \beta_0^2 \cos^2 \vartheta)} \right] + \ln \left(\frac{s}{m_e^2} \right) \right\}, \quad (2.83)$$

(iii) for $|\cos \vartheta| > |c_i^+|$ with $y_i \pm Az_i < 0$ (case $(i)^{--}$):

$$I_i^0 = -\frac{1}{sz_i} \ln \left(\frac{y_i + Az_i}{y_i - Az_i} \right). \quad (2.84)$$

It can be shown that the resulting number of cases for the angular distribution, depending on the value of $\cos \vartheta$ with respect to c_i^\pm and on R , is at most four in regions II and III, as only certain combination of signs of c_i^\pm are possible (see also Appendix B.1). These are for $\cos \vartheta \geq 0$ with the abbreviations given in (2.82) to (2.84) [145]:

$$\text{a.} \quad (1)^{++} \quad \text{combined with} \quad (2)^{++}, \quad (2.85)$$

$$\text{b.} \quad (1)^{+-} \quad \text{combined with} \quad (2)^{+-}, \quad (2.86)$$

$$\text{c.} \quad (1)^{++} \quad \text{combined with} \quad (2)^{+-}, \quad (2.87)$$

$$\text{d.} \quad (1)^{--} \quad \text{combined with} \quad (2)^{++}. \quad (2.88)$$

For $\cos \vartheta < 0$, cases c. and d. are exchanged by c.' and d.' (formally by interchanging indices (1) and (2)):²

$$\text{a.} \quad (1)^{++} \quad \text{combined with} \quad (2)^{++}, \quad (2.89)$$

$$\text{b.} \quad (1)^{+-} \quad \text{combined with} \quad (2)^{+-}, \quad (2.90)$$

$$\text{c.}' \quad (1)^{+-} \quad \text{combined with} \quad (2)^{++}, \quad (2.91)$$

$$\text{d.}' \quad (1)^{++} \quad \text{combined with} \quad (2)^{--}. \quad (2.92)$$

² For region I in (2.52), only case b. is possible.

For the hard photon parts of the total cross section $\sigma_T(c)$ or forward-backward asymmetry $A_{FB}(c)$ with acceptance cut c , we finally have to integrate over $\cos \vartheta$ within cut boundaries $\pm c$:

$$\sigma_T^{hard}(c) = \int_{-c}^c d\cos \vartheta \frac{d\sigma^{hard}}{d\cos \vartheta}; \quad (2.93)$$

$$\sigma_{FB}^{hard}(c) = \left(\int_0^c - \int_{-c}^0 \right) d\cos \vartheta \frac{d\sigma^{hard}}{d\cos \vartheta} \quad (2.94)$$

$$= \left(\int_0^c + \int_0^{-c} \right) d\cos \vartheta \frac{d\sigma^{hard}}{d\cos \vartheta}. \quad (2.95)$$

Looking at the possible logarithmic expressions which have to be integrated, like the ones in (2.82) to (2.84), one immediately sees that these are, except for some rational factors in R , merely reproduced with the variable $\cos \vartheta$ now replaced by c (see Appendix B.1). The treatment of mass singularities for $m_e \rightarrow 0$ and the distinction of different regions in phase space therefore has to be repeated for the totally integrated case where the cut-off c now plays the role of $\cos \vartheta$. Depending on the relative position of c with respect to the values c_i^\pm , we have to integrate over different expressions of the angular distribution in the $\cos \vartheta$ - R phase space (see cases a. to d. or a. to d.' above).

For the corresponding hard radiator functions $H_T(R, A, c)$ and $H_{FB}(R, A, c)$, defined for example by (2.41), one finally gets at most four or respectively six different analytical expressions from different regions of phase space. This is because of symmetric cancellations when integrating over $\cos \vartheta$ for σ_T^{hard} , while in the definition of σ_{FB}^{hard} there is the additional occurrence of $c = 0$ which leads to more cases; see (2.93) and (2.94).

If the acceptance cut is omitted, i.e. setting $c = 1$, only case d. (or respectively d.') from above remains for $\sigma_T^{hard} = \sigma(1) - \sigma(-1)$ in regions II and III because then $-1 < c_i^\pm < 1$. For σ_{FB}^{hard} with $\sigma_{FB}^{hard} = \sigma(1) - 2\sigma(0) + \sigma(-1)$, two cases are left because the additional integrated contributions from $\cos \vartheta = 0$ depend on whether $c_2^- > 0$ from (2.80) or not. The conditions (2.77) to (2.80) are fulfilled for $\cos \vartheta = 0$ with

$$A_0(R) = \frac{1 - R}{1 + R}, \quad (2.96)$$

so that, depending on the sign of $(A(R) - A_0(R))$, one or the other analytical expression has to be used. This will lead for $c = 1$ to quite compact results for σ_T and σ_{FB} , presented in the next Subsection 2.3.3 and published in [37].

One can check that the integrated results $\sigma_{T,FB}^{hard}$ are continuous when $c \rightarrow c_i^\pm$, while $d\sigma^{hard}/d\cos\vartheta$ can be regularized at $\cos\vartheta = c_i^\pm$, taking the exact logarithmic results in m_e for the integrals. So, the artificially introduced mass ‘singularities’ when neglecting m_e have to cancel. Also, as a further check, the contributions proportional to the Born cross section σ^0 and Born asymmetry A_{FB} are (anti)symmetric respectively, as it should be for the one loop corrected initial state results.

The phase space splitting discussed above also has an influence on the initial-final state interference corrections since there the initial state propagators with $Z_{1,2}^{-1}$ appear linearly. The discussion of the different steps of integration can be done completely analogously as for the initial state case. These propagators, however, do not contribute in the *final state expressions* so that the phase space splitting is not necessary there.

Summarizing, we observe that neglecting the initial and final state masses at the mentioned high energies necessitates a separation of the phase space formed by the cosines of the remaining two angles of integration $\cos\vartheta$ and $\cos\theta_{acol}$ into several different regions. Only where necessary, the masses are kept in order to regularize the mass singularities from collinear radiation of bremsstrahlung photons. This splitting of phase space delivers for each region different analytical expressions for the calculated observables [145]. For the special cases of either full angular acceptance, i.e. no cut on $\cos\vartheta$, or no cut on the acollinearity angle θ_{acol} , the number of different expressions can be substantially reduced and very compact formulae can be obtained [37].

2.3.3 Cross section formulae

Beginning with the soft and virtual photon corrections, these are of course independent of the applied cuts and we can use the results for the initial, final, interference, and box corrections from [32, 34, 35]. Concerning the hard corrections with acollinearity cut, see the phase space discussion in the previous Subsection (2.3.1). We have seen that the hard photon part of the total cross section including initial state radiation can be written as the sum of different contributions from three regions in phase space:

$$\sigma_T^{hard}(s) = \left[\int_I + \int_{II} - \int_{III} \right] ds' dx d\cos\vartheta \frac{d\sigma(A)}{ds' dx d\cos\vartheta}, \quad (2.97)$$

with the parameter $A = A(s'/s)$ and its different meanings in these regions given in (2.52), (2.53), and (2.54).

Initial state radiation

For the total cross section, the analytical formula with cuts on acollinearity and minimal fermion energy is remarkably compact for the full angular acceptance ($c = 1$). For the initial state hard radiator function $H_T^{ini}(R, A)$ we have, replacing the Bonneau-Martin function $H_{BM}(R)$ from (2.40) in (2.37) and (2.39):

$$H_T^{ini}(R, A) = \frac{3\alpha}{4\pi} Q_e^2 \left[\left(A + \frac{A^3}{3} \right) \frac{1+R^2}{1-R} \left(\ln \frac{s}{m_e^2} - 1 \right) + (A - A^3) \frac{\mathcal{B}R}{1-R} \right], \quad (2.98)$$

with $\mathcal{B} = 2$. In $\sigma_{FB}^{ini}(s)$, the corresponding hard radiator part is:

$$\begin{aligned} H_{FB}^{ini}(R, A \geq A_0) = & \frac{\alpha}{\pi} Q_e^2 \left\{ \frac{1+R^2}{1-R} \left[\frac{4R}{(1+R)^2} \left(\ln \frac{s(1+R)^2}{4m_e^2 R} - 1 \right) \right. \right. \\ & - \frac{1}{(1+R)^2} [y_+ y_- \ln |y_+ y_-| + 4R \ln(4R)] \\ & \left. \left. - (1-A^2) \left(\ln \frac{s}{4m_e^2 (1+A)^2 R} - 1 \right) \right] + \frac{4A(1-A)R}{1-R} \right\}, \end{aligned} \quad (2.99)$$

$$\begin{aligned} H_{FB}^{ini}(R, A < A_0) = & \frac{\alpha}{\pi} Q_e^2 \left\{ \frac{1+R^2}{1-R} \left[-\frac{y_+ y_-}{(1+R)^2} \ln \left| \frac{y_+}{y_-} \right| + (1-A^2) \ln \frac{1+A}{1-A} \right] \right. \\ & \left. + \frac{8AR^2}{(1+R)(1-R)} \right\}. \end{aligned} \quad (2.100)$$

The following definition is used:

$$y_{\pm} = (1-R) \pm A(1+R). \quad (2.101)$$

In region I, ($A \rightarrow 1$), the above expressions (2.98) and (2.99) reduce to those known from [137] and [32]. The phase space regions II and III do not contribute there. In this region the radiators diverge for $R \rightarrow 1$, and soft photon exponentiation and the subtraction $\beta/(1-R)$ is applied there in order to get $\bar{H}_B^{ini}(R)$, $B = T, FB$; see (2.39). For phase space regions II and III, i.e. $A \neq 1$, safe of infrared divergent contributions we immediately have $\bar{H}_B^{ini}(R, A) = H_B^{ini}(R, A)$.

The additional contributions for $A = 1$ from final state radiation and the initial-final state interference to σ_T (and also those to σ_{FB}) may be found in [32]. Important to note is that, differing from (2.98), the coding in the program **ZFITTER** corresponds to $\mathcal{B} = 4/3$ if one looks there into the limit $c = 1$. The resulting numerical deviations are typically of the order of 0.5% to 2%. They will not lead to drastical improvements in the comparisons shown later in Section 2.4.

Initial-final state interferences

In the initial-final state interferences, the effective Born cross sections depend on both s and s' as well as on the type of exchanged vector particles V_i (e.g. photon and or Z):

$$\sigma_B^{int}(s) = \int dR \sum_{V_i, V_j=\gamma, Z} \sigma_B^0(s, s', i, j) \rho_B^{int}(R, A, i, j). \quad (2.102)$$

The radiator functions are:

$$\rho_B^{int}(R, A; i, j) = \delta(1 - R) [S_B + b_B(i, j)] + \theta(1 - R - \epsilon) H_B^{int}(R, A). \quad (2.103)$$

The soft corrections, already known from [32, 35], we give explicitly:

$$S_T^{int} = 8 \frac{\alpha}{\pi} Q_e Q_f \left(1 - \ln \frac{2\epsilon}{\lambda} \right), \quad (2.104)$$

$$S_{FB}^{int} = \frac{\alpha}{\pi} Q_e Q_f \left[- (1 + 8 \ln 2) \ln \frac{2\epsilon}{\lambda} + 4 \ln^2 2 + \ln 2 + \frac{1}{2} + \frac{1}{3} \pi^2 \right]. \quad (2.105)$$

The box contributions $b_T(i, j)$ may be taken from equations (116) and (118) (to be multiplied by 4/3) of [35] and the $b_{FB}(i, j)$ from equations (123) and (126). Finally, the hard radiator parts are:

$$H_T^{int}(R, A) = -\frac{\alpha}{\pi} Q_e Q_f \frac{4AR(1+R)}{1-R}, \quad (2.106)$$

and

$$\begin{aligned} H_{FB}^{int}(R, A \geq A_0) = & \frac{\alpha}{\pi} Q_e Q_f \left\{ \frac{3R}{2} \left[\ln \frac{z_+}{z_-} + \frac{2 - R + \frac{5}{3}R^2}{1 - R} \ln R \right] \right. \\ & - \frac{1 + R}{2(1 - R)} (5 - 2R + 5R^2) \ln \frac{(1 + R)(1 + A)}{2} \\ & + \frac{1}{4(1 - R)} \left[\frac{(1 - 4R + R^2)[A(1 + R)^2 - (1 - R)^2]}{1 + R} \right. \\ & \left. \left. + 2A(1 - A)(1 + R^3) \right] \right\}, \end{aligned} \quad (2.107)$$

$$H_{FB}^{int}(R, A < A_0) = \frac{3\alpha}{2\pi} Q_e Q_f R \left\{ \ln \frac{z_+}{z_-} - \frac{2 - R + \frac{5}{3}R^2}{1 - R} \ln \frac{1 + A}{1 - A} + A(1 - R) \right\}, \quad (2.108)$$

with

$$z_{\pm} = (1 + R) \pm A(1 - R). \quad (2.109)$$

Again, for $A \rightarrow 1$ the radiators $H_T^{int}(R, A)$ and $H_{FB}^{int}(R, A \geq A_0)$ approach the known expressions of the s' -cut given in [32]. A misprint could be found in eq. (22) of [32]: The non-logarithmic terms there have to be multiplied by $1/(1+R)$.

Final state radiation

The final state corrections to order $O(\alpha)$ are:

$$\sigma_B^{fin}(s) = \sigma_B^0(s) \int dR \rho_B^{fin}(R, A), \quad (2.110)$$

with

$$\rho_B^{fin}(R, A) = \delta(1-R)S_f + \theta(1-R-\epsilon)H_B^{fin}(R, s, A), \quad (2.111)$$

$$S_f = \bar{S}_f + \beta_f \ln \epsilon, \quad (2.112)$$

where \bar{S}_f and β_f can trivially be obtained from the initial state terms \bar{S} and β , replacing s/m_e^2 by s'/m_f^2 and Q_e by Q_f . The hard radiators are:

$$H_T^{fin}(R, s, A) = \frac{\alpha}{\pi} Q_f^2 \left[\frac{1+R^2}{1-R} \ln \frac{1+A}{1-A} - \frac{8Am_f^2/s}{(1-A^2)(1-R)} - A(1-R) \right], \quad (2.113)$$

$$H_{FB}^{fin}(R, s, A) = H_T^{fin}(R, A) + \frac{\alpha}{\pi} Q_f^2 \left[A(1-R) - (1+R) \ln \frac{z_+}{z_-} \right]. \quad (2.114)$$

Some analytical formulae for the final state corrections are also given in [157]. This will be treated in more detail in Appendix B.3.

If one is interested in considering the leading higher order effects of multiple soft photon emission and virtual corrections, a *common initial and final state soft photon exponentiation* may be performed, following [35, 159]:

$$\sigma_B^{ini+fin}(s) = \int dR \sigma^0(s') \rho_B^{ini}(R, A) \bar{\rho}_B^{fin}(R, s', A), \quad (2.115)$$

with

$$\bar{\rho}_B^{fin}(R, s', A) = (1-R_E)^{\beta'_f} (1+S'_f) \quad (2.116)$$

$$+ \int_{R_{min}/R}^1 du \left[H_B^{fin}(u, s', A') - \frac{\beta'_f}{1-u} \theta(R-R_E) \right]. \quad (2.117)$$

The soft part of $\rho_B^{fin}(u, s', A')$, $A' = A(u)$, and β'_f are derived from (2.37) by replacing there Q_e by Q_f and s/m_e^2 by s'/m_f^2 . Such a procedure for resumming the leading photonic higher order corrections is straightforward and for the theoretical confirmation of the experimental precision results on the Z peak absolutely mandatory there.

It shall be mentioned here that in the hard radiators the integration over u may also be performed analytically. In region III one has to interchange for this the order of integration over u and x [157]. There the over $R = s'/s$ analytically fully integrated result for $\sigma_B^{fin}(s)$ was calculated. The recalculation could also correct for some smaller misprints there. The general results with acceptance cut in [157] can be easily compared with the results here setting $c = 1$. A complete derivation of the angular distribution $d\sigma^{fin}/d\cos\vartheta$ is illustrated in Appendix B.3.

General example: Hard photon initial state radiator with general cuts

We want to present here as an example of one of the main results obtained during this dissertation. These are radiator functions

$$H_{T,FB}^{ini} = H_{T,FB}^{ini}(R, \theta_{acol}^{\max}, E_{\min}, c) \quad (2.118)$$

for the hard initial state bremsstrahlung to total and forward-backward cross sections $\sigma_{T,FB}(\theta_{acol}^{\max}, E_{\min}, c)$. We cut on the maximal acollinearity angle θ_{acol} of the final state fermions, on the minimal energy of the fermions E_{\min} , and on the scattering angle ϑ of one fermion. As general convolution integrals with all cuts we have:

$$\sigma_T^{ini}(\theta_{acol}^{\max}, E_{\min}, c) = \int dR \sigma^0(s') \rho_{T,FB}^{ini}(R, A, c), \quad (2.119)$$

$$\sigma_{FB}^{ini}(\theta_{acol}^{\max}, E_{\min}, c) = \int dR \sigma^0(s') \rho_{T,FB}^{ini}(R, A, c), \quad (2.120)$$

$$\rho_{T,FB}^{ini}(R, A, c) = (1 + \bar{S}) \beta_e (1 - R)^{\beta_e - 1} + \bar{H}_{T,FB}^{ini}(R, A, c). \quad (2.121)$$

The soft photon part \bar{S} can be looked up with the factor β_e in (2.38), the function A depending on

$$A = A(R, \theta_{acol}^{\max}, E_{\min}). \quad (2.122)$$

For each region of phase space depending on R for fixed cut-off value c we then have to insert the appropriate hard photon flux function $\bar{H}_{T,FB}^{ini}(R, A, c)$. For region I, $A \approx 1$, the regularized result for the radiator is given by

$$\bar{H}_{T,FB}^{ini}(R, 1, c) = H_{T,FB}(R, 1, c) - \frac{\beta_e}{1 - R}, \quad (2.123)$$

while for regions II and III, safely away from the soft photon region, we have $\bar{H}_{T,FB}^{ini}(R, A, c) = H_{T,FB}^{ini}(R, A, c)$.

Following the discussion in Section 2.3.2 for the treatment of the phase space with respect to mass singularities, we have to distinguish 4 regions for $H_{T,FB}^{ini}$ with a further separation into two cases for the antisymmetric radiator H_{FB}^{ini} . This is due to additional contributions from $\sigma(0)$ from the lower bound of the integration over $\cos \vartheta$ which cancel in $H_{T,FB}^{ini}$. The generic structure of $H_{T,FB}^{ini}$ with cut-off $c \geq 0$ can be written as ($i = 0, 1$):

$$H_T^{ini}(R, A, c) = \frac{3\alpha}{4\pi} Q_e^2 \left\{ \mathcal{F}_{ii}(R, A, c) \mp \mathcal{F}_{ii}(R, A, c) + \mathcal{C}_0(R, A, c) \left[\pm \mathcal{F}_{10}(R) \right] \right\}, \quad (2.124)$$

$$H_{FB}^{ini}(R, A, c) = \frac{\alpha}{\pi} Q_e^2 \left\{ \mathcal{G}_{ii}(R, A, c) \pm \mathcal{G}_{ii}(R, A, c) + \mathcal{G}_{0,1}(R, A) \left[\pm (2) \mathcal{G}_{10}(R, A) \right] \right\}, \quad (2.125)$$

with functions $\mathcal{F}_{ii}(R, A, c)$ and $\mathcal{G}_{ii}(R, A, c)$ which depend on the acceptance cut c and further functions independent of c , $\mathcal{F}_{10}(R)$, $\mathcal{G}_0(R)$, $\mathcal{G}_1(R)$, and $\mathcal{G}_{10}(R)$. The functions \mathcal{F}_{ij} and \mathcal{G}_{ij} , $i, j = 0, 1$ contain different logarithmic expressions

$$\mathcal{L}_{Ac}^\pm(R, A, c), \quad L_z(R, c), \quad L_{me}(R), \quad L^\pm(c), \quad \text{and} \quad L^\pm(A). \quad (2.126)$$

These depend on $R = s'/s$ as last variable for the numerical integration and on the cuts c , θ_{acol}^{\max} , and E_{\min} , the latter two contained in the function A . The detailed structure of the hard radiators $H_{T,FB}^{ini}$ we give below following the distinction of cases given in (2.85) ($c > 0$):

I. Case $(1)^{++} \leftrightarrow (2)^{++} \quad (\Rightarrow A \geq A_0(R)) :$

$$H_T^{ini}(R, A, c) = \frac{3\alpha}{4\pi} Q_e^2 \left\{ \mathcal{F}_{00}(R, A, c) - \mathcal{F}_{00}(R, A, -c) + \mathcal{C}_0(R, A, c) \right\}, \quad (2.127)$$

$$H_{FB}^{ini}(R, A, c) = \frac{\alpha}{\pi} Q_e^2 \left\{ \mathcal{G}_{00}(R, A, c) + \mathcal{G}_{00}(R, A, -c) + \mathcal{G}_0(R, A) \right\}, \quad (2.128)$$

II. Case $(1)^{+-} \leftrightarrow (2)^{+-} \quad (\Rightarrow A < A_0(R)) :$

$$H_T^{ini}(R, A, c) = \frac{3\alpha}{4\pi} Q_e^2 \left\{ \mathcal{F}_{11}(R, A, c) - \mathcal{F}_{11}(R, A, -c) + \mathcal{C}_0(R, A, c) \right\}, \quad (2.129)$$

$$H_{FB}^{ini}(R, A, c) = \frac{\alpha}{\pi} Q_e^2 \left\{ \mathcal{G}_{11}(R, A, c) + \mathcal{G}_{11}(R, A, -c) + \mathcal{G}_1(R, A) \right\}, \quad (2.130)$$

III. Case $(1)^{++} \leftrightarrow (2)^{+-}$:

$$H_T^{ini}(R, A, c) = \frac{3\alpha}{4\pi} Q_e^2 \left\{ \mathcal{F}_{11}(R, A, c) - \mathcal{F}_{00}(R, A, -c) + \mathcal{F}_{10}(R) + \mathcal{C}_0(R, A, c) \right\}, \quad (2.131)$$

a. $A < A_0(R)$:

$$H_{FB}^{ini}(R, A, c) = \frac{\alpha}{\pi} Q_e^2 \left\{ \mathcal{G}_{11}(R, A, c) + \mathcal{G}_{00}(R, A, -c) + \mathcal{G}_1(R, A) + \mathcal{G}_{10}(R, A) \right\}, \quad (2.132)$$

b. $A \geq A_0(R)$:

$$H_{FB}^{ini}(R, A, c) = \frac{\alpha}{\pi} Q_e^2 \left\{ \mathcal{G}_{11}(R, A, c) + \mathcal{G}_{00}(R, A, -c) + \mathcal{G}_0(R, A) - \mathcal{G}_{10}(R, A) \right\}, \quad (2.133)$$

IV. Case $(1)^{--} \leftrightarrow (2)^{++}$:

$$H_T^{ini}(R, A, c) = \frac{3\alpha}{4\pi} Q_e^2 \left\{ \mathcal{F}_{11}(R, A, c) + \mathcal{F}_{11}(R, A, -c) + \mathcal{C}_0(R, A, c) \right\}, \quad (2.134)$$

a. $A < A_0(R)$:

$$H_{FB}^{ini}(R, A, c) = \frac{\alpha}{\pi} Q_e^2 \left\{ \mathcal{G}_{11}(R, A, c) - \mathcal{G}_{11}(R, A, -c) + \mathcal{G}_1(R, A) \right\}, \quad (2.135)$$

b. $A \geq A_0(R)$:

$$H_{FB}^{ini}(R, A, c) = \frac{\alpha}{\pi} Q_e^2 \left\{ \mathcal{G}_{11}(R, A, c) - \mathcal{G}_{11}(R, A, -c) + \mathcal{G}_0(R, A) - 2\mathcal{G}_{10}(R, A) \right\}. \quad (2.136)$$

\mathcal{F}_{00} , \mathcal{G}_{00} , \mathcal{F}_{11} , and \mathcal{G}_{11} are now illustrated below:

$$\begin{aligned} \mathcal{F}_{00}(R, A, c) = & \frac{1}{v} \left\{ \left(c + \frac{1}{3}c^3 \right) [L_z(R, c) + L_{m_e}(R)] + \frac{1}{3}c(1 - c^2) \ln(1 - c^2) \right. \\ & \left. - \frac{4}{3} [(1 + c) L^+(c) - (1 - c) L^-(c)] \right\} \\ & + \frac{1}{6v} [(3 + c^2 + A^2) \mathcal{L}_{Ac}^+(R, A, c) - Ac \mathcal{L}_{Ac}^-(R, A, c)] \\ & + f_1(z, R, A, c) \mathcal{L}_{Ac}^+(R, A, c) + A f_2(z, R, c) \mathcal{L}_{Ac}^-(R, A, c) \\ & + \frac{2}{3}(1 + R) [L^+(c) - L^-(c)] \end{aligned}$$

$$\begin{aligned}
 & + f_{01}(z, R, c) \left[L_z(R, c) + L_{m_e}(R) - \ln(1 - c^2) \right] \\
 & + f_{02}(z, R, c) + f_{03}(R, A, c), \tag{2.137}
 \end{aligned}$$

$$\begin{aligned}
 \mathcal{F}_{11}(R, A, c) &= \frac{1}{2} \frac{1 + R^2}{v} \left\{ \left(A + \frac{1}{3} A^3 \right) L_{m_e}(R) + \frac{1}{3} A(1 - A^2) \ln(1 - A^2) \right. \\
 & \quad \left. - \frac{4}{3} \left[(1 + A) L^+(A) - (1 - A) L^-(A) \right] \right\} \\
 & \quad + \frac{1}{6v} \left\{ (3 + c^2 + A^2) \mathcal{L}_{Ac}^-(R, A, c) - Ac \mathcal{L}_{Ac}^+(R, A, c) \right\} \\
 & \quad + f_1(z, R, A, c) \mathcal{L}_{Ac}^-(R, A, c) + A f_2(z, R, c) \mathcal{L}_{Ac}^+(R, A, c) \\
 & \quad + f_{11}(z, R, A, c) + f_{12}(R, A, c), \tag{2.138}
 \end{aligned}$$

$$\begin{aligned}
 \mathcal{G}_{00}(R, A, c) &= \frac{1}{2v} \left\{ c \mathcal{L}_{Ac}^+(R, A, c) - A \mathcal{L}_{Ac}^-(R, A, c) \right. \\
 & \quad \left. - 2(1 - c^2) \left[L_z(R, c) + L_{m_e}(R) - \ln(1 - c^2) \right] \right\} \\
 & \quad + g_1(z, R, c) \mathcal{L}_{Ac}^+(R, A, c) + A g_2(z, R, c) \mathcal{L}_{Ac}^-(R, A, c) \\
 & \quad + g_{01}(z, R, c) \left[L_z(R, c) + L_{m_e}(R) - \ln(1 - c^2) \right] \\
 & \quad + g_{02}(R, A, c), \tag{2.139}
 \end{aligned}$$

$$\begin{aligned}
 \mathcal{G}_{11}(R, A, c) &= \frac{1}{2v} \left[c \mathcal{L}_{Ac}^-(R, A, c) - A \mathcal{L}_{Ac}^+(R, A, c) \right] \\
 & \quad + g_1(z, R, c) \mathcal{L}_{Ac}^-(R, A, c) + A g_2(z, R, c) \mathcal{L}_{Ac}^+(R, A, c) \\
 & \quad + g_{11}(R, A, c), \tag{2.140}
 \end{aligned}$$

$$\mathcal{C}_0(R, A, c) = \frac{c}{R} c_0(R, A) = -2Ac(1 - R), \tag{2.141}$$

with the coefficient functions

$$\begin{aligned}
 f_1(z, R, A, c) &= \frac{1}{6z} \left\{ \frac{2(1 - c^2)}{z} \left[c + \frac{y + 2R(1 + R)}{z} \right] \right. \\
 & \quad \left. - \left[(1 - c)^2(1 + c) + 4(c + R) \right] - A^2(c + R) \right\}, \tag{2.142}
 \end{aligned}$$

$$g_1(z, R, c) = \frac{1}{2z} \left[1 - c^2 - (c + R) \frac{y}{z} \right], \quad (2.143)$$

$$f_2(z, R, c) = -\frac{1}{3} g_1(z, R, c), \quad (2.144)$$

$$g_2(z, R, c) = \frac{1}{2z} (c + R), \quad \text{with } y \equiv y(R, c), \quad z \equiv z(R, c), \quad (2.145)$$

and other simple coefficient functions f_{01} , f_{02} , f_{03} , f_{11} , f_{12} and g_{01} , g_{02} , g_{11} , as rational functions in terms of $z(R, c)$, R , A , and c . They are listed in Appendix (B.1), (B.131) to (B.136). In (2.124) and (2.125) we have also introduced the additional expressions:

$$\mathcal{F}_{10}(R) = -\frac{2}{3} \frac{1 + R^2}{v} \ln R, \quad (2.146)$$

$$\begin{aligned} \mathcal{G}_0(R, A) &= \frac{1 + R^2}{1 + R} \left[\frac{1}{v} A \mathcal{L}_A^- - \frac{1}{1 + R} \mathcal{L}_A^+ \right] \\ &\quad + \frac{4R}{1 + R} \frac{1 + R^2}{1 + R} \frac{1}{v} [L_0(R) + L_{m_e}(R)], \end{aligned} \quad (2.147)$$

$$\mathcal{G}_1(R, A) = \frac{1 + R^2}{1 + R} \left[\frac{1}{v} A \mathcal{L}_A^+ - \frac{1}{1 + R} \mathcal{L}_A^- \right] - \frac{4R}{1 + R} A, \quad (2.148)$$

$$\mathcal{G}_{10}(R, A) = \frac{1}{2} \frac{1 + R^2}{v} (1 - A^2) [L_{m_e}(R) - \ln(1 - A^2)] + \frac{2A^2 R}{v}, \quad (2.149)$$

with following basic logarithms,

$$\mathcal{L}_A^\pm(R, A) = y(R, A) \ln |y(R, A)| \pm y(R, -A) \ln |y(R, -A)|, \quad (2.150)$$

$$\begin{aligned} \mathcal{L}_{Ac}^\pm(R, A, c) &= [y(R, c) + A z(R, c)] \ln |y(R, c) + A z(R, c)| \\ &\quad \pm [y(R, c) - A z(R, c)] \ln |y(R, c) - A z(R, c)|, \end{aligned} \quad (2.151)$$

$$\begin{aligned} &= [y(R, A) + c z(R, A)] \ln |y(R, A) + c z(R, A)| \\ &\quad \pm [y(R, -A) + c z(R, -A)] \ln |y(R, -A) + c z(R, -A)|, \end{aligned} \quad (2.152)$$

$$L^\pm(c) = \ln(1 \pm c), \quad L^\pm(A) = \ln(1 \pm A), \quad (2.153)$$

$$L_z(R, c) = \ln \left[\frac{z^2(R, c)}{4R} \right], \quad L_0(R) = \ln \left[\frac{(1 + R)^2}{4R} \right] = L_z(R, 0), \quad (2.154)$$

$$L_{m_e}(R) = \ln\left(\frac{s}{m_e^2}\right) - 1 - \ln(4R), \quad (2.155)$$

$$y(R, c) = (1 - R) + c(1 + R), \quad z(R, c) = (1 + R) + c(1 - R). \quad (2.156)$$

If we only consider an acollinearity and energy cut, A , without an acceptance, i.e. $c = 1$, only the case $(1)^{- -} \leftrightarrow (2)^{+ +}$ in (2.134) to (2.136) is possible. For H_{FB}^{ini} there is still the further distinction into cases $A(R) \geq A_0(R)$ and $A(R) < A_0(R)$. We then obtain the very compact results already shown in (2.98), (2.99), and (2.100) and published in [37]. Equivalently, one can show for omitted acollinearity cut, i.e. for $A = 1$, corresponding to a simple s' -cut that the results with acceptance cut c and s' -cut given in [35] can be obtained.

A nice consistency check can also be done for the forward-backward radiators when setting

$$y(R, -A) = 0 \quad \leftrightarrow \quad A = A_0(R) = \frac{1 - R}{1 + R}. \quad (2.157)$$

Relation (2.157) immediately gives

$$1/v \cdot A_0(R) \mathcal{L}_A^\pm - 1/(1 + R) \cdot \mathcal{L}_A^\mp = 0, \quad (2.158)$$

and therefore:

$$\begin{aligned} H_{FB}^{ini, A < A_0}(R, 1) &= H_{FB}^{ini, A \geq A_0}(R, 1) \\ &= \frac{\alpha}{\pi} Q_e^2 \left\{ -\frac{4R(1 + R^2)}{(1 + R)^2} \frac{1}{v} \ln(R) + \frac{8R^2}{(1 + R)^2} \right\}. \end{aligned} \quad (2.159)$$

That is, the results $H_{FB}^{ini, A < A_0}(R, 1)$ and $H_{FB}^{ini, A \geq A_0}(R, 1)$ are continuous at the phase space boundaries for $A \rightarrow A_0(R)$. Without any angular or energy cuts at all, i.e. $c = A = 1$, we can at last reproduce the classical results for a simple cut on s' with the Bonneau-Martin term from (2.40) [32, 137].³

$$H_T^{ini}(R, 1) = \int_0^1 d\cos\vartheta \, h_T^{ini}(R, \cos\vartheta) = \frac{\alpha}{\pi} Q_e^2 \frac{1 + R^2}{v} \left[\ln\left(\frac{s}{m_e^2}\right) - 1 \right], \quad (2.160)$$

$$\begin{aligned} H_{FB}^{ini}(R, 1) &= \int_0^1 d\cos\vartheta \, h_{FB}^{ini}(R, \cos\vartheta) \\ &= \frac{\alpha}{\pi} Q_e^2 \frac{4R(1 + R^2)}{(1 + R)^2} \frac{1}{v} \left\{ \ln\left(\frac{s}{m_e^2}\right) - 1 + \ln\left[\frac{(1 + R)^2}{4R}\right] \right\}. \end{aligned} \quad (2.161)$$

³ In this limit, only region $A \geq A_0(R)$ is possible, i.e. only one function $H_{FB}^{ini, A \geq A_0}(R, 1)$ remains for the forward-backward radiator.

For a description of the calculation of the radiators $H_{T,FB}^{ini}$ please refer to Appendix B.1. The evaluation of the interference results $H_{T,FB}^{int}$ is absolutely analogous to the initial state case with the final expressions summarized in B.2.

All analytical formulae for the hard radiators presented in this Chapter and contained in the Appendix were numerically checked by comparing them with the squared matrix element, numerically integrated over the angular phase space.⁴ This was done for each hard flux function separately. Different acollinearity, energy, and acceptance cuts were applied for values of $s'/s = m_f^2/s \dots (1 - \varepsilon)$ at different center-of-mass energies $\sqrt{s} = 30 \dots 10^3$ GeV. Also the single steps of the analytical integration were numerically checked for each integrand listed in Appendix B.1.

While in the flux functions all mass terms except for the logarithmic terms are omitted, the squared matrix element contains the mass terms in the propagators in order to numerically regularize the mass singularities described above. The analytically and numerically integrated results agree at the 10^{-8} to 10^{-4} level, depending on the functions compared, the phase space region examined, and the cuts applied. The agreement is naturally restricted due to the partly omitted mass terms and deteriorates from the final state to the interference term, and is worst for the initial state results. This is due to the critical, numerically instable propagators of order $1/Z_{1,2} = -1/(2pk_{1,2})$ for the interference terms and even of order $1/Z_{1,2}^2$ for the initial state terms which are regularized by the initial state mass terms m_e^2/s . These propagators are not contained in the hard photon final state radiators.

2.4 Numerical results of ZFITTER and comparisons

2.4.1 Hard bremsstrahlung corrections in ZFITTER

The corrections of the new formulae on the $O(\alpha)$ bremsstrahlung to $e^+e^- \rightarrow \bar{f}f$ implemented in the semi-analytical program ZFITTER versions v.6 were compared with the results of versions v.5.20 and earlier.

The main modifications in the new coding are corrected terms in the QED initial state and interference radiator parts. For the case of initial state radiation, it was possible to trace back the origin of the numerical inaccuracies related to the acollinearity cut of ZFITTER below version 6. It is the result of leaving out a certain class of non-logarithmic, simple terms of order $O(\alpha)$. For σ_T , polynomials

⁴ For simplicity, the straightforward integration over the azimuthal photon angle ϕ_γ was done analytically in order to get shorter expressions which were easier to numerically integrate.

proportional to $\cos \vartheta$ (and their integrals) are concerned, and for σ_{FB} polynomials of the type $(a + b \cos^2 \vartheta)$ (and their integrals). At first glance the corresponding contributions seem to vanish for symmetric acceptance cuts. But this is not the case ! As was explained in Section (2.3.2), the cross section formulae lose the usual simple symmetry/anti-symmetry behaviour under the transformation $\cos \vartheta \leftrightarrow (-\cos \vartheta)$ in regions II and III of the phase space since different analytical expressions may be needed depending on the location of the parameters c_i^\pm in (2.77) to (2.80). Then, the symmetry behaviour as a function of $\cos \vartheta$ is ‘hidden’ since different regions contribute differently to the net result. Omitting these terms in earlier versions is justified with the then anticipated experimental precision of only 5×10^{-3} at LEP 1, but not with the higher accuracy now at the Z resonance peak. For the hard final state radiators implemented in **ZFITTER** some misprints could be corrected for. These modifications are completely negligible for total cross sections (only at the level 10^{-5} or less), and only of minor importance for the forward-backward asymmetries, i.e. always stay below per mil level. The final state radiators $H_{T,FB}^{fin}(R, A, c)$ and the over R analytically integrated results we could also compare – for the general case with acceptance cut – with the results of [157], obtaining complete agreement except for some smaller misprints there.

The corresponding Fortran package is **acol.f**. We merged package **acol.f** with photonic corrections for the integrated total cross section and the integrated forward-backward asymmetry (with and without acceptance cut) into **ZFITTER** v.5.21, thus creating **ZFITTER** v.6.04/06 [38, 160] onwards. The angular distribution is available in v.6.2 [38] onwards. The remarkably compact expressions for the case that no angular acceptance cut is applied are published [37] and also implemented in an extra branch of **ZFITTER** [38] for quick cross section or asymmetry evaluations in the case of less cuts. A complete collection of the most general analytical expressions with cuts on maximal acollinearity, minimal energies, and minimal acceptance is given in the Appendix.

Numerical predictions of **ZFITTER** v.5.20 [36, 161] and **ZFITTER** v.6.11 [162] were systematically compared with default flag settings. Version 5.20 was used as released, while version 6.11 was prepared such that the changes due to the recalculation of initial state corrections, final state corrections, their interferences, and the net effect could be isolated. To look at the single cross section and asymmetry contributions is also interesting from the point of view that experimentalists very often use two different approaches to data: Sometimes the initial-final state interference contributions are subtracted from measured data, and sometimes the interference effects remain in the data sample. We begin with a study of the changes related to *initial state radiation*.

Initial state corrections

For σ_T , the changes are at most one unit in the fifth digit at LEP 1 energies and thus considered to be completely negligible. In Tables 2.3 and 2.4 the predictions for σ_T and for A_{FB} are shown for two acollinearity cuts $\theta_{\text{acol}} < 10^\circ, 25^\circ$ and three different acceptance cuts $\theta_{\text{acc}} = 0^\circ, 20^\circ, 40^\circ$. The numbers are given in the first row of each box for a certain acceptance angle θ_{acc} , for both versions v.6.11 and v.5.20. The changes are less than the theoretical accuracies demanded. It was checked that the numbers for flag value $\text{ICUT} = 0$ (see [38]) agree with the ZFITTER predictions shown in Tables 26 and 27 of [152].

Initial-final state interference corrections

The ZFITTER v.5 predictions of photonic corrections from the *initial-final state interference* also receive modifications after the recalculation for the versions v.6. The explanation given above for the case of initial state radiation is also applicable for a part of the deviations here. The codings for the initial-final state interference also show additional deviations in the hard photonic corrections and the resulting numerical differences are much larger.

The absolute values of σ_T and A_{FB} are also listed in Tables 2.3 and 2.4 in the second row of each box, while the third rows show the shifts when switching on the initial-final state interference. For the cross sections these are relative shifts in per mil, for the asymmetries they are absolute values also in per mil. The two tables are the analogues to Tables 37–40 of [152] where TOPAZ0 v.4.3 [130, 131] and ZFITTER v.5.20 were compared. At the Z peak, the predictions for the influence of the initial-final state interference from ZFITTER v.5.20 and ZFITTER v.6.11 deviate from each other only negligibly, with maximal deviations of up to 0.015%. At the wings, the situation is quite different, we observe deviations of up to several per mil for cross sections and up to a per mil for asymmetries. The deviations between the two codings decrease if the acollinearity cut is weakened.

Final state corrections

For LEP 1, the numerical outcome of the minor improvements to the code is shown in Tables 2.5 for A_{FB} with $\theta_{\text{acol}} < 10^\circ, 25^\circ$ and several different acceptance cuts: $\theta_{\text{acc}} = 0^\circ, 20^\circ, 40^\circ$. Again, the numbers for $\text{ICUT} = 0$ agree with those shown in Tables 26 and 27 of [152]. All the changes are though visible, but negligible. For the cross sections, the differences are completely negligible and not tabulated here.

For the case of *final state radiation*, common soft photon exponentiation together with initial state radiation is foreseen in ZFITTER. For an s' -cut, ZFITTER

σ_μ [nb] with $\theta_{\text{acol}} < 10^\circ$						σ_μ [nb] with $\theta_{\text{acol}} < 25^\circ$					
θ_{acc}	$M_Z - 3$	$M_Z - 1.8$	M_Z	$M_Z + 1.8$	$M_Z + 3$	θ_{acc}	$M_Z - 3$	$M_Z - 1.8$	M_Z	$M_Z + 1.8$	$M_Z + 3$
Z6 0°	0.21928	0.46285	1.44780	0.67721	0.39360	Z6 0°	0.22328	0.46968	1.46598	0.68688	0.40031
	0.21772	0.46082	1.44776	0.67898	0.39489		0.22228	0.46836	1.46602	0.68816	0.40128
	-7.16	-4.41	-0.03	+2.60	+3.27		-4.51	-2.82	+0.03	+1.86	+2.41
Z5 0°	0.21928	0.46285	1.44781	0.67722	0.39361	Z5 0°	0.22328	0.46968	1.46598	0.68688	0.40031
	0.21852	0.46186	1.44782	0.67814	0.39429		0.22281	0.46905	1.46603	0.68754	0.40081
	-3.48	-2.14	+0.01	+1.36	+1.72		-2.11	-1.34	+0.03	+0.96	+1.25
Z6 20°	0.19987	0.42205	1.32053	0.61756	0.35881	Z6 20°	0.20357	0.42834	1.33718	0.62647	0.36505
	0.19869	0.42046	1.32018	0.61877	0.35972		0.20281	0.42729	1.33689	0.62731	0.36572
	-5.96	-3.79	-0.27	+1.95	+2.53		-3.74	-2.46	-0.21	+1.35	+1.83
Z5 20°	0.19987	0.42205	1.32053	0.61756	0.35881	Z5 20°	0.20357	0.42833	1.33718	0.62647	0.36505
	0.19892	0.42075	1.32021	0.61857	0.35959		0.20321	0.42781	1.33689	0.62684	0.36536
	-4.78	-3.09	-0.24	+1.63	+2.17		-1.77	-1.22	-0.22	+0.59	+0.85
Z6 40°	0.15032	0.31760	0.99416	0.46475	0.26983	Z6 40°	0.15318	0.32243	1.00682	0.47164	0.27477
	0.14974	0.31675	0.99349	0.46515	0.27019		0.15280	0.32183	1.00619	0.47188	0.27502
	-3.88	-2.72	-0.67	+0.87	+1.32		-2.48	-1.88	-0.62	+0.51	+0.91
Z5 40°	0.15032	0.31760	0.99415	0.46474	0.26983	Z5 40°	0.15318	0.32243	1.00682	0.47164	0.27477
	0.14978	0.31680	0.99350	0.46511	0.27016		0.15287	0.32192	1.00619	0.47180	0.27496
	-3.61	-2.53	-0.65	+0.80	+1.22		-2.03	-1.58	-0.63	+0.34	+0.69

Table 2.3: Comparison of ZFITTER v.6.11 [38] (first row) with ZFITTER v.5.20 [36, 161] (second row) for muon pair production cross sections with angular acceptance cuts ($\theta_{\text{acc}} = 0^\circ, 20^\circ, 40^\circ$) and acollinearity cut ($\theta_{\text{acol}} < 10^\circ, 25^\circ$). First row is without initial-final state interference, second row with, third row the relative effect of that interference in per mil. Final state radiation is treated as in v.5.20 [145].

A_{FB}^{μ} with $\theta_{\text{acol}} < 10^{\circ}$						A_{FB}^{μ} with $\theta_{\text{acol}} < 25^{\circ}$					
θ_{acc}	$M_Z - 3$	$M_Z - 1.8$	M_Z	$M_Z + 1.8$	$M_Z + 3$	θ_{acc}	$M_Z - 3$	$M_Z - 1.8$	M_Z	$M_Z + 1.8$	$M_Z + 3$
Z6 0°	-0.28462	-0.16916	0.00024	0.11482	0.16063	Z6 0°	-0.28651	-0.17051	-0.00043	0.11292	0.15680
	-0.28187	-0.16689	0.00083	0.11379	0.15907		-0.28554	-0.16960	-0.00000	0.11285	0.15669
	+2.75	+2.27	+0.60	-1.03	-1.56		+0.97	+0.91	+0.43	-0.06	-0.11
Z5 0°	-0.28453	-0.16911	0.00025	0.11486	0.16071	Z5 0°	-0.28647	-0.17049	-0.00043	0.11293	0.15682
	-0.28282	-0.16783	0.00070	0.11475	0.16059		-0.28555	-0.16975	-0.00005	0.11307	0.15701
	+1.71	+1.28	+0.45	-0.11	-0.12		+0.92	+0.74	+0.48	+0.14	+0.19
Z6 20°	-0.27521	-0.16355	0.00032	0.11141	0.15602	Z6 20°	-0.27727	-0.16499	-0.00038	0.10942	0.15201
	-0.27285	-0.16167	0.00080	0.11053	0.15467		-0.27659	-0.16436	-0.00006	0.10943	0.15199
	+2.35	+1.88	+0.47	-0.89	-1.35		+0.68	+0.63	+0.32	+0.00	-0.02
Z5 20°	-0.27506	-0.16347	0.00035	0.11148	0.15616	Z5 20°	-0.27722	-0.16497	-0.00037	0.10944	0.15204
	-0.27408	-0.16261	0.00070	0.11133	0.15594		-0.27657	-0.16447	-0.00009	0.10963	0.15229
	+0.98	+0.86	+0.35	-0.15	-0.22		+0.65	+0.50	+0.28	+0.19	+0.25
Z6 40°	-0.24230	-0.14398	0.00045	0.09881	0.13868	Z6 40°	-0.24452	-0.14549	-0.00027	0.09675	0.13449
	-0.24063	-0.14277	0.00073	0.09825	0.13780		-0.24423	-0.14527	-0.00010	0.09687	0.13464
	+1.67	+1.22	+0.28	-0.56	-0.88		+0.29	+0.22	+0.17	+0.12	+0.15
Z5 40°	-0.24207	-0.14386	0.00050	0.09893	0.13891	Z5 40°	-0.24445	-0.14545	-0.00026	0.09678	0.13454
	-0.24151	-0.14343	0.00069	0.09890	0.13888		-0.24444	-0.14542	-0.00011	0.09700	0.13483
	+0.56	+0.43	+0.19	-0.03	-0.03		+0.01	+0.03	+0.15	+0.22	+0.29

Table 2.4: Comparison of ZFITTER v.6.11 (first row) with ZFITTER v.5.20 (second row) for the muonic forward-backward asymmetry with angular acceptance cuts ($\theta_{\text{acc}} = 0^{\circ}, 20^{\circ}, 40^{\circ}$) and acollinearity cut ($\theta_{\text{acol}} < 10^{\circ}, 25^{\circ}$). First row is without initial-final state interference, second row with, third row the relative effect of that interference in per mil. Final state radiation is treated as in v.5.20 [145].

A_{FB}^μ with $\theta_{\text{acol}} < 10^\circ$					
θ_{acc}	$M_Z - 3$	$M_Z - 1.8$	M_Z	$M_Z + 1.8$	$M_Z + 3$
0°	-0.28487	-0.16932	0.00025	0.11500	0.16091
	-0.28453	-0.16911	0.00025	0.11486	0.16071
20°	-0.27539	-0.16367	0.00035	0.11162	0.15635
	-0.27506	-0.16347	0.00035	0.11148	0.15616
40°	-0.24236	-0.14404	0.00050	0.09905	0.13908
	-0.24207	-0.14386	0.00050	0.09893	0.13891

A_{FB}^μ with $\theta_{\text{acol}} < 25^\circ$					
θ_{acc}	$M_Z - 3$	$M_Z - 1.8$	M_Z	$M_Z + 1.8$	$M_Z + 3$
0°	-0.286732	-0.170647	-0.000428	0.113029	0.156963
	-0.286474	-0.170493	-0.000427	0.112927	0.156821
20°	-0.277471	-0.165114	-0.000370	0.109537	0.152173
	-0.277221	-0.164965	-0.000370	0.109438	0.152036
40°	-0.244669	-0.145582	-0.000255	0.096867	0.134658
	-0.244449	-0.145451	-0.000255	0.096780	0.134537

Table 2.5: Comparison of ZFITTER v.6.11 (first row) with ZFITTER v.5.20 (second row) for the muonic forward-backward asymmetry with angular acceptance cut ($\theta_{\text{acc}} = 0^\circ, 20^\circ, 40^\circ$) and acollinearity cuts ($\theta_{\text{acol}} < 10^\circ$) and ($\theta_{\text{acol}} < 25^\circ$). The initial-final state interference is switched off and only final state radiation is corrected [145].

follows [157]. As may be seen from [69] (for the angular distributions) or from [37] (for integrated observables), the predictions for common soft photon exponentiation include one additional integration, namely that over the invariant mass of the final state fermion pair at a given reduction of s into s' after initial state radiation.⁵ This additional integration is done partly analytically, for not too involved integrands, and partly numerically using a Lagrange interpolating formula for the integrand. Common exponentiation was always included in the comparisons shown here.

Net corrections

In case of the net corrections, first the corrections for the initial and final state calculations in v.6.11 were combined and compared with the old coding in v.5.20. Then the corrected initial-final state interference was added and compared with the earlier formulae to see the overall effect of the modifications. One can state

⁵With acollinearity cut, there remains some arbitrariness in the choice of the region with exponentiation. In ZFITTER, the acollinearity cut is simulated by an effective s' -cut for this purpose. For details see also [38].

σ_μ [nb] with $\theta_{\text{acol}} < 10^\circ$					
θ_{acc}	$M_Z - 3$	$M_Z - 1.8$	M_Z	$M_Z + 1.8$	$M_Z + 3$
0°	0.21772	0.46081	1.44776	0.67898	0.39489
	0.21852	0.46186	1.44782	0.67814	0.39429
20°	0.19869	0.42046	1.32018	0.61877	0.35972
	0.19892	0.42075	1.32021	0.61857	0.35959
40°	0.14974	0.31675	0.99349	0.46515	0.27019
	0.14978	0.31680	0.99350	0.46511	0.27016
A_{FB}^μ with $\theta_{\text{acol}} < 10^\circ$					
0°	-0.28222	-0.16710	0.00083	0.11392	0.15926
	-0.28282	-0.16783	0.00070	0.11475	0.16059
20°	-0.27319	-0.16187	0.00080	0.11066	0.15486
	-0.27408	-0.16261	0.00070	0.11133	0.15594
40°	-0.24093	-0.14294	0.00074	0.09837	0.13797
	-0.24151	-0.14343	0.00069	0.09890	0.13888

Table 2.6: Comparison of net corrections from ZFITTER v.6.11 (first row) with ZFITTER v.5.20 (second row) for muon pair production with angular acceptance cut ($\theta_{\text{acc}} = 0^\circ, 20^\circ, 40^\circ$) and acollinearity cut ($\theta_{\text{acol}} < 10^\circ$). The initial-final state interference is switched on [145].

that the net corrections without initial-final state interference are negligible for the cross section. The corrections to the numerical output from ZFITTER with acollinearity cut increased when the corrected initial-final state interference is taken into account. The resulting net corrections for the total cross section and the forward-backward asymmetry at LEP 1 are shown in Table 2.6 for $\theta_{\text{acol}} < 10^\circ$ and different acceptance cuts.

2.4.2 Comparisons of ZFITTER with different numerical programs

The s' -cut was studied for LEP 1 in [149] and more recently by [147, 148, 150, 152–155]. The agreement of two-fermion codes for s -channel observables is now better than 0.1 per mil on resonance and quite sufficient for experimental applications at LEP 1 [114, 149].

Numerical results with acollinearity cut are given in Table 3 of [148] for the s -channel part of Bhabha scattering for programs TOPAZ0 and ALIBABA. In [146] this was compared with ZFITTER v.5.14 [163] and one gets in both cases roughly a 3 per mil agreement. Out to the wings of the Z resonance region, i.e. $\sqrt{s} = M_Z \pm 3 \text{ GeV}$, this numerical agreement remains for the comparison with TOPAZ0,

but deteriorates to several per mil for the ALIBABA case. For the accuracies demanded from theory by experiment at the starting phase of LEP 1 in 1989, i.e. roughly 0.5% [114], this was quite sufficient, but not anymore now with the better than per mil precision at the Z peak [15–21].

After the update of the ZFITTER code for combined cuts on energies, acollinearity, and acceptance angle [37, 38] and after comparisons with other numerical programs [130–132], the situation for LEP 1 energies shown in Fig. 2.5 and Table 2.7 can be stated as quite satisfactory [145, 146, 152, 164–166]:

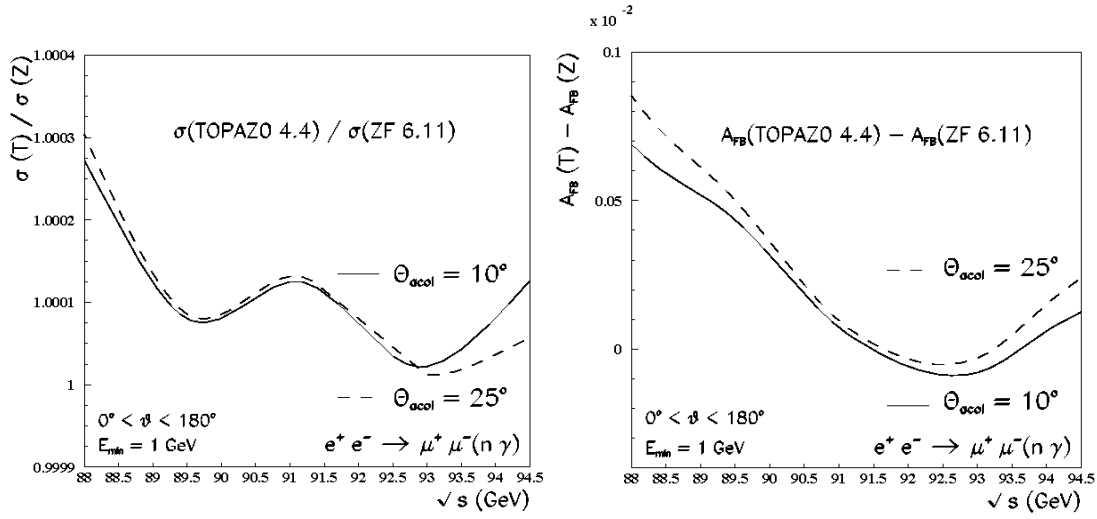


Figure 2.5: Ratios of muon pair production cross sections and differences of forward-backward asymmetries at the Z resonance: ZFITTER v.6.11 [38, 162] vs. TOPAZO v.4.4 [131] for different acollinearity cuts (full acceptance) [165].

The numerical comparison of the newly updated ZFITTER version v.6.11 [38] with TOPAZO’s latest release version v.4.4 [131] now delivers for LEP 1 energies the same high level of agreement as for the s' -cut (Fig. 2.5): At the peak itself we have a deviation of the codes of $O(10^{-4})$ or less for σ_T and A_{FB} , with an acceptable increase to maximally 3×10^{-4} for σ_T and a slightly worse value for A_{FB} of 7×10^{-4} at $\sqrt{s} = M_Z \pm 3 \text{ GeV}$ for a maximal acollinearity angle of 10° . This is also listed in more detail in Table 2.7. The agreement at the Z peak is now as good as for the s' -cut which was checked recently in [149, 152].

For LEP 2, the s' -cut is estimated to be ‘under control’ in [156], while a warning was given there that ‘the agreement between TOPAZO and ZFITTER somehow degrades when implementing an acollinearity cut’. However, one should mention here that both programs were originally designed for applications around the Z boson resonance and using them at higher energies deserves dedicated checks and, if necessary, further improvements. A detailed comparison of the situation of the

codes at LEP 2 energies, before and after our corrections to the ZFITTER code will follow in the next Chapter.

σ_μ [nb] with $\theta_{\text{acol}} < 10^\circ$					
$\theta_{\text{acc}} = 0^\circ$	$M_Z - 3$	$M_Z - 1.8$	M_Z	$M_Z + 1.8$	$M_Z + 3$
TOPAZO	0.21932	0.46287	1.44795	0.67725	0.39366
	0.21776	0.46083	1.44785	0.67894	0.39491
	-7.16	-4.43	-0.07	+2.49	+3.17
ZFITTER	0.21928	0.46284	1.44780	0.67721	0.39360
	0.21772	0.46082	1.44776	0.67898	0.39489
	-7.16	-4.40	-0.03	+2.60	+3.27
$A_{FB\mu}$ with $\theta_{\text{acol}} < 10^\circ$					
$\theta_{\text{acc}} = 0^\circ$	$M_Z - 3$	$M_Z - 1.8$	M_Z	$M_Z + 1.8$	$M_Z + 3$
TOPAZO	-0.28450	-0.16914	0.00033	0.11512	0.16107
	-0.28158	-0.16665	0.00088	0.11385	0.15936
	+2.92	+2.49	+0.55	-1.27	-1.71
ZFITTER	-0.28497	-0.16936	0.00024	0.11496	0.16083
	-0.28222	-0.16710	0.00083	0.11392	0.15926
	+2.75	+2.27	+0.60	-1.03	-1.56

Table 2.7: A comparison of predictions from ZFITTER v.6.11 [38, 162] and TOPAZO v.4.4 [131] for muonic cross sections and forward-backward asymmetries around the Z peak. First row is without initial-final state interference, second row with, third row the relative effect of that interference in per mil [145, 165, 166].

2.4.3 Effects on the experimental analysis at LEP

The LEP 1 data taking phase happened between 1989 and 1995 with about 17 million Z decays reported, i.e. 15.5×10^6 hadronic and 1.7×10^6 leptonic decays. Several energy scans were undertaken around the Z peak during this period with a high statistics run exactly on the peak in 1992 and 1994 [16, 124]. The theoretical description of the experimental results by available two-fermion programs taking into account all radiative corrections was reported to be in good shape then in [149]. Since then, there has been theoretical progress in several branches of the programs ZFITTER [38], TOPAZO [131], and others, especially for the description of hard bremsstrahlung and the inclusion of higher order corrections. As an example, the effects of the latest changes can be discussed for the typical peak cross section parameters M_Z , Γ_Z , and σ_{had}^0 as total hadronic peak cross section. The LEP average value for the latter is $\sigma_{\text{had}}^0 = 41.491 \pm 0.058$ nb [16, 124], while M_Z , Γ_Z were given in Table 2.1.

To start with, in 1998 there were some changes to the extracted values of M_Z and Γ_Z using programs ZFITTER [38] and TOPAZ0 [131] due to newly implemented leading logarithmic $O(\alpha^3)$ QED corrections to the initial state [119, 150]. There are in principle two different schemes for the estimate of the higher order QED corrections which are included in the programs and used by the experiments. Either the exact two-loop results for initial state bremsstrahlung [62] are applied together with a soft and virtual photon exponentiation including the third order results by [119, 150]. Or secondly, there is the possibility of an inclusive exponentiation scheme via Yennie-Frautschi-Suura [57] treated by [119, 167]. The differences of both schemes, however, are documented to be small with 0.1 MeV uncertainties to M_Z and Γ_Z and a 0.01% correction to σ_{had}^0 . Much larger theoretical errors are estimated to arise from the inclusion of corrections due to QED initial state pair creation. These uncertainties are $\Delta M_Z \approx \pm 0.3$ MeV, $\Delta \Gamma_Z \approx \pm 0.2$ MeV, and $\Delta \sigma_{\text{had}}^0 \approx \pm 0.02\%$ [124].

Since 1999, the version ZFITTER v.6.10/6.11 [162, 168] are used together with TOPAZ0 [131] by all four LEP collaborations. The addition of new leading logarithmic $O(\alpha^3)$ and $O(\alpha^4)$ QED radiators calculated recently in [123] will lead to the main uncertainties from QED corrections. For example, for M_Z and Γ_Z these new terms will lead to changes of +0.5 MeV with a final theoretical error of roughly ± 0.3 MeV [124].

In [151, 152] there was a detailed comparison of both programs at the precision level 10^{-4} to estimate the effect on cross section and SM observables by the different approaches used for SM or model independent calculations. The main focus there was on the s' -cut branch for total cross sections and asymmetries. Adding the comparisons with the new results on the acollinearity cut in the previous sections and partly presented in [145, 146, 164–166], one can summarize as general outcome of all analysis that the errors from these different approaches are negligible with respect to the uncertainties from the higher order QED effects stated above. They are only at the order ± 0.1 MeV for M_Z and Γ_Z and not more than ± 1 pb for σ_{had}^0 . The new hard photon calculation therefore guarantees that both codes perfectly describe with their predictions for cross sections and other observables the experimental results, for both cut options using different approaches.

2.5 Conclusions

A derivation of analytical formulae for the $O(\alpha)$ hard QED bremsstrahlung corrections to $e^+e^- \rightarrow \bar{f}f$ was presented with cuts to the fermions' acollinearity angle and energies ($f \neq e$). Very compact formulae can be obtained and pose an alternative for lepton pair final states to the usually applied kinematically simpler cut on the final state fermions' invariant mass squared s' . The hard radiators for

the integrated total and forward-backward cross sections with an additional cut on angular acceptance also have been derived within this dissertation (see Section 2.3.3 and Appendix B.1, B.2, and B.3).

This was done in the context of the semi-analytical program **ZFITTER** [38] which calculates radiatively corrected observables with realistic experimental cuts, e.g. for LEP/SLC applications. Several numerical applications of the above formulae were applied. For this purpose, the package **acol.f** was added. As a result, it was concluded that older versions of **ZFITTER**, i.e. versions v.5.20 [161] and earlier, derive the $O(\alpha)$ QED corrections to the total cross section σ_T with acollinearity cut with a numerical accuracy of about 0.4% in the Z resonance region ($M_Z \pm 3$ GeV), and similarly for the forward-backward asymmetry A_{FB} with about 0.13%.

The determined modifications to hard photon radiators for the initial and final state radiation and its interference are certain non-logarithmic terms. When the code was created in 1989 [70], an accuracy of 0.5% at LEP 1 was assumed to be needed, so these corrected terms could be neglected then. This accuracy is not sufficient anymore now with the high level of experimental precision (e.g. $\delta M_Z/M_Z = 2.2 \times 10^{-5}$ [78]) and demanded the recalculation of the hard photonic corrections. The new and improved coding starting from **ZFITTER** v.6.11 [38] with **acol.f** gave a numerical agreement of σ_T for leptons, with $\theta_{acol} \leq 10^\circ$ and $E_{min} = 1$ GeV, with predictions from **TOPAZ0** v.4.4 [131] at LEP 1 of 0.03% (at the wings) or better (at resonance). For A_{FB} , the accuracy at LEP 1 energies is now estimated to be better than 0.1% for the same cuts.

The numerical limitations at LEP 1 before had been mainly due to the initial-final state interference which is now corrected after the recalculation. At the Z peak itself, however, the accuracy had already been quite satisfactory before, i.e. better than 10^{-4} , due to suppressed hard photon radiation. The new coding in **ZFITTER** now reproduces the very nice agreement with program **TOPAZ0**, already obtained for the s' -cut [152]. These findings were partly published in [145, 146, 164–166]. The influence of higher order corrections in these and other two-fermion codes has been recently treated in [123, 153–155].

Chapter 3

Fermion Pair Production at LEP 2 Energies

While data taking at energies around the Z boson resonance ended at LEP 1 in 1995, a new phase started after a brief run around an intermediate energy scale of $\sqrt{s} \approx 135$ GeV: The LEP 2 went into operation with center-of-mass energies at the W pair production threshold $\sqrt{s} \approx 161$ GeV [16, 156] and is expected to reach up to 208 GeV at the final end of LEP [169]. The above said already marks the main physics goal at LEP 2: High precision physics to the charged weak gauge bosons W^\pm , is the main objective, i.e. determining the mass M_W , width Γ_W , and properties of the W boson. Especial focus is here also put on details of triple gauge boson couplings (TGC) in the electroweak sector of the SM. Especially interesting are contributions from the $(\gamma, Z)WW$ vertex which is contained in the s -channel part of the processes $e^+e^- \rightarrow W^+W^-$. Also additional Z pair production sets in above $\sqrt{s} = 2M_Z$ for which additional searches of anomalous TGC, not described in the SM, are conducted [156]. As the massive gauge bosons are instable particles and cannot be observed directly, one has to reconstruct the W pair decays from the corresponding 4-fermion final states arising from decays of the W and Z pairs. But this demands the inclusion of 4-fermion final states which did not originate from the W and Z pair decays as background processes [156].

But though the main interest at LEP 2 naturally lies on the above sketched physics program, two-fermion physics still is an interesting branch which is quite actively pursued [170, 171]. Fermion pair production is still one of the most copious processes at these energies having to be treated as possible background to 4-fermion final states. Moreover, precision physics with fermion pairs at LEP 2 extends the indirect searches for ‘New Physics’ already undertaken on the Z boson resonance [172–174].

The main introductory facts to fermion pair production at LEP 2 energies sufficiently above the Z boson resonance can be summarized as follows [118]:

- The effective Born cross section $\sigma^0(s)$ for $e^+e^- \rightarrow \bar{f}f$ (including electroweak and QCD corrections) drop by roughly three orders of magnitude from the peak cross section $\sigma_{peak}^0(M_Z^2)$ down to $O(10\text{ pb})$.
- The estimated statistical error by experiment will be approximately $\Delta\sigma \approx 1\%$, while at LEP 1 we typically had $\Delta\sigma \approx 10^{-3}$.
- For loose cuts, one observes in cross section distributions for different c.m. energies a second peak arising from events with hard photons emitted with energies $E_\gamma \approx \sqrt{s} - M_Z$ (radiative return events). This can be explained, by a shift of the gauge boson propagator onto the Z boson resonance after initial state hard photon emission. This gives a strong increase of $\sigma_T(s)$ by the resonant effective Born term.
- The weak box corrections from box diagrams with WW and ZZ exchange, which are usually only approximately treated at energies around the Z resonance, may grow, depending on the calculational gauge chosen and the cuts applied, roughly up to 1 or 2% effects. Also other weak corrections from massive top quark or weak gauge boson loops play an important role.
- Comparing LEP 2 fermion pair production data with theory, can also be used for SM Higgs boson or New Physics searches. In this context, also looking at processes $e^+e^- \rightarrow \gamma\gamma$ and $e^+e^- \rightarrow \nu\bar{\nu}\gamma(\gamma)$ allows further search options. More on this general issue can be seen in Chapter 4.

3.1 Physics effects in virtual radiative corrections

First let us have a look at two examples on virtual radiative corrections with special focus on the interplay between pure QED and electroweak corrections and their relative importance. We will especially have to realize that QED and electroweak corrections may start to be of similar importance at center-of-mass energies well above the Z boson resonance and it will give us some feeling on the importance of precisely knowing the different QED contributions better than one per cent also at LEP 2 energies. This shall be discussed before we go to the details of the recalculated QED radiation with cuts at higher energies.

The $Zb\bar{b}$ Vertex at LEP 2

An instructive example for different behaviour of weak corrections on and off the Z peak is $b\bar{b}$ production. The corrections differ from those to $d\bar{d}$ production due to the huge t -quark mass, which is depicted in Fig. 3.1. Only in the $b\bar{b}$ case, we

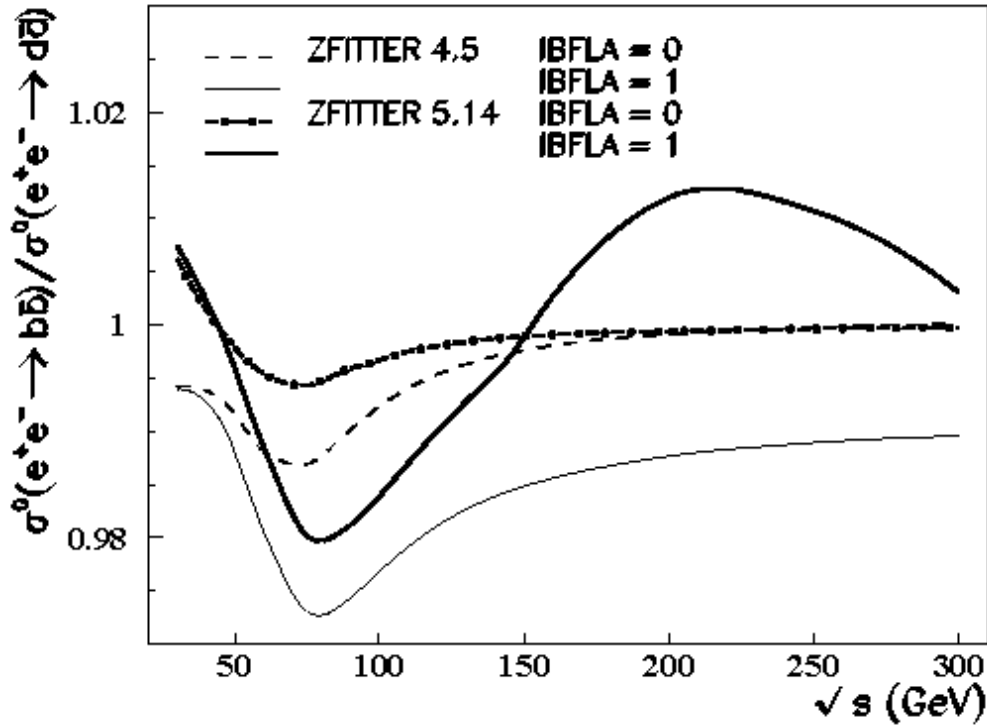


Figure 3.1: Ratios of improved Born cross sections for $b\bar{b}$ and $d\bar{d}$ production from ZFITTER v.4.5 (1992) [36] and v.5.14 (1998) [163] ; the latter has the correct t mass dependence at LEP 2 [146].

have large per cent level corrections from the large mixing to virtual top quarks in the loop, with $|V_{tb}|^2 \approx 1$ for the top-bottom mixing matrix element squared. The one-loop results to the $Zb\bar{b}$ vertex including the effects by a heavy quark exchange were first treated in [42–46].

While at LEP 1, the off-resonant WW box corrections and the $\gamma b\bar{b}$ vertex corrections are negligible compared to the $Zb\bar{b}$ vertex, they become more and more important with increasing c.m. energy. Further, one has to correctly include the s -dependence of the vertices and for the box also its different angular dependence. The net effect is taken into account in ZFITTER since v.5.12 [175], which contains the complete one-loop virtual EW corrections to the $(\gamma, Z)f\bar{f}$ vertex, and is shown in Fig. 3.1. It may be switched off with flag IBFLA=0 [36, 38]. It amounts up to about 2–4 % and is thus of the order of the statistical error [146]. Deviations from SM predictions for corrections to the $Zb\bar{b}$ vertex would of course immediately imply effects from *New Physics* through virtual corrections. A brief report on such searches for non-SM physics in the next Chapter will be given in connection with the possibilities at a future e^+e^- linear colliding machine.

The QED interference and electroweak box corrections – a comparison

While at LEP 1 the EW and QCD corrections can in general be considered as small in comparison to the QED bremsstrahlung, this observation is not necessarily valid anymore at higher energies, where EW and QED corrections can grow to comparable magnitudes. In order to underline this, in Fig. 3.2 the ef-

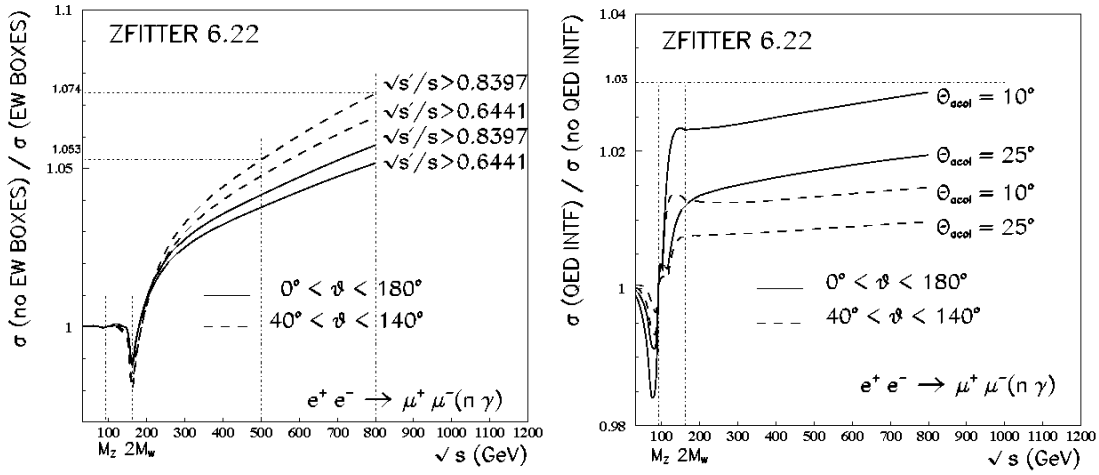


Figure 3.2: a. Effect of electroweak box corrections at LEP and LC energies, b. QED radiative corrections from initial-final state interference, calculated by ZFITTER v.6.22 [38], with cuts on $s' = M_{\mu^+\mu^-}^2$, on maximal acollinearity θ_{acol} , and on total acceptance ϑ [165].

fect of virtual ZZ and WW box corrections as important EW corrections was compared with corrections from the QED initial-final state interference for muon pair production cross sections σ_T . In Fig. 3.2a, the ZZ and WW box corrections are switched off in order to visualize a positive effect. Correspondingly, the QED interference was switched on and off in the right-hand plot (Fig. 3.2b). The net effect of these EW box corrections grows with increasing c.m. energy roughly up to per cent level at LEP 2 energies, with the QED interference corrections being slightly larger depending on the cut applied. At LC energies, however, the EW contributions can even surpass the QED interference contribution by roughly a factor of 2, while the effect from the QED interference approaches a more or less constant value of 2 to 3%. For this comparison, the ZFITTER code version v.6.22 [38] was run ‘blindly’ as it stands, i.e. without considering possible extra effects above the $t\bar{t}$ threshold due to the top quark mass [146].

At higher energies, all virtual corrections will start to become equally relevant introducing large gauge cancellations. Logarithmic and double logarithmic ‘Sudakov-type’ contributions could lead to measurable 1% or larger effects at a LC for $\sigma_T(b\bar{b})$ and R_b at 500 GeV or higher, but only to per mil level modifications for different $b\bar{b}$ asymmetries [176] (see (2.15) for R_b). For an estimate of the EW situation at energies up to 1 TeV also consult for example [177].

3.2 Photonic corrections above the Z resonance

The cross section ratios and the absolute differences of the asymmetries of ZFITTER v.6.11 [38, 162], containing the new results, are compared with v.5.20 [36, 161], still with the old coding, for different acollinearity cut values. First the single corrected contributions in the new code were compared with the old code, i.e. when the initial state corrections were compared, the final state radiation and the QED interference were switched off and so on.

Initial state corrections

In Fig. 3.3, the ratios of total cross sections σ_T and the differences of forward-

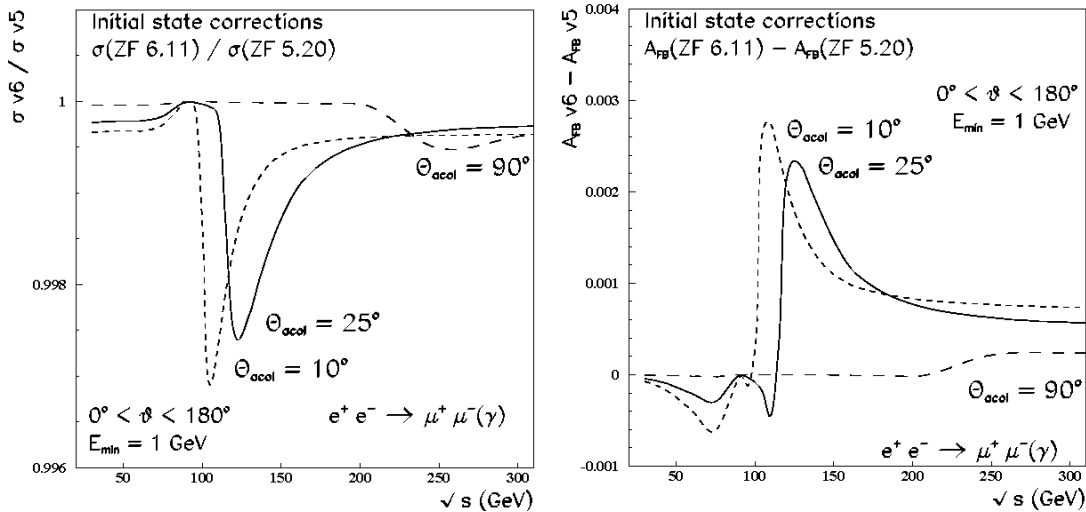


Figure 3.3: Ratios of muon pair production cross sections and differences of forward-backward asymmetries predicted by ZFITTER v.6.11 [38] and v.5.20 [36, 161] without and with acceptance cut and with three different acollinearity cuts: $\theta_{acol} < 10^\circ, 25^\circ, 90^\circ$; $E_{min} = 1$ GeV; programs differ by initial state radiation [145].

backward asymmetries A_{FB} for muon pair production are plotted from the two codes. The figure shows a wide range of c.m. energies from 30 to 300 GeV. We only discuss the energy regime above the Z^0 resonance, i.e. at c.m. energies of roughly $\sqrt{s} > 100$ GeV, as the resonance region was already discussed in the preceding Chapter 2, while the low energy region below $\sqrt{s} = M_Z$ is not interesting here and just given for completeness.

While at energies slightly above the Z peak the differences of the predictions show local peaks, at LEP 2 energies and beyond they are negligible for σ_T and amount to only 0.1% – 0.2% for A_{FB} . The peaking structures in Fig. 3.3 disappear at energies for which the radiative return is prohibited by the cuts. Depending on the acollinearity cut, this happens for energies $\sqrt{s} > \sqrt{s^{min}}$ with $\sqrt{s^{min}}$ being an effective s' -cut defined by the acollinearity cut. The values of s^{min} were given in Table 2.2.

Initial-final state interference corrections

In Fig. 3.4 the corresponding changes to the code are shown for the QED interference corrections. For total cross sections, the deviations may reach at most

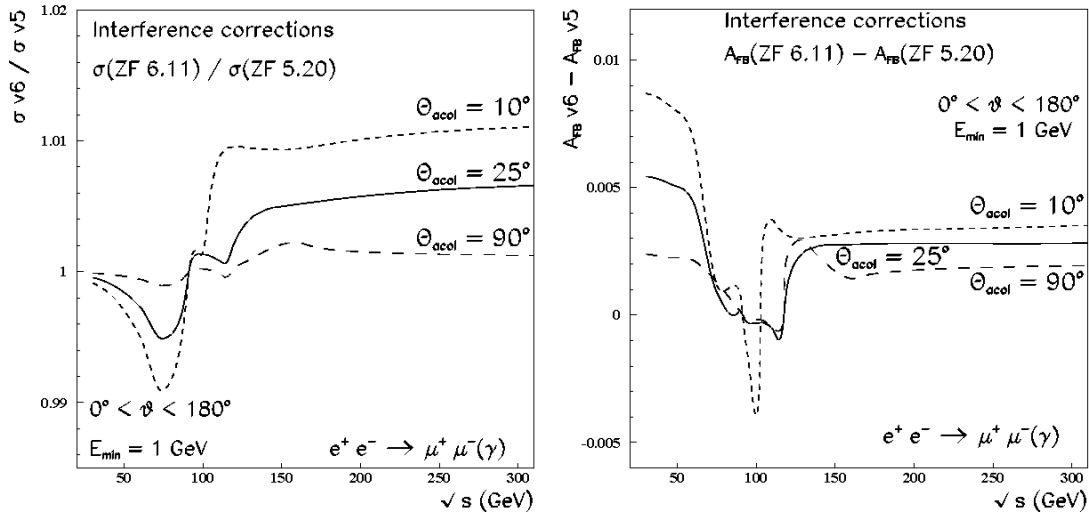


Figure 3.4: Ratios of muon pair production cross sections and differences of forward-backward asymmetries predicted by ZFITTER v.6.11 [38] and v.5.20 [36,161], cuts as in Fig. 3.3; programs differ by the initial-final state interference [145].

up to 1% at LEP 2 energies, while for asymmetries they stay below 0.5% there. Both shifts are more than the precision we aim at for the theoretical predictions.

Final state corrections

In Fig. 3.5, omitting an acceptance cut, we see that the deviations from the corrected final state radiators are negligible in the wide energy range, never exceeding 0.01% for the cross section and 0.1% for the asymmetry. If an acceptance cut is applied, the changes are yet smaller.

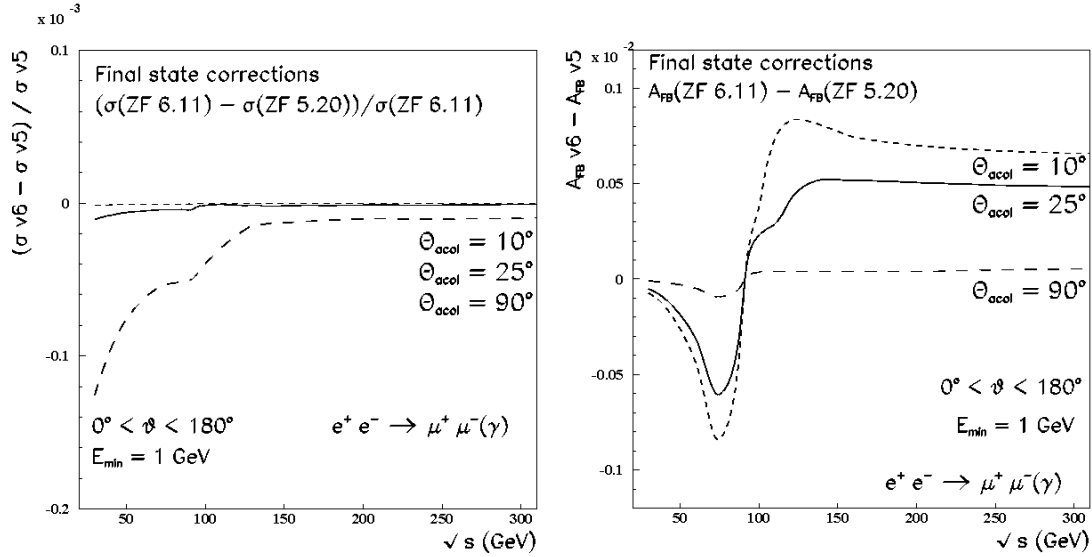


Figure 3.5: Ratios of muon pair production cross sections and differences of forward-backward asymmetries predicted by ZFITTER v.6.11 [38] and v.5.20 [36, 161], cuts as in Fig. 3.3; programs differ by final state radiation [145].

Net corrections

We have to distinguish two different approaches to data. Sometimes experimentalists subtract the initial-final state interference contributions from measured data, and sometimes the interference effects remain in the data sample. The resulting effects of all photonic corrections discussed in the foregoing sections are shown in Fig. 3.6. The net corrections for the muon pair production cross section and the forward-backward asymmetry at LEP 1 we had shown in Table 2.6.

For the wider energy range, the changes without initial-final interferences are below what is expected to be relevant at LEP 2 energies. The corrections to the numerical output from ZFITTER with acollinearity cut, however, increased when the corrected initial-final state interference is taken into account (see Fig. 3.6).

The numerical effects are dominated by the initial-final state interference and never exceed 1% at LEP 2 energies [145, 164, 165]. The corrected initial state and

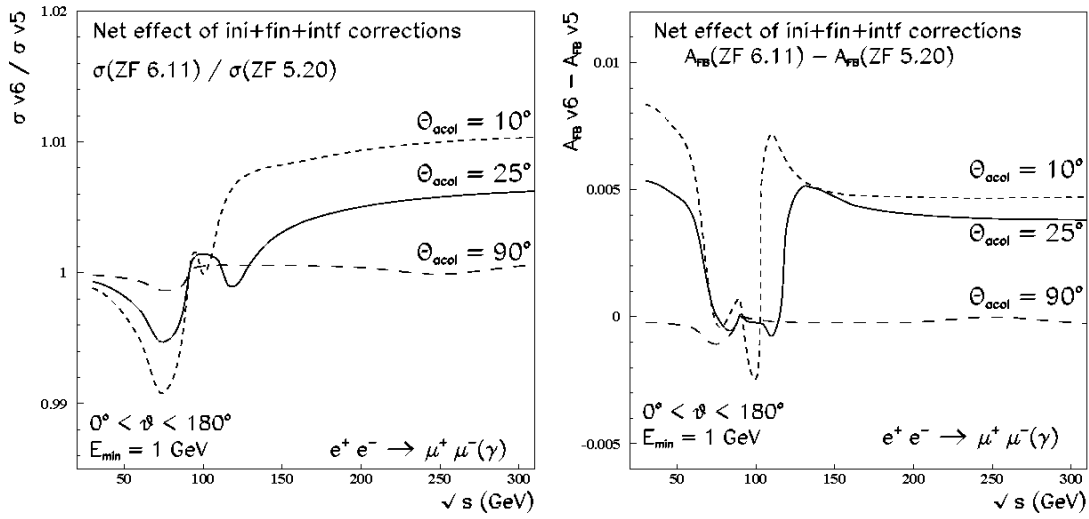


Figure 3.6: Net ratios of muon pair production cross sections and differences of forward-backward asymmetries predicted by ZFITTER v.6.11 [38] and v.5.20 [36, 161], cuts as in Fig. 3.3; initial-final state interference included [145, 164, 165].

final state terms only have minor effects on σ_T and A_{FB} and amount at most to corrections at the order of 0.1% – 0.2% for A_{FB} at LEP 2 energies for different cuts. The net corrections are largest where the radiative return to the Z starts to be prevented by the acollinearity cut. For $\theta_{acol} < 10^\circ$ or 25° this sets in at roughly $\sqrt{s} > 100$ GeV, or 115 GeV respectively. These corrections to the code are at most roughly 0.5% for σ_T and 1% for A_{FB} and shrink below 1% at higher energies. A detailed analysis of all new modifications to the code can be found in [145].

3.3 Comparisons with different programs

In 1992, a comparison of ALIBABA v.1 (1991) [132] and ZFITTER v.4.5 (1992) [36] showed deviations between the predictions of the two programs of up to 10% cent [178]; one of the plots of that study is shown in Fig. 3.7.

These deviations were observed only above the Z peak and only when an acollinearity cut on the fermions was applied; the agreement was much better without this cut. The comparison was repeated in 1998 with ALIBABA v.2 (1991) [132], TOPAZO v.4.3 (1998) [130, 131, 179], and ZFITTER v.5.14 (1998) [36, 163]. ALIBABA v.2 was used with the default settings and in ZFITTER v.5.14 one flag was modified (PHOT2=2). TOPAZO v.4.3 was run in accordance with ZFITTER v.5.14. The outcome was basically unchanged compared to 1992 as may be seen in Fig. 3 of reference [146] which shows cross section ratios as functions of s with

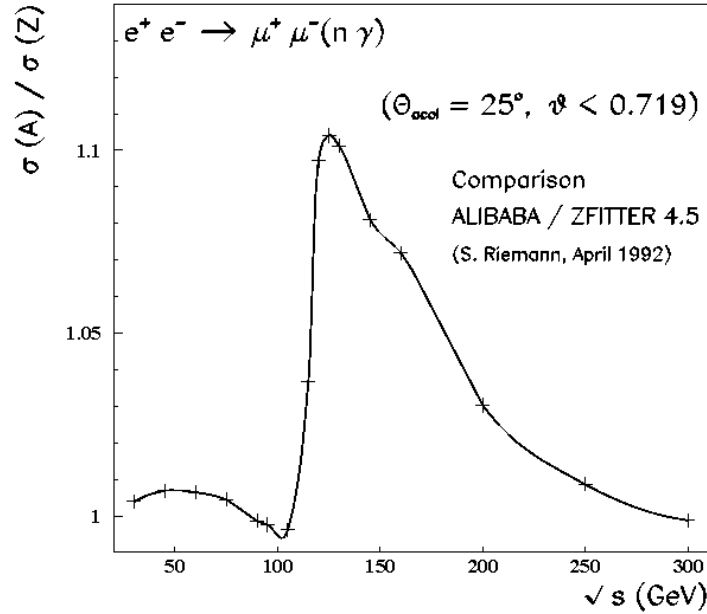


Figure 3.7: Muon pair production cross section ratios ALIBABA v.1 (1990) [132] versus ZFITTER v.4.5 (1992) [36]. An acollinearity cut was applied with $\theta_{\text{acol}} = 25^\circ$ [145, 165].

a cut on the maximal acollinearity angle θ_{acol} between the fermions. In addition, selected predictions had been shown in [146] at 120 GeV arising from a variation of flags (IORDER, NONLOG, IFINAL) in ALIBABA: upper ones at (4,n,m), lower ones at (3,n,m), with $n=0,1$, $m=1,2$ (best choice: (4,1,2)), with the deviations strongly depending on the calculated higher order corrections. All numbers were produced with the default settings of the programs.

Finally, the same version of ALIBABA was compared with ZFITTER v.6.22 (1999) [38, 162] and the same was done for TOPAZO v.4.3 and v.4.4 [130, 131] and ZFITTER v.6.04/06 [160] and v.6.22 (1999) [38], all depicted in Fig. 3.8.

Concerning the TOPAZO v.4.4 ratios, we register a different behaviour (compared to v.4.3) for $\theta_{\text{acc}} = 40^\circ$ which is now much closer to the ALIBABA ratios at energies above roughly 100 GeV. Between about 100 GeV and 200 GeV, the deviations in the predictions from different programs are huge and heavily depending on the maximally allowed acollinearity angle θ_{acol} , here shown for $\theta_{\text{acol}} = 10^\circ, 25^\circ$. The ratios stabilize at higher (or smaller) energies. The ZFITTER numbers are produced with the default settings (if not otherwise stated).

At LEP 2 energies the deviation of ZFITTER v.6.22 and TOPAZO v.4.4 is at the order of 1% or less for different acollinearity cuts and an acceptance cut of $40^\circ < \vartheta < 140^\circ$. In both cases, however, there is a clear peak of the cross section ratios at energies where the Z radiative return is not prevented by the

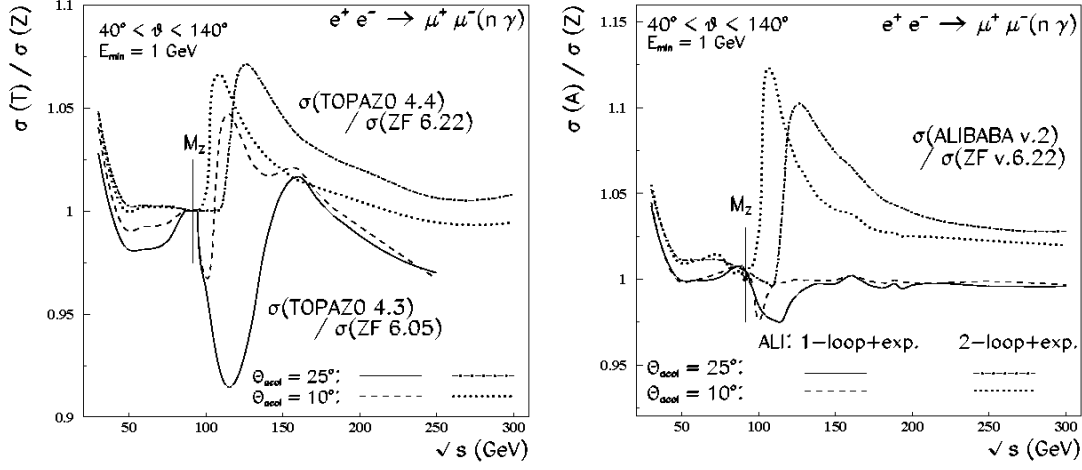


Figure 3.8: Muon pair production cross section ratios with $\theta_{\text{acol}} = 10^\circ, 25^\circ$ and $\theta_{\text{acc}} = 40^\circ$; a. TOPAZO v.4.3 and v.4.4 [130, 131] versus ZFITTER v.6.04/06 [160] and v.6.22 [38] (1999), b. ALIBABA v.2 (1990) [132] versus ZFITTER v.6.22 [145, 164, 165]. Flag setting: ISPP=0 [38].

cuts. While for the s' -cut this discrepancy stays moderate at the per cent level, it grows up to several per cent for the acollinearity cut.¹ Corrections by initial state pair production or different exponentiation of initial and final state higher orders, however, do not have a large effect here [164, 165].²

Furthermore, when the two-loop contributions in ALIBABA (with setting IORDER=3) were switched off, the agreement improved considerably. This visualizes the strong dependence of predictions on the details of the theoretical input chosen, e.g. the treatment of higher order contributions or the correct inclusion of non-logarithmic $O(\alpha)$ corrections. Evidently, the largest deviations arise from the radiative return of $\sqrt{s'}$ to the Z boson resonance due to hard initial state radiation. Interest in the high energy part of the data anyhow means to cut this away and so there should not be a serious problem. If instead one is interested in the radiative return, one has to be concerned about accuracies. These observations confirm similar statements from other studies [150].

On the other hand, a cross check of the ZFITTER and TOPAZO programs ap-

¹The flip of sign of these effects compared to the older versions, TOPAZO v.4.3 and ZFITTER v.6.04/06, is mainly due to a corrected interference contribution in the TOPAZO code. Changes to code ZFITTER v.6.04/06 were negligible here.

²In ZFITTER, the treatment of some higher order corrections was varied via flags FOT2 and PAIRS.

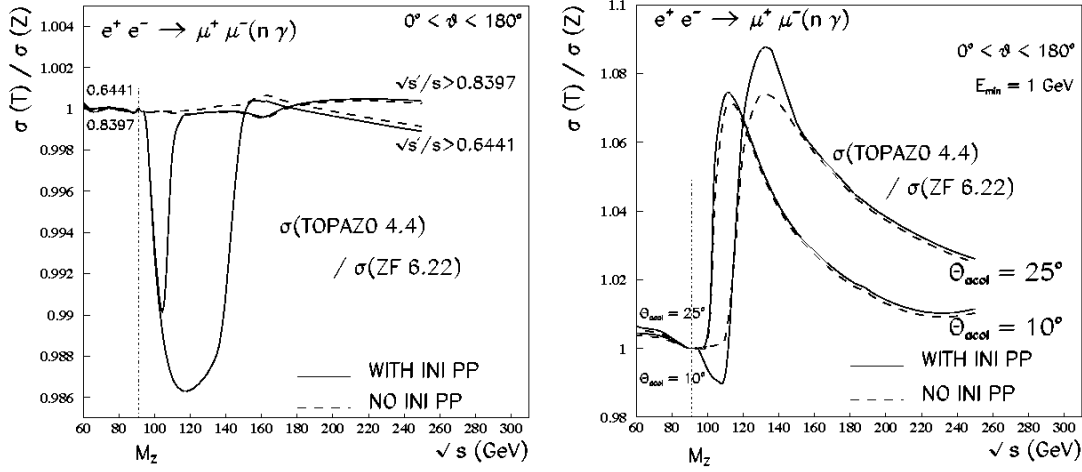


Figure 3.9: Comparison of predictions from ZFITTER v.6.22 [38] and TOPAZ0 v.4.4 [131] for muon pair production cross section ratios with a. an s' -cut or b. an acollinearity cut [165] (Flag setting: ISPP=0,1, FINR=0; further: SIPP=S_PR [38]).

plying s' -cuts comparable to the acollinearity cuts show a very high level of agreement between the two, at LEP 1 ($< O(3 \cdot 10^{-4})$), but also at LEP 2 energies at the order of less than a per mil ³ and is under control with respect to the experimentally demanded accuracy [152]. Initial state pair production and exponentiation of higher orders do not spoil this high level of agreement for the s' -cut. For the acollinearity cut branch, the deviation of the codes increases to few per cent, even with stringent hard photon cuts [164–166]. This may be seen in Fig. 3.9 and 3.10.

Our s' -cut dependent ratios deviate from unity mostly in the regions where the radiative return is not prevented. The same is true for the ratios with acollinearity cut; since this cut is not as effective in preventing the radiative return as the s' -cut, the deviations survive at higher energies to some extent. This fact and the higher order corrections, which remained untouched by our study, seem to be the main sources of the remaining deviations between the different programs.

Preliminary studies show that a correct description of hard two-loop QED corrections, especially for the acollinearity cut option in the ZFITTER code, together with a correct resummation of the soft and virtual initial-final state interference contribution, not contained in the ZFITTER code so far, seem to play a key role

³For this, a sufficiently large invariant mass cut preventing the radiative return to the Z boson resonance is applied. For LEP 2 energies flag FINR was set to 0 for the final state corrections which is the recommended choice.

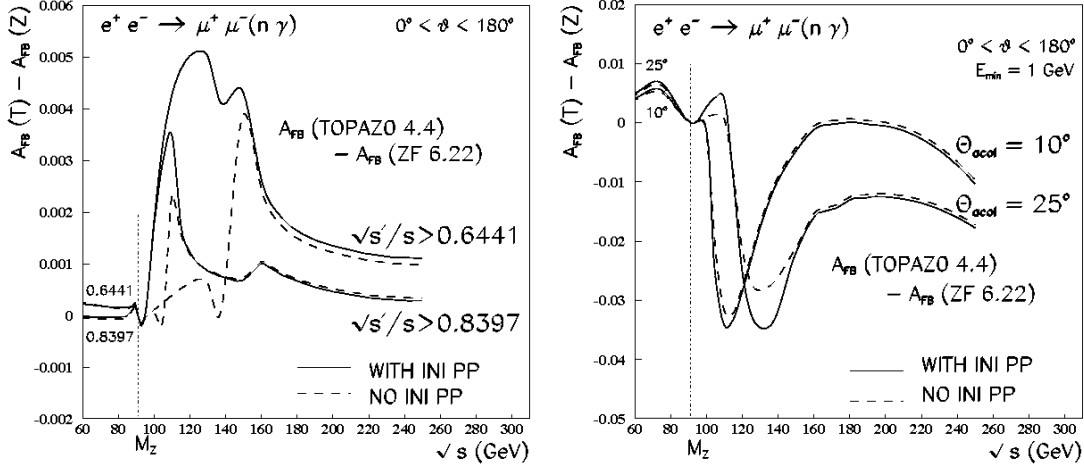


Figure 3.10: Comparison of predictions from ZFITTER v.6.22 [38] and TOPAZO v.4.4 [131] for differences of muon pair forward-backward asymmetries with a. an s' -cut or b. an acollinearity cut [165] (Flag setting: ISPP=0,1, FINR=0; further: SIPP=S_PR [38]).

here. Since the acollinearity cut is not as effective in preventing the radiative return to the Z boson as the s' -cut, these deviations also survive more profoundly for the acollinearity cut than for the s' -cut.

3.4 Conclusions

Analytical formulae were derived for the photonic corrections with acollinearity cut and substantial deviations were obtained from the coding in ZFITTER until version 5. The essentials of the changes have been described and numerical comparisons were performed in great detail.

At LEP 1 energies and for the s' -cut branch we had shown in Chapter 2 that the situation of the ZFITTER code up to versions v.5.x (1998) in comparison with the code TOPAZO can be stated as quite satisfactory. At $M_Z \pm 3$ GeV the agreement is better than 10^{-4} [149,152]. And also at LEP 2 energies and higher we can meet the demands by experiment with a deviation of the codes of not more than 1 or 2 per mil for different cut values and with a substantial decrease of this difference below 1 per mil in case of a sufficiently large s' -cut. This situation does not change when an extra cut on the maximal scattering angle $\cos \vartheta$ is applied [145,164,165].

If one introduces an acollinearity cut instead of the s' -cut, a comparable

agreement was obtained around the Z resonance as long as only initial state bremsstrahlung was considered. But as soon as we include the initial-final state corrections this agreement deteriorates to $O(3 \times 10^{-3})$ which grows to a large discrepancy between the two codes of several per cent at larger energies ($\sqrt{s} \approx 100 \dots 200$ GeV) [146]. An earlier comparison of the **ZFITTER** code with the **ALIBABA** code for the s-channel part of the Bhabha scattering branch had already shown similar deviations [145, 178]. At higher energies, $\sqrt{s} > 200$ GeV, the agreement with s' -cut is better than per mil, but still only 1 to 2% for the acollinearity cut. Especially in the intermediate energy range where the Z radiative return events are not prevented this discrepancy peaks and amounts up to several per cent. A similar effect is also visible for the s' -cut, although to a much lesser extent (below 1%).

We can therefore conclude that in the case of a cut on the acollinearity angle the correct treatment of the higher order hard photonic corrections is crucial in order to obtain better than per cent predictions. This is especially important at energies above the Z peak where the Z^0 radiative return effect is just approximately prevented by the applied cut. Due to the specific phase space for the acollinearity cut (see Fig. 2.4), a complete removal of the Z^0 radiative return via hard photon emission is not possible, no matter how strong the applied cut. These effects therefore also survive stronger at the 1 to 2 per cent level at LEP 2 energies $\sqrt{s} \approx 200$ GeV than for an s' -cut where the deviations are only few per mil.

In the **ZFITTER** code an approximation is implemented for the inclusion of hard two-loop corrections from initial state bremsstrahlung [62] with acollinearity cut, including an exponentiation of soft and virtual photonic corrections. For this, the acollinearity cut is simulated by an effective s' -cut which seems to be too crude at these energies. A delicate cancellation of the infrared divergences is at play here demanding a precise matching of the soft, virtual, and hard higher order corrections. The approximation is especially problematic at energies where the hard photonic corrections are strongly reduced. This has to be done as an analytical calculation for the hard two-loop radiator functions with acollinearity cut is not available. Cuts on the minimal and maximal scattering (acceptance) angle of $\vartheta_{min} < \vartheta < 180^\circ - \vartheta_{min}$ with $\vartheta_{min} = 20^\circ$ and 40° had no effect on the outcome of these comparisons.

Fortunately, we may conclude that the numerical changes at the interesting LEP 2 energy range above roughly 160 GeV are not as big as one could expect. Applying an extra s' -cut on top of the acollinearity cut for the intermediate energy region, could possibly reduce the large discrepancies between the codes. This would perhaps be a possibility for experimental fitting procedures in order to assure the necessary level of agreement between the different codes. If one is interested in performing investigations in this kinematical region, further studies with the codes are necessary.

Chapter 4

The e^+e^- Linear Collider and Fermion Pairs

With the experience of LEP in mind, there appear two equally fascinating opportunities for studying fermion pair production processes at a future e^+e^- Linear Collider (LC). One option, the Giga-Z option, would be to run with high luminosity on the Z boson resonance. This may be performed in a quick and feasible few months run in order to pin down the symmetry breaking mechanism of the electroweak sector by indirectly determining the masses of a light SM or MSSM Higgs boson or looking for effects of supersymmetric particles from virtual corrections [180, 181]. The main motivation to build such a machine of course is to look for such particles or other ‘New Physics’ in direct particle production at energies typically reaching the TeV scale like the *Tesla project* [182].

These two scenarios for the LC shall be sketched at the beginning of this Chapter. We then want to put particular emphasis on what this means for the QED description to fermion pair production and on what is provided in this respect by the semi-analytical program ZFITTER [36, 38] in comparison with the numerical programs TOPAZ0 [130, 131] and KK2f [133, 135, 136].

4.1 Searches for *Physics beyond the Standard Model*

High precision measurements to the SM and MSSM

Starting with the Giga-Z option, it was demonstrated in [180] that with a factor of 100 or so higher statistics than at LEP running on the Z boson resonance,¹

¹ In comparison to SLD at SLAC, it would be even a factor of roughly 2000.

which corresponds to a luminosity of $\mathcal{L} \sim 5 \cdot 10^{33} \text{cm}^{-2} \text{s}^{-1}$ or roughly 10^9 hadronic Z boson decays after just a few months of running, especially fermion pair production asymmetries like A_{LR} or the polarized $b\bar{b}$ forward-backward asymmetry A_{FB}^b could be measured with very high precision when using one or both beams polarized. This latter condition together with good b -tagging techniques and the collected experiences at LEP and SLD should help to keep the systematic errors under control. The implication of this from the theoretical side on extracted **SM** parameters, like e.g. on the W boson mass M_W or the effective weak mixing angle $\sin^2 \theta_{eff}$ was illustrated in [181]: With expected experimental accuracies at the Giga-Z one obtains $\Delta M_W = 6 \text{ MeV}$ or $\Delta \sin^2 \theta_{eff} = 4 \times 10^{-5}$. This is to be compared with the presently achievable total experimental errors by the end of LEP of $\Delta M_W = 40 \text{ MeV}$ or $\Delta \sin^2 \theta_{eff} = 1.8 \times 10^{-4}$ [180]. Due to loop corrections M_W and $\sin^2 \theta_{eff}$ are sensitive to the mass of a light Higgs boson M_H , the top quark mass m_t , and in the supersymmetric case, also on the mass scale M_{susy} . These much improved experimental values for M_W and $\sin^2 \theta_{eff}$ thus allow at the Giga-Z, together with the precise knowledge of m_t , an indirect determination of the mass of a light Higgs boson in the **SM** at the 10% level. Moreover, strong consistency checks can be performed on the **SM**/**MSSM** values of M_W and $\sin^2 \theta_{eff}$ with m_t and supersymmetric masses as input parameters [181].

Virtual corrections and New Physics Phenomena

Probably one of the most fascinating applications of fermion pair production processes at higher energies is then the search for ‘New Physics Phenomena’ (NPP), i.e. new effects which would be observed, but not described by the **SM** [182, 183]. This is of course quite actively pursued already at existing e^+e^- high energy facilities, giving quite stringent bounds on masses and couplings of exchanged ‘exotic’ particles or minimal interaction scales of NPP. With a future LC, however, reaching much higher energies close to the TeV scale and using high luminosities, there is the justified hope of really uncovering this ‘beyond the **SM**’ domain of particle physics. Examples of such investigations are e.g. setting lower limits on four-fermion contact interaction scales or on masses and couplings of extra heavy neutral or charged gauge bosons, Z' and W' , [61, 184–186], of **susy** particles in \mathcal{R} parity violating supersymmetric models, or for interaction-unifying models (**GUTs**). Also searches for excited leptons, leptoquarks, preons, or heavy fermions from Technicolor models could be conducted or [187], one could look for effects in angular cross section distributions from spin-2 boson exchanges predicted in string-inspired, low-scale quantum gravity models [188].

LEP 1 and LEP 2, for example, already have some potential for the observation of new virtual effects in the $2f$ final state [172, 173, 189]:

- Heavy neutral Z' bosons may be searched for in two respects: At the Z peak, limits on a ZZ' mixing angle may be derived, typically $|\theta_M| < 0.003$ [61, 184]. While, at LEP 2 limits on the mass of a Z' boson are obtained in the range $M_{Z'} > 250 - 725$ GeV depending on the models studied [189].
- A limit on the energy scale Λ at which contact interactions could appear is $\Lambda > 4 - 10$ TeV. Typical limits from atomic parity violation searches are $\Lambda > 15$ TeV. They are not sensitive to the \mathcal{P} conserving $VV, AA, LL + RR, LR + RL$ type models [173].
- Leptoquarks and also sneutrinos and squarks from supersymmetric theories with \mathcal{R} -parity breaking may be exchanged in addition to γ and Z . The leptoquark mass limits, $m_{LQ} > 120 - 430$ GeV, are for some models competitive with direct searches [172].
- Extra dimensions naturally arising in quantum gravity models could be probed through the relation $M_{Pl} = \mathcal{R}^n M_S^{n+2}$ which relates the Planck mass scale $M_{Pl} \approx 10^{19}$ GeV with an effective gravity scale M_S in usual 4-dimensional space-time assuming a maximal spatial extension R of the extra dimensions [173, 188]. This delivers lower bounds on the energy scale at which gravity effects could appear of $M_S > 0.7 - 1$ TeV.

With a LC, the so far checked energy region for NPP from LEP or SLC can be extended from typically $O(\text{few TeV})$ up to several tenths of TeV at a LC. A complete presentation of these activities is given in [183].

Recently collected evidence of neutrino-oscillations at the Super Kamiokande experiment [72] makes another application in the context of the Giga-Z option quite interesting: looking for lepton flavor number violating Z decays like $Z \rightarrow \mu\tau, e\tau$, or $e\mu$ when heavy neutrinos are exchanged in virtual corrections (Dirac or Majorana type). The estimated branching ratios in the case of $Z \rightarrow e\tau$ or $\mu\tau$ could be large enough in some models to be observable at the Giga-Z. A first calculation had been done in [190] and studies for the LC were presented in [191].

4.2 Higher order QED corrections

In order to successfully look at the Giga-Z for such small corrections by NPP, the large QED corrections have to be subtracted reliably from data with an exact treatment of the other radiative corrections. This means that the **SM** corrections have to be known precisely at least at the level of the New Physics effects. The

per mil precision obtained at LEP 1 and SLC naturally sets a lower benchmark for the expected accuracies at the Giga-Z. For the **ZFITTER** program and other two-fermion codes it was shown in Chapter 2 that a relative precision for cross section observables of the order 10^{-4} can already be guaranteed on the Z peak. This could especially be proven for the new QED bremsstrahlung calculation with general cuts on final state angles and energies, shown there.

At energies approaching the TeV scale, the QED interference between initial and final state radiation starts to become as equally important as the initial state contribution and also higher order corrections grow in importance. Furthermore, the removal of Z radiative return events from the experimental data through kinematical cuts to the hard photon phase space is important in order to remove most of the, for particle searches uninteresting **SM** background.

Therefore, the comparison of total cross section predictions by codes **ZFITTER** v.6.22, **TOPAZ0** v.4.4, and **KK2f** v.4.12 [136] was now extended up to typical LC energies of 500 to 800 GeV for the invariant mass cut option. This is shown in Fig. 4.1 and Fig. 4.2. The general result of this analysis is that the deviation of the cross section predictions by the three codes is not more than 5 per mil for the complete energy range for the **TOPAZ0**–**ZFITTER** comparison. This observation also holds for the case of initial state QED bremsstrahlung (ISR) alone when comparing code **KK2f** with **ZFITTER**, applying sufficiently strong invariant mass cuts and taking into account different higher order corrections (Fig. 4.1). Including QED initial-final state interference (IFI), the comparisons with **KK2f** delivered a maximal deviation of roughly 1 % (Fig. 4.2).

In detail, this meant: The numerical precision of **TOPAZ0** and **ZFITTER** was better than 10^{-5} everywhere, while the accuracy of the Monte Carlo (MC) event generator **KK2f** was necessarily restricted due to limited CPU time: Calculating ISR with an accuracy of at least 10^{-3} required samples of 100000 events for each energy point. When including the resummed IFI, smaller samples of 30000 events had to be used, resulting in a lower precision of roughly 2×10^{-3} . For ISR only, the typical CPU time per MC data point e.g. on an HP-UX 9000 workstation was about 25 minutes, increasing to roughly 100 minutes if IFI is added for the event samples stated above. In comparison, **TOPAZ0** calculated one cross section value in a few minutes, while **ZFITTER** with its semi-analytical approach calculated all 32 cross section values for one cut in a few seconds. On the other hand, when interested in more complex setups, i.e. calculating multi-differential observables, using a wider variety of cuts, or including extra higher order effects to the initial-final state interference, which **ZFITTER** cannot or only partly provide, the numerical programs **TOPAZ0**, or respectively **KK2f**, clearly have their advantages.

The effect of ISR was compared alone (Fig. 4.1) or of ISR together with IFI (Fig. 4.2) for three different cut values: $\sqrt{s'}/s > 0.6441$, 0.8397, and 0.9164, in

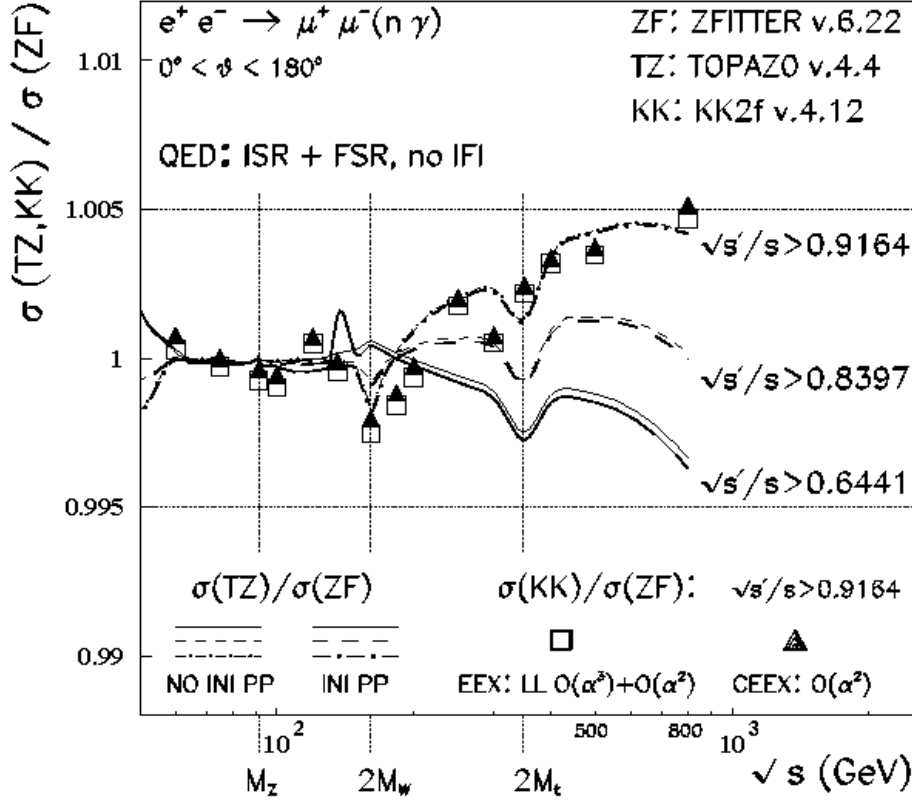


Figure 4.1: Cross section ratios for muon pair production with different s' -cuts for codes ZFITTER v.6.22 [38], TOPAZO v.4.4 [131], KK2f v.4.12 [136] (1999) from 60 to 800 GeV c.m. energy; without initial-final state interference [166] (INI PP: initial state pair production; LL: leading logarithmic terms).

the case of the TOPAZO–ZFITTER comparison, and $\sqrt{s'/s} > 0.9164$ when comparing with KK2f.² The value s' is defined here as the invariant mass squared of the γ or Z propagator after ISR, which is equal to the final state invariant mass squared including the emitted final state photons. For this, final state radiation (FSR) was treated in form of a global correction factor. Alternatively, cutting on the minimal final state invariant mass squared $M_{f\bar{f}}^2$ after FSR, though it slightly worsened the good agreement at LEP 1 energies [152], it did not change the overall agreement in Fig. 4.1 and Fig. 4.2 substantially. A recent discussion on this issue, defining kinematical cuts with radiative corrections for the experimental

²The cut values correspond approximately to a relatively strong cut on the maximal final state leptons' acollinearity angle of 25°, 10°, and 5° respectively.

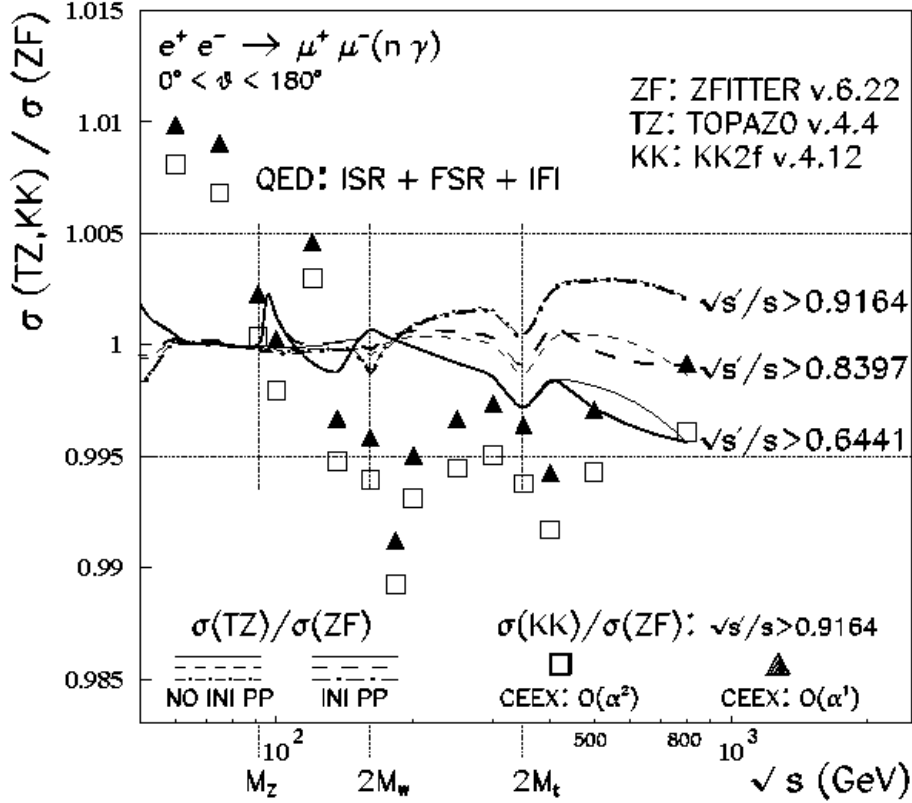


Figure 4.2: Cross section ratios for muon pair production with different s' -cuts for codes ZFITTER v.6.22 [38], TOPAZ0 v.4.4 [131], KK2f v.4.12 [136] (1999) from 60 to 800 GeV c.m. energy; with initial-final state interference [166] (INI PP: initial state pair production; LL: leading logarithmic terms).

and computational situation – e.g. when including mixed QED and QCD contributions from photonic and gluonic emission in the case of hadronic final states – was given in [152]. In particular, at LEP 2 energies the predictions of the codes lie well inside the estimated experimental accuracies of e.g. $\Delta\sigma_{\mu\mu} \approx 1.2\%$, $\Delta\sigma_{had} \approx 0.5\%$ for sufficiently strong cuts [152].

Except where otherwise stated, the default settings of the programs were used, thus taking into account the $O(\alpha^2)$ photonic initial state corrections [62] with the leading logarithmic $O(\alpha^3)$ [120] corrections together with the exactly added $O(\alpha)$ IFI and QED box contribution [38, 131, 136]. In ZFITTER and TOPAZ0, the two-loop corrections are complete. All three programs have installed higher order corrections to ISR where the finite soft and virtual photonic corrections

are resummed.³ In contrast to codes **ZFITTER** and **TOPAZ0**, **KK2f** also possesses a procedure to exponentiate IFI corrections with its newly implemented *coherent exclusive exponentiation* (*CEEX*) [134,136,154].⁴ To be more precise, *CEEX* does not include $O(\alpha^3)$ contributions to initial state bremsstrahlung up to now, while the *EEX* option in **KK2f** does not contain the second order, subleading $O(\alpha^2 L)$ corrections, so both options are complementary to each other when interested in estimating these higher order effects for the initial state bremsstrahlung with **KK2f** ($L = \ln(s/m_e^2)$). In both cases **KK2f** lacks the $O(\alpha^2 L^0)$ terms which, however, are estimated to be of the order 10^{-5} and so do not play a visible role in this comparison [136].

In Fig. 4.1, the predictions by **KK2f** were compared with those by **ZFITTER** for ISR alone, first for the *EEX* option with the leading logarithmic (LL) $O(\alpha^3 L^3)$ and $O(\alpha^2 L^2)$ corrections (**ZFITTER** flag values: **FOT2** = 3, 5) [38]. Then we used the *CEEX* option for **KK2f** and compared the $O(\alpha^2)$ results (**ZFITTER**: **FOT2** = 2). The cross section ratios and the maximally 5 per mil deviation of the codes did not change considerably. The values were calculated with a numerical uncertainty of 0.4×10^{-3} at the Z peak, and 1×10^{-3} overall.

In Fig. 4.2 the cross section ratios, now with the IFI contribution, are compared for *CEEX* $O(\alpha^1)$ and *CEEX* $O(\alpha^2)$. There is roughly a 2 per mil shift of the central values – always having in mind calculational uncertainties of 2×10^{-3} – when going to the $O(\alpha^2)$ calculation, but they stay inside the overall, $\pm 1\%$ margin.

Another, in **ZFITTER** recently updated contribution are initial state pair corrections [38,123]. These originate from bremsstrahlung photons dissociating into light fermion pairs: **TOPAZ0** and **ZFITTER** versions contain the $O(\alpha^2)$ leptonic and hadronic initial state pairs and a realization for simultaneous exponentiation of the photonic and pair radiators [62,121,122]. According to [136], initial state pair corrections are not included in the **KK2f** code. Since **ZFITTER** v.6.20 [38], also the leading and subleading terms of $O(\alpha^3)$ and the LL $O(\alpha^4)$ corrections from initial state pair emission may be included through convolution of the photonic and pair flux functions [123]. The effect of the pair corrections is e.g. with strong cuts roughly 2.5 per mil at the Z peak, slightly decreases to approximately 2 per mil at LEP 2 energies, and is not more than roughly 1 per mil at 500 to 800 GeV c.m. energy. In Fig. 4.1 and Fig. 4.2, switching on the pair corrections for different cuts, does not change the level of agreement between **ZFITTER** v.6.22 and **TOPAZ0** v.4.4 substantially. One interesting feature at lower energies between roughly 100 and 150 GeV – just where the Z radiative return is not prevented anymore by the applied cuts – is the fact that the several per mil deviation of the two codes there disappears when the pair corrections are switched off. From

³In **KK2f**, the Yennie-Frautschi-Suura (EEX) prescription was used [136].

⁴ The initial-final state interference contribution in **KK2f** is only available with the *CEEX* option; for *EEX* it is neglected.

Fig. 4.1 and Fig. 4.2 it can also be seen that such deviations can also be prevented by a sufficiently large s' -cut of e.g. $s'/s > 0.9$ if initial state pair corrections shall be included.

The inclusion of 4-fermion final states in this context, e.g. from final state pair creation, with their rather large, per cent level corrections at LEP 2 and higher energies [155] is another task which has to be pursued for an update of the codes for the LC. Especially, the definition of background and signal diagrams in the hadronic case together with kinematical cuts will be one of the major obstacles to overcome for experiment and theory [155].

4.3 Conclusions

A possible quick usage of a future e^+e^- Linear Collider (LC) as a high luminosity Z factory in a Giga- Z mode leads to strong demands on theoretical cross section predictions by two-fermion codes like **ZFITTER**. The analysis done in Chapter 2 for LEP 1 and SLC precisions can of course also be applied here. Cross section results are now calculated by **ZFITTER** with 10^{-4} precision on the Z resonance itself which is a good start for the estimated high precisions at a Giga- Z with a factor of 10^2 or 10^3 more Z decays than at LEP.

For typical LC energies, a first comparison of programs **ZFITTER**, **TOPAZ0**, and **KK2f** for the standard s' -cut option shows very nice agreement for the whole center-of-mass energy range from $\sqrt{s} \approx 60$ GeV to 800 GeV. The maximal deviation is 5 per mil for initial state radiation alone, which also holds for codes **ZFITTER** and **TOPAZ0** when switching on the QED interference. The maximal deviation grows up to 1% when comparing with **KK2f**, but can be explained with a resummation of soft interference terms, installed in **KK2f** [134, 136], but not yet for the other codes [166]. This analysis included different initial state photonic corrections and corrections from initial state QED pair creation with different cuts. It can be concluded that the codes already fulfil the minimal precision requirements at the $O(1\%)$ or better for the higher energies at a LC . Still a lot has to be done having in mind for example an update of codes for top pair production with final state masses and cuts or for an experimentally realistic description of beamstrahlung effects with polarized beams, higher luminosities, and higher energies.

Summary

Results

QED flux functions with cuts on maximal acollinearity, minimal energies, and minimal and maximal acceptance

Summarizing, new and more general formulae for flux functions for hard bremsstrahlung were derived for total and forward-backward cross sections σ_T , and σ_{FB} and the angular cross section distribution $d\sigma/d\cos\vartheta$, for s -channel fermion pair production, $e^+e^- \rightarrow \bar{f}f$, $f \neq e, \nu_e$. The semi-analytical results contain different kinematical cuts to the hard photon phase space which had not or only incompletely been treated in the literature so far [69]:

- Cuts on the final state fermions' maximal acollinearity angle $\theta_{\text{acol}}^{\text{max}}$ and minimal energies E_{min} :

$$\sigma_T = \sigma_T(\theta_{\text{acol}}^{\text{max}}, E_{\text{min}}), \quad (5.1)$$

$$\sigma_{FB} = \sigma_{FB}(\theta_{\text{acol}}^{\text{max}}, E_{\text{min}}), \quad (5.2)$$

- with an additional symmetrical cut c on the cosine of the scattering angle ϑ of one of the final state fermions:

$$\sigma_T(c, \theta_{\text{acol}}, E_{\text{min}}) = \int_{-c}^c d\cos\vartheta \frac{d\sigma}{d\cos\vartheta}(\cos\vartheta; \theta_{\text{acol}}^{\text{max}}, E_{\text{min}}), \quad (5.3)$$

$$\sigma_{FB}(c, \theta_{\text{acol}}^{\text{max}}, E_{\text{min}}) = \left(\int_0^c - \int_{-c}^0 \right) d\cos\vartheta \frac{d\sigma}{d\cos\vartheta}(\cos\vartheta; \theta_{\text{acol}}^{\text{max}}, E_{\text{min}}), \quad (5.4)$$

$$\rightarrow A_{FB}(c, \theta_{\text{acol}}^{\text{max}}, E_{\text{min}}) = \frac{\sigma_{FB}}{\sigma_T}(c, \theta_{\text{acol}}^{\text{max}}, E_{\text{min}}). \quad (5.5)$$

A set of simplified and handy expressions for flux functions (*radiators*) was determined for $O(\alpha)$ hard QED corrections to s -channel processes $e^+e^- \rightarrow \bar{f}f$

with the above listed general cuts. These are radiators H_A^a , $A = T, FB$, $a = ini, int, fin$, for the initial state, final state, and initial-final state interference hard photonic corrections. They are regularized by cancelling all infrared singularities after adding the corresponding $O(\alpha)$ radiator functions from [32, 34, 35] for soft and virtual photon corrections S_A^a , including corrections B_A from $\gamma\gamma$ and γZ exchange box diagrams.

The complete, regularized radiator functions R_A^a , containing all soft, virtual, and hard photonic terms, can be integrated in an effective Born approximation together with improved Born observables over s' . See Sections 2.2 and 2.3.3 in Chapter 2 on these issues. For brevity, the radiators for $d\sigma/d\cos\vartheta$ were not presented here, but are available and will be published later.

The results were implemented in the semi-analytical program **ZFITTER** for fermion pair production in e^+e^- annihilation from version 6.04/6.06 onwards [38, 160]. The program with the new results is used by the experimental communities at the LEP and SLC experiments e.g. for an analysis of the Z line shape. The considered cuts are an experimentally requested option for leptonic final states as alternative to a kinematically simpler cut on s' and on $\cos\vartheta$.

The semi-analytical calculation of the hard photon flux functions consisted in a two- or respectively three-fold analytical integration over three angles of phase space, while the convolution integrals over s' are done numerically in the program **ZFITTER**. The convolution integrals over s' are done numerically. The phase space parameterization was done in accordance with [158]. There, the hard-photon corrections with acollinearity and energies cut had been calculated completely numerically. The phase space was shown for two variables of integration in Fig. 2.4. Details of the parameterization can be seen in Section 2.3.1 and Appendix A.

It is naturally split into three separate parts due to the cuts applied. A nice observation is that all three regions of phase space can be treated equivalently, using one general parameter $A = A_{I,II,III}(s'/s)$ as function of $R \equiv s'/s$, and for each region only depending on m_f or on one of the two cuts applied. This was first illustrated in [69, 158]. The insertion of the specific value of $A(s'/s)$ for each region yields the corresponding expression of a radiator in each of the three phase space regions [37, 145, 164].

In order to analytically integrate over the final two angles of phase space θ_γ and θ , the fermion masses m_e and m_f had to be neglected, which is safe, having applications at LEP or a LC in mind and not considering top pair production. The calculation demanded a separation of phase space into different regions providing different analytical expressions for each region. The necessity for this phase space splitting is due to artificial poles which arise in the squared matrix element for collinear photon emission from the initial state, i.e. in the case $\cos\theta_\gamma = \pm\cos\vartheta$ and when neglecting masses. While this separation of phase space into different

regions is necessary for the initial state and initial-final state interference terms, the critical electron and positron propagator terms do not occur in the final state matrix element and therefore no phase space splitting is necessary there.

It can be shown that these unphysical poles cancel when combining all terms, i.e. the expressions from different phase space regions transform continuously into each other for $\cos \vartheta \rightarrow \pm \cos \theta_\gamma$. Only logarithmic mass terms of the form $\ln(s/m_e^2)$ and $\ln[(1+c)/(1-c)]$ with c as symmetric acceptance cut remain, or $\ln(s'/m_f^2)$ respectively for the final state, from collinear photon emission remain. This is discussed for the initial state case in Section 2.3.2 and Appendix B.1. The QED interference can be treated completely analogously.

Each flux function with general cuts consists of not more than approximately 50 terms and can be straightforwardly implemented into a semi-analytical Fortran program like **ZFITTER** [38]. Allowing full acceptance, i.e. omitting the cut on the scattering angle $\cos \vartheta$ ($c=1$), strongly reduces the number of different expressions for the totally integrated radiators – only one expression remains for the c -even terms H_T^a , and only two are possible for the c -odd ones, H_{FB}^a . This yields very compact formulae of less than 10 terms in each case. The short formulae were published in [37], while a collection of all general radiator formulae are given in the Appendix B.2 and B.3 or were presented for the initial state case in Chapter 2. The cross section distribution over s' , $d\sigma^{fin}/ds'$, can be analytically integrated further over s' in order to reproduce the results given in [157], where some misprints could be corrected there.

Programming in *ZFITTER*

The update to the **ZFITTER** code from version 6.04/06 [38, 160] onwards consisted in a correction of the up-to-now mainly undocumented flux functions for hard bremsstrahlung to $e^+e^- \rightarrow \bar{f}f$ for the calculational branch with acollinearity cut. Results for the integrated initial state and initial-final state interference radiators had been given in [69], but with errors there.

The new formulae implemented in the code now only contain terms proportional to $P = 1/(1 - s'/s)$ which formally correspond to the infrared poles of the unregularized expressions for $s' \rightarrow s$. All unphysical powers P^n for $n \geq 2$ could be removed in these first order results. The formulae with all non-logarithmic fermion mass terms being neglected are still sufficiently compact for a convenient description in the Fortran code. The initial state and initial-final state interference contributions can be calculated in parallel in the different subroutines with a small distinction for the soft and virtual photonic terms. For initial state radiation the finite part is resummed in a soft-photon exponentiation, while the QED interference radiators are added in first order approximation. The expressions in the code for final state radiation could also be corrected.

The very short formulae on cross section and asymmetry flux functions without acceptance cut [37] allow a numerically fast, additional branch of the code, when one is only interested in cuts on the maximal acollinearity angle and the minimal energies. All analytical formulae were numerically checked by comparing them with the squared matrix element which was numerically integrated over the angular phase space. Only the trivial integration over the photon angle φ_γ was performed analytically. We obtained complete agreement, solely restricted by the numerical precision of the applied Simpson integration routine and neglected mass terms in the analytical formulae. The Fortran package `acol.f` was written containing the new results and linked to `ZFITTER`. This is described in [38].

Numerical analysis of codes

The other major part of this thesis consisted of numerical comparisons of the earlier `ZFITTER` codes [36] with the new versions from version 6.04/06 [38, 160] onwards which were updated with the new results. This internal comparison was extended to other 2-fermion programs with special focus on QED radiative corrections for center-of-mass energies of $\sqrt{s} = 30 \dots 800$ GeV:

- (1) `ALIBABA` versions 1 and 2 [148] were compared with `ZFITTER` v.4.5 to v.6.11 [36, 38] for the s -channel contribution to Bhabha scattering $e^+e^- \rightarrow e^+e^-$ with cuts on acollinearity, acceptance, and energies for $\sqrt{s} = 30 \dots 300$ GeV [145, 146, 164–166].
- (2) A comparison for `TOPAZ0` versions 4.3 and 4.4 [130, 131] and `ZFITTER` v.4.5 to v.6.11 was performed [36, 38] for $e^+e^- \rightarrow \mu^+\mu^-$ with cuts on acollinearity, acceptance, and energies, or alternatively on s' and acceptance for $\sqrt{s} = 30 \dots 300$ GeV [145, 146, 164–166].
- (3) `KK2f` version 4.12 [136] was treated together with `ZFITTER` v.6.22 [38] and `TOPAZ0` v.4.4 [131] for muon pairs with cuts on s' and acceptance for $\sqrt{s} = 60 \dots 800$ GeV [166].

The main result of the numerical comparisons is that now a numerical agreement for codes `ZFITTER` v.6.04/06 onwards and `TOPAZ0` v.4.4 can be guaranteed of better than 1 per mil for the Z -boson resonance region: For σ_T , results agree now better than 0.3×10^{-3} for $\sqrt{s} = M_Z \pm 3$ GeV, and better than 10^{-4} at the Z peak itself. For A_{FB} we have: $\delta A_{FB} < 10^{-4}$ for $\sqrt{s} = M_Z$, and $\delta A_{FB} < 10^{-3}$ for $\sqrt{s} = M_Z \pm 3$ GeV. The numerical accuracy of the codes now meets the precision already obtained earlier for the kinematically simpler s' -cut [152]. The results were presented in Fig. 2.5 and Table 2.7 in Chapter 2. For the internal `ZFITTER` comparisons please refer to Tables 2.3, 2.4, 2.5, and 2.6.

At energies slightly above the Z peak, around $\sqrt{s} \approx 100 \dots 130$ GeV, deviations were observed of several per cent between codes **ZFITTER**, **ALIBABA**, and **TOPAZ0**. The energy interval describes the region where the Z radiative return effect is still active for the applied cuts of $\theta_{acol}^{\max} = 10^\circ, 25^\circ$, i.e. where the invariant mass squared s' is shifted back onto the Z resonance through initial state hard photon emission [145, 164, 165]. Switching off the resummed QED two-loop corrections in **ALIBABA** and just applying the exponentiated one-loop corrections, however, substantially reduces this discrepancy down to roughly 1 to 2 per cent which decreases to few per mil above typical LEP 2 energies of roughly 160 GeV [164, 165]. Repeating these comparisons for similarly strong s' -cuts instead, shows an agreement of better than one per cent which does not depend on higher order corrections [145, 164, 165] and also observed by [123, 150, 155]. These findings are summarized in Fig. 3.2 to 3.10 in Chapter 3.

The studies conducted here show that higher order photonic corrections, in particular the $O(\alpha^2)$ hard photon initial state contribution together with a correct resumming of soft and virtual photons for an acollinearity cut seem to be the major underlying cause for the observed discrepancies [134, 154]. Analytically, an exact soft and virtual photon exponentiation procedure is only known for an s' -cut [35, 58, 59, 62], so an approximation has to be used for the semi-analytical approach in **ZFITTER** [36, 38] for an acollinearity cut. The resummation is done here with an effective s' -cut which removes the bulk of the hard photon effects but does not take into account some higher order hard photonic contributions, still allowed by the phase space with acollinearity cut. So, while this procedure exactly reproduces the first order results, higher order photonic corrections are only approximately described for the acollinearity cut.

This explains the large deviations of codes at energies, where the Z radiative return is approximately prevented because here a very delicate removal of hard photons has to occur by the applied cut which cannot be done exactly for the higher order terms in **ZFITTER**. Around the Z boson resonance, however, hard photon emission is strongly suppressed due to the resonant Born term, resulting there in the better than per mil agreement with other numerical codes. Since the acollinearity cut is not so effective in preventing the radiative return to the Z as the s' -cut, these deviations also survive more profoundly for the acollinearity cut at higher energies than for the s' -cut.

With this work being done in the finishing phase of LEP, it is of course interesting to ask how the predictions of the codes look like when going to higher energies at a future e^+e^- Linear Collider (LC) as e.g. the TESLA project [192]. The overall outcome of our analysis for the LC [166] is that the codes **ZFITTER**, **TOPAZ0**, and **KK2f** deviate with initial state bremsstrahlung not worse than 5 per mil, with a better than per mil agreement exactly at the Z peak as reference point. This was achieved for strong hard photon cuts using the default settings of the code. The agreement deteriorated slightly with increasing s' -cut value, but stayed

within a ± 5 per mil margin. The comparison included different resummed higher order corrections, up to three-loop order [35, 62, 120]. Final state bremsstrahlung was also taken into account, but cuts had no considerable effects here. The same is true for QED initial state pair creation [123, 155] contained in **ZFITTER** [38] and **TOPAZ0** [131] but not in **KK2f** [136]. The effects always stayed below the 1 to 2 per mil level.

Including the QED initial-final state interference did not change these observations for the **ZFITTER** – **TOPAZ0** comparison but led to an increase of the discrepancies with **KK2f** up to 1 per cent. This is due to an additional exponentiation of the soft interference terms which is available for **KK2f** [134, 154], but not for the other two codes. This is a clear indication that codes like **ZFITTER** and **TOPAZ0** may have to include higher order corrections from the QED interference considering its increasing importance at higher energies. An exponentiation of the soft photon terms could be done straightforwardly [35]. A recent comparison at the LEP 2 Monte-Carlo Workshop [193] using the full possibilities of **KK2f** as Monte-Carlo event generator even showed e.g. a better than 2 per mil agreement at $\sqrt{s} = 189$ GeV for **KK2f** and a quickly modified version of **ZFITTER** in which the soft QED interference terms were resummed. All results were combined in Fig. 4.1 and Fig. 4.2 in Chapter 4.

Computing time is also an important issue which one has to reconcile when the programs shall be utilized for quick data-fitting routines: While **ZFITTER** needs few seconds for 30 cross section values on a typical HP-UX workstation or PC, **TOPAZ0** calculates roughly 30 minutes for the same amount of numbers, and **KKf** needs 1 or 2 days [166]. The advantages of the slower numerical programs on the other hand can be clearly seen in the possibility of calculating multi-differential observables, including more complex kinematical cuts, helicities, or resummed QED interference corrections. These issues can only be treated in a very limited way by **ZFITTER** due to its semi-analytical approach, so the code should be considered complementary to other numerical programs [156].

Outlook

Updates to the QED part of *ZFITTER*

Thinking of an upgrade of the **ZFITTER** code for later applications, we discussed in Chapter 4 two different options for which the **ZFITTER** code be used at an e^+e^- Linear Collider (LC): First, precision physics could again be performed on the Z boson resonance, but this time in a very high-luminosity mode at the LC, to indirectly search e.g. for Higgs and supersymmetric particles. Secondly, particle searches at TeV scale energies will also need a precise and fast numerical evaluation of cross sections with all theoretically available radiative corrections.

On the Z boson resonance, we have shown that the present level of agreement between codes like **ZFITTER**, **TOPAZ0**, and **KK2f** for cross section predictions is now better than 10^{-4} itself and better than 0.3×10^{-3} for $\sqrt{s} = M_Z \pm 3$ GeV and therefore quite satisfactory in comparison with the present experimental accuracies there. With a possible later Giga Z option at a LC, experimental accuracies could increase by a factor of 100 or more and then a re-analysis of higher order predictions with kinematical cuts by the codes would become necessary.

At energies up to roughly 800 GeV like for the *Tesla project* [182], of course, issues like experimental and theoretical precisions are still quite vague, but it is clear that the demands on 2-fermion codes will be quite challenging due to higher energies, higher luminosities, and more refined analysis techniques compared to the LEP/SLC situation. On the one hand, for example, electroweak and QED corrections become equally important which may demand a critical look at the numerical validity of the effective Born approach at higher energies. On the other hand, higher order QED corrections will also grow in importance with increasing energies. Just to give an impression what might lie ahead in the near future on updates for the semi-analytical program **ZFITTER** concerning its QED branch, some examples have been listed below:

- For the forward-backward asymmetries A_{FB} still the leading logarithmic $O(\alpha^2)$ corrections for initial state pair creation have to be determined and included in the code.
- Already at LEP 2 energies an exponentiation of the soft and virtual interference part in **ZFITTER** appears necessary in case of no or only loose cuts [193]. The corresponding formulae for the one-loop case with cuts on s' and $\cos\vartheta$ are already available [35].
- In order to account for incoherent higher order corrections from final state leptonic or hadronic pair emission [155], a merger between programs **ZFITTER** and **GENTLE** [194] would be a convenient first approach.
- The Bhabha scattering case is has to be correctly dealt with, analytically and numerically in **ZFITTER**, for an acollinearity cut. This is even more important due to the high statistics of this channel or considering applications like small-angle Bhabha scattering for high-precision luminosity measurements. The formulae presented in this dissertation can be directly applied to the s -channel part, while the t -channel and s - t -interference terms with their different angular dependence still have to be calculated. For this, especially the treatment of mass singularities and the phase-space splitting procedure presented here for the s -channel case would be a helpful guideline.
- Further options like the inclusion of beamstrahlung effects, already contained in some Monte-Carlo programs [156] are also thinkable for **ZFITTER**

in order to obtain results for more realistic, experimental set-ups.

All of this, of course, will have to go hand-in-hand with further comparisons between codes `ZFITTER`, `TOPAZO`, `KK2f`, `ALIBABA`, and other programs. Only then can one hope to guarantee the correctness and accuracy of the analytical and numerical results and meet the experimental precision demands.

Top pair production at LC energies

One very interesting topic for the LC is top pair production above $\sqrt{s} \approx 350$ GeV [195], with real and virtual radiative corrections including final state mass effects and will have to be treated accurately by the codes, at least sufficiently above the threshold region. The correct inclusion of mass effects is crucial here. `SM` and `MSSM` calculations to $e^+e^- \rightarrow t\bar{t}$ with final state masses and virtual and real QED [196], EW [197], and QCD [198] corrections are already available. But work still has to be done concerning a description in the context of EW form factors or the inclusion of hard QED and QCD bremsstrahlung corrections with final state masses [199]. First preliminary comparisons show some several per cent corrections from hard final state bremsstrahlung close to the threshold region [199].

Possible *beyond-the-SM* applications

Finally, I would like to end our discussion on fermion pair production by giving some interesting possibilities of how one could extend the `ZFITTER` code for applications beyond a `SM` description:

- *Flavor number violation in Z decays:* Numerical branches for the calculation of branching ratios of `SM` flavor changing neutral currents through virtual one-loop corrections with massive quarks and *CKM* mixing in hadronic Z decays like $Z \rightarrow ds$ etc. are feasible. The corresponding extension to the ν `SM` case for non-diagonal leptonic Z decays due to massive neutrinos with neutrino-lepton mixing [190], strongly suggested by recent experimental results [72], would be straightforward. For this, a recent discussion of branching ratios for different scenarios has been done [191].
- *Supersymmetry:* The inclusion of virtual corrections in the *minimal supersymmetric model* (`MSSM`) would be the natural next step in expanding the code also to non-`SM` physics. The complete one-loop results in the `MSSM` together with masses and some two-loop effects are already available [181] and could be implemented straightforwardly with the effective Born approach.

- *Z', W' physics*: Subroutines like ZEFIT [200] calculating cross sections with the exchange of extra heavy gauge bosons, Z' and W' , predicted in certain *GUTs*, already exist. This could be refined having different models, higher center-of-mass energies, etc. in mind.
- *Quantum gravity effects above the electroweak scale*: Recently, possible effects by the exchange of spin-2 bosons in pair-production processes, especially on angular cross section distributions have been examined in [188]. This is motivated by string-inspired models which may allow effects of *extra dimensions* at TeV energy scales. For this, only the Born level part of ZFITTER would have to be extended.

These are just a few issues which could be addressed in the not so far future for the existing ZFITTER code. It also illustrates the still rich predictive power on *New Physics* scenarios when looking at the classical fermion pair production channel.

At the beginning of LEP 1 or SLC data taking, the precision of the codes had been sufficient, due to the lower experimental statistics then and the hard QED corrections being strongly suppressed at the Z peak. The increased experimental accuracy now demands a precise, better than per-mil determination of QED bremsstrahlung in the resonance region. This is now guaranteed for the semi-analytical code ZFITTER with the new results. The new formulae pose a realistic alternative to a kinematically simpler s' -cut for leptonic final states and are a direct generalization of the up-to-now known analytical results including cuts.

Also for LEP 2 and especially for later LC energies and luminosities one is for example interested in removing a disturbing radiative return to the Z boson through hard photon emission when searching for *New Physics* effects. For this, hard photon effects have to be known accurately with kinematical cuts. The new results derived in this dissertation finally form an important contribution in the larger framework of precision tests to the SM or for *New Physics* searches performed at present or future e^+e^- collider experiments.

Appendix A

Cross Sections and Phase Space

A.1 Feynman diagrams and matrix element

The real photon emission from the initial and final state of s -channel processes $e^+e^- \rightarrow \bar{f}f$ is described by the two Feynman diagrams depicted in the Fig. A.1.

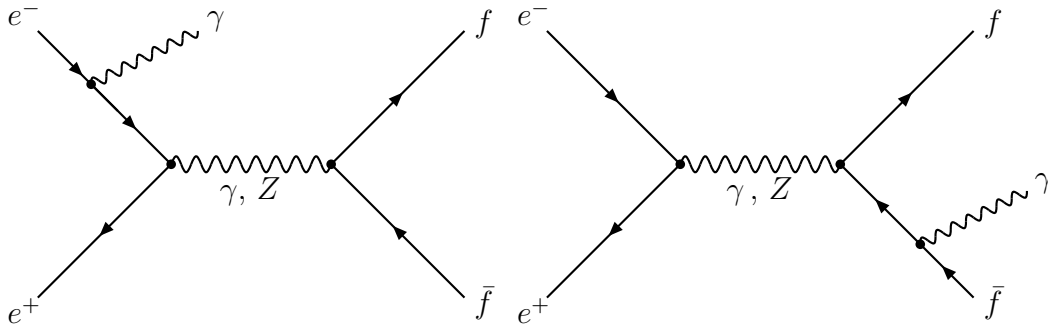


Figure A.1: Examples of Feynman diagrams for real photon initial and final state radiation.

The four-momenta of the 5 particles are denoted as $k_{1,2}$ for $e^-, +$, $p_{1,2}$ for f, \bar{f} and p for the photon γ . The c.m. energy is designated as $s := (k_1 + k_2)^2$ and the electron and fermion masses as m_e, m_f . The corresponding S -matrix element \mathcal{M} for the scattering processes $e^+e^- \rightarrow \bar{f}f$ with $O(\alpha)$ initial and final state real *bremsstrahlung* is:

$$\mathcal{M} = (2\pi)^4 \delta^{(4)}(k_1 + k_2 - p_1 - p_2 - p) \frac{M_{ini} + M_{fin}}{(2\pi)^6 (2\pi)^{3/2} (2k_1^0 2k_2^0 2p_1^0 2p_2^0 2p^0)^{1/2}}. \quad (\text{A.1})$$

The Born S -matrix element is:

$$\mathcal{M}^{Born} = (2\pi)^4 \delta^{(4)}(k_1 + k_2 - p_1 - p_2) \frac{M^{Born}}{(2\pi)^6 (2k_1^0 2k_2^0 2p_1^0 2p_2^0)^{1/2}}, \quad (\text{A.2})$$

The current structure for these amplitudes M_{ini} , M_{fin} , and M^{Born} is given below:

$$M^{Born} = i e^2 \frac{1}{s} \left(Q_e Q_f J_e^\mu(\gamma) J_{f\mu}(\gamma) + \chi_Z(s) J_e^\mu(Z) J_{f\mu}(Z) \right), \quad (\text{A.3})$$

$$M_{ini} = i e^3 \frac{Q_e \epsilon_\alpha}{s'} \left(Q_e Q_f I^{\mu,\alpha}(\gamma) J_{f\mu}(\gamma) + \chi_Z(s') I^{\mu,\alpha}(Z) J_{f\mu}(Z) \right), \quad (\text{A.4})$$

$$M_{fin} = i e^3 \frac{Q_f \epsilon_\alpha}{s} \left(Q_e Q_f J_e^\mu(\gamma) F_\mu^\alpha(\gamma) + \chi_Z(s) J_e^\mu(Z) F_\mu^\alpha(Z) \right). \quad (\text{A.5})$$

The vector ϵ_α denotes the photon polarization vector. Q_e and Q_f are the charges of the initial electron, $Q_e = -1$, and final state fermion f . The Z boson propagator $\chi_Z(s)$ and the weak neutral current couplings v_e , v_f , a_e , and a_f are defined as:

$$\chi_Z(s) = \chi(s) \equiv \kappa \frac{s}{s - M_Z^2 + i \frac{s}{M_Z} \Gamma_Z}, \quad (\text{A.6})$$

$$\kappa = \frac{g^2}{4e^2 \cos^2 \theta_W} = \frac{1}{4 \sin^2 \theta_W \cos^2 \theta_W} = \frac{G_\mu}{\sqrt{2}} \frac{M_Z^2}{2\pi\alpha}, \quad (\text{A.7})$$

$$v_e = -\frac{1}{2} + 2 \sin^2 \theta_W, \quad a_e = -\frac{1}{2}, \quad (\text{A.8})$$

$$v_f = I_3^f - 2Q_f \sin^2 \theta_W, \quad a_f = I_3^f. \quad (\text{A.9})$$

The values M_Z and Γ_Z are the Z boson mass and width. The currents for real photon emission from the initial state, $I^{\mu,\alpha}(\gamma)$ and $I^{\mu,\alpha}(Z)$, and from the final state $F_\mu^\alpha(\gamma)$ and $F_\mu^\alpha(Z)$ are given below together with the Born terms, $J_e^\mu(\gamma)$, $J_e^\mu(Z)$, $J_{f\mu}(\gamma)$, and $J_{f\mu}(Z)$:

$$I^{\mu,\alpha}(\gamma) = \bar{u}(-k_2) \left[\frac{2k_2^\alpha - \gamma^\alpha \not{p}}{Z_2} \gamma^\mu - \gamma^\mu \frac{2k_1^\alpha - \not{p} \gamma^\alpha}{Z_1} \right] u(k_1), \quad (\text{A.10})$$

$$I^{\mu,\alpha}(Z) = \bar{u}(-k_2) \left[\frac{2k_2^\alpha - \gamma^\alpha \not{p}}{Z_2} \gamma^\mu (v_e + a_e \gamma_5) - \gamma^\mu (v_e + a_e \gamma_5) \frac{2k_1^\alpha - \not{p} \gamma^\alpha}{Z_1} \right] u(k_1), \quad (\text{A.11})$$

$$F_\mu^\alpha(\gamma) = \bar{u}(p_1) \left[\frac{2p_1^\alpha + \gamma^\alpha \not{p}}{V_1} \gamma_\mu - \gamma_\mu \frac{2p_2^\alpha + \not{p} \gamma^\alpha}{V_2} \right] u(-p_2), \quad (\text{A.12})$$

$$F_\mu^\alpha(Z) = \bar{u}(p_1) \left[\frac{2p_1^\alpha + \gamma^\alpha \not{p}}{V_1} \gamma_\mu (v_f + a_f \gamma_5) - \gamma_\mu (v_f + a_f \gamma_5) \frac{2p_2^\alpha + \not{p} \gamma^\alpha}{V_2} \right] u(-p_2). \quad (\text{A.13})$$

$$J_e^\mu(\gamma) = \bar{u}(-k_2) \gamma^\mu u(k_1), \quad (\text{A.14})$$

$$J_e^\mu(Z) = \bar{u}(-k_2) \gamma^\mu (v_e + a_e \gamma_5) u(k_1), \quad (\text{A.15})$$

$$J_{f\mu}(\gamma) = \bar{u}(p_1) \gamma_\mu u(-p_2), \quad (\text{A.16})$$

$$J_{f\mu}(Z) = \bar{u}(p_1) \gamma_\mu (v_f + a_f \gamma_5) u(-p_2). \quad (\text{A.17})$$

For brevity, in order to have a compact illustration of the amplitudes, the initial and final state masses m_e and m_f have been neglected in (A.4) to (A.3). In the later calculation they will, however, be correctly considered.

For the calculation of the matrix element there are the following important invariants for the QED corrected scattering process given in (A.10) to (A.17):

$$s := (k_1 + k_2)^2 = 2k_1 k_2 + 2m_e^2, \quad (\text{A.18})$$

$$s' := (p_1 + p_2)^2 = 2p_1 p_2 + 2m_f^2, \quad (\text{A.19})$$

$$Z_1 := 2pk_1 = -[(k_1 - p)^2 - m_e^2], \quad (\text{A.20})$$

$$Z_2 := 2pk_2 = -[(k_2 - p)^2 - m_e^2], \quad (\text{A.21})$$

$$V_1 := 2pp_1 = [(p_1 + p)^2 - m_f^2], \quad (\text{A.22})$$

$$V_2 := 2pp_2 = [(p_2 + p)^2 - m_f^2]. \quad (\text{A.23})$$

Using total four-momentum conservation one arrives at the following important relations between these invariants:

$$\left. \begin{aligned} s &= (p_1 + p_2 + p)^2 = s' + V_1 + V_2 \\ s' &= (k_1 + k_2 - p)^2 = s - Z_1 - Z_2 \end{aligned} \right\} \rightarrow Z_1 + Z_2 = V_1 + V_2 = s - s'. \quad (\text{A.24})$$

We define the invariants λ_s , λ_1 , λ_2 , and λ_p with $k \equiv k_1 + k_2$:

$$\lambda_s = \lambda(k^2, k_1^2, k_2^2) = s^2 - 4sm_e^2 = s^2 \beta_0^2, \quad (\text{A.25})$$

$$\lambda_1 = \lambda([k - p_1]^2, k^2, p_1^2) = (s - V_2)^2 - 4sm_f^2, \quad (\text{A.26})$$

$$\lambda_2 = \lambda([k - p_2]^2, k^2, p_2^2) = (s' + V_2)^2 - 4sm_f^2, \quad (\text{A.27})$$

$$\lambda_p = \lambda([k-p]^2, k^2, p^2) = (s-s')^2, \quad (\text{A.28})$$

$$\text{with} \quad \lambda = \lambda(x, y, z) = x^2 + y^2 + z^2 - 2xy - 2xz - 2yz. \quad (\text{A.29})$$

We will also need the invariants:

$$T = 2 k_1 \cdot p_2 = \frac{1}{2} \left(s' + V_2 + \beta_0 \sqrt{\lambda_2} \cos \vartheta \right), \quad (\text{A.30})$$

$$U = 2 k_2 \cdot p_2 = \frac{1}{2} \left(s' + V_2 - \beta_0 \sqrt{\lambda_2} \cos \vartheta \right). \quad (\text{A.31})$$

The differential cross sections to the bremsstrahlung and Born matrix elements have the form:

$$d\sigma^{Born} = \frac{1}{j} (2\pi)^4 \delta^{(4)}(k_1 + k_2 - p_1 - p_2) \frac{1}{4} \frac{\sum_{spin} |M^{Born}|^2}{(2\pi)^{12} 2k_1^0 2k_2^0 2p_1^0 2p_2^0} \cdot d^3\vec{p}_1 d^3\vec{p}_2, \quad (\text{A.32})$$

$$d\sigma = \frac{1}{j} (2\pi)^4 \delta^{(4)}(k_1 + k_2 - p_1 - p_2 - p) \frac{1}{4} \frac{\sum_{spin} |M|^2}{(2\pi)^{15} 2k_1^0 2k_2^0 2p_1^0 2p_2^0 2p^0} \cdot d^3\vec{p}_1 d^3\vec{p}_2 d^3\vec{p}, \quad (\text{A.33})$$

where the flux of the initial particles is:

$$j = \frac{\sqrt{(k_1 \cdot k_2)^2 - m_e^4}}{2(2\pi)^6 k_1^0 k_2^0} = \frac{s\beta_0}{(2\pi)^6 2k_1^0 k_2^0}, \quad \beta_0 = \sqrt{1 - \frac{4m_e^2}{s}}. \quad (\text{A.34})$$

With (A.32), (A.33), and (A.34) the differential cross-sections can therefore finally be written in the form:

$$d\sigma^{Born} = \frac{1}{4} \frac{\sum_{spin} |M^{Born}|^2}{2s\beta_0} d\Gamma^{(2)}, \quad (\text{A.35})$$

$$d\sigma = \frac{1}{4} \frac{\sum_{spin} |M|^2}{2s\beta_0} d\Gamma^{(3)}, \quad (\text{A.36})$$

where $d\Gamma^{(2)}$ and $d\Gamma^{(3)}$ are the two- and three-particle differential phase space volumes of the outgoing particles respectively.

$$d\Gamma^{(2)} = (2\pi)^4 \delta^{(4)}(k_1 + k_2 - p_1 - p_2) \frac{d^3\vec{p}_1}{(2\pi)^3 2p_1^0} \frac{d^3\vec{p}_2}{(2\pi)^3 2p_2^0}, \quad (\text{A.37})$$

$$d\Gamma^{(3)} = (2\pi)^4 \delta^{(4)}(k_1 + k_2 - p_1 - p_2 - p) \frac{d^3\vec{p}_1}{(2\pi)^3 2p_1^0} \frac{d^3\vec{p}_2}{(2\pi)^3 2p_2^0} \frac{d^3\vec{p}}{(2\pi)^3 2p^0}. \quad (\text{A.38})$$

A.2 Kinematics

Angles of phase space

The main objective of this discussion is to calculate the contributions of the $O(\alpha)$ hard bremsstrahlung corrections to cross section observables for fermion pair production processes $e^+e^- \rightarrow \bar{f}f$, $f \neq e, \nu_e$. The first order soft and virtual photonic corrections are then added to derive finite and physical results for the inclusive processes $e^+e^- \rightarrow \bar{f}f(\gamma)$. Leading effects from multiple soft and virtual photon emission can be included straightforwardly in our flux function description; see also (0.4) and (2.41).

We are interested in different kinematical cuts, which includes a cut on the maximal *acollinearity angle* of the two final state fermions. The acollinearity angle $\xi \equiv \theta_{\text{acol}}$ of the two final state fermions is depicted in Fig. A.2. The directions of motion of the initial state electron and positron in the center-of-mass system (c.m.s.) define the beam axis. In case of the emission of an energetic photon

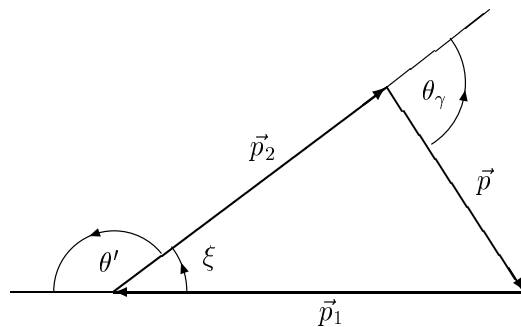


Figure A.2: Acollinearity angle $\xi \equiv \theta_{\text{acol}}$.

from the initial or final state, the final state fermions will not move back-to-back anymore due to four-momentum conservation, but will be acollinear. The acollinearity angle can be reexpressed by the fermionic polar angle θ' defined in the plane of the two fermions' three-momenta: $\xi := \pi - \theta'$. For the description of the hard photon phase space with acollinearity cut one can also refer to [158] and [69].

The number of independent degrees of freedom for a $2 \rightarrow 3$ scattering process amounts to four taking into account four-momentum conservation, on-shell conditions, and a rotational symmetry of the scattering process around the beam axis in the c.m.s. Having in mind a cut on the maximal acollinearity angle, one can use the following independent kinematic variables to parameterize the total phase space:

- $s' := (p_1 + p_2)^2$ as invariant mass squared of the fermion pair,
- $\cos \vartheta$ as cosine of the scattering angle of \bar{f} with respect to the e^- beam axis in the c.m.s.,
- $\cos \theta_\gamma$ as cosine of the polar angle between the three-momenta of \bar{f} and the photon in the c.m.s.,
- φ_γ as azimuthal angle of the photon in the rest frame of (f, γ) (z -axis defined by \vec{p}_2 of \bar{f} in the c.m.s.).

The different angles of phase space are shown in Fig. A.3.

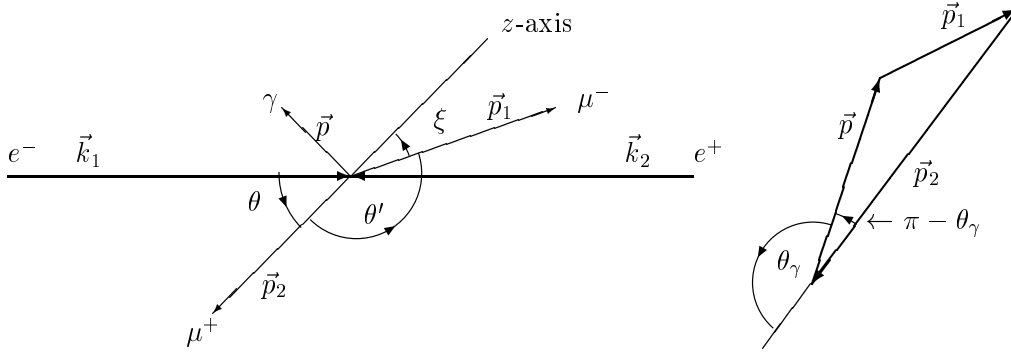


Figure A.3: Angles of phase space and photon angle θ_γ .

For brevity, we will from now on use the notation ξ during the calculations for the acollinearity angle.

Energies and three-momenta

The energies and three-momenta in the c.m.s. can now be extracted easily from the invariants in (A.25) to (A.28) using four-momenta conservation and the on-shell conditions. For the energy component q^0 and the three-momentum \vec{q} of an arbitrary 4-momentum q in the c.m.s. with $\vec{k} = \vec{k}_1 + \vec{k}_2 = 0$, it holds:

$$2k^0 q^0 = 2kq \quad \longrightarrow \quad q^0 = \frac{2kq}{2k^0} = \pm \frac{(k \pm q)^2 - k^2 - q^2}{2k^0}, \quad (\text{A.39})$$

$$|\vec{q}| = \sqrt{(q^0)^2 - q^2} = \frac{\sqrt{\lambda([k \pm q]^2, k^2, q^2)}}{2k_0}. \quad (\text{A.40})$$

We can therefore derive with (A.18) to (A.21) and λ_s , λ_1 , λ_2 , and λ_p defined in (A.25) to (A.28):

$$k_1^0 = k_2^0 = \frac{\sqrt{s}}{2}, \quad |\vec{k}_1| = |\vec{k}_2| = \frac{1}{2}\sqrt{s - 4m_e^2}, \quad (\text{A.41})$$

$$p^0 = \frac{s - s'}{2\sqrt{s}}, \quad |\vec{p}| = \frac{\sqrt{\lambda_p}}{2\sqrt{s}}, \quad (\text{A.42})$$

$$p_1^0 = \frac{s - V_2}{2\sqrt{s}}, \quad |\vec{p}_1| = \frac{\sqrt{\lambda_1}}{2\sqrt{s}}, \quad (\text{A.43})$$

$$p_2^0 = \frac{s' + V_2}{2\sqrt{s}}, \quad |\vec{p}_2| = \frac{\sqrt{\lambda_2}}{2\sqrt{s}}. \quad (\text{A.44})$$

A.3 The three-particle phase space with acollinearity cut

Kinematical constraints

For a separation of the two phase space regions for soft and hard photon emission one generally introduces an arbitrary parameter ε in order to integrate over vanishing, $p^0 < \varepsilon$, or sufficiently energetic photon momenta, $p^0 \geq \varepsilon$. The parameter ε is unphysical and has to cancel in physical quantities when combining the soft and virtual corrections with the hard photonic contributions. Together with the kinematically minimally allowed s' value this gives the following bounds on s' for the hard photon phase space:

$$4m_f^2 \leq s' \leq s(1 - \varepsilon). \quad (\text{A.45})$$

Furthermore, with (A.41) to (A.42) it is straightforward to express $\cos \theta_\gamma$ as function of the invariants s , s' , and V_2 :

$$\cos \theta_\gamma = \frac{|\vec{p}_1|^2 - |\vec{p}_2|^2 - |\vec{p}|^2}{2|\vec{p}_1||\vec{p}_2|} = \frac{\lambda_1 - \lambda_2 - \lambda_p}{2\sqrt{\lambda_p\lambda_2}}. \quad (\text{A.46})$$

From (A.46) we gain a limiting condition on the kinematically maximally accessible phase space:

$$\sin^2 \theta_\gamma = \frac{\lambda(\lambda_1, \lambda_2, \lambda_p)}{4\lambda_2\lambda_p} \geq 0 \quad \longrightarrow \quad \lambda(\lambda_1, \lambda_2, \lambda_p) \geq 0, \quad (\text{A.47})$$

$$4\lambda_2\lambda_p - (\lambda_1 - \lambda_2 - \lambda_p)^2 \geq 0. \quad (\text{A.48})$$

Thus we have the following combined kinematical constraint for the variables s' and V_2 :

$$V_2^{\min}(s') \leq V_2 \leq V_2^{\max}(s') \quad (\text{A.49})$$

with

$$V_2^{\max, \min}(s') = \frac{s - s'}{2} (1 \pm \beta), \quad \beta = \beta(s') := \sqrt{1 - \frac{4m_f^2}{s'}}. \quad (\text{A.50})$$

The differential phase space volume

The differential phase space volume $d\Gamma^{(3)}$ of a three-particle final state was given in (A.38):

$$d\Gamma = (2\pi)^4 \frac{d^3\vec{p}_1}{(2\pi)^3 2p_1^0} \frac{d^3\vec{p}_2}{(2\pi)^3 2p_2^0} \frac{d^3\vec{p}}{(2\pi)^3 2p^0} \delta^4(\underbrace{k_1 + k_2}_{=k_{12}} \underbrace{-p_1 - p_2}_{=-p_{12}} - p) \quad (\text{A.51})$$

$$= (2\pi)^{-5} d^4p_1 \delta(p_1^2 - m^2) d^4p_2 \delta(p_2^2 - m^2) d^4p \delta(p^2) \delta^4(k_{12} - p_{12} - p). \quad (\text{A.52})$$

When transforming the differentials of the four-momenta into those of the independent variables s' , $\cos\vartheta$, $\cos\theta_\gamma$, and φ_γ , it is convenient to separate the three-particle phase space into the two-particle phase spaces of two subsystems: We chose one fermion and the photon, f and γ , in their rest frame as one subsystem and boost it in the center-of-mass system, with the anti-fermion \bar{f} and this subsystem creating the second subsystem. This choice of subsystems is given by the definition of the photon angle θ_γ with respect to the direction of motion of the anti-fermion \bar{f} (Fig. A.3).

We therefore have the following separation of the three-particle phase space

$$d\Gamma^{(3)} = \frac{dM_{f\gamma}^2}{2\pi} d\Gamma_I^{(2)} d\Gamma_{II}^{(2)}, \quad (\text{A.53})$$

into the two-particle phase spaces

$$\text{I.} \quad d\Gamma_I^{(2)} = \frac{1}{(2\pi)^2} d^4P \delta(P^2 - M_{f\gamma}^2) d^4p_2 \delta(p_2^2 - m^2) \delta^4(k_1 + k_2 - P - p_2), \quad (\text{A.54})$$

$$\text{II.} \quad d\Gamma_{II}^{(2)} = \frac{1}{(2\pi)^2} d^4p_1 \delta(p_1^2 - m^2) d^4p \delta(p^2) \delta^4(P - p - p_1), \quad (\text{A.55})$$

after inserting

$$1 = d^4P \delta^4(P - p_1 - p) dM_{f\gamma}^2 \delta(P^2 - M_{f\gamma}^2) \quad (\text{A.56})$$

into (A.51) and using

$$\begin{aligned} & \delta^4(k_1 + k_2 - p - p_1 - p_2) \delta^4(P - p - p_1) \\ &= \delta^4(k_1 + k_2 - P - p_2) \delta^4(P - p - p_1). \end{aligned} \quad (\text{A.57})$$

The value $M_{f\gamma}^2 := P^2$ is the invariant mass squared of the fermion-photon subsystem (f, γ) with $P := p + p_1 = k_1 + k_2 - p_2$.

The integration of $d\Gamma_I$ and $d\Gamma_{II}$ can now be done by inserting the invariants (A.22) to (A.21) into (A.54) and (A.55) and using the on-shell conditions and four-momentum conservation defined by the δ -distributions. Starting with $d\Gamma_I$, we have:

$$\begin{aligned} d\Gamma_I^{(2)} &= \frac{1}{(2\pi)^2} d^4 p_2 \delta(p_2^2 - m_f^2) \delta((k_1 + k_2 - p_2)^2 - M_{f\gamma}^2) \\ &= \frac{1}{(2\pi)^2} \frac{|\vec{p}_2| dp_2^0}{2} \delta(s' + V_2 - 2\sqrt{s} p_2^0) d\Omega_{\vec{p}_2}, \quad d\Omega_{\vec{p}_2} = 2\pi d\cos\vartheta, \end{aligned} \quad (\text{A.58})$$

$$\rightarrow \quad d\Gamma_I^{(2)} = \frac{1}{2\pi} \frac{\sqrt{\lambda_2}}{8s} d\cos\vartheta \quad \text{with} \quad \lambda_2 = (s' + V_2)^2 - 4m^2 s^2. \quad (\text{A.59})$$

The relation (A.58) was obtained using the rotational symmetry around the beam axis and the on-shell condition $p_2^{0^2} = |\vec{p}_2|^2 + m_f^2$, which leads to $2p_2^0 dp_2^0 = 2|\vec{p}_2| d|\vec{p}_2|$. Similarly, we can treat $d\Gamma_{II}$:

$$\begin{aligned} d\Gamma_{II}^{(2)} &= \frac{1}{(2\pi)^2} d^4 p \delta(p^2) \delta((P - p)^2 - m_f^2) \\ &= \frac{1}{(2\pi)^2} \frac{|\vec{p}| dp^0}{2} \delta(s - s' - 2\sqrt{s} p^0) d\Omega_{\vec{p}}, \quad d\Omega_{\vec{p}} = d\varphi_\gamma d\cos\theta_\gamma, \end{aligned} \quad (\text{A.60})$$

$$\rightarrow \quad d\Gamma_{II}^{(2)} = \frac{1}{(2\pi)^2} \frac{\sqrt{\lambda_p}}{8s} d\varphi_\gamma d\cos\theta_\gamma. \quad (\text{A.61})$$

Combining the results of (A.59) and (A.61) in (A.53) delivers the complete differential phase space volume in the independent variables φ_γ , $\cos\theta_\gamma$, $M_{f\gamma}^2$, and $\cos\vartheta$:

$$d\Gamma^{(3)} = \frac{1}{(2\pi)^4} \frac{\sqrt{\lambda_2 \lambda_p}}{(8s)^2} d\varphi_\gamma d\cos\theta_\gamma dM_{f\gamma}^2 d\cos\vartheta. \quad (\text{A.62})$$

We have in mind a description of the QED bremsstrahlung effects to cross sections by flux functions which are convoluted over the final state fermions' invariant

mass squared s' with effective Born observables. For this, one can make the substitution:

$$M_{f\gamma}^2, \quad \cos \theta_\gamma \quad \longrightarrow \quad s', \quad V_2, \quad (\text{A.63})$$

with the two independent variables s' and V_2 which depends linearly on $\cos \theta_\gamma$. Introducing V_2 as a new variable of integration will also prove to be appropriate when applying a cut on the maximal acollinearity of the final state fermions. Using the relations

$$M_{f\gamma}^2 = (p_1 + p)^2 = -s' - V_2 + s + m_f^2, \quad (\text{A.64})$$

$$V_2 = 2pp_2 = 2p^0(p_2^0 - \sqrt{p_2^{02} - m_f^2} \cos \theta_\gamma), \quad (\text{A.65})$$

and expressing p^0 and p_2^0 by their invariant expressions according to (A.42) and (A.44), this finally delivers as differential phase volume in the new variables:

$$\rightarrow d\Gamma^{(3)} = \frac{1}{(2\pi)^5} \frac{\pi}{16s} d\varphi_\gamma dV_2 ds' d\cos \vartheta \quad (\text{A.66})$$

$$= \frac{1}{2} \frac{s}{(4\pi)^4} d\varphi_\gamma d\left(\frac{V_2}{s}\right) d\left(\frac{s'}{s}\right) d\cos \vartheta \quad (\text{A.67})$$

$$= \frac{1}{2} \frac{s}{(4\pi)^4} d\varphi_\gamma dx dR d\cos \vartheta. \quad (\text{A.68})$$

In (A.66) to (A.68) we have introduced for the later calculation the more suitable dimensionless variables

$$R \equiv \frac{s'}{s} \quad \text{and} \quad x \equiv \frac{V_2}{s}. \quad (\text{A.69})$$

Before calculating cross section observables with (A.36) and (A.66), the constraints onto the integration variables R , x , $\cos \vartheta$, and φ_γ , introduced by the kinematical cuts considered, have to be determined.

Kinematical cuts and limits of integration

The different kinematical cuts which shall be treated are stated below. They will not affect the azimuthal photon angle φ_γ . It will be integrated over the complete angular range:

$$\varphi_\gamma \in [0; 2\pi]. \quad (\text{A.70})$$

The kinematical boundaries defined by the cuts are also shown in Fig. 2.4 and Fig. A.4 below.

1. Cuts on the minimal and maximal scattering angle $\cos \vartheta$ (acceptance cut):

$$-c \leq \cos \vartheta \leq c. \quad (\text{A.71})$$

2. A cut on the minimal fermion energies:

For simplicity, equal cuts are applied on the minimal fermion energies $E_{\min} = E_{\min}^{f, \bar{f}}$. With (A.43) and (A.44) we obtain for the variable x kinematical limits depending on R :

$$\left. \begin{array}{l} \text{For } f : p_1^0 \geq E_{\min} \quad , \quad p_1^0 = \frac{s - V_2}{2\sqrt{s}} \\ \text{For } \bar{f} : p_2^0 \geq E_{\min} \quad , \quad p_2^0 = \frac{s' + V_2}{2\sqrt{s}} \end{array} \right\} \longrightarrow \quad (\text{A.72})$$

$$R_E - R \leq x \leq 1 - R_E, \quad R_E = \frac{2E_{\min}}{\sqrt{s}}. \quad (\text{A.73})$$

The upper and lower bounds on x defined in (A.72) intersect with the kinematical boundaries $x^{\min, \max}(R)$, derived in (A.49) ($x \equiv V_2/s$) in a point with the R -value \bar{R}_E :

$$\begin{aligned} \text{I.} \quad & 1 - R_E = x^{\max}(R) = \frac{1}{2}(1 - R)(1 + \beta(R)) \\ \text{II.} \quad & R_E - R = x^{\min}(R) = \frac{1}{2}(1 - R)(1 - \beta(R)), \\ \rightarrow \quad & \bar{R}_E = \frac{2\frac{m_f^2}{s} + (1 - R_E) \left(R_E + \sqrt{R_E^2 - 4\frac{m_f^2}{s}} \right)}{2(1 - R_E + \frac{m_f^2}{s})}. \end{aligned} \quad (\text{A.74})$$

Neglecting final state masses for $m_f^2 \ll s$, we simply have: $\bar{R}_E = R_E$. This automatically also defines a minimally allowed R -value R_{cut} from the minimal energy cut:

$$\max(4m_f^2, R_{\text{cut}}) \leq R \leq 1 - \varepsilon \quad \text{with} \quad R_{\text{cut}} := 2R_E - 1. \quad (\text{A.75})$$

3. A cut on the maximal acollinearity angle ξ :

With $\bar{\xi}$ being a cut on the maximal acollinearity angle ξ of the final state fermions, one can derive in analogy to (A.46), (A.47), and (A.49) a further kinematical boundary for the phase space given by the variables R and x :

$$\begin{aligned} \cos \xi &= \frac{|\vec{p}_1|^2 + |\vec{p}_2|^2 - |\vec{p}|^2}{2|\vec{p}_1||\vec{p}_2|} = \frac{\lambda_1 + \lambda_2 - \lambda_p}{2\sqrt{\lambda_1\lambda_2}} \\ \rightarrow \quad \sin^2 \frac{\bar{\xi}}{2} &\geq \sin^2 \frac{\xi}{2} = \frac{1}{2}(1 - \cos \xi) = \frac{\lambda_p - (\sqrt{\lambda_1} - \sqrt{\lambda_2})^2}{4\sqrt{\lambda_1\lambda_2}}. \end{aligned} \quad (\text{A.76})$$

This yields in terms of x , R , and $\bar{\xi}$ the relation ($m_f^2 \ll s$):

$$\cos^2 \frac{\bar{\xi}}{2} x^2 - \cos^2 \frac{\bar{\xi}}{2} (1 - R) x + \sin^2 \frac{\bar{\xi}}{2} R \geq 0. \quad (\text{A.77})$$

Solving relation (A.77) for R , we receive the following curve $R^{\min}(x)$ for minimal values of R depending on the second variable x :

$$R \geq R^{\min}(x) := \frac{x(1-x)(1 - \sin^2 \frac{\bar{\xi}}{2})}{x + (1-x) \sin^2 \frac{\bar{\xi}}{2}}. \quad (\text{A.78})$$

This can be translated equivalently into a minimal and a maximal bound on x depending on R . That we have either

$$x \leq x_{\xi}^{\min}(R) \quad \text{or} \quad x \geq x_{\xi}^{\max}(R) \quad \text{for} \quad R \leq R_{\xi}, \quad (\text{A.79})$$

where

$$x_{\xi}^{\max, \min}(R) = \frac{1-R}{2} \left[1 \pm \sqrt{1 - \frac{R}{R_{\xi}} \frac{(1-R_{\xi})^2}{(1-R)^2}} \right], \quad (\text{A.80})$$

if $R \leq R_{\xi}$ where R_{ξ} defines the R -value of the turning point P_t of the acollinearity bound, depicted in Fig. 2.4.

$$R_{\xi} = \frac{1 - \sin(\bar{\xi}/2)}{1 + \sin(\bar{\xi}/2)}, \quad (\text{A.81})$$

$$P_t \equiv [R_t, x_t] = \left[R_{\xi}, \frac{1}{2}(1 - R_{\xi}) \right]. \quad (\text{A.82})$$

For $R > R_{\xi}$, the variable x is limited by the relation in (A.49) with $x \equiv V_2/s$.

4. A cut on the minimal invariant mass squared s' of the fermions:

This cut can be trivially applied in addition to the above mentioned cuts and introduces a new minimum R -value \bar{R} :

$$\max(4m_f^2, R_{\text{cut}}, \bar{R}) \leq R \leq 1 - \varepsilon. \quad (\text{A.83})$$

It is equivalent to a cut on the maximal energy \bar{E}_{γ} of the emitted photon.

$$E_{\gamma} \leq \bar{E}_{\gamma} \quad \leftrightarrow \quad \bar{R} = 1 - \frac{2\bar{E}_{\gamma}}{\sqrt{s}}. \quad (\text{A.84})$$

For the allowed complete phase space region, depending on the numerical values of the cuts, two different cases may arise:

$$R_{\text{cut}} < R_{\xi} \quad \text{or} \quad R_{\text{cut}} \geq R_{\xi}, \quad (\text{A.85})$$

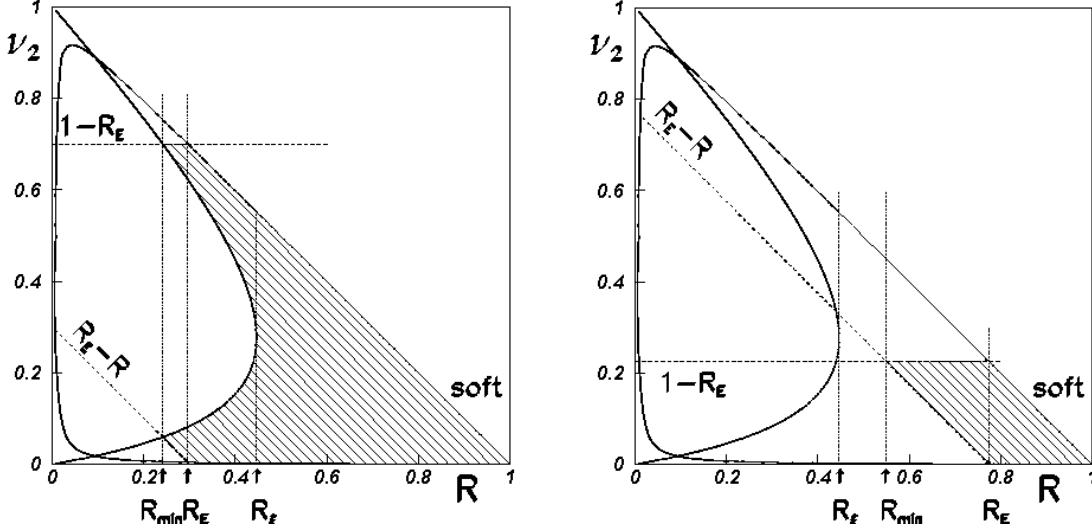


Figure A.4: Phase space with acollinearity cut R_ξ and equal muon energy cuts R_E : a. $R_{cut} < R_\xi$, b. $R_{cut} \geq R_\xi$; $\nu_2 := V_2/s \equiv x$.

where R_{cut} was defined in (A.75). The two corresponding Dalitz plots are shown in Fig. A.4. In the first case, $R_{cut} < R_\xi$, the acollinearity cut has an effect and the absolute minimum of R is given by the R -value of the intersection of the kinematical bounds inflicted by the maximal acollinearity and minimal energy cut.

$$R_{\min} = R_E \left(1 - \frac{\sin^2(\bar{\xi}/2)}{1 - R_E \cos^2(\bar{\xi}/2)} \right). \quad (\text{A.86})$$

The complete phase space $\Gamma = \int d\Gamma^{(3)}$ can then be divided into three parts where each one depends separately on one of the applied cuts:

$$\Gamma = \Gamma_I + \Gamma_{II} - \Gamma_{III} \quad (\text{A.87})$$

$$= \int_{\bar{R}_E}^1 dR \int_{x^{\min}(R)}^{x^{\max}(R)} dx + \int_{R_{\min}}^{\bar{R}_E} dR \int_{R_E-R}^{1-R_E} dx - \int_{R_{\min}}^{R_\xi} dR \int_{x_\xi^{\min}(R)}^{x_\xi^{\max}(R)} dx. \quad (\text{A.88})$$

In the other case, $R_{cut} \geq R_\xi$, the energy cuts are so stringent that the acollinearity cut has no influence. The minimum value of R is

$$R_{\min} = R_{cut}, \quad (\text{A.89})$$

and the integration region is simplified to a trapezoid:

$$\Gamma = \Gamma_I + \Gamma_{II} = \int_{\bar{R}_E}^1 dR \int_{x^{\min}(R)}^{x^{\max}(R)} dx + \int_{R_{\min}}^{\bar{R}_E} dR \int_{R_E-R}^{1-R_E} dx. \quad (\text{A.90})$$

These findings have been summarized in Table A.1, introducing the parameter $A = A_a(R)$, $a = m, E, \xi$, as defined in (2.52), (2.53), and (2.54):

$$A_m = [1 - 4m_f^2/(sR)]^{\frac{1}{2}}, \quad A_E = (1 + R - 2R_E)/(1 - R),$$

and $A_\xi = [1 - R(1 - R_\xi)^2/(R_\xi(1 - R)^2)]^{\frac{1}{2}}.$

Neglecting the final state mass for the integration limits of regions II and III, $m_f^2 \ll s$, allows to set $\bar{R}_E \approx R_E$ and is justified as they will only play a role for integrands proportional to $1/(1 - R)$ for $R \rightarrow 1$, i.e. in region I.

The above relations are independent of the scattering angle and thus, as mentioned, compatible with the angular acceptance cut. The acollinearity cut has an indirect influence on the acceptance cut. It is easy to see that the maximal scattering angle of the other final state fermion becomes limited by an acollinearity cut, i.e. the scattering angle of the second fermion is limited to $[-(\xi + \vartheta^{\max}), (\xi + \vartheta^{\max})]$.

Region I:	$\bar{R}_E \leq R \leq 1 - \varepsilon,$	$x^{\min}(R) \leq x \leq x^{\max}(R),$
	$x^{\min}(R) = (1 - R)d(R),$	$x^{\max}(R) = (1 - R)(1 - d(R)),$
	$d(R) = (1 - A_m(R))/2,$	$1 - d(R) = (1 + A_m(R))/2,$
Region II:	$R_{\min} \leq R \leq \bar{R}_E,$	$x_E^{\min}(R) \leq x \leq x_E^{\max}(R),$
	$x_E^{\min}(R) = (1 - R)d_E(R),$	$x_E^{\max}(R) = (1 - R)(1 - d_E(R)),$
	$d_E(R) = (1 - A_E(R))/2,$	$1 - d_E(R) = (1 + A_E(R))/2,$
Region III:	$R_{\min} \leq R \leq R_\xi,$	$x_\xi^{\min}(R) \leq x \leq x_\xi^{\max}(R),$
	$x_\xi^{\min}(R) = (1 - R)d_\xi(R),$	$x_\xi^{\max}(R) = (1 - R)(1 - d_\xi(R)),$
	$d_\xi(R) = (1 - A_\xi(R))/2,$	$1 - d_\xi(R) = (1 + A_\xi(R))/2.$

Table A.1: Regions of phase space with cuts on maximal acollinearity and minimal energy of the final state fermions.

Appendix B

Hard bremsstrahlung corrections

B.1 Initial state radiation

Matrix element and differential cross section

The matrix element for real initial state bremsstrahlung is given below:

$$\begin{aligned} \mathcal{M}_{ini} = & (2\pi)^4 \delta^{(4)}(k_1 + k_2 - p_1 - p_2 - p) \\ & \left[(2\pi)^{15} 2k_1^0 2k_2^0 2p_1^0 2p_2^0 2p^0 \right]^{-\frac{1}{2}} \mathbf{M}_{ini}. \end{aligned} \quad (\text{B.1})$$

The initial state differential cross section with its contributions from the three phase space regions I, II, and III created by the cuts (see Appendix A.3) is:

$$\frac{d\sigma_{ini}^{hard}}{d\cos\vartheta} = \frac{1}{2} \frac{s}{(4\pi)^4} \left[\int_I + \int_{II} - \int_{III} \right] \frac{1}{4} \frac{\sum_{spin} |M_{ini}|^2}{2s\beta_0} d\varphi_\gamma dx dR. \quad (\text{B.2})$$

Introducing the coupling constant combinations $\mathcal{V}(s')$ and $\mathcal{A}(s')$, with the neutral current couplings v_e, a_e, v_f, a_f and Z propagator $\chi(s')$ defined in (A.6) to (A.9),

$$\mathcal{V}(s) = Q_e^2 Q_f^2 + 2Q_e Q_f v_e v_f \Re \chi(s') + [v_e^2 + a_e^2] [v_f^2 + a_f^2] |\chi(s')|^2, \quad (\text{B.3})$$

$$\mathcal{A}(s) = 2Q_e Q_f a_e a_f \Re \chi(s') + 4v_e a_e v_f a_f |\chi(s')|^2, \quad (\text{B.4})$$

the squared amplitude $|M_{ini}|^2$, including all mass terms reads ($e^2 = 4\pi\alpha$):

$$\begin{aligned}
|M_{ini}|^2 = & (4\pi\alpha)^3 \left\{ \frac{\mathcal{V}(s')}{ss'} \left[-\frac{2m_e^2}{Z_1^2} (2T^2 - 2Ts' + s'^2 + 2m_f^2 s') \right. \right. \\
& - \frac{2m_e^2}{Z_2^2} (2U^2 - 2Us' + s'^2 + 2m_f^2 s') \\
& + \frac{s'}{Z_1 Z_2} (2T^2 + 2U^2 + 2s'^2 - 2(T+U)s' + 4m_f^2 s') \\
& + \frac{1}{Z_1} (ss' - 2Us' + s'^2 + 2m_f^2 (s+s')) \\
& + \frac{1}{Z_2} (ss' - 2Ts' + s'^2 + 2m_f^2 (s+s')) - 2s' - 4m_f^2 \left. \right] \\
& + \frac{\mathcal{A}(s)}{ss'} \left[-\frac{2m_e^2 s' (s' - 2T)}{Z_1^2} + \frac{2m_e^2 s' (s' - 2U)}{Z_2^2} \right. \\
& - \frac{2(T-U)s'^2}{Z_1 Z_2} - \frac{s'(s+s' - 2U)}{Z_1} + \frac{s'(s+s' - 2T)}{Z_2} \left. \right] \\
& + \frac{2m_f^2}{ss'} a_f^2 (v_e^2 + a_e^2) |\chi(s')^2| \\
& \cdot \left[\frac{4m_e^2 s'}{Z_1^2} + \frac{4m_e^2 s'}{Z_2^2} - \frac{4s'^2}{Z_1 Z_2} - \frac{2(s+s')}{Z_1} - \frac{2(s+s')}{Z_2} \right] \Big\}. \quad (\text{B.5})
\end{aligned}$$

The bremsstrahlung kinematic invariants Z_1 , Z_2 , V_1 , V_2 , T , and U are taken from (A.18) to (A.23) and (A.30) and (A.31). It is important to note that the coupling constant functions $\mathcal{V}(s')$ and $\mathcal{A}(s')$ in (B.5) depend on the final state invariant mass squared s' . This is immediately clear due to the emission of the hard photon from the initial state, with the propagators of the effective Born terms then depending on s' , and not on s .

The integration shall be performed analytically over the variables φ_γ , $x \equiv V_2/s$, and $\cos\vartheta$ to deliver QED flux functions for hard photon emission. A convolution integral of these flux functions with effective Born terms over $R \equiv s'/s$ is kept for numerical integration (see (0.4) and (2.41)).

The hard photon radiator functions $H_{T,FB}^{ini}(R)$ together with the soft and virtual correction terms S_{ini} for the totally integrated results σ_T^{ini} and A_{FB}^{ini} have been presented in the main part of this dissertation in Section 2.3.3. Here, we just want to present the basic steps of the analytical integration and describe especially the treatment of mass singularities arising during the calculation: The denominators $1/Z_i$, $i = 1, 2$ appearing in (B.5) are the propagators of the electron and positron and will determine the logarithmic structure of the final integrated results for $d\sigma_{ini}^{hard}/d\cos\vartheta$ and σ_{ini}^{hard} . These propagator terms deliver artificial singularities, i.e. mass singularities, when neglecting the initial state mass m_e for the analytical integration over $\cos\vartheta$ (see Section 2.3.2). These unphysical

singularities will however cancel each other when combining all integrated terms in the completely integrated radiator $H_{T,FB}^{ini}(R)$. This shall be presented and discussed below.

Integration over φ_γ

Performing the first integration over φ_γ in (B.2), only the denominators $1/Z_i$, $i = 1, 2$ are relevant. They depend linearly on $\cos \varphi_\gamma$.

Table of integrals:

$$\frac{1}{2\pi} \int_0^{2\pi} d\varphi_\gamma = 1, \quad (\text{B.6})$$

$$\frac{1}{2\pi} \int_0^{2\pi} \frac{d\varphi_\gamma}{Z_i} = \frac{1}{2\pi} \int_0^{2\pi} \frac{d\varphi_\gamma}{A_i \pm b \cos \varphi_\gamma} = \frac{1}{\sqrt{A_i^2 - B^2}}, \quad (\text{B.7})$$

$$\frac{1}{2\pi} \int_0^{2\pi} \frac{d\varphi_\gamma}{Z_i^2} = \frac{1}{2\pi} \int_0^{2\pi} \frac{d\varphi_\gamma}{(A_i \pm B \cos \varphi_\gamma)^2} = \frac{A_i}{(A_i^2 - B^2)^{\frac{3}{2}}}, \quad (\text{B.8})$$

with

$$\begin{aligned} \frac{1}{2\pi} \int_0^{2\pi} \frac{d\varphi_\gamma}{A_i \pm B \cos \varphi_\gamma} &= \frac{1}{2\pi} \frac{2}{\sqrt{A_i^2 - B^2}} \arctan \frac{\sqrt{A_i^2 - B^2} \tan(\varphi_\gamma/2)}{A \pm B} \Bigg|_0^{2\pi} \\ &= \frac{1}{\sqrt{A_i^2 - B^2}}, \end{aligned} \quad (\text{B.9})$$

$$\frac{1}{2\pi} \int_0^{2\pi} \frac{d\varphi_\gamma}{(A_i \pm B \cos \varphi_\gamma)^2} = \frac{1}{2\pi} \frac{A_i}{A_i^2 - B^2} \int_0^{2\pi} \frac{d\varphi_\gamma}{A_i \pm B \cos \varphi_\gamma} = \frac{A_i}{(A_i^2 - B^2)^{\frac{3}{2}}}. \quad (\text{B.10})$$

The coefficients A_i , $i = 1, 2$ and B depend on $\cos \vartheta_\gamma$, or equivalently V_2 , and s' :

$$A_i = \frac{s}{2}(1 - R)[1 \pm \beta_0 \cos \vartheta \cos \vartheta_\gamma] \quad (i = 1 \rightarrow +, 2 \rightarrow -), \quad (\text{B.11})$$

$$B = \frac{s}{2}(1 - R)\beta_0 \sin \vartheta \sin \vartheta_\gamma, \quad (\text{B.12})$$

with

$$R = \frac{s'}{s}, \quad v = 1 - R, \quad \beta_0 = \sqrt{1 - \frac{4m_e^2}{s}}, \quad \beta = \sqrt{1 - \frac{4m_f^2}{sR}}. \quad (\text{B.13})$$

Integration over V_2

The dependence of the integrals in (B.6) to (B.8) on $\cos \vartheta_\gamma$ can be transformed into a dependence on V_2 and s' using the identities from (A.46) and (A.47) with the definitions (A.25) to (A.28):

$$\cos \vartheta_\gamma = \frac{\lambda_1 - \lambda_2 - \lambda_p}{2\sqrt{\lambda_2}\sqrt{\lambda_p}}, \quad \sin \vartheta_\gamma = \frac{\sqrt{-\lambda(\lambda_1, \lambda_2, \lambda_p)}}{2\sqrt{\lambda_2}\sqrt{\lambda_p}}. \quad (\text{B.14})$$

With (B.11) and (B.12) and (B.14) one gets the following results depending on V_2 and s' :

$$\frac{1}{2\pi} \int_0^{2\pi} \frac{d\varphi_\gamma}{Z_i} = \frac{\sqrt{\lambda_2}}{C_i^{\frac{1}{2}}} \quad , \quad \frac{1}{2\pi} \int_0^{2\pi} \frac{d\varphi_\gamma}{Z_i^2} = \frac{\sqrt{\lambda_2} B_i}{C_i^{\frac{3}{2}}}, \quad (\text{B.15})$$

with

$$B_i = \frac{1}{2} \left[(s - s')\lambda_2 \pm (2ss' - (V_2 + s')(s + s'))\sqrt{\lambda_2}\beta_0 \cos \vartheta \right], \quad (\text{B.16})$$

$$C_i = \frac{1}{4} [2ss' - (V_2 + s')(s + s') \pm (s - s')\sqrt{\lambda_2}\beta_0 \cos \vartheta]^2 \\ + 4m_e^2 [s'V_2(s - s' - V_2) - (s - s')^2 m_f^2], \quad (\text{B.17})$$

$$\lambda_2 = (s' + V_2)^2 - 4m_f^2 s \approx (s' + V_2)^2 \quad \text{for } m_f \approx 0. \quad (\text{B.18})$$

Rewriting (B.16) and (B.17) in a more suitable form for the integration over V_2 and later over $\cos \vartheta$, we get:

$$C_i(x, R, \cos \vartheta) = s^2 a_i x^2 - 2s b_i x + c_i, \quad (\text{B.19})$$

$$B_i(x, R, \cos \vartheta) = s^3 \left[(x + R)^2 y_i \pm (x + R) R \beta_0 \cos \vartheta \right], \quad (\text{B.20})$$

$$a_i(R, \cos \vartheta) = s^2 \left(z_i^2 - (1 - \beta_0^2) R \right), \quad (\text{B.21})$$

$$b_i(R, \cos \vartheta) = s^3 \left[R z_i (1 - z_i) - \frac{1}{2} (1 - \beta_0^2) R (1 - R) \right], \quad (\text{B.22})$$

$$c_i(R, \cos \vartheta) = s^4 R^2 (1 - z_i)^2, \quad (\text{B.23})$$

$$z_1(R, \cos \vartheta) = \frac{1 - \beta_0 \cos \vartheta}{2} + R \frac{1 + \beta_0 \cos \vartheta}{2}, \quad (\text{B.24})$$

$$z_2(R, \cos \vartheta) = \frac{1 + \beta_0 \cos \vartheta}{2} + R \frac{1 - \beta_0 \cos \vartheta}{2}, \quad (\text{B.25})$$

$$y_1(R, \cos \vartheta) = \frac{1 - \beta_0 \cos \vartheta}{2} - R \frac{1 + \beta_0 \cos \vartheta}{2}, \quad (\text{B.26})$$

$$y_2(R, \cos \vartheta) = \frac{1 + \beta_0 \cos \vartheta}{2} - R \frac{1 - \beta_0 \cos \vartheta}{2}. \quad (\text{B.27})$$

Alternatively, one can also write:

$$y_1 = \frac{1}{2} [(1 - R) - (1 + R)\beta_0 \cos \vartheta], \quad y_2(R, \cos \vartheta) = y_1(R, -\cos \vartheta), \quad (\text{B.28})$$

$$z_1 = \frac{1}{2} [(1 + R) - (1 - R)\beta_0 \cos \vartheta], \quad z_2(R, \cos \vartheta) = z_1(R, -\cos \vartheta), \quad (\text{B.29})$$

$$\eta_0^2 := 1 - \beta_0^2 = \frac{4m_e^2}{s}. \quad (\text{B.30})$$

From (B.19) to (B.27), it is immediately obvious that the possible integrands are symmetric to each other with respect to a change of sign of $\cos \vartheta$.

In (B.18), the final state mass m_f is neglected. This is justified as for initial state bremsstrahlung only final state mass terms proportional to m_f^2/s may arise which can be neglected having in mind applications at energies around or above the Z boson resonance, $m_f^2 \ll M_Z^2 \leq s$. This approximation also greatly simplifies the analytical integrations over x and $\cos \vartheta$.

We will perform an integration over x in the three different regions of phase space I, II, and III, suggested by the cuts and depending on the variables x and R . This was summarized in Table (A.1).

$$\frac{d\sigma_{ini_I}^{hard}}{d\cos \vartheta} = \int_{\bar{R}_E}^1 dR \int_{x_m^{\min}(R)}^{x_m^{\max}(R)} dx \frac{d\sigma_{ini}^{hard}}{dR dx d\cos \vartheta}, \quad (\text{B.31})$$

$$\frac{d\sigma_{ini_{II}}^{hard}}{d\cos \vartheta} = \int_{R_{\min}}^{\bar{R}_E} dR \int_{x_E^{\min}(R)}^{x_E^{\max}(R)} dx \frac{d\sigma_{ini}^{hard}}{dR dx d\cos \vartheta}, \quad (\text{B.32})$$

$$\frac{d\sigma_{ini_{III}}^{hard}}{d\cos \vartheta} = \int_{R_{\min}}^{R_\xi} dR \int_{x_\xi^{\min}(R)}^{x_\xi^{\max}(R)} dx \frac{d\sigma_{ini}^{hard}}{dR dx d\cos \vartheta}. \quad (\text{B.33})$$

All three regions of phase space can be described equivalently by introducing a general, cut dependent parameter $0 \leq A_a(R) \leq 1$, $a = m, E, \xi$ defined in (2.52), (2.53), and (2.54). The limits of integration $x_a^{\max}(R)$ and $x_a^{\min}(R)$ can then be treated according to (A.1) in the general form:

$$x_a^{\max, \min}(R) = \frac{1}{2} (1 - R) [1 \pm A_a(R)], \quad a = m, E, \xi. \quad (\text{B.34})$$

In order to obtain short analytical formulae which can later be integrated analytically over $\cos \vartheta$, we will have to make different approximations for small initial state masses, $m_e^2 \ll s$. This will essentially define three intervals for $\cos \vartheta$ with different analytical expressions for the hard photon radiators. The boundaries of these intervals depend on R and the cut parameter $A_a = A_a(R)$.

defined in (2.52), (2.53), and (2.54). For brevity, we will use from now on $A \equiv A_a$ and only consider the integrands (B.15) with index ‘1’, as the results with index ‘2’ can trivially be obtained by the substitution ‘ $\cos \vartheta \rightarrow -\cos \vartheta$ ’ (see (B.19) to (B.27)).

Integrands proportional to $C_i^{-\frac{1}{2}}$

We have as basic set of integrals arising from integrands proportional to $C_i^{-\frac{1}{2}}$:

$$I_1^0 = \int_{V_2^{\min}}^{V_2^{\max}} \frac{dV_2}{\sqrt{C_1(V_2, s', \cos \vartheta)}} = s \int_{x^{\min}}^{x^{\max}} \frac{dx}{\sqrt{C_1(x, R, \cos \vartheta)}}, \quad (\text{B.35})$$

$$I_1^i = \int_{V_2^{\min}}^{V_2^{\max}} \frac{dV_2}{\sqrt{C_1(V_2, s', \cos \vartheta)}} (V_2 + s')^i = s^{i+1} \int_{x^{\min}}^{x^{\max}} \frac{dx}{\sqrt{C_1(x, R, \cos \vartheta)}} (x + R)^i, \quad (\text{B.36})$$

$i = 1, 2, 3.$

We will start with the basic integral I_1^0 :

$$I_1^0 = \frac{1}{\sqrt{a_1}} \ln \left[\sqrt{a_1} C_1^{\frac{1}{2}}(x, R, \cos \vartheta) + s a_1 x - b_1 \right] \Big|_{x^{\min}}^{x^{\max}}. \quad (\text{B.37})$$

With (B.28) and (B.16) we can express e.g. $C_1(x^{\max}, R, \cos \vartheta)$ and $C_1(x^{\min}, R, \cos \vartheta)$ as:

$$C_1(x^{\max}, R, \cos \vartheta) = \frac{1}{4} s^4 (1 - R)^2 \left[(y_1 + A z_1)^2 + R (1 - A^2) \eta_0^2 \right], \quad (\text{B.38})$$

$$C_1(x^{\min}, R, \cos \vartheta) = \frac{1}{4} s^4 (1 - R)^2 \left[(y_1 - A z_1)^2 + R (1 - A^2) \eta_0^2 \right]. \quad (\text{B.39})$$

The function $(y_1 \pm A z_1)$ can change sign, which means that $C_1(x^{\max, \min}, R, \cos \vartheta)$ can be of the order $O(\eta_0^2 = \frac{4m_e^2}{s})$, if $y_1 \pm A z_1$ disappears. As we want to integrate all angles of phase space analytically and fermion masses do not play a role at the center-of-mass energies in mind, we will neglect all non-logarithmic contributions of m_e^2 . So, the exact analytical result for I_1^0 from (B.37) can first be summarized as follows:

$$I_1^0 = \frac{1}{s} \frac{1}{\sqrt{z_1^2 - R \eta_0^2}} \ln \left(\frac{Z}{N} \right). \quad (\text{B.40})$$

Depending on the signs of $(y_1 \pm A z_1)$, it is useful to apply the following expressions for $\ln Z$ and $\ln N$ because otherwise the nominator Z or denominator N will lead

to an exact zero under the logarithm, when neglecting small mass terms of $O(\eta_0^2)$. This occurs for (2.76):

$$R(1 - A(R)^2)\eta_0^2 = [y_1(R, \cos \vartheta) \pm A(R)z_1(R, \cos \vartheta)]^2, \quad (\text{B.41})$$

which defines the following limiting parameters:

$$c_1^+(R) = -\frac{1 - R + A(R)(1 + R)}{1 + R + A(R)(1 - R)}, \quad (\text{B.42})$$

$$c_1^-(R) = -\frac{1 - R - A(R)(1 + R)}{1 + R - A(R)(1 - R)}, \quad (\text{B.43})$$

$$c_2^+(R) = -c_1^+(R), \quad (\text{B.44})$$

$$c_2^-(R) = -c_1^-(R), \quad (\text{B.45})$$

with $c_1^+ \leq c_1^-$ and $c_2^- \leq c_2^+$. These values were already given in (2.77) to (2.79) but for convenience are presented here again. Therefore we use:

a. for $y_1 + Az_1 > 0$:

$$\ln Z = \begin{cases} \ln \left[A\sqrt{z_1^2 - R\eta_0^2} + \sqrt{(y_1 + Az_1)^2 + R(1 - A^2)\eta_0^2} + \sqrt{y_1^2 + R\eta_0^2} \right] \\ + \ln \left[A\sqrt{z_1^2 - R\eta_0^2} + \sqrt{(y_1 + Az_1)^2 + R(1 - A^2)\eta_0^2} - \sqrt{y_1^2 + R\eta_0^2} \right] \\ - \ln(2A); \end{cases} \quad (\text{B.46})$$

b. for $y_1 + Az_1 \leq 0$:

$$\ln Z = \begin{cases} -\ln \left[\sqrt{y_1^2 + R\eta_0^2} - \sqrt{(y_1 + Az_1)^2 + R(1 - A^2)\eta_0^2} + A\sqrt{z_1^2 - R\eta_0^2} \right] \\ -\ln \left[\sqrt{y_1^2 + R\eta_0^2} + \sqrt{(y_1 + Az_1)^2 + R(1 - A^2)\eta_0^2} - A\sqrt{z_1^2 - R\eta_0^2} \right] \\ + \ln(2A) + \ln[R^2\eta_0^2\beta_0^2(1 - \cos^2 \vartheta)]; \end{cases} \quad (\text{B.47})$$

c. for $y_1 - Az_1 \geq 0$:

$$\ln N = \begin{cases} \ln \left[-A\sqrt{z_1^2 - R\eta_0^2} + \sqrt{(y_1 - Az_1)^2 + R(1 - A^2)\eta_0^2} + \sqrt{y_1^2 + R\eta_0^2} \right] \\ + \ln \left[A\sqrt{z_1^2 - R\eta_0^2} - \sqrt{(y_1 - Az_1)^2 + R(1 - A^2)\eta_0^2} + \sqrt{y_1^2 + R\eta_0^2} \right] \\ - \ln(2A); \end{cases} \quad (\text{B.48})$$

d. for $y_1 - Az_1 < 0$:

$$\ln N = \begin{cases} -\ln \left[\sqrt{y_1^2 + R\eta_0^2} + \sqrt{(y_1 - Az_1)^2 + R(1-A^2)\eta_0^2} - A\sqrt{z_1^2 - R\eta_0^2} \right] \\ -\ln \left[-\sqrt{y_1^2 + R\eta_0^2} + \sqrt{(y_1 - Az_1)^2 + R(1-A^2)\eta_0^2} + A\sqrt{z_1^2 - R\eta_0^2} \right] \\ +\ln(2A) + \ln[R^2\eta_0^2\beta_0^2(1 - \cos^2\vartheta)] \end{cases} \quad (\text{B.49})$$

Now we neglect terms of $O(\eta_0^2)$ in (B.46) to (B.49). The parameters c_1^+ and c_1^- from (B.42) and (B.43) thus distinguish three different intervals for the variable $\cos\vartheta$ with different analytical expressions for I_1^0 in each interval:

1. $\cos\vartheta < c_1^- \quad (y_1 \pm Az_1 > 0) :$

$$\begin{aligned} I_1^0 &= \frac{1}{sz_1} \ln \left(\frac{y_1 + Az_1}{y_1 - Az_1} \right) \quad (\text{B.50}) \\ &= \frac{1}{sz_1} \ln \left\{ \frac{[(1-R) + A(1+R)] - [(1+R) + A(1-R)] \cos\vartheta}{[(1-R) - A(1+R)] - [(1+R) - A(1-R)] \cos\vartheta} \right\}, \end{aligned} \quad (\text{B.51})$$

2. $c_1^- < \cos\vartheta < c_1^+ \quad (y_1 + Az_1 > 0 \wedge y_1 - Az_1 < 0) :$

$$\begin{aligned} I_1^0 &= \frac{1}{sz_1} \{ \ln [(y_1 + Az_1)(Az_1 - y_1)] + 2 \ln z_1 \\ &\quad - \ln(1 - \cos^2\vartheta) + \ln \left(\frac{s}{m_e^2} \right) - 2 \ln R \}, \end{aligned} \quad (\text{B.52})$$

3. $\cos\vartheta > c_1^+ \quad (y_1 \pm Az_1 < 0) :$

$$\begin{aligned} I_1^0 &= -\frac{1}{sz_1} \ln \left(\frac{y_1 + Az_1}{y_1 - Az_1} \right) \quad (\text{B.53}) \\ &= -\frac{1}{sz_1} \ln \left\{ \frac{[(1-R) + A(1+R)] - [(1+R) + A(1-R)] \cos\vartheta}{[(1-R) - A(1+R)] - [(1+R) - A(1-R)] \cos\vartheta} \right\}. \end{aligned} \quad (\text{B.54})$$

In case 2., the term $\ln(1 - \cos^2\vartheta)$ in (B.52) does not pose a problem for $\cos\vartheta \rightarrow \pm 1$ because it cancels with the logarithm $\ln[(y_1 + Az_1)(Az_1 - y_1)]$. To see this one has to take into account that the condition $\cos\vartheta \rightarrow \pm 1$ demands $c_1^\pm \pm 1$ which only occurs for $A \rightarrow 1$ (see (B.42) and (B.43)) This finally implies:

$$\ln [(y_1 + Az_1)(Az_1 - y_1)] \rightarrow \ln [z_1^2 - y_1^2] = \ln(1 - \cos^2\vartheta) + O(\eta_0^2). \quad (\text{B.55})$$

In the limit $\cos \vartheta \rightarrow c_1^-$ or $\cos \vartheta \rightarrow c_1^+$, I_1^0 simplifies to:

$$I_1^0 \rightarrow \frac{1}{s z_1} \left[\frac{1}{2} \ln \left(\frac{s}{m_e^2} \right) + \ln z_1 - \frac{1}{2} \ln R - \frac{1}{2} \ln \left(\frac{1 - A^2}{4 A^2} \right) \right]. \quad (\text{B.56})$$

In order to determine the remaining integrals

$$I_1^i = \int_{V_2^{\min}}^{V_2^{\max}} \frac{dV_2}{\sqrt{C_1(V_2, s', \cos \vartheta)}} (V_2 + s')^i = s^{i+1} \int_{x^{\min}}^{x^{\max}} \frac{dx}{\sqrt{C_1(x, R, \cos \vartheta)}} (x + R)^i, \quad (\text{B.57})$$

we can use the recurrence relations:

$$\hat{I}_1^1 = \frac{\sqrt{C_1}}{a_1} \Big|_{x^{\min}}^{x^{\max}} + \frac{b_1}{a_1} \hat{I}_1^0 \rightarrow I_1^1 = \hat{I}_1^1 + s' \hat{I}_0^1, \quad (\text{B.58})$$

$$\hat{I}_1^2 = \frac{s x \sqrt{C_1}}{2 a_1} \Big|_{x^{\min}}^{x^{\max}} + \frac{3 b_1}{2 a_1} \hat{I}_1^1 - \frac{1}{2} \frac{c_1}{a_1} \hat{I}_1^0 \rightarrow I_1^2 = \hat{I}_1^2 + 2 s' \hat{I}_1^1 + \hat{I}_0^2, \quad (\text{B.59})$$

$$\begin{aligned} \hat{I}_1^3 &= \frac{s^2 x^2 \sqrt{C_1}}{3 a_1} \Big|_{x^{\min}}^{x^{\max}} + \frac{5 b_1}{3 a_1} \hat{I}_1^2 - \frac{2 c_1}{3 a_1} \hat{I}_1^1 \rightarrow I_1^3 = \hat{I}_1^3 + 3 s' \hat{I}_1^2 \\ &\quad + 3 s'^2 \hat{I}_1^1 + s'^3 \hat{I}_0^1, \end{aligned} \quad (\text{B.60})$$

with the integrals

$$\hat{I}_1^i = \int_{V_2^{\min}}^{V_2^{\max}} \frac{dV_2}{\sqrt{C_1(V_2, s', \cos \vartheta)}} V_2^i = s^{i+1} \int_{x^{\min}}^{x^{\max}} \frac{dx}{\sqrt{C_1(x, R, \cos \vartheta)}} x^i \quad (\text{B.61})$$

which can be calculated via recurrence relations from the basic integral I_1^0 . In (B.58), the approximations for $m_e^2 \ll s$ were used:

$$\frac{c_1}{a_1} \approx \left(\frac{b_1}{a_1} \right)^2, \quad \frac{b_1}{a_1} \approx s R \frac{1 - z_1}{z_1}, \quad \frac{1}{a_1} \approx \frac{1}{s^2 z_1^2}. \quad (\text{B.62})$$

So, for the three intervals in $\cos \vartheta$, given e.g. through (B.51), (B.52), and (B.54), we obtain for I_1^i :

1. $\cos \vartheta < c_1^-$ ($y_1 \pm Az_1 > 0$) :

$$I_1^1 = \frac{A(1-R)}{z_1} + \left(\frac{sR}{z_1}\right) I_1^0, \quad (\text{B.63})$$

$$I_1^2 = s \frac{A(1-R)}{z_1} \left(\frac{1+R}{2} + \frac{R}{z_1}\right) + \left(\frac{sR}{z_1}\right)^2 I_1^0, \quad (\text{B.64})$$

$$I_1^3 = s^2 \frac{A(1-R)}{z_1} \left\{ \left[\frac{A^2(1-R)^2}{12} + \frac{(1+R)^2}{4} \right] + \frac{R(1+R)}{2z_1} + \frac{R^2}{z_1^2} \right\} + \left(\frac{sR}{z_1}\right)^3 I_1^0, \quad (\text{B.65})$$

2. $c_1^- < \cos \vartheta < c_1^+$ ($y_1 + Az_1 > 0 \wedge y_1 - Az_1 < 0$) :

$$I_1^1 = \frac{1}{z_1} \left[(1+R) - \frac{2R}{z_1} \right] + \left(\frac{sR}{z_1}\right) I_1^0, \quad (\text{B.66})$$

$$I_1^2 = s \frac{1}{z_1} \left\{ \frac{1}{4} [(1+R)^2 + A^2(1-R)^2] + \frac{R(1+R)}{z_1} - \frac{3R^2}{z_1^2} \right\} + \left(\frac{sR}{z_1}\right)^2 I_1^0, \quad (\text{B.67})$$

$$I_1^3 = s^2 \frac{1}{z_1} \left\{ \frac{1+R}{12} [(1+R)^2 + 3A^2(1-R)^2] + \frac{R}{4z_1} [(1+R)^2 + A^2(1-R)^2] + \frac{R^2(1+R)}{z_1^2} - \frac{11R^3}{3z_1^3} \right\} + \left(\frac{sR}{z_1}\right)^3 I_1^0, \quad (\text{B.68})$$

3. $\cos \vartheta > c_1^+$ ($y_1 \pm Az_1 < 0$) :

$$I_1^1 = -\frac{A(1-R)}{z_1} + \left(\frac{sR}{z_1}\right) I_1^0, \quad (\text{B.69})$$

$$I_1^2 = -s \frac{A(1-R)}{z_1} \left(\frac{1+R}{2} + \frac{R}{z_1}\right) + \left(\frac{sR}{z_1}\right)^2 I_1^0, \quad (\text{B.70})$$

$$I_1^3 = -s^2 \frac{A(1-R)}{z_1} \left\{ \frac{1}{12} [3(1+R)^2 + A^2(1-R)^2] + \frac{R(1+R)}{2z_1} + \frac{R^2}{z_1^2} \right\} + \left(\frac{sR}{z_1}\right)^3 I_1^0. \quad (\text{B.71})$$

This type of integrals I_1^i can generally be transformed into a sum of *rational functions* in powers of $1/z_1(\cos \vartheta)$ and the logarithmic function $I_1^0(\cos \vartheta)$ with powers of $1/z_1$ as coefficient.

Integrands proportional to $m_e^2 C_i^{-\frac{3}{2}}$

For the second type of integrands proportional to $m_e^2 C_i^{-\frac{3}{2}}$ is stated below:

$$J_1^0 = m_e^2 \int_{V_2^{\min}}^{V_2^{\max}} \frac{dV_2}{C_1^{\frac{3}{2}}} = s \int_{x^{\min}}^{x^{\max}} \frac{dx m_e^2}{C_1(x, R, \cos \vartheta)^{\frac{3}{2}}}, \quad (\text{B.72})$$

$$J_1^i = \int_{V_2^{\min}}^{V_2^{\max}} \frac{dV_2 m_e^2 B_1 (V_2 + s')^i}{C_1^{\frac{3}{2}}} = s^{i+1} \int_{x^{\min}}^{x^{\max}} \frac{dx m_e^2 B_1(x, R, \cos \vartheta) (x + R)^i}{C_1(x, R, \cos \vartheta)^{\frac{3}{2}}},$$

$$i = 1, 2, 3, \quad (\text{B.73})$$

with C_1 and B_1 defined in (B.19) and (B.20). We again start with the basic integral J_1^0 . Its integration yields:

$$J_1^0 = \frac{1}{4s^4} \frac{z_1}{R^2(1-z_1)(z_1-R)} \left\{ \frac{y_1 + Az_1}{\sqrt{(y_1 + Az_1)^2 + R(1-A^2)\eta_0^2}} - \frac{y_1 - Az_1}{\sqrt{(y_1 - Az_1)^2 + R(1-A^2)\eta_0^2}} \right\}. \quad (\text{B.74})$$

It can be shown that this integral J_1^0 cancels in the integrated matrix element, but all other integrals of the type J_1^i will be related to J_1^0 by recurrence relations. The denominator in (B.74) vanishes if $R(1-A^2)\eta_0^2 \ll (y_1 \pm Az_1)^2$. Thus, an approximation for small m_e^2 again delivers three different analytical expressions for J_1^0 depending on the relative values of $\cos \vartheta$ and c_1^\pm defined in (B.42) and (B.43):

$$1. \quad \cos \vartheta < c_1^- \quad (y_1 \pm Az_1 > 0) : \quad J_1^0 \approx \eta_0^2 \frac{1}{4s^4} \frac{2A(1-A^2)z_1^2 y_1}{R(1-z_1)(z_1-R)(y_1^2 - A^2 z_1^2)^2} \quad (\text{B.75})$$

$$= \frac{\eta_0^2}{s^4} \frac{2A(1-A^2)z_1^2 y_1}{R(1-R)^2(1-\beta_0^2 \cos^2 \vartheta)}, \quad (\text{B.76})$$

$$2. \quad c_1^- < \cos \vartheta < c_1^+ \quad (y_1 + Az_1 > 0 \wedge y_1 - Az_1 < 0) : \quad J_1^0 \approx \frac{1}{4s^4} \frac{2z_1}{R^2(1-z_1)(z_1-R)} = \frac{1}{s^4} \frac{2z_1}{R^2(1-R)^2(1-\beta_0^2 \cos^2 \vartheta)}, \quad (\text{B.77})$$

$$3. \quad \cos \vartheta > c_1^+ \quad (y_1 \pm Az_1 < 0) : \quad (B.78)$$

$$J_1^0 \approx -\eta_0^2 \frac{1}{4s^4} \frac{2A(1-A^2)z_1^2 y_1}{R(1-z_1)(z_1-R)(y_1^2 - A^2 z_1^2)^2}$$

$$= -\frac{\eta_0^2}{s^4} \frac{2A(1-A^2)z_1^2 y_1}{R(1-R)^2(1-\beta_0^2 \cos^2 \vartheta)}. \quad (B.79)$$

So, for J_1^0 we have the interesting situation that after integration over $\cos \vartheta$ the expressions in (B.76) and (B.79) are suppressed by an additional factor

$$\eta_0^2 = \frac{4m_e^2}{s} \quad (B.80)$$

and can be neglected in the integrated matrix element. This ‘drop’ of J_1^0 by a factor η_0^2 occurs in a very narrow region with a width of the order $O(\eta_0^2)$, i.e. for $|\cos \vartheta - c_1^-| < \eta_0^2$ and $|\cos \vartheta - c_1^+| < \eta_0^2$. In the limit $\cos \vartheta \rightarrow c_1^-$ or $\cos \vartheta \rightarrow c_1^+$, we have:

$$J_1^0 \rightarrow \frac{1}{4s^4} \frac{z_1}{R^2(1-z_1)(z_1-R)} = \frac{1}{s^4} \frac{z_1}{R^2(1-R)^2(1-\beta_0^2 \cos^2 \vartheta)}. \quad (B.81)$$

The remaining integrals J_1^i from (B.73) can be written as

$$J_1^i = \frac{1}{1-R} \left\{ [(1+R)z_1 - 2R] \hat{J}_1^{i+2} + R[(1+R) - 2z_1] \hat{J}_1^{i+1} \right\}, \quad (B.82)$$

with z_1 from (B.24) and where we introduce the integrals

$$\hat{J}_1^i = \int_{V_2^{\min}}^{V_2^{\max}} \frac{dV_2 m_e^2 (V_2 + s')^i}{C_1(V_2)^{\frac{3}{2}}} = s^{i+1} \int_{x^{\min}}^{x^{\max}} \frac{dx m_e^2 (x + R)^i}{C_1(x)^{\frac{3}{2}}}. \quad (B.83)$$

If we neglect terms of $O(\eta_0^2)$, (B.82) simplifies with (B.62) to:

$$\hat{J}_1^i \approx \left(\frac{b_1}{a_1} + s' \right)^i \cdot J_1^0 \approx \left(\frac{sR}{z_1} \right)^i \cdot J_1^0, \quad (B.84)$$

which produces with (B.77) for only the interesting case, $c_1^- < \cos \vartheta < c_1^+$:

$$J_1^i = \frac{2s(1-z_1)(z_1-R)}{1-R} \left(\frac{sR}{z_1} \right)^{i+2} J_1^0 \quad (B.85)$$

$$= \frac{1}{2} s(1-R)(1-\beta_0^2 \cos^2 \vartheta) \left(\frac{sR}{z_1} \right)^{i+2} J_1^0, \quad (B.86)$$

$$J_1^i = \frac{1}{s(1-R)z_1} \left(\frac{sR}{z_1} \right)^i. \quad (B.87)$$

At the end we discover the remarkable result that all integrands proportional to $m_e^2 C_i^{-\frac{3}{2}}$ yield integrals proportional to the basic integral J_1^0 . They will therefore, just like J_1^0 , only lead to non-neglectable contributions in the defined region $c_1^- < \cos \vartheta < c_1^+$. So, the dependence on the parameter $A(R)$, which contains the cut dependence of the different phase space regions I, II, and III, is only introduced through the basic integral J_1^0 .

The only terms, however, which arise in integrated matrix element are proportional to J_1^i with $i = 1, 2, 3$. All other terms proportional to J_1^0 have to cancel for $c_1^- < \cos \vartheta < c_1^+$ due to its mass singular behaviour there. From (B.77) we see:

$$J_1^0 \sim \frac{1}{1 - \beta_0^2 \cos^2 \vartheta} \approx \frac{1}{\eta_0^2} \quad (\text{B.88})$$

for $\cos \vartheta \approx \pm 1$, and $c_1^\pm \approx 1$ respectively which can happen for $A(R) \approx 1$ in phase space region I (see (B.42) and (B.43)). Due to [139,140] these poles have to cancel. In J_1^i , $i \geq 1$, this problem does not occur because the factor $1/(1 - \beta_0^2 \cos^2 \vartheta)$ is cancelled.

All the results obtained in this section can now be used straightforwardly for the corresponding integrands proportional to $C_2^{-\frac{1}{2}}$ and $m_e^2 C_2^{-\frac{3}{2}}$, just by replacing formally in the expressions the term ‘ z_1 ’ by ‘ z_2 ’, or, more explicitly, substituting ‘ $\cos \vartheta$ ’ by ‘ $-\cos \vartheta$ ’.

Integration over $\cos \vartheta$

Following the discussion, above the zero conditions defined in (2.76) and (B.41) fix different values $c_1^+(R)$, $c_1^-(R)$, $c_2^+(R)$, and $c_2^-(R)$ (see (B.42) to (B.45)) which separate the symmetric integration interval $[-c; c]$ into several different regions with different analytical expressions for the hard radiator functions. With $c \geq 0$, we define below the different intervals for an integration over $\cos \vartheta$. $H_{T,FB}^{ini}(R, c, A)$ and $h_{T,FB}^{ini}(\cos \vartheta, R, A)$ are the total or differential hard flux functions which factorize from the (improved) Born cross sections or asymmetries, not demonstrated here.

1. $0 \leq c < c_2^-$ ($c_2^- > 0$) :

$$H_{T,FB}^{ini}(R, c, A) = \int_{c_2^-}^c d\cos\vartheta h_{T,FB}^{ini}(\cos\vartheta, R, A), \quad (\text{B.89})$$

2. $0 \leq c < c_1^-$ ($c_1^- \geq 0$) :

$$H_{T,FB}^{ini}(R, c, A) = \int_{c_1^-}^c d\cos\vartheta h_{T,FB}^{ini}(\cos\vartheta, R, A), \quad (\text{B.90})$$

3. $c_1^-, c_2^- \leq c < c_1^+$:

- a. $c_1^- \geq 0$:

$$H_{T,FB}^{ini}(R, c, A) = \left\{ \int_0^{c_1^-} d\cos\vartheta + \int_{c_1^-}^c d\cos\vartheta \right\} h_{T,FB}^{ini}(\cos\vartheta, R, A), \quad (\text{B.91})$$

- b. $c_2^- > 0$:

$$H_{T,FB}^{ini}(R, c, A) = \left\{ \int_0^{c_2^-} d\cos\vartheta + \int_{c_2^-}^c d\cos\vartheta \right\} h_{T,FB}^{ini}(\cos\vartheta, R, A), \quad (\text{B.92})$$

4. $c_1^+ \leq c \leq 1$:

- a. $c_1^- \geq 0$:

$$H_{T,FB}^{ini}(R, c, A) = \left\{ \int_0^{c_1^-} d\cos\vartheta + \int_{c_1^-}^{c_1^+} d\cos\vartheta + \int_{c_1^+}^c d\cos\vartheta \right\} h_{T,FB}^{ini}(\cos\vartheta, R, A), \quad (\text{B.93})$$

- b. $c_2^- > 0$:

$$H_{T,FB}^{ini}(R, c, A) = \left\{ \int_0^{c_2^-} d\cos\vartheta + \int_{c_2^-}^{c_1^+} d\cos\vartheta + \int_{c_1^+}^c d\cos\vartheta \right\} h_{T,FB}^{ini}(\cos\vartheta, R, A). \quad (\text{B.94})$$

For $H_T^{ini}(R, c, A)$ the results for $c_1^- \geq 0$ and $c_2^- \geq 0$ have to reproduce which serves as a check of the analytical integration.

Integral types of the integration over $\cos \vartheta$

Introducing the the following abbreviations,

$$R_c^+ = (1 + R) + c(1 - R) = 2z_2(c), \quad (\text{B.95})$$

$$R_c^- = (1 + R) - c(1 - R) =: R_c = 2z_1(c), \quad (\text{B.96})$$

$$R_A^+ = (1 + R) + A(1 - R) = 2z_2(A), \quad (\text{B.97})$$

$$R_A^- = (1 + R) - A(1 - R) = 2z_1(A), \quad (\text{B.98})$$

$$\bar{R}_A^+ = (1 - R) + A(1 + R) = 2y_2(A), \quad (\text{B.99})$$

$$\bar{R}_A^- = (1 - R) - A(1 + R) = 2y_1(A), \quad (\text{B.100})$$

$$R_{Ac}^+ = (1 - R)(1 - cA) - (1 + R)(c - A) = 2(y_1(c) + Az_1(c)), \quad (\text{B.101})$$

$$R_{Ac}^- = (1 - R)(1 + cA) - (1 + R)(c + A) = 2(y_2(c) + Az_2(c)). \quad (\text{B.102})$$

It is obvious that all integrals with z_2 in the integrand can uniformly be obtained from those with index ‘1’ by introducing an extra overall minus sign and substituting c by $-c$.¹

We first have the following rational integrals over $\cos \vartheta$:

Table of integrals

Type 0:

$$[f_0(\cos \vartheta)]_{(c)} = \int_0^c d(\cos \vartheta) f_0(\cos \vartheta), \quad (\text{B.103})$$

$$\left[\frac{1}{z_1}\right]_{(c)} = \int_0^c d\xi \frac{2}{1 - R} \frac{1}{\frac{1+R}{1-R} - \xi} = -\frac{2}{1 - R} [\ln R_c^- - \ln(1 + R)], \quad (\text{B.104})$$

$$\left[\frac{1}{z_1^2}\right]_{(c)} = -\frac{4}{1 - R} \left[\frac{1}{1 + R} - \frac{1}{R_c^-}\right] = \frac{4c}{R_c^-(1 + R)}, \quad (\text{B.105})$$

$$\left[\frac{1}{z_1^3}\right]_{(c)} = -\frac{4}{1 - R} \left[\frac{1}{(1 + R)^2} - \frac{1}{R_c^{-2}}\right] = \frac{4c}{R_c^-(1 + R)} \left[\frac{1}{1 + R} + \frac{1}{R_c^-}\right], \quad (\text{B.106})$$

$$\begin{aligned} \left[\frac{1}{z_1^4}\right]_{(c)} &= -\frac{16}{3(1 - R)} \left[\frac{1}{(1 + R)^3} - \frac{1}{R_c^{-3}}\right] \\ &= \frac{16c}{3R_c^-(1 + R)} \left[\frac{1}{(1 + R)^2} + \frac{1}{R_c^-(1 + R)} + \frac{1}{R_c^{-2}}\right], \end{aligned} \quad (\text{B.107})$$

¹To see this, just substitute $\cos \vartheta$ in the integrand by $-\cos \vartheta$ with $z_1(R, -\cos \vartheta) = z_2(R, \cos \vartheta)$ and the new upper limit $-c$

$$\left[\frac{1}{z_2} \right]_{(c)} = \frac{2}{1-R} \left[\ln R_c^+ - \ln(1+R) \right], \quad (\text{B.108})$$

$$\left[\frac{1}{z_2^2} \right]_{(c)} = \frac{4}{1-R} \left[\frac{1}{1+R} - \frac{1}{R_c^+} \right] = \frac{4c}{R_c^+(1+R)}, \quad (\text{B.109})$$

$$\left[\frac{1}{z_2^3} \right]_{(c)} = \frac{4}{1-R} \left[\frac{1}{(1+R)^2} - \frac{1}{R_c^{+2}} \right] = \frac{4c}{R_c^+(1+R)} \left[\frac{1}{1+R} + \frac{1}{R_c^+} \right], \quad (\text{B.110})$$

$$\begin{aligned} \left[\frac{1}{z_2^4} \right]_{(c)} &= \frac{16}{3(1-R)} \left[\frac{1}{(1+R)^3} - \frac{1}{R_c^{+3}} \right] \\ &= \frac{16c}{3R_c^+(1+R)} \left[\frac{1}{(1+R)^2} + \frac{1}{R_c^+(1+R)} + \frac{1}{R_c^{+2}} \right]. \end{aligned} \quad (\text{B.111})$$

And secondly, there are the following logarithmic integrals, just showing the integrals with index ‘1’ and $R_c := R_c^-$ and keeping the above said in mind:

Type 1:

$$\left[\frac{1}{z_i^k} \ln \left(\frac{s}{m_e^2} \frac{z_i^2}{R} \right) \right]_{(c)} = \ln \left(\frac{s}{m_e^2} \frac{1}{R} \right) \int_0^c d(\cos \vartheta) \frac{1}{z_i^k} + 2 \int_0^c d(\cos \vartheta) \frac{\ln z_i}{z_i^k} \quad (\text{B.112})$$

$$= \pm \frac{2}{1-R} \left\{ \ln \left(\frac{s}{m_e^2} \frac{1}{R} \right) \int_{\frac{1}{2}(1+R)}^{\frac{1}{2}R_c^\pm} dz_i \frac{1}{z_i^k} + 2 \int_{\frac{1}{2}(1+R)}^{\frac{1}{2}R_c^\pm} dz_i \frac{\ln z_i}{z_i^k} \right\}, \quad (\text{B.113})$$

with $i = 1$ (‘-’) or 2 (‘+’), $k = 2, 3, 4$,

$$\frac{1}{2} \left[\frac{\ln z_1}{z_1^2} \right]_{(c)} = 2 \left\{ \frac{1}{v} \frac{1}{1+R} \ln \left(\frac{R_c}{1+R} \right) + \frac{c}{R_c(1+R)} \left[\ln \left(\frac{R_c}{2} \right) + 1 \right] \right\}, \quad (\text{B.114})$$

$$\begin{aligned} \frac{1}{2} \left[\frac{\ln z_1}{z_1^3} \right]_{(c)} &= 2 \left\{ \frac{1}{v} \left(\frac{1}{1+R} \right)^2 \ln \left(\frac{R_c}{1+R} \right) \right. \\ &\quad \left. + \frac{c}{R_c(1+R)} \left(\frac{1}{R_c} + \frac{1}{1+R} \right) \left[\ln \left(\frac{R_c}{2} \right) + \frac{1}{2} \right] \right\}, \end{aligned} \quad (\text{B.115})$$

$$\begin{aligned} \frac{1}{2} \left[\frac{\ln z_1}{z_1^4} \right]_{(c)} &= \frac{8}{3} \left\{ \frac{1}{v} \left(\frac{1}{1+R} \right)^3 \ln \left(\frac{R_c}{1+R} \right) \right. \\ &\quad \left. + \frac{c}{R_c(1+R)} \left[\frac{1}{R_c^2} + \frac{1}{R_c(1+R)} + \frac{1}{(1+R)^2} \right] \left[\ln \left(\frac{R_c}{2} \right) + \frac{1}{3} \right] \right\}. \end{aligned} \quad (\text{B.116})$$

Type 2:

$$\begin{aligned} \left[\frac{\ln(1 - \beta_0^2 \cos^2 \vartheta)}{z_i^k} \right]_{(c)} &= \int_0^c d(\cos \vartheta) \frac{\ln[(z_i - R)(1 - z_i)] - 2 \ln\left(\frac{1-R}{2}\right)}{z_i^k} \quad (\text{B.117}) \\ &= \pm \frac{2}{1-R} \int_{\frac{1}{2}(1+R)}^{\frac{1}{2}R_c^\pm} dz_i \frac{\ln[(z_i - R)(1 - z_i)] - 2 \ln\left(\frac{1-R}{2}\right)}{z_i^k}, \end{aligned}$$

$$\text{with } i = 1 \text{ ('-')} \text{ or } 2 \text{ ('+'), } k = 2, 3, 4, \quad (\text{B.118})$$

$$\begin{aligned} &\frac{1}{2} \left[\frac{\ln(1 - \beta_0^2 \cos^2 \vartheta)}{z_1^2} \right]_{(c)} \\ &= \frac{1}{v} \frac{1+R}{R} \ln\left(\frac{R_c}{1+R}\right) + \frac{1+c}{R_c} \ln(1+c) - \frac{1-c}{RR_c} \ln(1-c), \quad (\text{B.119}) \end{aligned}$$

$$\begin{aligned} &\frac{1}{2} \left[\frac{\ln(1 - \beta_0^2 \cos^2 \vartheta)}{z_1^3} \right]_{(c)} \\ &= \frac{1}{2} \left\{ \frac{1}{v} \frac{1+R^2}{R^2} \ln\left(\frac{R_c}{1+R}\right) + \left(\frac{2}{R_c} + 1\right) \frac{1+c}{R_c} \ln(1+c) \right. \\ &\quad \left. - \left(\frac{2}{R_c} + \frac{1}{R}\right) \frac{1-c}{RR_c} \ln(1-c) - \frac{2c}{RR_c} \right\}, \quad (\text{B.120}) \end{aligned}$$

$$\begin{aligned} &\frac{1}{2} \left[\frac{\ln(1 - \beta_0^2 \cos^2 \vartheta)}{z_1^4} \right]_{(c)} \quad (\text{B.121}) \\ &= \frac{1}{3} \left\{ \frac{1}{v} \frac{1+R^3}{R^3} \ln\left(\frac{R_c}{1+R}\right) + \left(\frac{4}{R_c^2} + \frac{2}{R_c} + 1\right) \frac{1+c}{R_c} \ln(1+c) \right. \\ &\quad \left. - \left(\frac{4}{R_c^2} + \frac{2}{RR_c} + \frac{1}{R^2}\right) \frac{1-c}{RR_c} \ln(1-c) - \frac{2c}{RR_c} \left[\frac{1}{R_c} + \frac{1+R+R^2}{R(1+R)} \right] \right\}. \end{aligned}$$

Type 3:

$$\begin{aligned} \left[\frac{1}{z_i^k} \ln \left| \frac{y_i + Az_i}{y_i - Az_i} \right| \right]_{(c)} &= \pm \frac{2}{1-R} \int_{\frac{1}{2}(1+R)}^{\frac{1}{2}R_c^\pm} dz_i \frac{1}{z_i^k} \ln \left| \frac{y_i + Az_i}{y_i - Az_i} \right| \\ &\text{with } i = 1 \text{ ('-')} \text{ or } 2 \text{ ('+'), } k = 2, 3, 4, \quad (\text{B.122}) \end{aligned}$$

$$\begin{aligned}
& \frac{1}{2} \left[\frac{1}{z_1^2} \ln \left| \frac{y_1 + Az_1}{y_1 - Az_1} \right| \right]_{(c)} \\
= & \frac{A}{R} \ln \left(\frac{R_c}{1+R} \right) + \frac{1}{2R(1+R)} \left[\bar{R}_A^+ \ln(\bar{R}_A^+) - \bar{R}_A^- \ln |\bar{R}_A^-| \right] \\
& + \frac{1}{2RR_c} \left[R_{Ac}^+ \ln |R_{Ac}^+| - R_{Ac}^- \ln |R_{Ac}^-| \right], \tag{B.123}
\end{aligned}$$

$$\begin{aligned}
& \frac{1}{2} \left[\frac{1}{z_1^3} \ln \left| \frac{y_1 + Az_1}{y_1 - Az_1} \right| \right]_{(c)} \\
= & \frac{1}{2} \left\{ \frac{A(1+R)}{R^2} \ln \left(\frac{R_c}{1+R} \right) + \frac{1}{2R(1+R)} \left[\left(\frac{2}{1+R} + \frac{R_A^+}{2R} \right) \bar{R}_A^+ \ln(\bar{R}_A^+) \right. \right. \\
& \left. \left. - \left(\frac{2}{1+R} + \frac{R_A^-}{2R} \right) \bar{R}_A^- \ln |\bar{R}_A^-| \right] \right. \\
& \left. + \frac{1}{2RR_c} \left[\left(\frac{2}{R_c} + \frac{R_A^+}{2R} \right) R_{Ac}^+ \ln |R_{Ac}^+| - \left(\frac{2}{R_c} + \frac{R_A^-}{2R} \right) R_{Ac}^- \ln |R_{Ac}^-| \right] \right. \\
& \left. - \frac{2Ac}{RR_c} \frac{1-R}{1+R} \right\}, \tag{B.124}
\end{aligned}$$

$$\begin{aligned}
& \frac{1}{2} \frac{1}{z_1^4} \left[\ln \left| \frac{y_1 + Az_1}{y_1 - Az_1} \right| \right]_{(c)} \\
= & \frac{1}{3} \left\{ \frac{A}{4R^3} \left[A^2(1-R)^2 + 3(1+R)^2 \right] \ln \left(\frac{R_c}{1+R} \right) \right. \\
& + \frac{1}{2R(1+R)} \left[\left(\frac{4}{(1+R)^2} + \frac{R_A^+}{R(1+R)} + \frac{R_A^{+2}}{4R^2} \right) \bar{R}_A^+ \ln(\bar{R}_A^+) \right. \\
& \left. \left. - \left(\frac{4}{(1+R)^2} + \frac{R_A^-}{R(1+R)} + \frac{R_A^{-2}}{4R^2} \right) \bar{R}_A^- \ln |\bar{R}_A^-| \right] \right. \\
& + \frac{1}{2RR_c} \left[\left(\frac{4}{R_c^2} + \frac{R_A^+}{RR_c} + \frac{R_A^{+2}}{4R^2} \right) R_{Ac}^+ \ln |R_{Ac}^+| \right. \\
& \left. \left. - \left(\frac{4}{R_c^2} + \frac{R_A^-}{RR_c} + \frac{R_A^{-2}}{4R^2} \right) R_{Ac}^- \ln |R_{Ac}^-| \right] \right. \\
& \left. - \frac{2Ac(1-R)}{RR_c(1+R)} \left(\frac{1}{R_c} + \frac{1}{1+R} + \frac{1+R}{R} \right) \right\}. \tag{B.125}
\end{aligned}$$

Type 4:

$$\left[\frac{1}{z_i^k} \ln |(y_i + Az_i)(Az_i - y_i)| \right]_{(c)} = \pm \frac{2}{1-R} \int_{\frac{1}{2}(1+R)}^{\frac{1}{2}R_c^\pm} dz_i \frac{1}{z_i^k} \ln |(y_i + Az_i)(Az_i - y_i)|,$$

with $i = 1$ ('-') or 2 ('+'), $k = 2, 3, 4$, (B.126)

$$\begin{aligned} & \frac{1}{2} \left[\frac{1}{z_1^2} \ln |(y_1 + Az_1)(Az_1 - y_1)| \right]_{(c)} \\ = & \frac{1}{v} \frac{1+R}{R} \ln \left(\frac{R_c}{1+R} \right) + \frac{1}{2R(1+R)} \left[\bar{R}_A^+ \ln(\bar{R}_A^+) + \bar{R}_A^- \ln |\bar{R}_A^-| \right] \\ & - \frac{1}{2RR_c} \left[R_{Ac}^+ \ln |R_{Ac}^+| + R_{Ac}^- \ln |R_{Ac}^-| \right], \quad (\text{B.127}) \end{aligned}$$

$$\begin{aligned} & \frac{1}{2} \left[\frac{1}{z_1^3} \ln |(y_1 + Az_1)(Az_1 - y_1)| \right]_{(c)} \\ = & \frac{1}{2} \left\{ \frac{1}{2R^2} \left[\frac{1}{v} (1+R)^2 + A^2(1-R) \right] \ln \left(\frac{R_c}{1+R} \right) \right. \\ & + \frac{1}{2R(1+R)} \left[\left(\frac{2}{1+R} + \frac{R_A^+}{2R} \right) \bar{R}_A^+ \ln(\bar{R}_A^+) \right. \\ & \quad \left. + \left(\frac{2}{1+R} + \frac{R_A^-}{2R} \right) \bar{R}_A^- \ln |\bar{R}_A^-| \right] \\ & - \frac{1}{2RR_c} \left[\left(\frac{2}{R_c} + \frac{R_A^+}{2R} \right) R_{Ac}^+ \ln |R_{Ac}^+| + \left(\frac{2}{R_c} + \frac{R_A^-}{2R} \right) R_{Ac}^- \ln |R_{Ac}^-| \right] \\ & \left. - \frac{2c}{RR_c} \right\}, \quad (\text{B.128}) \end{aligned}$$

$$\begin{aligned} & \frac{1}{2} \left[\frac{1}{z_1^4} \ln |(y_1 + Az_1)(Az_1 - y_1)| \right]_{(c)} \\ = & \frac{1}{3} \left\{ \frac{(1+R)}{4R^3} \left[\frac{1}{v} (1+R)^2 + 3A^2(1-R) \right] \ln \left(\frac{R_c}{1+R} \right) \right. \\ & + \frac{1}{2R(1+R)} \left[\left(\frac{4}{(1+R)^2} + \frac{R_A^+}{R(1+R)} + \frac{R_A^{+2}}{4R^2} \right) \bar{R}_A^+ \ln(\bar{R}_A^+) \right. \\ & \quad \left. + \left(\frac{4}{(1+R)^2} + \frac{R_A^-}{R(1+R)} + \frac{R_A^{-2}}{4R^2} \right) \bar{R}_A^- \ln |\bar{R}_A^-| \right] \end{aligned}$$

$$\begin{aligned}
& -\frac{1}{2RR_c} \left[\left(\frac{4}{R_c^2} + \frac{R_A^+}{RR_c} + \frac{R_A^{+2}}{4R^2} \right) R_{Ac}^+ \ln |R_{Ac}^+| \right. \\
& \quad \left. + \left(\frac{4}{R_c^2} + \frac{R_A^-}{RR_c} + \frac{R_A^{-2}}{4R^2} \right) R_{Ac}^- \ln |R_{Ac}^-| \right] \\
& - \frac{c}{RR_c} \left[\frac{(1+R)^2 + A^2(1-R)^2}{R(1+R)} + 2 \left(\frac{1}{R_c} + \frac{1}{1+R} \right) \right] \Big\}. \quad (\text{B.129})
\end{aligned}$$

As the integrals of (B.126) always appear in combination with the integrals of (B.117) as differences of the form

$$\int_0^c d(\cos \vartheta) \frac{1}{z_i^k} \left\{ \ln |(y_i + Az_i)(Az_i - y_i)| - \ln(1 - \beta_0^2 \cos^2 \vartheta) \right\}, \quad (\text{B.130})$$

we can show that powers of the order $\frac{1}{v^k}$, $k \geq 2$, with $v := 1 - R$ being proportional to the photon energy, completely cancel out, as they should. So, the unregularized hard photon radiators will only contain physical poles in the photon energy of the order $\frac{1}{v}$. After adding the soft terms and integrating over R also the remaining singularities proportional to $\ln \varepsilon$ will disappear (ε : cut-off between soft and hard photon phase space).

Some coefficient functions

The hard photon radiator functions $H_{T,FB}^{ini} = H_{T,FB}^{ini}(c, \theta_{\text{acol}}, E_{\text{min}})$ for total cross sections and asymmetries were presented in Section 2.3.3. For completeness we just give some additional coefficient functions here appearing in $H_{T,FB}^{ini}$ which were not shown there for brevity (functions $y(R, c)$ and $z(R, c)$ defined in (2.145)).

$$\begin{aligned}
f_{01}(R, c) = & -\frac{4}{3z^3} (7 + 12c + 8c^2 + 4c^3 + c^4 + 8R) \\
& + \frac{2}{3z^2} (24 + 25c + 11c^2 + c^3 - c^4 + 12R) \\
& - \frac{1}{3z} (26 + 19c + 3c^2 - c^3 + c^4 + 12R) \\
& + \frac{2}{3} (4 + R), \quad (\text{B.131})
\end{aligned}$$

$$\begin{aligned}
f_{02}(R, c) = & \frac{4}{3z^3} (15 + 28c + 22c^2 + 12c^3 + 3c^4 + 16R) \\
& - \frac{2}{3z^2} (52 + 63c + 37c^2 + 9c^3 - c^4 + 24R) \\
& + \frac{1}{3z} (52 + 2R + 41c + 10c^2 - 3c^3) \\
& - \frac{1}{12} [23 - 9R + 2(11 - R)c - (5 + R)c^2], \quad (\text{B.132})
\end{aligned}$$

$$\begin{aligned}
f_{03}(R, A, c) = & \frac{A^2}{12} \left\{ -\frac{4}{z} [(1 + c)^2 + 2R] \right. \\
& + [3 - R + 12c + 3(1 + R)c^2 - 2(1 - R)c^3] \Big\} \\
& + \frac{2}{3} \frac{c(1 - A^2)}{v} + \frac{c}{2} \left(1 + \frac{1}{3} A^2 c^2 \right) (1 - R), \quad (\text{B.133})
\end{aligned}$$

$$f_{11}(R, A, c) = A \left\{ -\frac{2}{3} g_{Lz}(R, c) + \frac{1}{4v} \left[y^2 - \frac{1}{3} A^2 (z^2 + 8R) \right] \right\}, \quad (\text{B.134})$$

$$f_{12}(R, A, c) = \frac{2}{3} \frac{A(1 - c^2)}{v} + \frac{A}{2} \left(1 + \frac{1}{3} A^2 c^2 \right) (1 - R), \quad (\text{B.135})$$

$$g_{01}(R, c) = \frac{1 - c^2}{z} \left[c + \frac{y + 2R(1 + R)}{z} \right], \quad (\text{B.136})$$

$$g_{02}(R, A, c) = \frac{1}{2} c(1 + R) \left\{ A^2 + \left[\frac{y}{z} \right]^2 \right\}, \quad (\text{B.137})$$

$$g_{11}(R, A, c) = A \left[\frac{2R}{v} + (1 + R)c \right] \frac{y}{z}. \quad (\text{B.138})$$

B.2 Initial-final state interference

Matrix element and differential cross section

The matrix element for the initial-final state interference contribution to real bremsstrahlung is given by:

$$\begin{aligned} \mathcal{M}_{int} &= (2\pi)^4 \delta^{(4)}(k_1 + k_2 - p_1 - p_2 - p) \\ &\cdot \left[(2\pi)^{15} 2k_1^0 2k_2^0 2p_1^0 2p_2^0 2p^0 \right]^{-\frac{1}{2}} \frac{1}{4} \frac{\sum_{spin} 2 \Re \{M_{ini} M_{fin}^*\}}{2 s \beta_0}. \end{aligned} \quad (\text{B.139})$$

The hard photon cross section part

$$\frac{d\sigma_{int}^{hard}}{d\cos\vartheta} = \frac{1}{2} \frac{s}{(4\pi)^4} \left[\int_I + \int_{II} - \int_{III} \right] \frac{1}{4} \frac{\sum_{spin} 2 \Re \{M_{ini} M_{fin}^*\}}{2 s \beta_0} d\varphi_\gamma dx dR, \quad (\text{B.140})$$

then contains the following squared amplitude $|M_{ini}|^2$ including all mass terms:

$$\begin{aligned} &2 \Re \{M_{ini} M_{fin}^*\} = \\ &= (4\pi\alpha)^3 \left\{ \frac{\mathcal{V}(s, s')}{s s'} \left[\frac{1}{V_1} \left(s(Z_1 - Z_2) + (U - T)(3s - s' - 4m_f^2) \right) \right. \right. \\ &\quad + \frac{1}{V_2} \left(-(Z_1 - Z_2)(s' + 4m_f^2) + (U - T)(-3s' + s - 4m_f^2) \right) \\ &\quad + \frac{s - T}{Z_1 V_1} \left(T^2 + (s' - T)^2 + 2m_f^2 s' - 2TU + s^2 + 2m_f^2 s \right) \\ &\quad - \frac{s' - U}{Z_1 V_2} \left(U^2 + (s - U)^2 + 2m_f^2 s - 2TU + s'^2 + 2m_f^2 s' \right) \\ &\quad + \frac{s' - T}{Z_2 V_2} \left(T^2 + (s - T)^2 + 2m_f^2 s - 2TU + s'^2 + 2m_f^2 s' \right) \\ &\quad - \frac{s - U}{Z_2 V_1} \left(U^2 + (s' - U)^2 + 2m_f^2 s' - 2TU + s^2 + 2m_f^2 s \right) \\ &\quad \left. + \left(\frac{1}{Z_2} - \frac{1}{Z_1} \right) \left(s^2 + s'^2 + 2m_f^2(s + s') \right) \right] \\ &\quad + \frac{\mathcal{A}(s, s')}{s s'} \left[2(s + s') + 4m_f^2 + 2s s' \left(\frac{1}{V_1} - \frac{1}{V_2} \right) \right. \\ &\quad + (-sU + s'T) \frac{1}{Z_1} + (s'U - sT) \frac{1}{Z_2} \\ &\quad + (V_2 - 2s) \frac{2m_f^2}{V_1} + (V_1 - 2s') \frac{2m_f^2}{V_2} \\ &\quad \left. + \frac{s - U}{Z_1 V_1} \left(s'^2 - 2s'T - s(T - U) \right) \right] \end{aligned}$$

$$\begin{aligned}
& + \frac{s-T}{Z_2 V_1} (s'^2 - 2s'U + s(T-U)) \\
& + \frac{s'-T}{Z_1 V_2} (s^2 - 2sU + s'(T-U)) \\
& + \frac{s'-U}{Z_2 V_2} (s^2 - 2sT - s'(T-U)) \Big] \\
& + \frac{m_f^2}{s s'} \mathcal{C}_1(s, s') \left[(Z_1 - Z_2) \left(\frac{1}{V_2} - \frac{1}{V_1} \right) \right. \\
& + (s + s') \left(-\frac{s-U}{Z_1 V_1} + \frac{s-T}{Z_2 V_1} + \frac{U}{Z_1 V_2} - \frac{T}{Z_2 V_2} \right) \Big] \\
& + \frac{m_f^2}{s s'} \mathcal{C}_2(s, s') (s + s') \left(\frac{1}{V_1} + \frac{1}{V_2} \right) \Big\}. \tag{B.141}
\end{aligned}$$

The coupling functions $\mathcal{V}(s, s')$ and $\mathcal{A}(s, s')$ are generalizations of (B.3) and (B.4) with the kinematic invariants Z_1 , Z_2 , V_1 , V_2 , T , and U from (A.18) to (A.23) and (A.30) and (A.31), while the extra coupling factors $\mathcal{C}_{1,2}(s, s')$ are new for the interference part:

$$\begin{aligned}
\mathcal{V}(s, s') &= Q_e^2 Q_f^2 + Q_e Q_f v_e v_f (|\chi(s)|\eta(s) + |\chi(s')|\eta(s')) \\
&+ (v_e^2 + a_e^2)(v_f^2 + a_f^2) |\chi(s)\chi(s')| (\eta(s)\eta(s') + \zeta(s)\zeta(s')), \tag{B.142}
\end{aligned}$$

$$\begin{aligned}
\mathcal{A}(s, s') &= Q_e Q_f a_e a_f (|\chi(s)|\eta(s) + |\chi(s')|\eta(s')) \\
&+ 4 v_e v_f a_e a_f |\chi(s)\chi(s')| (\eta(s)\eta(s') + \zeta(s)\zeta(s')), \tag{B.143}
\end{aligned}$$

$$\mathcal{C}_1(s, s') = 4(v_e^2 + a_e^2) a_f^2 |\chi(s)\chi(s')| (\eta(s)\eta(s') + \zeta(s)\zeta(s')), \tag{B.144}$$

$$\mathcal{C}_2(s, s') = 2 a_e a_f Q_e Q_f (|\chi(s)|\eta(s) - |\chi(s')|\eta(s')), \tag{B.145}$$

$$\text{with } \eta(s) = \kappa \frac{s - M_Z^2}{\sqrt{(s - M_Z^2)^2 + \left(\frac{s}{M_Z} \Gamma_Z\right)^2}}, \tag{B.146}$$

$$\zeta(s) = \kappa \frac{s \Gamma_Z / M_Z}{\sqrt{(s - M_Z^2)^2 + \left(\frac{s}{M_Z} \Gamma_Z\right)^2}}, \tag{B.147}$$

$$\chi_Z(s) = \chi(s) \equiv \kappa \frac{s}{s - M_Z^2 + i \frac{s}{M_Z} \Gamma_Z}, \tag{B.148}$$

$$\kappa = \frac{g^2}{4e^2 \cos^2 \theta_W} = \frac{1}{4 \sin^2 \theta_W \cos^2 \theta_W} = \frac{G_\mu}{\sqrt{2}} \frac{M_Z^2}{2\pi\alpha}. \tag{B.149}$$

All other neutral current properties are summarized in Appendix A.1. Interesting to note is that the coupling constant functions $\mathcal{V}(s, s')$, $\mathcal{A}(s, s')$, and $\mathcal{C}_{1,2}(s, s')$ in the interference term naturally depend on both s' and s . It holds: $\mathcal{V}(s') = \mathcal{V}(s', s')$, $\mathcal{A}(s') = \mathcal{A}(s', s')$, which reproduces the initial state factors $\mathcal{V}(s')$ and $\mathcal{A}(s')$. In (B.141) we again will neglect final state mass terms proportional to m_f^2/s as for the initial state bremsstrahlung.

Furthermore, (B.141) contains as denominators

$$\frac{1}{V_i}, \quad \frac{1}{Z_i}, \quad \text{and} \quad \frac{1}{Z_i V_j}, \quad i, j = 1, 2. \quad (\text{B.150})$$

In comparison, the matrix elements for initial state or final state bremsstrahlung terms are proportional to $1/Z_i$, $1/(Z_i Z_j)$, and $1/Z_i^2$, or to $1/V_i$, $1/(V_i V_j)$, and $1/V_i^2$ respectively. For the integration of terms proportional to $\frac{1}{Z_i}$ in the matrix element for the QED interference the same separation of phase space into different regions for the variables $\cos \vartheta$ occurs as in Appendix B.1. This is done in order to treat the occurring mass singularities after neglecting initial mass terms m_e^2/s . The invariants $\frac{1}{V_i}$, whether appearing by themselves or as factors of $1/(Z_j)$ are regular and do not possess this singular behaviour and therefore do not affect the phase space splitting for the variable $\cos \vartheta$.

Finally, there is a symmetric description of the initial state and initial-final state interference results possible, for the angular cross section distributions, as well as for the totally integrated results. This fact also went into the implementation of these new results in the updated program version ZFITTER [38].

The integrated hard radiators $H_{T,FB}^{int}$

The integrated results $H_{T,FB}^{int}(R, A(R), c)$, for the interference of initial and final state hard photon emission are presented below. They can be factorized in one-loop approximation from an improved Born cross section or asymmetry $\sigma_{T,FB}^0(s, s')$ for the differential cross section contribution $d\sigma^{int}$. From $d\sigma^{int}$ then the QED interference contributions $\sigma_{T,FB}^{int}(s, \bar{\xi}, E_{\min}, c)$ can be derived.

Again, the value c is defined as symmetric cut on the minimal and maximal scattering angle of one final-state fermion and $\bar{\xi}$ and E_{\min} as cuts on the maximal acollinearity and minimal energy of the fermions. In the hard photon radiators $H_{T,FB}^{int}(R, A(R), c)$ the dependence on the acollinearity and energy cut is introduced through the value $A = A(R; \bar{\xi}, E_{\min})$. It parameterizes the three different contributions from different regions of phase space for the variables x and R , each region depending on only one of the cuts (see (2.52), (2.53), and (2.54)).

The distinction of analytical expressions according to the splitting of phase space due to mass singularities, which was discussed in Section 2.3.2, follows the

same lines as Section 2.3.3 and Appendix B.1. See for this also the analytical results on $H_{T,FB}^{ini}(R, A(R), c)$ in (2.127) to (2.150).

$$\sigma_{int_A}^{hard}(s, \bar{\xi}, E_{\min}, c, \varepsilon) = \int_{R_{min}}^{1-\varepsilon} dR \left[H_A^{int}(R, A(R), c) \sigma_A^0(s, s') \right], \quad A = T, FB, \quad (\text{B.151})$$

$$\begin{aligned} \text{I. case :} \quad & (1)^{++} \leftrightarrow (2)^{++} \quad (\Rightarrow A \geq A_0(R)) \\ H_T^{int}(R, A, c) &= \frac{\alpha}{\pi} Q_e Q_f \left\{ \mathcal{F}_{00}(R, A, c) - \mathcal{F}_{00}(R, -c, A) + \mathcal{C}_0(R, A, c) \right\}, \end{aligned} \quad (\text{B.152})$$

$$H_{FB}^{int}(R, A, c) = \frac{\alpha}{\pi} Q_e Q_f \left\{ \mathcal{G}_{00}(R, A, c) + \mathcal{G}_{00}(R, -c, A) \right\}, \quad (\text{B.153})$$

$$\begin{aligned} \text{II. case :} \quad & (1)^{+-} \leftrightarrow (2)^{+-} \quad (\Rightarrow A < A_0(R)) \\ H_T^{int}(R, A, c) &= \frac{\alpha}{\pi} Q_e Q_f \left\{ \mathcal{F}_{11}(R, A, c) - \mathcal{F}_{11}(R, -c, A) + \mathcal{C}_0(R, A, c) \right\}, \end{aligned} \quad (\text{B.154})$$

$$\begin{aligned} H_{FB}^{int}(R, A, c) &= \frac{\alpha}{\pi} Q_e Q_f \left\{ \mathcal{G}_{11}(R, A, c) + \mathcal{G}_{11}(R, -c, A) + \mathcal{G}_1(R, A, c) \right. \\ &\quad \left. + 2 \mathcal{G}_{10}(R, A, c) \right\}, \end{aligned} \quad (\text{B.155})$$

$$\begin{aligned} \text{III. case :} \quad & (1)^{++} \leftrightarrow (2)^{+-} \\ H_T^{int}(R, A, c) &= \frac{\alpha}{\pi} Q_e Q_f \left\{ \mathcal{F}_{11}(R, A, c) - \mathcal{F}_{00}(R, -c, A) + \mathcal{F}_{10}(R, c) \right. \\ &\quad \left. + \mathcal{C}_0(R, A, c) \right\}, \end{aligned} \quad (\text{B.156})$$

$$\begin{aligned} a. \ A < A_0(R) \quad : \\ H_{FB}^{int}(R, A, c) &= \frac{\alpha}{\pi} Q_e Q_f \left\{ \mathcal{G}_{11}(R, A, c) + \mathcal{G}_{00}(R, -c, A) + \mathcal{G}_1(R, A, c) \right. \\ &\quad \left. - \mathcal{G}_0(R, A, c) + \mathcal{G}_{10}(R, A, c) \right\}, \end{aligned} \quad (\text{B.157})$$

$$\begin{aligned} b. \ A \geq A_0(R) \quad : \\ H_{FB}^{int}(R, A, c) &= \frac{\alpha}{\pi} Q_e Q_f \left\{ \mathcal{G}_{11}(R, A, c) + \mathcal{G}_{00}(R, -c, A) + \mathcal{G}_0(R, A, c) \right. \\ &\quad \left. + \mathcal{G}_{10}(R, A, c) \right\}, \end{aligned} \quad (\text{B.158})$$

IV. case : $(1)^{- -} \leftrightarrow (2)^{+ +}$

$$H_T^{int}(R, A, c) = \frac{\alpha}{\pi} Q_e Q_f \left\{ \mathcal{F}_{11}(R, A, c) + \mathcal{F}_{11}(R, -c, A) + \mathcal{C}_0(R, A, c) \right\}, \quad (\text{B.159})$$

a. $A < A_0(R)$:

$$H_{FB}^{int}(R, A, c) = \frac{\alpha}{\pi} Q_e Q_f \left\{ \mathcal{G}_{11}(R, A, c) - \mathcal{G}_{11}(R, -c, A) + \mathcal{G}_1(R, A, c) + 2 \mathcal{G}_{10}(R, A, c) \right\}, \quad (\text{B.160})$$

b. $A \geq A_0(R)$:

$$H_{FB}^{int}(R, A, c) = \frac{\alpha}{\pi} Q_e Q_f \left\{ \mathcal{G}_{11}(R, A, c) - \mathcal{G}_{11}(R, -c, A) + 2 \mathcal{G}_0(R, A, c) + 2 \mathcal{G}_{10}(R, A, c) \right\}. \quad (\text{B.161})$$

The functions $\mathcal{F}_{i(j)}$, $\mathcal{G}_{i(j)}$, and \mathcal{C}_0 appearing above depend on the following logarithms, linear functions, variables, and cut parameters ($A = A(R)$) ($i, j = 0, 1$):

$$\mathcal{F}_{ii}(R, A, c) = \mathcal{F}_{ii}(L_z(R, c); L_z(R, \pm A); L^\pm(c); L^\pm(A); z(R, c); R, A, c), \quad (\text{B.162})$$

$$\mathcal{G}_{ii}(R, A, c) = \mathcal{G}_{ii}(L_z(R, c); L_z(R, \pm A); L^\pm(c); L^\pm(A); z(R, c); R, A, c), \quad (\text{B.163})$$

$$\mathcal{G}_{0,1,10}(R, A, c) = \mathcal{G}_{0,1,10}(L_z(R, \pm A); L^\pm(A); R, A, c), \quad (\text{B.164})$$

$$\mathcal{C}_0 = \mathcal{C}_0(R, A, c), \quad (\text{B.165})$$

$$\mathcal{F}_{10} = \mathcal{F}_{10}(R, c). \quad (\text{B.166})$$

\mathcal{F}_{00} , \mathcal{G}_{00} , \mathcal{F}_{11} , and \mathcal{G}_{11} together with \mathcal{C}_0 , \mathcal{F}_{10} , and $\mathcal{G}_{0,1,10}$ are now illustrated below ($v \equiv 1 - R$):

$$\begin{aligned} \mathcal{F}_{00}(R, A, c) = & \frac{2}{v} \left[(1 - c^2) \ln \left(\frac{1 + c}{1 - c} \right) - 2c \right] \\ & - (1 + 2R - c^2 + 2cR) \left[\ln \left(\frac{1 + c}{1 - c} \right) - \ln R \right] \\ & - \frac{1}{2} \left[(1 - R)^2 - c^2(1 + R)^2 \right] \end{aligned} \quad (\text{B.167})$$

$$\left\{ \ln \left[\frac{z^2(R, c)}{4R^2(1-c)^2} \right] + \ln(1-A^2) + 1 \right\} \\ + c(3 + 2R + R^2) - (1 + R^2),$$

$$\begin{aligned} \mathcal{F}_{11}(R, A, c) &= \frac{2}{v} \left[(1-c^2) \ln \left(\frac{1+A}{1-A} \right) - 2A \right] \\ &\quad - \frac{1}{2} \left[(1-c^2)(3 + 2R + R^2) + 4cR \right] \ln \left(\frac{1+A}{1-A} \right) \\ &\quad + A \left[2(1 + R + R^2) + \frac{1}{2}(1+c^2)(1-R^2) - c(1-R)^2 \right], \end{aligned} \quad (\text{B.168})$$

$$\mathcal{C}_0(R, c) = 2Ac(1 - R^2), \quad (\text{B.169})$$

$$\mathcal{F}_{10}(R, c) = \frac{2}{v}(1 - c^2) \ln R, \quad (\text{B.170})$$

$$\begin{aligned} \mathcal{G}_{00}(R, A, c) &= -\frac{2}{v} \left\{ \left(c + \frac{c^3}{3} \right) \left[\ln \left(\frac{1+c}{1-c} \right) - \ln R \right] \right. \\ &\quad \left. + \frac{1}{3} \left[4 \ln(1-c^2) - 8 \ln \left[\frac{z(R, c)}{1+R} \right] + c^2 \right] \right\} \\ &\quad + (1 + 2R - c^2 + 2cR) \ln \left(\frac{1+c}{1-c} \right) \\ &\quad + \frac{1}{3}(1 + 8R + 5R^2) \left\{ \ln(1-c) - \ln \left[\frac{z(R, c)}{1+R} \right] \right\} \\ &\quad + \left[\frac{c^3}{3}(1 + R + R^2) + \frac{c^2}{2}(1 - R^2) + c(1 - R + R^2) \right] \\ &\quad \left\{ \ln \left[\frac{z^2(R, c)}{4R^2(1-c)^2} \right] + \ln(1-A^2) \right\} \\ &\quad + \frac{1}{2}c^2 \left\{ (1 - R^2) \ln \left(\frac{1+A}{1-A} \right) + 2R \ln \left[\frac{z(R, A)}{z(R, -A)} \right] \right\} \\ &\quad + c(c - 2R) \ln R \\ &\quad - \frac{4}{z(R, c)} \left[2(1 + R) + 4c + \frac{c}{1+R} + \frac{5c^2}{1+R} + \frac{2c^3}{(1+R)^2} \right] \\ &\quad + \frac{c^3}{12} [A^2(1 - R)^2 + 5(1 + R)^2] \\ &\quad + c^2 \left[-\frac{A}{2}(1 - R^2) - \frac{1}{2}R^2 + \frac{4}{3}R + \frac{19}{6} + \frac{2}{1+R} + \frac{4}{(1+R)^2} \right] \\ &\quad + c \left[\frac{A^2}{4}(1 - R)^2 + \frac{1}{4}R^2 - \frac{1}{6}R + \frac{17}{4} + \frac{8}{1+R} \right] + 8, \end{aligned} \quad (\text{B.171})$$

$$\begin{aligned}
\mathcal{G}_{11}(R, A, c) = & -\frac{2}{v} \left(c + \frac{c^3}{3} \right) \ln \left(\frac{1+A}{1-A} \right) \\
& + \frac{1}{2} \left\{ 2 \left[c + \frac{c^3}{3} \right] (1+R+R^2) - c^2(1+R^2) - \frac{1}{3} (5-4R+5R^2) \right\} \\
& \ln \left(\frac{1+A}{1-A} \right) \\
& + \frac{1}{2} A(1+c^2)(1-R) [(1-R) + c(1+R)], \tag{B.172}
\end{aligned}$$

$$\begin{aligned}
\mathcal{G}_0(R, A, c) = & -\frac{2}{3v} \left\{ 4 \left[\ln(1-A^2) + \ln \left[\frac{(1+R)^2}{4R} \right] \right] + A^2 \right\} \\
& + \frac{1}{6} (11+8R+5R^2) \left\{ \ln(1-A^2) + \ln \left[\frac{(1+R)^2}{4R} \right] - \ln R \right\} \\
& + (1+2R) \ln R \\
& - \frac{1}{2} A c^2 (1-R^2) \\
& + \frac{1}{3} A^2 (1+R+R^2) \\
& - \frac{2}{1+R} + \frac{11}{6} - R + \frac{1}{6} R^2, \tag{B.173}
\end{aligned}$$

$$\begin{aligned}
\mathcal{G}_1(R, A, c) = & \frac{1}{3} (5-4R+5R^2) \ln \left(\frac{1+A}{1-A} \right) \\
& - A(1-R) [(1-R) + c^2(1+R)], \tag{B.174}
\end{aligned}$$

$$\mathcal{G}_{10}(R, A, c) = \frac{1}{2} c^2 \left\{ (1-R^2) \ln \left(\frac{1+A}{1-A} \right) + 2R \ln \left[\frac{z(R, A)}{z(R, -A)} \right] \right\}. \tag{B.175}$$

B.3 Final state radiation

Matrix element and differential cross section

The kinematically allowed phase space region is given in Fig. B.1. For the third region of phase space III, it will be necessary to exchange the order of the last two integrations over x and R in order to integrate the final state terms analytically completely for total or differential cross sections.

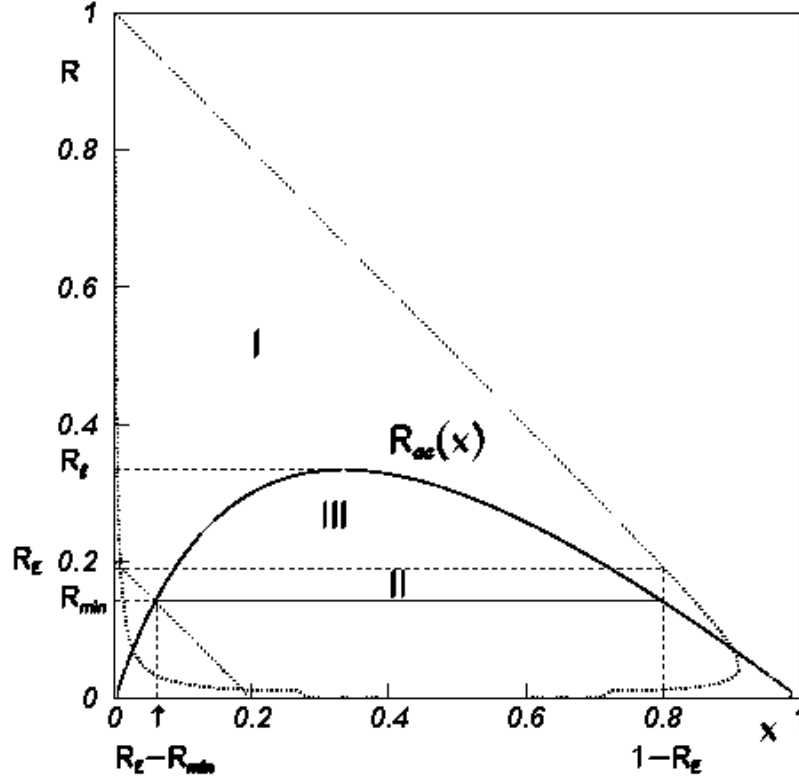


Figure B.1: Phase space with cuts on maximal acollinearity and minimal fermion energy.

The kinematics for the hard photon phase space has been extensively discussed in Appendix A with all kinematical variables, invariants, and boundaries defined by the cuts on maximal acollinearity and minimal energy of the final state. A cut on one scattering angle can be treated in addition.

The equation of the phase space boundary defined by the acollinearity cut, shown in Fig. B.1, can be written as

$$R = R_{ac}(x) = \frac{x(1-x)}{x + \rho - 1}, \quad (\text{B.176})$$

$$R_{\min} = \frac{R_E(1 - R_E)}{\rho - R_E}, \quad (\text{B.177})$$

$$\rho = 1 + \tan^2 \frac{\bar{\xi}}{2} = \frac{(1 + R_\xi)^2}{4R_\xi} \geq 1. \quad (\text{B.178})$$

Here we have introduced R_{\min} as starting value of the variable R which can be substituted by a sufficiently large see (A.83) and the parameter ρ following the notation of [157]. Results on the complete final state corrections to the total cross section σ_T were derived there first. The calculation is repeated here and some small misprints in the original work can be corrected. Moreover, the complete differential cross section $d\sigma/d\cos\vartheta$ is presented here from which σ_T and also the forward-backward asymmetry A_{FB} , not given in [157], trivially can be extracted.

Using the separation of phase space into three different regions I, II, and III, discussed in Section 2.3 and Appendix A.3 (see also Fig. 2.4 and Fig. B.1), hard photonic final state contribution to the differential cross section can be written as:

$$\frac{d\sigma_{fin}^{hard}}{d\cos\vartheta} = \left[\int_I + \int_{II} - \int_{III} \right] d\varphi_\gamma dx dR \frac{d\sigma_{fin}^{hard}}{d\varphi_\gamma dx dR d\cos\vartheta}. \quad (\text{B.179})$$

Starting from the final state bremsstrahlung matrix element

$$\begin{aligned} \mathcal{M}_{fin} &= (2\pi)^4 \delta^{(4)}(k_1 + k_2 - p_1 - p_2 - p) \\ &\quad \left[(2\pi)^{15} 2k_1^0 2k_2^0 2p_1^0 p_2^0 2p^0 \right]^{-\frac{1}{2}} M_{fin}, \end{aligned} \quad (\text{B.180})$$

with M_{fin} given in (A.5), one can write the contribution of the final state hard bremsstrahlung in terms of the four independent kinematic variables φ_γ , x , R , and $\cos\vartheta$:

$$\frac{d\sigma_{fin}^{hard}}{d\cos\vartheta} = \frac{s}{(4\pi)^4} \left[\int_I + \int_{II} - \int_{III} \right] \frac{\sum_{spin} |M_{fin}|^2}{2s\beta_0} d\varphi_\gamma dx dR. \quad (\text{B.181})$$

The squared amplitude $|M_{fin}|^2$ is given as:

$$\begin{aligned}
|M_{fin}|^2 = & (4\pi\alpha)^3 \left\{ \frac{\mathcal{V}(s)}{s^2} \left[\frac{2}{V_1 V_2} (s^2 - T U - (U + Z_1)(T + Z_2) + 2 s' m_f^2) \right. \right. \\
& + \frac{V_2}{V_1} + \frac{V_1 - 2s}{V_2} + 4 \frac{m_f^2}{s} \left(\frac{U}{V_1} + \frac{U + Z_1}{V_2} \right) \left(\frac{T}{V_1} + \frac{T + Z_2}{V_2} \right) \\
& \left. \left. - 2m_f^2 (s + 2m_f^2) \left(\frac{1}{V_1} + \frac{1}{V_2} \right)^2 \right] \right. \\
& + \frac{\mathcal{A}(s)}{s^2} \left[\left(-\frac{2m_f^2}{V_1} + \frac{s' - 2m_f^2}{V_2} + 1 \right) \frac{U - T}{V_1} \right. \\
& + \left(-\frac{2m_f^2}{V_2} + \frac{s' - 2m_f^2}{V_1} + 1 \right) \frac{U + Z_1 - T - Z_2}{V_2} \left. \right] \\
& \left. + \frac{8m_f^2}{s} (v_e^2 + a_e^2) a_f^2 \frac{1}{s^2} |\chi(s)|^2 \left[\frac{Z_1 Z_2 - s s'}{V_1 V_2} + s m_f^2 \left(\frac{1}{V_1} + \frac{1}{V_2} \right)^2 \right] \right\}, \tag{B.182}
\end{aligned}$$

where $\mathcal{V}(s)$ and $\mathcal{A}(s)$ are functions of the center-of-mass energy squared s in the final state case. They contain the neutral current couplings and Z boson propagator and are given in (B.3) and (B.4). The bremsstrahlung kinematic invariants Z_1 , Z_2 , V_1 , V_2 , T , and U are taken from (A.18) to (A.23) and (A.30) and (A.31). It is useful to also introduce the dimensionless quantities:

$$v_1 \equiv \frac{V_1}{s}, \quad t \equiv \frac{T}{s}, \quad u \equiv \frac{U}{s}, \quad \text{and} \quad v \equiv 1 - R = 1 - \frac{s'}{s}. \tag{B.183}$$

Integration over φ_γ

The only invariants depending on φ_γ are:

$$Z_{1,2} = a_{1,2} \pm b \cos \varphi_\gamma, \tag{B.184}$$

where

$$a_{1,2} = \frac{1}{2} s v (1 \pm \beta_0 \cos \vartheta \cos \theta_\gamma), \tag{B.185}$$

$$b^2 = \frac{1}{4} s^2 v^2 \beta_0^2 (1 - \cos^2 \theta) (1 - \cos^2 \theta_\gamma), \tag{B.186}$$

$$\cos \theta_\gamma = \frac{R v_1 - x}{v \sqrt{\lambda_2}}. \tag{B.187}$$

Table of integrals:

$$\frac{1}{2\pi} \int_0^{2\pi} d\varphi_\gamma = 1, \quad \frac{1}{2\pi} \int_0^{2\pi} d\varphi_\gamma \cos \varphi_\gamma = 0, \quad \frac{1}{2\pi} \int_0^{2\pi} d\varphi_\gamma \cos^2 \varphi_\gamma = \frac{1}{2}. \quad (\text{B.188})$$

The complete integration over φ_γ yields:

$$\begin{aligned} \frac{1}{2\pi} \int_0^{2\pi} d\varphi_\gamma |M_{fin}|^2 &= (4\pi\alpha)^3 \left\{ \frac{\mathcal{V}(s)}{s} \left[\frac{1 + \cos^2 \vartheta}{2} \left(-\frac{2m_f^2}{s} \left(\frac{1}{v_1^2} + \frac{1}{x^2} \right) + \frac{2}{v_1 x} \right. \right. \right. \\ &\quad \left. \left. - \frac{1+R}{v_1} + \frac{1+R}{x} - 2 \right) + (1 - 3 \cos^2 \vartheta) \frac{R}{(R+x)^2} \right] \\ &\quad + \frac{\mathcal{A}(s)}{s} \cos \vartheta \left[-\frac{2m_f^2}{s} \left(\frac{1}{v_1^2} + \frac{1}{x^2} \right) + \frac{2}{v_1 x} \right. \\ &\quad \left. \left. - \frac{1+R}{v_1} + \frac{1+R}{x} - 2 \frac{1+R}{R+x} \right] \right\}. \end{aligned} \quad (\text{B.189})$$

We only keep terms proportional to $m_f^2/v_{1,2}^2$ because their contributions could be non-negligible. Elsewhere we set $m_f = 0$.

Integration over x

The integration over x can be performed using the parameterization with $A(R)$ in (2.52), (2.53), and (2.54). So we integrate over x in the limits:

$$(1-R) \frac{1-A(R)}{2} \leq x(R) \leq (1-R) \frac{1+A(R)}{2}. \quad (\text{B.190})$$

The variable R then remains as last variable of integration:

Table of integrals

$$[f(x)]_{(x)} = \int_{v^{\frac{1-A(R)}{2}}}^{v^{\frac{1+A(R)}{2}}} dx f(x), \quad (\text{B.191})$$

$$[1]_{(x)} = v A(R), \quad (\text{B.192})$$

$$\left[\frac{1}{v_{1,2}} \right]_{(x)} = \ln \frac{1+A(R)}{1-A(R)}, \quad (\text{B.193})$$

$$\left[\frac{1}{v_1^2, x^2} \right]_{(x)} = \frac{1}{v} \frac{4 A(R)}{1-A(R)^2}, \quad (\text{B.194})$$

$$\left[\frac{1}{x+R} \right]_{(x)} = \ln \frac{1+R+A(R)(1-R)}{1+R-A(R)(1-R)}, \quad (\text{B.195})$$

$$\left[\frac{1}{(x+R)^2} \right]_{(x)} = \frac{4 A(R) v}{(1+R)^2 - A(R)^2 v^2}. \quad (\text{B.196})$$

The result of the integration of (B.181) with (B.189) over x is:

$$\begin{aligned} \frac{d\sigma_{fin}^{hard}}{d \cos \vartheta} &= \frac{\pi \alpha^2}{s} \frac{\alpha}{\pi} Q_f^2 \left[\int_I + \int_{II} - \int_{III} \right] dR \\ &- \left\{ \mathcal{V}(s) \left[\frac{1 + \cos^2 \vartheta}{2} \left(\frac{1+R^2}{v} \ln \frac{1+A}{1-A} - Av \right. \right. \right. \\ &\quad \left. \left. - \frac{8m_f^2 A}{sv(1-A^2)} \right) + \frac{1-3\cos^2 \vartheta}{2} \frac{4AvR}{(1+R)^2 - A^2 v^2} \right] \\ &+ \mathcal{A}(s) \cos \vartheta \left[\frac{1+R^2}{v} \ln \frac{1+A}{1-A} \right. \\ &\quad \left. \left. - (1+R) \ln \frac{1+R+A(1-R)}{1+R-A(1-R)} - \frac{8m_f^2 A}{sv(1-A^2)} \right] \right\}. \end{aligned} \quad (\text{B.197})$$

Integration over R

Region I

The value R varies in the interval

$$R_E \leq R \leq 1 - \varepsilon, \quad (\text{B.198})$$

where $\varepsilon/2$ is the normalized minimal photon energy. The value ε separates soft and hard photon phase space and cancels when adding the soft contributions (see Appendix A.3).

Only region I has to take into account the soft-photon corner of phase space, i.e. only the expressions derived there have to be regularized. For this, the soft and virtual photonic corrections from (C.91) with (C.92) have to be added, with the necessary modifications for the final state case. The hard-photon results for regions II and III are finite.

For region I, logarithmic mass terms $L_f = \ln(s'/m_f^2)$ have to be taken into account. The parameter $A(R)$ for the final state expressions of region I therefore has to be taken correctly with mass:

$$1 - A^2(R) = 4 \frac{m_f^2}{sR}. \quad (\text{B.199})$$

For the initial state bremsstrahlung and initial-final state interference expressions this be could set to $A \cong 1$ (see Sections 2.3.3 and 2.3.3). Inserting (B.199) into (B.197), we get:

$$\begin{aligned} \frac{d\sigma_{finI}^{hard}}{d\cos\vartheta} = & \frac{\pi\alpha^2}{s} \frac{\alpha}{\pi} Q_f^2 \int_I dR \left\{ \mathcal{V}(s) \left[\frac{1 + \cos^2\vartheta}{2} \left(\ln \frac{s}{m_f^2} - 1 + \ln R \right) \frac{1 + R^2}{v} \right. \right. \\ & \left. \left. + \frac{1 - 3\cos^2\vartheta}{2} v \right] \right. \\ & \left. + \mathcal{A}(s) \cos\vartheta \left[\left(\ln \frac{s}{m_f^2} - 1 \right) \frac{1 + R^2}{v} + \frac{2}{v} \ln R + v \right] \right\}. \quad (\text{B.200}) \end{aligned}$$

The over $\cos\vartheta$ in region I integrated flux functions of (B.200) are given for the total cross section σ_T in [35] and for the forward-backward cross section σ_{FB} in [32]. The final integration of (B.200) over R uses the following

Table of integrals

$$[f(R)]_{(R)} = \int_{R_E}^{1-\varepsilon} dR f(R), \quad (\text{B.201})$$

$$[1]_{(R)} = 1 - R_E, \quad (\text{B.202})$$

$$[\ln R]_{(R)} = -1 + R_E - R_E \ln R_E, \quad (\text{B.203})$$

$$[R]_{(R)} = \frac{1}{2} (1 - R_E^2), \quad (\text{B.204})$$

$$[R \ln R]_{(R)} = \frac{1}{4} (-1 + R_E^2) - \frac{1}{2} R_E^2 \ln R_E, \quad (\text{B.205})$$

$$\left[\frac{1}{1-R} \right]_{(R)} = -\ln \frac{2\varepsilon}{\sqrt{s}} + \ln(1 - R_E), \quad (\text{B.206})$$

$$\left[\frac{\ln R}{1-R} \right]_{(R)} = -\text{Li}_2(1) + \text{Li}_2(R_E) + \ln R_E \ln(1 - R_E). \quad (\text{B.207})$$

After integration over R we have obtained the hard bremsstrahlung contribution to the differential cross-section for region I:

$$\begin{aligned} \frac{d\sigma_{finI}^{hard}}{d\cos\vartheta} = & \frac{\pi\alpha^2}{s} \frac{\alpha}{\pi} Q_f^2 \left\{ \mathcal{V}(s) \left[\frac{1 + \cos^2\vartheta}{2} \left(\left(\ln \frac{s}{m_f^2} - 1 \right) (-2\ln\varepsilon - 2\ln 2 \right. \right. \right. \\ & + 2\ln(1 - R_E) - \frac{3}{2} + R_E + \frac{R_E^2}{2} \Big) + \frac{5}{4} - R_E - \frac{R_E^2}{4} \\ & + R_E \left(1 + \frac{R_E}{2} \right) \ln R_E - \frac{\pi^2}{3} + 2\text{Li}_2(R_E) + 2\ln R_E \ln(1 - R_E) \Big) \\ & + \frac{1 - 3\cos^2\vartheta}{4} (1 - R_E)^2 \Big] \\ & + \mathcal{A}(s) \cos\vartheta \left[\left(\ln \frac{s}{m_f^2} - 1 \right) \left(-\ln \frac{(2\varepsilon)^2}{s} + 2\ln(1 - R_E) - \frac{3}{2} \right. \right. \\ & + R_E + \frac{R_E^2}{2} \Big) + \frac{1}{2} (1 - R_E)^2 - \frac{\pi^2}{3} + 2\text{Li}_2(R_E) \\ & \left. \left. + 2\ln R_E \ln(1 - R_E) \right] \right\}. \quad (\text{B.208}) \end{aligned}$$

Adding the soft and virtual contributions (see e.g. (C.91) with (C.92)), the regularized result for phase space region I can be written as:

$$\frac{d\sigma_{finI}}{d\cos\vartheta} = \frac{d\sigma_{fin}^{soft+virtual}}{d\cos\vartheta} + \frac{d\sigma_{finI}^{hard}}{d\cos\vartheta} \quad (\text{B.209})$$

$$\begin{aligned} &= \frac{\pi\alpha^2}{s} \frac{\alpha}{\pi} Q_f^2 \\ &\cdot \left\{ \mathcal{V}(s) \left[\frac{1+\cos^2\vartheta}{2} \left(\left(\ln \frac{s}{m_f^2} - 1 \right) \left(2\ln(1-R_E) + R_E + \frac{R_E^2}{2} \right) + \frac{3}{4} \right. \right. \right. \\ &\quad \left. \left. - R_E - \frac{1}{4}R_E^2 + R_E \left(1 + \frac{1}{2}R_E \right) \ln R_E + 2\text{Li}_2(R_E) \right. \right. \\ &\quad \left. \left. + 2\ln R_E \ln(1-R_E) \right) + \frac{1-3\cos^2\vartheta}{4} (1-R_E)^2 \right] \\ &\quad + \mathcal{A}(s) \cos\vartheta \left[\left(\ln \frac{s}{m_f^2} - 1 \right) \left(2\ln(1-R_E) \right. \right. \\ &\quad \left. \left. + R_E + \frac{R_E^2}{2} \right) - R_E + \frac{R_E^2}{2} + 2\text{Li}_2(R_E) + 2\ln R_E \ln(1-R_E) \right] \right\}. \end{aligned} \quad (\text{B.210})$$

One can see that this expression does not contain divergences nor the parameter ε used to distinguish the soft photons from hard photons.

Region II

The value for $A(R)$ here is given in (2.53). The value R varies in the interval

$$R_{\min} \leq R \leq \bar{R}_E, \quad (\text{B.211})$$

where $\bar{R}_E \cong R_E$ (see Fig. B.1). The final state mass m_f^2 has now been neglected because only mass terms proportional to m_f^2 or $m_f^2 L_f$ can appear which vanish for $m_f^2 \rightarrow 0$. Inserting $A(R)$ from (2.53) into (B.197) we get after partial fraction decomposition:

$$\begin{aligned} \frac{d\sigma_{finII}^{hard}}{d\cos\vartheta} &= \frac{\pi\alpha^2}{s} \frac{\alpha}{\pi} Q_f^2 \int_{II} dR \\ &\cdot \left\{ \mathcal{V}(s) \left[\frac{1+\cos^2\vartheta}{2} \left(\frac{1+R^2}{v} \ln \frac{1-R_E}{R_E-R} - 1 - R + 2R_E \right) \right. \right. \\ &\quad \left. \left. + \frac{1-3\cos^2\vartheta}{2} \left(\frac{R}{R_E} - \frac{R}{1+R-R_E} \right) \right] \right. \\ &\quad \left. + \mathcal{A}(s) \cos\vartheta \left[\frac{1+R^2}{v} \ln \frac{1-R_E}{R_E-R} - (1+R) \ln \frac{1+R-R_E}{R_E} \right] \right\}. \end{aligned} \quad (\text{B.212})$$

Introducing the notation from [157],

$$x_\rho = 1 - R_E + R_{\min} = \frac{\rho(1-R_E)}{\rho - R_E}, \quad (\text{B.213})$$

$$R_{\min} = R_{\text{cut}} = 2R_E - 1, \quad (\text{B.214})$$

we have with (B.177) and (B.178) the general inequalities:

$$R_{\text{emin}} \leq R_{\text{min}}, \quad 1 + R_{\text{min}} - 2R_E \geq 0, \quad (\text{B.215})$$

$$R_{\text{min}} \leq R_E, \quad 0 \leq R_E - R_{\text{min}} \leq 1 - R_E, \quad (\text{B.216})$$

$$R_E \leq x_\rho \leq 1, \quad 0 \leq 1 - x_\rho \leq 1 - R_E. \quad (\text{B.217})$$

Now we can integrate over R using the following

Table of integrals

$$[f(R)]_{(R)} = \int_{R_{\text{min}}}^{R_E} dR f(R), \quad (\text{B.218})$$

$$[1]_{(R)} = R_E - R_{\text{min}}, \quad (\text{B.219})$$

$$[R]_{(R)} = \frac{1}{2}(R_E^2 - R_{\text{min}}^2), \quad (\text{B.220})$$

$$\left[\frac{1}{1 + R - R_E} \right]_{(R)} = -\ln(1 + R_{\text{min}} - R_E), \quad (\text{B.221})$$

$$\left[\ln \frac{1 - R_E}{R_E - R} \right]_{(R)} = (R_E - R_{\text{min}}) \left(1 + \ln \frac{1 - R_E}{R_E - R_{\text{min}}} \right), \quad (\text{B.222})$$

$$\left[R \ln \frac{1 - R_E}{R_E - R} \right]_{(R)} = \frac{1}{2}(R_E^2 - R_{\text{min}}^2) \left(\frac{1}{2} + \ln \frac{1 - R_E}{R_E - R_{\text{min}}} \right) \quad (\text{B.223})$$

$$\begin{aligned} & + \frac{1}{2} R_E (R_E - R_{\text{min}}), \\ \left[\frac{1}{1 - R} \ln \frac{1 - R_E}{R_E - R} \right]_{(R)} & = -\frac{1}{2} \ln^2 \frac{1 - R_E}{1 - R_{\text{min}}} + \text{Li}_2(1) - \text{Li}_2\left(\frac{1 - R_E}{1 - R_{\text{min}}}\right), \end{aligned} \quad (\text{B.224})$$

$$\begin{aligned} \left[\ln \frac{1 + R - R_E}{R_E} \right]_{(R)} & = -(R_E - R_{\text{min}}) (1 + \ln R_E) \\ & - (1 + R_{\text{min}} - R_E) \ln(1 + R_{\text{min}} - R_E), \end{aligned} \quad (\text{B.225})$$

$$\begin{aligned} \left[R \ln \frac{1 + R - R_E}{R_E} \right]_{(R)} & = -\frac{1}{2}(R_E^2 - R_{\text{min}}^2) \left(\frac{1}{2} + \ln R_E \right) \\ & + \frac{1}{2}((1 - R_E)^2 - R_{\text{min}}^2) \ln(1 + R_{\text{min}} - R_E) \\ & + \frac{1}{2}(1 - R_E)(R_E - R_{\text{min}}). \end{aligned} \quad (\text{B.226})$$

So, performing the integration over R in (B.212) we obtain the hard bremsstrahlung contribution to the differential cross-section for region II:

$$\begin{aligned}
\frac{d\sigma_{finII}^{hard}}{d\cos\vartheta} = & \frac{\pi\alpha^2}{s} \frac{\alpha}{\pi} Q_f^2 \left\{ \mathcal{V}(s) \left[\frac{1+\cos^2\vartheta}{2} \left(-2(R_E - R_{\min}) + \frac{3}{4}(R_E - R_{\min})^2 \right. \right. \right. \\
& \left. \left. - \ln^2 \frac{1-R_E}{1-R_{\min}} + \frac{\pi^2}{3} - 2\text{Li}_2\left(\frac{1-R_E}{1-R_{\min}}\right) \right. \right. \\
& \left. \left. + \left[R_E(1 + \frac{R_E}{2}) - R_{\min}(1 + \frac{R_{\min}}{2}) \right] [\ln(R_E - R_{\min}) - \ln(1 - R_E)] \right] \right. \\
& \left. \frac{1-3\cos^2\vartheta}{2} \left(-\frac{(R_E - R_{\min})^2}{2R_E} - (1 - R_E) \ln x_\rho \right) \right] \\
& + \mathcal{A}(s) \cos\vartheta \left[-\frac{R_E}{2} + \frac{R_{\min}}{2} + x_\rho \left(R_E + \frac{x_\rho}{2} \right) \ln x_\rho \right. \\
& \left. - \ln^2 \frac{1-R_E}{1-R_{\min}} + \frac{\pi^2}{3} - 2\text{Li}_2\left(\frac{1-R_E}{1-R_{\min}}\right) \right. \\
& \left. + \left[R_E(1 + \frac{R_E}{2}) - R_{\min}(1 + \frac{R_{\min}}{2}) \right] \right. \\
& \left. \cdot [\ln R_E + \ln(R_E - R_{\min}) - \ln(1 - R_E)] \right] \left. \right\}. \tag{B.227}
\end{aligned}$$

Region III

Region III is parameterized by:

$$III : \quad R_E - R_{\min} \leq x \leq 1 - R_E, \tag{B.228}$$

$$R_{\min} \leq R \leq R_{ac}(x), \tag{B.229}$$

where the acollinearity bound $R_{ac}(x)$ was defined in (B.176). Starting from the expression (B.181) with (B.189), one sees that for a complete analytical integration over x and R one should integrate over R first, and then over x :

Table of integrals

$$[f(R)]_{(R)} = \int_{R_{\min}}^{R_{ac}(x)} dR f(R), \tag{B.230}$$

$$[1]_{(R)} = R_{ac}(x) - R_{\min}, \tag{B.231}$$

$$[R]_{(R)} = \frac{1}{2} (R_{ac}^2 - R_{\min}^2), \tag{B.232}$$

$$\left[\frac{1}{v_1} \right]_{(R)} = -\ln \frac{1 - R_{ac}(x) - x}{1 - R_{\min} - x}, \quad (\text{B.233})$$

$$\left[\frac{1}{R+x} \right]_{(R)} = \ln \frac{R_{ac}(x) + x}{R_{\min} + x}, \quad (\text{B.234})$$

$$\left[\frac{1}{(R+x)^2} \right]_{(R)} = -\frac{1}{R_{ac}(x) + x} + \frac{1}{R_{\min} + x}. \quad (\text{B.235})$$

The result of the integration over R is:

$$\begin{aligned} \frac{d\sigma_{finIII}^{hard}}{d\cos\vartheta} &= \frac{\alpha}{\pi} Q_f^2 \int_{III} dx \\ &\left\{ \frac{d\sigma^{born}}{d\cos\vartheta} \left[\frac{1}{2} (1 + R_{\min}) + \frac{1}{4}x + \frac{R_{\min}}{2} \left(1 + \frac{R_{\min}}{2} \right) \frac{1}{x} \right. \right. \\ &\quad - \frac{\rho}{2} \left(1 + \frac{\rho}{2} \right) \frac{1}{x + \rho - 1} + \frac{1}{4} \rho^2 (\rho - 1) \frac{1}{(x + \rho - 1)^2} \\ &\quad \left. + \left(1 - \frac{x}{2} - \frac{1}{x} \right) \ln \frac{1 - R_{ac}(x) - x}{1 - R_{\min} - x} \right] \\ &\quad + \frac{\pi \alpha^2}{s} \left[\mathcal{V}(s) \frac{1 - 3 \cos^2 \vartheta}{2} \left(\frac{x - 1}{\rho} + \frac{R_{\min}}{x + R_{\min}} + \ln \frac{R_{ac}(x) + x}{R_{\min} + x} \right) \right. \\ &\quad \left. \left. \mathcal{A}(s) \cos \vartheta (x - 1) \ln \frac{R_{ac}(x) + x}{R_{\min} + x} \right] \right\}. \quad (\text{B.236}) \end{aligned}$$

Now one has to integrate over x in the interval $R_E - R_{\min} \leq x \leq 1 - R_E$. It is suitable to also introduce the notation [157]:

$$\rho_x = \rho - 1 + R_E - R_{\min} = \frac{\rho(\rho - 1)}{\rho - R_E}. \quad (\text{B.237})$$

From Figure (B.1) one observes one very nice property of the function $R_{ac}(x)$: It has the same value R_{\min} in two different points where $x = 1 - R_E$ and $x = R_E - R_{\min}$, which removes some of the logarithmic terms arising during the integration:

$$\ln \frac{1 - R_{ac}(x) - x}{1 - R_{\min} - x} \Big|_{1-R_E}^{1-R_E} = \ln \frac{1 - R_{ac}(x) - x}{1 - R_{\min} - x} \Big|_{R_E-R_{\min}}^{R_E-R_{\min}} = 0, \quad (\text{B.238})$$

$$\ln \frac{R_{ac}(x) + x}{R_{\min} + x} \Big|_{1-R_E}^{1-R_E} = \ln \frac{R_{ac}(x) + x}{R_{\min} + x} \Big|_{R_E-R_{\min}}^{R_E-R_{\min}} = 0. \quad (\text{B.239})$$

Table of integrals

$$[f(x)]_{(x)} = \int_{R_E - R_{\min}}^{1-R_E} dx f(x), \quad (\text{B.240})$$

$$[1]_{(x)} = x_\rho - R_E, \quad (\text{B.241})$$

$$[x]_{(x)} = \frac{1}{2}(x_\rho - R_E)(1 - R_{\min}), \quad (\text{B.242})$$

$$\left[\frac{1}{x}\right]_{(x)} = \ln(1 - R_E) - \ln(R_E - R_{\min}), \quad (\text{B.243})$$

$$\left[\frac{1}{x + R_{\min}}\right]_{(x)} = \ln x_\rho - \ln R_E, \quad (\text{B.244})$$

$$\left[\frac{1}{x + \rho - 1}\right]_{(x)} = \ln(\rho - R_E) - \ln(\rho - x_\rho), \quad (\text{B.245})$$

$$\left[\frac{1}{(x + \rho - 1)^2}\right]_{(x)} = \frac{1 + R_{\min} - 2R_E}{\rho(\rho - 1)}, \quad (\text{B.246})$$

$$\begin{aligned} \left[\ln \frac{1 - R_{ac}(x) - x}{1 - R_{\min} - x}\right]_{(x)} &= x_\rho - R_E + \ln \frac{x_\rho}{R_E} - (\rho - 1) \ln \frac{\rho - R_E}{\rho - x_\rho} \\ &\quad - (1 - R_{\min}) \ln \frac{1 - R_E}{R_E - R_{\min}}, \end{aligned} \quad (\text{B.247})$$

$$\begin{aligned} \left[\frac{1}{x} \ln \frac{1 - R_{ac}(x) - x}{1 - R_{\min} - x}\right]_{(x)} &= -\ln(1 - R_{\min}) \ln \frac{1 - R_E}{1 - x_\rho} + \text{Li}_2\left(\frac{1 - R_E}{1 - R_{\min}}\right) \\ &\quad - \text{Li}_2\left(\frac{1 - x_\rho}{1 - R_{\min}}\right) - \text{Li}_2(1 - R_E) + \text{Li}_2(1 - x_\rho) \\ &\quad + \text{Li}_2\left(\frac{1 - R_E}{1 - \rho}\right) - \text{Li}_2\left(\frac{1 - x_\rho}{1 - \rho}\right), \end{aligned} \quad (\text{B.248})$$

$$\begin{aligned} \left[\ln \frac{R_{ac}(x) + x}{R_{\min} + x}\right]_{(x)} &= x_\rho - R_E - R_{\min} \ln \frac{x_\rho}{R_E} \\ &\quad - (\rho - 1) \ln \frac{\rho - R_E}{\rho - x_\rho}, \end{aligned} \quad (\text{B.249})$$

$$\begin{aligned} \left[x \ln \frac{1 - R_{ac}(x) - x}{1 - R_{\min} - x}\right]_{(x)} &= \frac{1}{2}(x_\rho - R_E)(1 - \rho - R_{\min}) \\ &\quad + \frac{1}{4}(1 - R_E)^2 - \frac{1}{4}(R_E - R_{\min})^2 + \frac{1}{2} \ln \frac{x_\rho}{R_E} \end{aligned}$$

$$\begin{aligned}
& +\frac{1}{2}(\rho-1)^2 \ln \frac{\rho-R_E}{\rho-x_\rho} \\
& -\frac{1}{2}(1-R_{\min})^2 \ln \frac{1-R_E}{R_E-R_{\min}}, \tag{B.250}
\end{aligned}$$

$$\begin{aligned}
\left[x \ln \frac{R_{ac}(x)+x}{R_{\min}+x} \right]_{(x)} &= \frac{1}{2}(x_\rho-R_E)(1-\rho-R_{\min}) \\
& +\frac{1}{4}(1-R_E)^2 - \frac{1}{4}(R_E-R_{\min})^2 \\
& +\frac{1}{2}R_{\min}^2 \ln \frac{x_\rho}{R_E} + \frac{1}{2}(\rho-1)^2 \ln \frac{\rho-R_E}{\rho-x_\rho}. \tag{B.251}
\end{aligned}$$

This provides as hard photonic contribution of the third region to $d\sigma_{finIII}^{hard}/d\cos\vartheta$:

$$\begin{aligned}
\frac{d\sigma_{finIII}^{hard}}{d\cos\vartheta} &= \frac{\pi\alpha^2}{s} \frac{\alpha}{\pi} Q_f^2 \left\{ \mathcal{V}(s) \left(\frac{1+\cos^2\vartheta}{2} \left[\frac{1}{2}(x_\rho-R_E)(\rho+\frac{3R_{\min}}{2}+\frac{5}{2}) \right. \right. \right. \\
& +\rho(1+\frac{\rho}{2}) \ln \frac{\rho-x_\rho}{\rho-R_E} \\
& +\left[R_{\min}(1+\frac{R_{\min}}{2}) + \ln(1-R_{\min}) \right] \ln \frac{1-R_E}{1-x_\rho} \\
& +\text{Li}_2\left(\frac{1-x_\rho}{1-R_{\min}}\right) - \text{Li}_2\left(\frac{1-R_E}{1-R_{\min}}\right) + \text{Li}_2\left(\frac{1-x_\rho}{1-\rho}\right) \\
& \left. \left. -\text{Li}_2\left(\frac{1-R_E}{1-\rho}\right) + \text{Li}_2(1-x_\rho) - \text{Li}_2(1-R_E) \right] \right. \\
& +\frac{1-3\cos^2\vartheta}{2} \left[(x_\rho-R_E)(1-\frac{R_{\min}}{2\rho}-\frac{1}{2\rho}) - (1-\rho) \ln \frac{\rho-x_\rho}{\rho-R_E} \right] \\
& +\mathcal{A}(s) \cos\vartheta \left(x_\rho-R_E + \left[\frac{1}{2} + \rho + R_{\min}(1+\frac{R_{\min}}{2}) \right] \ln \frac{\rho-x_\rho}{\rho-R_E} \right. \\
& +\left[2R_{\min}(1+\frac{R_{\min}}{2}) + \ln(1-R_{\min}) \right] \ln \frac{1-R_E}{1-x_\rho} \\
& +\text{Li}_2\left(\frac{1-x_\rho}{1-R_{\min}}\right) - \text{Li}_2\left(\frac{1-R_E}{1-R_{\min}}\right) + \text{Li}_2\left(\frac{1-x_\rho}{1-\rho}\right) \\
& \left. \left. -\text{Li}_2\left(\frac{1-R_E}{1-\rho}\right) + \text{Li}_2(1-x_\rho) - \text{Li}_2(1-R_E) \right) \right\}. \tag{B.252}
\end{aligned}$$

Integration over $\cos \vartheta$

It is clear looking at the final results for $d\sigma_{fin(a)}^{hard}/d\cos\vartheta$, $a = I, II, III$ that it factorizes in each region into a term proportional to $\mathcal{V}(s)$ and a term proportional to $\mathcal{A}(s)$. The term with factor $\mathcal{V}(s)$ contributes solely to the total cross section, while the terms with factor $\mathcal{A}(s)$ only contribute to the integrated forward-backward result.

Table of integrals

$$[f(c)]_T = \int_{-c}^c d\cos\vartheta f(\cos\vartheta), \quad [f(c)]_{FB} = \left[\int_0^{+c} - \int_{-c}^0 \right] d\cos\vartheta f(\cos\vartheta), \quad (\text{B.253})$$

$$[1]_T = 2c, \quad [\cos\vartheta]_T = 0, \quad [\cos^2\vartheta]_T = \frac{2}{3}c^3, \quad (\text{B.254})$$

$$[1]_{FB} = 0, \quad [\cos\vartheta]_{FB} = c^2, \quad [\cos^2\vartheta]_{FB} = 0. \quad (\text{B.255})$$

One can trivially obtain the total cross section terms $\sigma_{T,fin(a)}$, $a = I, II, III$, from (B.209), (B.236), and (B.252) taking the terms proportional to $\mathcal{V}(s)$ and replacing the angular factors $(1 + \cos^2\vartheta)/2$ and $(1 - 3\cos^2\vartheta)/2$ by $c + c^3/3$ and $c - c^3$ respectively. Similarly the forward-backward cross section $\sigma_{FB,fin(a)}$ is given by the terms proportional to $\mathcal{A}(s)$ in (B.252) with the factor $\cos\vartheta$ replaced by a factor c^2 . This observation holds at any stage of the integration, i.e. the final state cross section distributions which appeared during the successive steps of integration all factorize into terms proportional to $(1 + \cos^2\vartheta)/2$, $(1 - 3\cos^2\vartheta)/2$, and $\cos\vartheta$.

The comparison of the integrated results with results given in [157] shows that they coincide, except for some small misprints there. In eq. (5) of [157] a term $\ln^2(y_b^-)$ is missing and in eq. (6) a minus sign is missing, i.e. one has to make the following replacement:

$$\frac{1}{\rho_e} + \frac{1}{\rho_x} \rightarrow -\frac{1}{\rho_e} + \frac{1}{\rho_x}. \quad (\text{B.256})$$

The term ρ^- has to be corrected there with an overall minus sign. Our R_E and R_{\min} are denoted there by e and y_b respectively and our results are more compact and simplified. The expressions for $d\sigma d\cos\vartheta$ and σ_{FB} , however, were not presented there and are therefore completely new.

Appendix C

Soft and virtual photonic corrections

C.1 Soft photonic corrections

For the general case with all soft photonic corrections and the real photon momentum $k \rightarrow 0$, one can show that the soft amplitudes M_{ini}^{soft} and M_{fin}^{soft} factorize from the Born amplitude [138]:

$$M_{ini}^{soft} = e Q_e \epsilon_\alpha \left(\frac{2k_2^\alpha}{Z_2} - \frac{2k_1^\alpha}{Z_1} \right) \cdot M^{Born}(s'), \quad (C.1)$$

$$M_{fin}^{soft} = e Q_f \epsilon_\alpha \left(\frac{2p_1^\alpha}{V_1} - \frac{2p_2^\alpha}{V_2} \right) \cdot M^{Born}(s). \quad (C.2)$$

So, having in mind that s' becomes s , the soft photon contribution to the differential cross section takes the form:

$$d\sigma^{soft} = -d\sigma^{Born} e^2 \left[Q_e \left(\frac{2k_2}{Z_2} - \frac{2k_1}{Z_1} \right) + Q_f \left(\frac{2p_1}{V_1} - \frac{2p_2}{V_2} \right) \right]^2 \theta(\bar{\varepsilon} - p^0) \cdot \frac{d^3 \vec{p}}{(2\pi)^3 2p^0}. \quad (C.3)$$

Here we have applied the sum rule for photon polarization vectors:

$$\sum_{spin} \epsilon_\alpha \epsilon_\beta = -g_{\alpha\beta}. \quad (C.4)$$

The soft photon cut-off parameter ε from (A.45) is related to $\bar{\varepsilon}$ through $\varepsilon = 2\bar{\varepsilon}/\sqrt{s}$. The expression in (C.3) can be written in the following way ($e^2 = 4\pi\alpha$):

$$d\sigma^{soft} = d\sigma_{ini}^{soft} + d\sigma_{fin}^{soft} + d\sigma_{int}^{soft} = \frac{\alpha}{\pi} \delta^{soft} d\sigma^{Born}. \quad (C.5)$$

The correction δ^{soft} , which we have to calculate, has the form:

$$\delta^{soft} = -4\pi^2 \int \frac{d^3\vec{p}}{(2\pi)^3 2p^0} \left[Q_e \left(\frac{2k_2}{Z_2} - \frac{2k_1}{Z_1} \right) + Q_f \left(\frac{2p_1}{V_1} - \frac{2p_2}{V_2} \right) \right]^2 \theta(\bar{\varepsilon} - p^0). \quad (C.6)$$

Taking the expression squared explicitly, we obtain:

$$\begin{aligned} \delta^{soft} &= 16\pi^2 \int \frac{d^3\vec{p}}{(2\pi)^3 2p^0} \left[Q_e^2 \left(-\frac{m_e^2}{Z_1^2} - \frac{m_e^2}{Z_2^2} + \frac{2k_1 \cdot k_2}{Z_1 Z_2} \right) \right. \\ &+ Q_e Q_f \left(\frac{2k_1 \cdot p_1}{Z_1 V_1} + \frac{2k_2 \cdot p_2}{Z_2 V_2} - \frac{2k_1 \cdot p_2}{Z_1 V_2} - \frac{2k_2 \cdot p_1}{Z_2 V_1} \right) \\ &+ \left. Q_f^2 \left(-\frac{m_f^2}{V_1^2} - \frac{m_f^2}{V_2^2} + \frac{2p_1 \cdot p_2}{V_1 V_2} \right) \right] \theta(\bar{\varepsilon} - p^0) \end{aligned} \quad (C.7)$$

$$\begin{aligned} &= 16\pi^2 \int \frac{d^3\vec{p}}{(2\pi)^3 2p^0} \left[Q_e^2 \left(-\frac{m_e^2}{Z_1^2} - \frac{m_e^2}{Z_2^2} + \frac{s - 2m_e^2}{Z_1 Z_2} \right) \right. \\ &+ Q_e Q_f \left(\frac{T}{Z_1 V_1} + \frac{T}{Z_2 V_2} - \frac{U}{Z_1 V_2} - \frac{U}{Z_2 V_1} \right) \\ &+ \left. Q_f^2 \left(-\frac{m_f^2}{V_1^2} - \frac{m_f^2}{V_2^2} + \frac{s - 2m_f^2}{V_1 V_2} \right) \right] \theta(\bar{\varepsilon} - p^0). \end{aligned} \quad (C.8)$$

The kinematic invariants are defined in (A.18) to (A.21) and in (A.30) and (A.31).

C.1.1 Initial state radiation

As an example, the soft photon factor δ_{ini}^{soft} for initial state bremsstrahlung to the differential cross section contribution $d\sigma_{ini}$ shall be explicitly evaluated. The differential cross section $d\sigma_{ini}$ can be separated into a hard and soft with virtual photon part, $d\sigma^{hard}$ and $d\sigma^{soft+virtual}$.

$$d\sigma_{ini} = d\sigma_{ini}^{hard} + d\sigma_{ini}^{soft} + d\sigma_{ini}^{virtual}. \quad (C.9)$$

The derivation of the virtual correction term $d\sigma_{ini}^{virtual}$ we will keep to the next Section C.2. The basic idea for the calculation of the soft photonic part is to introduce an arbitrary small cut-off $\bar{\varepsilon}$ for the photon energy p^0 , thus distinguishing the hard photon region of phase space, $p^0 \geq \bar{\varepsilon}$, from the soft photon region with $p^0 < \bar{\varepsilon}$.

$$d\sigma^{hard} + d\sigma^{soft} = -16\pi\alpha Q_e^2 \left(\frac{k_1}{Z_1} - \frac{k_2}{Z_2} \right)^2 d\sigma^{Born} d\Gamma^\gamma \left[\theta(\bar{\varepsilon} - p^0) + \theta(p^0 - \bar{\varepsilon}) \right], \quad (C.10)$$

$$= d\sigma^{Born} \cdot (\delta^{soft}(\bar{\varepsilon}) + \delta^{hard}(\bar{\varepsilon})), \quad (C.11)$$

$$\text{with} \quad d\sigma^{Born} = \frac{1}{2\sqrt{\lambda_s}} \sum_{spin} \overline{|M_{Born}|^2} d\Gamma^{(2)}, \quad (C.12)$$

$$\text{and} \quad \delta^{soft}(\bar{\varepsilon}) = 16\pi^2 Q_e^2 \int \left[\frac{s - 2m_e^2}{Z_1 Z_2} - \frac{m_e^2}{Z_1^2} - \frac{m_e^2}{Z_2^2} \right] d\Gamma^\gamma \Theta(\bar{\varepsilon} - p^0), \quad (C.13)$$

$$\text{and} \quad \delta^{hard}(\bar{\varepsilon}) = 16\pi^2 Q_e^2 \int \left[\frac{s - 2m_e^2}{Z_1 Z_2} - \frac{m_e^2}{Z_1^2} - \frac{m_e^2}{Z_2^2} \right] d\Gamma^\gamma \Theta(p^0 - \bar{\varepsilon}), \quad (C.14)$$

$$d\Gamma^\gamma = \frac{d^3\vec{p}}{(2\pi)^3 2p^0}, \quad d\Gamma^{(2)} = \frac{\beta}{16\pi} d(\cos\vartheta), \quad (C.15)$$

$$\lambda_s = s^2 \beta_0^2, \quad \beta_0 = \sqrt{1 - \frac{4m_e^2}{s}}, \quad \beta = \sqrt{1 - \frac{4m_f^2}{s'}}. \quad (C.16)$$

The Born squared amplitude $\overline{|M_{Born}|^2}$ for $e^+e^- \rightarrow \bar{f}f$ was given in Section A.1. The hard photon contribution $d\sigma_{ini}^{hard}(\bar{\varepsilon})$ has been calculated straightforwardly using the parameterization and the kinematical cuts presented in Appendix B.1. The corresponding phase space volume for hard photon emission is from (A.66) to (A.68) :

$$d\Gamma_{hard}^{(3)} = d\Gamma_{hard}^{(2)} \cdot d\Gamma^\gamma = \frac{1}{(2\pi)^5} \frac{\pi}{16s} d\varphi_\gamma dV_2 ds' d\cos\vartheta \Theta(p^0 - \bar{\varepsilon}). \quad (C.17)$$

In the soft photon case, if we introduce the Feynman parameter α and define $k_\alpha := k_1\alpha + k_2(1 - \alpha)$, we can transform δ^{soft} with the definitions of $Z_{1,2}$ into:

$$\delta^{soft}(\bar{\varepsilon}) = \frac{Q_e^2}{2\pi} \int_0^1 d\alpha \int \frac{d^3\vec{p}}{2p^0} \Theta(\bar{\varepsilon} - p^0) \left\{ \frac{s - 2m_e^2}{(k_\alpha p)^2} - \frac{m_e^2}{(k_1 p)^2} - \frac{m_e^2}{(k_2 p)^2} \right\}. \quad (C.18)$$

Before we can proceed, we have to be cautious as the underlying integrals

$$\int \frac{d^3\vec{p}}{2p^0} \frac{1}{(k_a p)^2} \Theta(\bar{\varepsilon} - p^0) = \int d^4p \delta(p^2) \frac{1}{(k_a p)^2} \Theta(\bar{\varepsilon} - p^0), \quad a = 1, 2, \alpha, \quad (C.19)$$

are infrared divergent, i.e. they become singular for vanishing photon momenta $p^0 \rightarrow 0$. According to [138], the infrared divergence has to cancel in the full scattering amplitude with soft and virtual corrections, i.e. when adding the term $d\sigma_{ini}^{virtual}$ (see Section C.2).

In order to calculate the integrals (C.19) over the photon momentum p , it is necessary to use a regularization technique to circumvent the infrared singular behaviour and to deal with regularized, i.e finite expressions. We use *dimensional regularization* [201–203]. The four-dimensional integration over p is replaced by an n -dimensional integration, using now the appropriately generalized on-shell condition $p^{02} := p_1^2 + p_2^2 + \dots + p_{n-1}^2$. For $n \neq 4$ the integrals (C.19) exist, and we can use $(n-1)$ -dimensional spherical coordinates to determine δ^{soft} . As side remark, dimensional regularization breaks the Lorentz structure, but preserves the symmetries and the gauge invariance of the theory and is therefore one strongly advocated regularization technique among other possible procedures.

In $(n-1)$ dimensional spherical coordinates (C.18) reads:

$$\begin{aligned} & \int \frac{d^3 \vec{p}}{2p^0} \Theta(\bar{\varepsilon} - p^0) \longrightarrow \int \frac{d^{n-1} \vec{p}}{2p^0} \Theta(\bar{\varepsilon} - p^0) = \\ & = \int_0^{\bar{\varepsilon}} \frac{dp^0}{2p^0} (p^0)^{n-2} \int_0^\pi d\theta_{n-2} (\sin \theta_{n-2})^{n-3} \dots \int_0^\pi d\theta_2 \sin \theta_2 \int_0^{2\pi} d\theta_1. \end{aligned} \quad (\text{C.20})$$

We can evaluate the integrals over p^0 and the first $(n-3)$ angles θ_i for each of the three integrals in (C.18), but have to keep the remaining angle $\theta_{n-2} =: \theta_p$ to parameterize each one of the propagators $k_a p = k_a^0 p^0 (1 - \beta_a \cos \theta_p)$ separately with $\beta_a = |\vec{k}_a|/k_a^0$, $a := 1, 2, \alpha$, for the last integration (isotropy of soft photon radiation). The integration of the first $(n-3)$ angular coordinates yields:

$$\int_0^\pi d\theta_{n-4} (\sin \theta_{n-3})^{n-4} \dots \int_0^\pi d\theta_2 \sin \theta_2 \int_0^{2\pi} d\theta_1 = 2\pi \pi^{\frac{n-4}{2}} \frac{\Gamma(1)}{\Gamma\left(\frac{n-2}{2}\right)}. \quad (\text{C.21})$$

So, for the propagators $1/(k_a p)^2$ we obtain:

$$\begin{aligned} & \frac{1}{2\pi \mu^{n-4}} \int_0^1 d\alpha \int \frac{d^{n-1} p}{2p^0} \frac{1}{(k_a p)^2} \Theta(\bar{\varepsilon} - p^0) = \\ & = \frac{1}{2} \pi^{\frac{n-4}{2}} \Gamma\left(\frac{n}{2} - 1\right) \int_0^1 \frac{d\alpha}{\mu^{n-4}} \int_0^{\bar{\varepsilon}} dp^0 (p^0)^{n-5} \int_0^\pi d\theta_p \frac{(\sin \theta_p)^{n-3}}{(k_a^0)^2 (1 - \beta_a \cos \theta_p)^2}. \end{aligned} \quad (\text{C.22})$$

We have used in (C.22) the additional parameter μ as regulator mass term for vanishing photon mass. It will eventually drop out as unphysical quantity when adding $\delta_{ini}^{virtual}$. We obtain further for (C.22):

$$\begin{aligned} 1. \quad & \frac{1}{\mu^{n-4}} \int_0^{\bar{\varepsilon}} dp^0 (p^0)^{n-5} = \frac{1}{n-4} \left(\frac{\bar{\varepsilon}}{\mu} \right)^{n-4} \\ & = \frac{1}{n-4} \left[1 + (n-4) \ln \left(\frac{\bar{\varepsilon}}{\mu} \right) + o\left((n-4)^2\right) \right], \end{aligned} \quad (\text{C.23})$$

$$\begin{aligned}
 2. \quad & \int_0^\pi d\theta_p \frac{(\sin \theta_p)^{n-3}}{(1 - \beta_a \cos \theta_p)^2} = \int_{-1}^1 d\xi \frac{(1 - \xi^2)^{\frac{n-4}{2}}}{(1 - \beta_a \xi)^2} \\
 & = \int_{-1}^1 d\xi \frac{1}{(1 - \beta_a \xi)^2} \left[1 + \frac{n-4}{2} \ln(1 - \xi^2) + o((n-4)^2) \right]. \quad (C.24)
 \end{aligned}$$

After isolating the infrared pole proportional to $1/(n-4)$, all terms of $o(n-4)$ and higher can be neglected, as the final results have to be derived with $n \rightarrow 4$ in the physical 4-dimensional Lorentz space. Inserting the results of (C.23) into (C.22), and with the definition (C: Euler constant)

$$P_{IR} := \frac{1}{n-4} + \frac{1}{2}C + \frac{1}{2} \ln \pi = \frac{1}{2\varepsilon_{IR}}, \quad (C.25)$$

we have ($\beta_{1,2} = \beta_0$):

$$\begin{aligned}
 \delta^{soft}(\bar{\varepsilon}, \varepsilon_{IR}, \mu) &= \frac{Q_e^2}{2(k_a^0)^2} \int_0^1 d\alpha \int_{-1}^{+1} d\xi \left[P_{IR}(\mu) + \ln\left(\frac{\bar{\varepsilon}}{\mu}\right) + \frac{1}{2} \ln(1 - \xi^2) \right] \\
 &\quad \cdot \left[\frac{s - 2m_e^2}{(1 - \beta_\alpha \xi)^2} - \frac{m_e^2}{(1 + \beta_0 \xi)^2} - \frac{m_e^2}{(1 - \beta_0 \xi)^2} \right], \quad (C.26)
 \end{aligned}$$

or eliminating the Feynman parameter α again for this simple case:

$$\begin{aligned}
 \delta^{soft}(\bar{\varepsilon}, \varepsilon_{IR}, \mu) &= \frac{2Q_e^2}{s} \int_{-1}^{+1} d\xi \left[P_{IR}(\mu) + \ln\left(\frac{\bar{\varepsilon}}{\mu}\right) + \frac{1}{2} \ln(1 - \xi^2) \right] \\
 &\quad \cdot \left[\frac{s - 2m_e^2}{1 - \beta_0^2 \xi^2} - \frac{m_e^2}{(1 + \beta_0 \xi)^2} - \frac{m_e^2}{(1 - \beta_0 \xi)^2} \right]. \quad (C.27)
 \end{aligned}$$

In (C.26) and (C.27) terms of $o(n-4)$ have been neglected. The integrals over ξ can be determined relatively easily, leading to logarithmic and dilogarithmic mass terms.

Table of integrals:

$$[f(\xi)]_{(\xi)} = \frac{1}{2} \int_{-1}^{+1} d\xi f(\xi), \quad (C.28)$$

$$[1]_{(\xi)} = 1, \quad (C.29)$$

$$\left[\frac{1}{1 \pm \beta_0 \xi} \right]_{(\xi)} = \frac{1}{2\beta_0} \ln \left(\frac{1 + \beta_0}{1 - \beta_0} \right) \approx \frac{1}{2} \ln \left(\frac{s}{m_e^2} \right), \quad (C.30)$$

$$\left[\frac{1}{(1 \pm \beta_0 \xi)^2} \right]_{(\xi)} = \frac{1}{1 - \beta_0^2} \approx \frac{s}{4m_e^2}, \quad (C.31)$$

$$\left[\frac{1}{2} \ln(1 - \xi^2) \right]_{(\xi)} = \ln 2 - 1, \quad (\text{C.32})$$

$$\left[\frac{1}{2} \frac{\ln(1 - \xi^2)}{1 \pm \beta_0 \xi} \right]_{(\xi)} = \frac{1}{2\beta_0} \left\{ \ln 2 \ln \left(\frac{1 + \beta_0}{1 - \beta_0} \right) + \frac{1}{2} \left[\Phi \left(\frac{2\beta_0}{\beta_0 - 1} \right) - \Phi \left(\frac{2\beta_0}{\beta_0 + 1} \right) \right] \right\} \quad (\text{C.33})$$

$$\approx \frac{1}{2} \ln 2 \ln \left(\frac{s}{m_e^2} \right) - \frac{1}{4} \left\{ \frac{\pi^2}{3} + \frac{1}{2} \left[\ln \left(\frac{s}{m_e^2} \right) \right]^2 \right\}, \quad (\text{C.34})$$

$$\left[\frac{1}{2} \frac{\ln(1 - \xi^2)}{(1 \pm \beta_0 \xi)^2} \right]_{(\xi)} = \frac{1}{1 - \beta_0^2} \left\{ \ln 2 - \frac{1}{2\beta_0} \ln \left(\frac{1 + \beta_0}{1 - \beta_0} \right) \right\} \quad (\text{C.35})$$

$$\approx \frac{s}{4m_e^2} \left\{ \ln 2 - \frac{1}{2} \ln \left(\frac{s}{m_e^2} \right) \right\}, \quad (\text{C.36})$$

$$\text{with } \Phi(y) := \text{Li}_2(y) = - \int_0^1 \frac{\ln(1 - xy)}{x} dx = - \int_0^y \frac{\ln(1 - x)}{x} dx. \quad (\text{C.37})$$

If we neglect mass terms for $4m_e^2 \ll s$ except for the logarithms $\ln(s/m_e^2)$, we obtain the right hand side of the above Table. Due to [139, 140] these are also the only mass singularities allowed to arise if one puts $m_e \rightarrow 0$. They are due to collinear photon emission from one of the initial state fermions. The final result for the initial state soft photon contribution δ^{soft} is:

$$\delta^{soft} = \delta^{soft}(\bar{\varepsilon}, \varepsilon_{IR}, \mu) \quad (\text{C.38})$$

$$= Q_e^2 \left[(L_e - 1) \left(2 \ln \frac{\bar{\varepsilon}}{\mu} + 2 \ln 2 + \ln \frac{m_e^2}{s} + \frac{1}{\varepsilon_{IR}} \right) + \frac{1}{2} L_e^2 - \frac{\pi^2}{3} \right],$$

$$\text{with } L_e := \ln \frac{s}{m_e^2}. \quad (\text{C.39})$$

C.1.2 The complete soft photonic corrections

Again using for the integration of (C.7), (C.8) dimensional regularization and the transformation into spherical coordinations as in (C.20), we arrive at:

$$d\sigma^{soft} = \frac{\alpha}{\pi} \left(\delta_{ini}^{soft} + \delta_{fin}^{soft} + \delta_{int}^{soft} \right) d\sigma^{Born} \quad (\text{C.40})$$

$$\begin{aligned} &= \frac{1}{4} \int_{-1}^{+1} d\xi \left[2P_{IR} + \ln \frac{\bar{\varepsilon}^2}{\mu^2} + \ln(1 - \xi^2) \right] 4p^{02} \\ &\cdot \left[Q_e^2 \left(-\frac{m_e^2}{Z_1^2} - \frac{m_e^2}{Z_2^2} + \frac{s - 2m_e^2}{Z_1 Z_2} \right) + Q_f^2 \left(-\frac{m_f^2}{V_1^2} - \frac{m_f^2}{V_2^2} + \frac{s - 2m_f^2}{V_1 V_2} \right) \right. \\ &\left. + Q_e Q_f \left(\frac{U}{Z_1 V_1} + \frac{U}{Z_2 V_2} - \frac{T}{Z_1 V_2} - \frac{T}{Z_2 V_1} \right) \right]. \end{aligned} \quad (\text{C.41})$$

We can repeat the calculation of the initial state case completely analogously for the final state terms, while for the interference contribution a suitable Feynman parameterization is necessary. Here, just the results from [32, 34, 35] are presented:

$$\begin{aligned}\delta_{ini}^{soft}(\bar{\varepsilon}, \varepsilon_{IR}, \mu) &= Q_e^2 \left[2 \left(P_{IR} + \ln \frac{\bar{\varepsilon}}{\mu} + \ln 2 \right) \left(\ln \frac{s}{m_e^2} - 1 \right) \right. \\ &\quad \left. + \ln \frac{s}{m_e^2} - \frac{1}{2} \ln^2 \frac{s}{m_e^2} - 2\text{Li}_2(1) \right],\end{aligned}\quad (\text{C.42})$$

$$\begin{aligned}\delta_{fin}^{soft}(\bar{\varepsilon}, \varepsilon_{IR}, \mu) &= Q_f^2 \left[2 \left(P_{IR} + \ln \frac{\bar{\varepsilon}}{\mu} + \ln 2 \right) \left(\ln \frac{s'}{m_f^2} - 1 \right) \right. \\ &\quad \left. + \ln \frac{s'}{m_f^2} - \frac{1}{2} \ln^2 \frac{s'}{m_f^2} - 2\text{Li}_2(1) \right],\end{aligned}\quad (\text{C.43})$$

$$\begin{aligned}\delta_{int}^{soft}(\bar{\varepsilon}, \varepsilon_{IR}, \mu) &= 2Q_e Q_f \left[2 \left(P_{IR} + \ln \frac{\bar{\varepsilon}}{\mu} + \ln 2 \right) \ln \left(\frac{c_-}{c_+} \right) \right. \\ &\quad \left. + \text{Li}_2(c_+) - \text{Li}_2(c_-) - \frac{1}{2} (\ln^2(c_+) - \ln^2(c_-)) \right],\end{aligned}\quad (\text{C.44})$$

$$\text{with} \quad c_{\pm} = \frac{1}{2}(1 \pm \beta\beta_0 \cos \vartheta). \quad (\text{C.45})$$

The unregularized soft photon contributions s_a and S_a , $a = ini, fin, int$ (without virtual corrections) to the total cross section σ_T and forward-backward asymmetry A_{FB} can be summarized as follows:

$$S_A^{ini}(c, \bar{\varepsilon}, \varepsilon_{IR}, \mu) = \frac{\alpha}{\pi} Q_e^2 D_A(c) \delta_{ini}^{soft}(\bar{\varepsilon}, \varepsilon_{IR}, \mu), \quad (\text{C.46})$$

$$S_A^{fin}(c, \bar{\varepsilon}, \varepsilon_{IR}, \mu) = \frac{\alpha}{\pi} Q_f^2 D_A(c) \delta_{fin}^{soft}(\bar{\varepsilon}, \varepsilon_{IR}, \mu), \quad (\text{C.47})$$

$$\begin{aligned}S_T^{int}(c, \bar{\varepsilon}, \varepsilon_{IR}, \mu) &= \frac{\alpha}{\pi} \int_{-c}^c d\cos \vartheta d_{FB}(\cos \vartheta) \delta_{int}^{soft}(\cos \vartheta, \bar{\varepsilon}, \varepsilon_{IR}, \mu) \\ &= \frac{\alpha}{\pi} Q_e Q_f \left\{ -4 \left(P_{IR} + \ln \frac{\bar{\varepsilon}}{\mu} + \ln 2 \right) \left[(c^2 - 1) \ln \frac{c_+}{c_-} + 2c \right] \right. \\ &\quad \left. + 2(c^2 - 1) [\text{Li}_2(c_+) - \text{Li}_2(c_-)] - (c^2 - 1) \ln(c_+ c_-) \ln \frac{c_+}{c_-} \right. \\ &\quad \left. - 4c \ln(c_+ c_-) - 4 \ln \frac{c_+}{c_-} + 8c, \right\}\end{aligned}\quad (\text{C.48})$$

$$\begin{aligned}\frac{3}{4} S_{FB}^{int}(c, \bar{\varepsilon}, \varepsilon_{IR}, \mu) &= \frac{3}{4} \frac{\alpha}{\pi} \left\{ \int_0^c - \int_{-c}^0 \right\} d\cos \vartheta d_T(\cos \vartheta) \delta_{int}^{soft}(\cos \vartheta, \bar{\varepsilon}, \varepsilon_{IR}, \mu) \\ &= \frac{\alpha}{\pi} Q_e Q_f \left\{ - \left(P_{IR} + \ln \frac{\bar{\varepsilon}}{\mu} + \ln 2 \right) \right.\end{aligned}$$

$$\begin{aligned}
& \cdot \left[3\left(\frac{1}{3}c^3 + c\right) \ln \frac{c_+}{c_-} + 4 \ln(c_+c_-) + c^2 + 8 \ln 2 \right] \\
& + \frac{3}{2}\left(\frac{1}{3}c^3 + c\right) [\text{Li}_2(c_+) - \text{Li}_2(c_-)] + 2 [\text{Li}_2(c_+) + \text{Li}_2(c_-)] \\
& - \frac{3}{4}\left(\frac{1}{3}c^3 + c\right) \ln(c_+c_-) \ln \frac{c_+}{c_-} - (\ln^2 c_+ + \ln^2 c_-) \\
& + \frac{1}{2}(1 - c^2) \ln(c_+c_-) + \frac{1}{2}c^2 + 4 \ln^2 2 + \ln 2 - 2\text{Li}_2(1) \Big\}, \tag{C.49}
\end{aligned}$$

$$\text{with} \quad D_T(c) = \frac{3}{4} \left(c + \frac{c^3}{3} \right), \quad D_{FB}(c) = c^2, \tag{C.50}$$

$$d_T(\cos \vartheta) = 1 + \cos^2 \vartheta, \quad d_{FB}(\cos \vartheta) = 2 \cos \vartheta, \tag{C.51}$$

$$c_{\pm} = \frac{1}{2}(1 \pm c), \quad (\beta = \beta_0 = 1). \tag{C.52}$$

The soft photon flux functions S_A^a , $a = ini, fin, int$, $A = T, FB$ are inserted into convolution integrals for total cross sections and asymmetries as for example given in (2.41) in Section 2.2.

The infrared pole term P_{IR} will be cancelled together with the regulator photon mass term μ^2 when combining the soft and virtual corrections. In the initial and final state case it is the initial and final state vertex corrections, while the soft interference term δ_{int}^{soft} has to be combined with the virtual corrections from the interference of the Born graphs with the $\gamma\gamma$ and γZ exchange box diagrams. This will be shown in the next Section C.2. The logarithmic soft-photon cut-off $2\ln(\varepsilon)$ cancels together with the corresponding term in the hard photon results derived in Appendix B.

C.2 Virtual corrections

C.2.1 Initial state and final state virtual corrections

The vertex function

In Fig. C.1 we depict the one-loop vertex corrections, i.e. the initial state and final state vertex diagrams. In order to completely cancel the infrared divergences from the initial and final state soft photon contributions, their contributions have to be added.

The integration is again done in dimensional regularization over the following matrix element, easily derived as real part of the interference between the Born

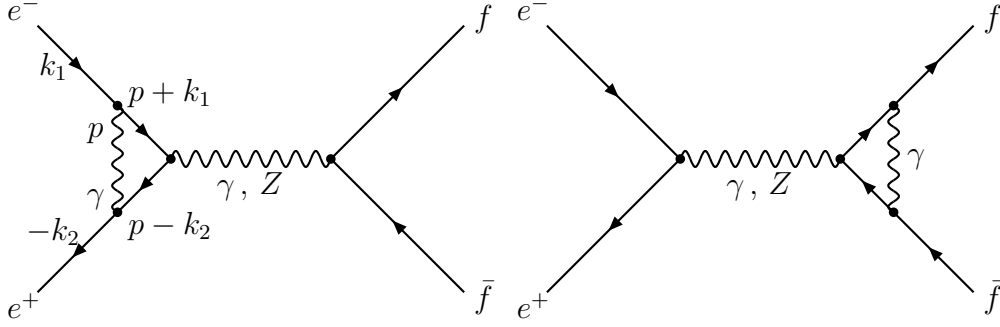


Figure C.1: The photonic vertex corrections.

diagram and the one-loop vertex diagrams illustrated above. The amplitude for the initial state vertex correction in Fig. C.1,

$$\mathcal{M}^{virtual} = (2\pi)^4 \delta^{(4)}(k_1 + k_2 - p_1 - p_2) \frac{M^{vertex}}{(2\pi)^6 (2k_1^0 2k_2^0 2p_1^0 2p_2^0)^{1/2}}, \quad (\text{C.53})$$

leads to the following cross section contribution:

$$d\sigma^{virtual} = \frac{1}{j} (2\pi)^4 \delta^{(4)}(k_1 + k_2 - p_1 - p_2) \frac{1}{4} \sum_{spin} 2 \Re e \left(M^{Born*} \cdot M^{vertex} \right) \cdot \frac{d^3 \vec{p}_1 d^3 \vec{p}_2}{(2\pi)^{12} 2k_1^0 2k_2^0 2p_1^0 2p_2^0} \quad (\text{C.54})$$

$$= (2\pi)^4 \delta^{(4)}(k_1 + k_2 - p_1 - p_2) \frac{1}{4} \frac{\sum_{spin} 2 \Re e \left(M^{Born*} \cdot M^{vertex} \right)}{2s \beta_0} \cdot \frac{d^3 \vec{p}_1}{(2\pi)^3 2p_1^0} \frac{d^3 \vec{p}_2}{(2\pi)^3 2p_2^0}. \quad (\text{C.55})$$

In (C.54) and (C.55) it is summed over the final state helicities and averaged over the initial state helicities. Here, we only sketch the initial state calculation as the final state calculation can trivially be deduced from the initial state one. For the initial state vertex we have to distinguish the two different contributions from the $\gamma e^+ e^-$ and $Z e^+ e^-$ vertices,¹ Γ_μ^γ and Γ_μ^Z , with their respective couplings:

$$\begin{aligned} M^{vertex} &= iQ_e Q_f e^2 \bar{v}(k_2) \Gamma_\mu^\gamma u(k_1) \frac{g^{\mu\nu}}{s} \bar{u}(p_1) \gamma_\nu v(p_2) \\ &+ i \frac{g^2}{4 \cos^2 \theta_W} \bar{v}(k_2) \Gamma_\mu^Z u(k_1) \frac{g^{\mu\nu} - \frac{k_\mu k_\nu}{M_Z^2}}{s - m_Z^2 + i\bar{\epsilon}} \bar{u}(p_1) \gamma_\nu (v_f + a_f \gamma_5) v(p_2), \\ m_z^2 &= M_Z^2 - i \Gamma_Z \frac{s}{M_Z}, \quad k = k_1 + k_2, \end{aligned} \quad (\text{C.56})$$

¹In the final state case, it is the $\gamma \bar{f} f$ and $Z \bar{f} f$ vertices correspondingly.

with the following vertex functions Γ_μ^γ and Γ_μ^Z as loop integrals over the virtual photon momentum p :

$$\Gamma_\mu^\gamma(k) = -iQ_e^2 e^2 \int \frac{d^4 p}{(2\pi)^4} \gamma^\alpha \frac{(\not{p} - \not{k}_2) + m_e}{(p - k_2)^2 - m_e^2 + i\bar{\varepsilon}} \gamma_\mu \frac{(\not{k}_1 + \not{p}) + m_e}{(k_1 + p)^2 - m_e^2 + i\bar{\varepsilon}} \gamma_\alpha \frac{1}{p^2}, \quad (\text{C.57})$$

$$\Gamma_\mu^Z(k) = -iQ_e^2 e^2 \int \frac{d^4 p}{(2\pi)^4} \gamma^\alpha \frac{(\not{p} - \not{k}_2) + m_e}{(p - k_2)^2 - m_e^2 + i\bar{\varepsilon}} \gamma_\mu (v_e + a_e \gamma_5) \cdot \frac{(\not{k}_1 + \not{p}) + m_e}{(k_1 + p)^2 - m_e^2 + i\bar{\varepsilon}} \gamma_\alpha \frac{1}{p^2}, \quad (\text{C.58})$$

with the final dependence on the momentum $k = k_1 - k_2$. There are the following three Feynman integrals to compute:

$$I_0^F = \mu^{4-n} \int d^4 p \frac{1}{[p^2 + 2pk_1][p^2 - 2pk_2]p^2}, \quad (\text{C.59})$$

$$I_\rho^F = \mu^{4-n} \int d^4 p \frac{p_\rho}{[p^2 + 2pk_1][p^2 - 2pk_2]p^2}, \quad (\text{C.60})$$

$$I_{\rho\sigma}^F = \mu^{4-n} \int d^4 p \frac{p_\rho p_\sigma}{[p^2 + 2pk_1][p^2 - 2pk_2]p^2}. \quad (\text{C.61})$$

Calculating these integrals using suitable Feynman parameterizations and isolating the infrared singularities finally delivers for the photonic vertex function:

$$\Gamma_\mu^\gamma(k) = -\frac{e^2 Q_e^2}{16\pi^2} [\gamma_\mu V^\gamma(-s, m_e, m_e) + m_e \sigma_{\mu\nu} k^\nu \mathcal{J}(-s, m_e, m_e)], \quad (\text{C.62})$$

$$\begin{aligned} \text{with } V^\gamma(-s, m_e, m_e) &= 2(s - 2m_e^2)C_0(-s, m_e, 0, m_e) \\ &\quad + B_0(-s, m_e, m_e) - 2(s - 3m_e^2)\mathcal{J}(-s, m_e, m_e) - 2. \end{aligned} \quad (\text{C.63})$$

B_0 and C_0 denote the well-known *Passarino-Veltman functions* as two- and three-point scalar one-loop integrals given in [96]. They deliver two singularities $1/\varepsilon_{UV}$ and $1/\varepsilon_{IR}$ which can be associated with an infrared and an ultraviolet divergence for vanishing or large photon momenta:

$$B_0(-s, m_e, m_e) = \frac{1}{\varepsilon_{UV}} - \ln \frac{m_e^2}{\mu^2} + 2 - \beta_0 \ln \frac{\beta_0 + 1}{\beta_0 - 1}, \quad (\text{C.64})$$

$$C_0(-s, m_e, 0, m_e) \approx \frac{1}{2\varepsilon_{IR}} \cdot \mathcal{J}(-s, m_e, m_e) + \frac{1}{2}\mathcal{K}(-s, m_e, m_e), \quad (\text{C.65})$$

$$\mathcal{J}(-s, m_e, m_e) = \int_0^1 dx \frac{1}{m_e^2 - x(1-x)s} \quad (\text{C.66})$$

$$\approx -\frac{2}{s\beta_0} \ln \frac{1+\beta_0}{1-\beta_0} = -\frac{2}{s} \ln \frac{s}{m_e^2}, \quad (\text{C.67})$$

$$\mathcal{K}(-s, m_e, m_e) = \int_0^1 dx \frac{1}{m_e^2 + x(1-x)s} \ln \left[\frac{m_e^2 + x(1-x)s}{\mu^2} \right] \quad (\text{C.68})$$

$$\approx -\frac{1}{s} \left[2 \ln \frac{s}{m_e^2} \frac{m_e^2}{\mu^2} + \ln^2 \frac{s}{m_e^2} - \frac{4}{3} \pi^2 \right]. \quad (\text{C.69})$$

The relations (C.65), (C.67), and (C.69) have been derived for small electron masses m_e^2 . We can show similarly for the Ze^+e^- vertex correction applying the Dirac equations for the bispinorial factors:

$$\begin{aligned} \Gamma_\mu^Z(k) = & \frac{e^2 Q_e^2}{16\pi^2} \left[\gamma_\mu (v_e + a_e \gamma_5) V^\gamma(-s, m_e, m_e) \right. \\ & \left. + m_e v_e \sigma_{\mu\nu} k^\nu \mathcal{J}(-s, m_e, m_e) + a_e A_\mu^Z(k) \right], \end{aligned} \quad (\text{C.70})$$

$$\begin{aligned} A_\mu^Z(k) = & -2m_e^2 \gamma_\mu \gamma_5 \mathcal{J}(-s, m_e, m_e) \\ & - m_e k_\mu \gamma_5 \left[\frac{4}{s} + \left(3 - \frac{4m_e^2}{s} \right) \mathcal{J}(-s, m_e, m_e) \right]. \end{aligned} \quad (\text{C.71})$$

So, neglecting masses, we can nicely correlate the two neutral current vertex functions simply by a vector- and axial-vector coupling term:

$$\Gamma_\mu^Z(k) = \Gamma_\mu^\gamma(k) (v_e + a_e \gamma_5). \quad (\text{C.72})$$

The final state vertex functions can be derived completely analogously, replacing m_e, Q_e, v_e, a_e by m_f, Q_f, v_f, a_f and repeating the above calculation with:

$$k_1 \rightarrow -p_2, \quad k_2 \rightarrow -p_1, \quad k \rightarrow -(k_1 + k_2) = p_1 + p_2. \quad (\text{C.73})$$

In order to finalize the calculation of the first order vertex correction, we now have to renormalize the vertex by adding the *counter terms* to the vertex. They are calculated from the self energy corrections to the external fermionic lines. They will remove the ultraviolet divergent contributions encountered in the B_0 function in (C.64).

The vertex counter terms

The procedure of renormalization can be looked up in any advanced textbook on quantum field theory or particle physics, so this will not be illustrated here [24–27]. We just want to give a quick illustration how to derive the necessary *counter terms* to the above calculated γ and Z vertex functions.

The counter term for the $\gamma e^+ e^-$ vertex function is nothing else but

$$\Gamma_\mu^{\gamma c.t.} = (Z - 1)\gamma_\mu, \quad (\text{C.74})$$

with the Z -factor still to be determined. This Z -factor arises from the renormalization of the fermion fields and can be extracted from the *self-energy corrections* to the external fermion legs. To see this connection, we use *on-mass-shell renormalization* and give the *renormalization conditions* which fix the Z -factor for the fermion fields' renormalization. The two renormalization conditions for the external fermion fields for on-mass-shell renormalization are:

1. The renormalized fermion mass is the pole of the renormalized fermion propagator on-mass shell.
2. On-mass shell, the residuum of the renormalized propagator is 1.

For this we need the *regularized* self-energy corrections to the fermion lines.

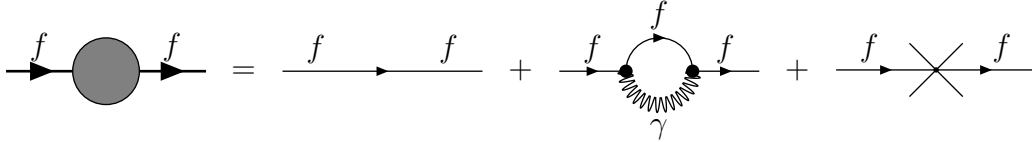


Figure C.2: Fermion line with QED self-energy insertion and counter term diagrams.

We can extract the two renormalization conditions:

$$\delta m = \Sigma^\gamma(m_e), \quad (\text{C.75})$$

$$Z - 1 = - \left. \frac{\partial \Sigma^\gamma(\not{p})}{\partial \not{p}} \right|_{\not{p} \rightarrow m_e}. \quad (\text{C.76})$$

For the fermionic QED self-energy correction we have the following loop integral after dimensional regularization:

$$\Sigma^\gamma(\not{p}) = -e^2 Q_e^2 \int \frac{d^4 q}{(2\pi)^4} \gamma_\alpha \frac{(\not{q} + \not{p}) + m_e}{(q + p)^2 - m_e^2 + i\epsilon} \gamma_\beta \frac{g_{\alpha\beta}}{q^2}, \quad (\text{C.77})$$

$$\rightarrow \frac{e^2 Q_e^2}{(2\pi)^4} \mu^{4-n} \int d^n q \frac{(2-n)(\not{q} + \not{p}) + n m_e}{[(q + p)^2 - m_e^2 + i\epsilon] q^2}, \quad (\text{C.78})$$

because in n dimensions we have:

$$\gamma^\alpha(\not{q} + \not{p})\gamma_\alpha = (2 - n)(\not{q} + \not{p}), \quad \gamma^\alpha\gamma_\alpha = n. \quad (\text{C.79})$$

Again with a suitable Feynman parameterization we have a scalar and a tensorial two-point function to compute and finally get for $\Sigma^\gamma(\not{p})$:

$$\Sigma^\gamma(\not{p}) = \frac{e^2 Q_e^2}{16\pi^2} \left[-2\not{p} B_1(p^2, 0, m_e) - 4m_e B_0(p^2, m_e, 0) - \not{p} + 2m_e \right]. \quad (\text{C.80})$$

Calculating the derivative of (C.80) produces the Z factor which we need to fix the vertex counter term:

$$Z - 1 = - \left. \frac{\partial \Sigma^\gamma(\not{p})}{\partial \not{p}} \right|_{\not{p} \rightarrow m_e} \longrightarrow \quad (\text{C.81})$$

$$Z - 1 = - \frac{e^2 Q_e^2}{16\pi^2} \left[\frac{1}{\varepsilon_{UV}} - 2 \frac{1}{\varepsilon_{IR}} - 3 \ln \frac{m_e^2}{\mu^2} + 4 \right], \quad (\text{C.82})$$

with

$$\frac{1}{\varepsilon_{UV}} = - \frac{2}{n_{UV} - 4} - C - \ln \pi = -2 P_{UV}, \quad (\text{C.83})$$

$$\frac{1}{\varepsilon_{IR}} = \frac{2}{n_{IR} - 4} + C + \ln \pi = 2 P_{IR}, \quad (\text{C.84})$$

thus fixing the vertex counter term to:

$$\Gamma_\mu^{\gamma c.t.} = (Z - 1)\gamma_\mu = - \frac{e^2 Q_e^2}{16\pi^2} \gamma_\mu \left[\frac{1}{\varepsilon_{UV}} - 2 \frac{1}{\varepsilon_{IR}} - 3 \ln \frac{m_e^2}{\mu^2} + 4 \right]. \quad (\text{C.85})$$

We can write down as regularized vertex function removing the ultra-violet pole of the bare vertex function $\Gamma_\mu^\gamma(q)$:

$$\begin{aligned} \Gamma_\mu^{\gamma reg}(q) &= \Gamma_\mu^\gamma(q) + \Gamma_\mu^{\gamma c.t.}(q) \\ &= \frac{e^2 Q_e^2}{16\pi^2} \left[\gamma_\mu V^{\gamma reg}(q^2, m_e, m_e) + m_e \sigma_{\mu\nu} (k_1^\nu - k_2^\nu) \mathcal{J}(q^2, m_e, m_e) \right], \end{aligned} \quad (\text{C.86})$$

$$\text{with} \quad V^{\gamma reg}(q^2, m_e, m_e) = V^\gamma(q^2, m_e, m_e) + \left[-\frac{1}{\varepsilon_{UV}} + 2 \frac{1}{\varepsilon_{IR}} + 3 \ln \frac{m_e^2}{\mu^2} - 4 \right]. \quad (\text{C.87})$$

Equivalently, we can show in absolutely the same manner for the corrected final state vertex function replacing the Lorentz index, the fermion mass and the momenta by the corresponding final state terms:

$$\begin{aligned}\Gamma_\mu^{\gamma reg}(q) &= \Gamma_\mu^\gamma(q) + \Gamma_\mu^{\gamma c.t.}(q) \\ &= \frac{e^2 Q_f^2}{16\pi^2} \left[\gamma_\mu V^{\gamma reg}(q^2, m_f, m_f) + m_f \sigma_{\mu\nu} (p_1^\nu + p_2^\nu) \right].\end{aligned}\quad (\text{C.88})$$

Inserting this (C.87) together with (C.72) into (C.55) and calculating the cross section contribution from the virtual corrections one can show that the ultraviolet pole $1/\varepsilon_{UV}$ cancels. We obtain as virtual correction factor $d\sigma_{ini}^{virtual}$:

$$d\sigma^{virtual} = \frac{\alpha}{\pi} \delta^{virtual}(\varepsilon_{IR}, \mu) d\sigma^{Born}, \quad (\text{C.89})$$

$$\delta^{virtual}(\varepsilon_{IR}, \mu) = Q_e^2 \left[(L_e - 1) \left(\frac{3}{2} - \ln \frac{m_e^2}{\mu^2} - \frac{1}{\varepsilon_{IR}} \right) - \frac{1}{2} L_e^2 - \frac{1}{2} + \frac{2\pi^2}{3} \right]. \quad (\text{C.90})$$

Combining the soft and virtual photon contributions from (C.38) and (C.90) to the fermion-pair production differential cross section we can see that finally also the infrared divergences cancel and the complete result for the initial state soft and virtual contribution to the cross sections can be given: ²

$$d\sigma^{soft+virtual} = \frac{\alpha}{\pi} \left(\delta^{soft}(\bar{\varepsilon}, \varepsilon_{IR}, \mu) + \delta^{virtual}(\varepsilon_{IR}, \mu) \right) d\sigma^{Born}, \quad (\text{C.91})$$

$$\delta^{soft+virtual}(\bar{\varepsilon}) = Q_e^2 \left[(L_e - 1) \left(\frac{3}{2} + 2 \ln \bar{\varepsilon} \right) - \frac{1}{2} + \frac{\pi^2}{3} \right]. \quad (\text{C.92})$$

The final state results for $\delta_{fin}^{virtual}$, δ_{fin}^{soft} , and $\delta_{fin}^{soft+virtual}$ are of course easily obtained merely replacing $L_e = \ln(s/m_e^2)$ by $L_f = \ln(s'/m_f^2)$.

The parameter $\bar{\varepsilon}$ is again the arbitrarily chosen soft photon cut-off to distinguish from the hard photon region. Adding the hard photon contribution – calculated for the initial state, final state, and initial-final state interference in Appendix B – then also removes this arbitrarily chosen and therefore unphysical parameter.

This can be shown of course separately for the initial state and the final state real and virtual photon contributions to $e^+e^- \rightarrow \bar{f}f$. For the initial-final state

²Of course, also the regulator term μ for the vanishing photon mass finally has to cancel and it does.

interference we have to combine the soft photon terms with the virtual corrections from the interference of Born and virtual box corrections for an infrared-finite result.

C.2.2 Virtual box corrections

After determining all first order soft and hard photonic contributions to $e^+e^- \rightarrow \bar{f}f$ adding the initial and final state vertex corrections, we also have to include the virtual QED corrections from the interference of the $\gamma\gamma$ and γZ box diagrams with the Born graphs in order to remove all infrared singularities. Due to the exchange of both photon and Z vector boson in the Born amplitudes also all box diagrams with $\gamma\gamma$ and γZ exchange have to be added in order to remove the divergences. The weak box contributions with ZZ and WW exchange are infrared-finite and are contained as weak virtual corrections in *improved Born observables* in an *effective Born approximation* (see e.g. Section 2.1).

As QED box diagrams (Fig. C.3) we have two different topologies: the *direct* and *crossed* graphs. The corresponding S -matrix element of the box graphs can

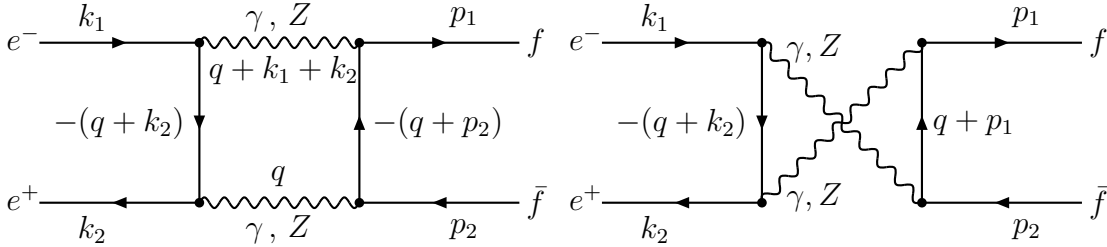


Figure C.3: The $\gamma\gamma$ and γZ direct and crossed box diagrams.

be written as

$$\mathcal{M}^{box} = (2\pi)^4 \delta^{(4)}(k_1 + k_2 - p_1 - p_2) \frac{M^{box}}{(2\pi)^6 (2k_1^0 2k_2^0 2p_1^0 2p_2^0)^{1/2}}, \quad (\text{C.93})$$

where M^{box} contains the direct and crossed diagrams with $\gamma\gamma$ and γZ (and $Z\gamma$) exchange.

$$M^{box} = M_{di}^{\gamma\gamma} + M_{cr}^{\gamma\gamma} + M_{di}^{\gamma Z} + M_{cr}^{\gamma Z} + M_{di}^{Z\gamma} + M_{cr}^{Z\gamma}. \quad (\text{C.94})$$

For the Born amplitude we of course similarly have:

$$\mathcal{M}^{Born} = (2\pi)^4 \delta^{(4)}(k_1 + k_2 - p_1 - p_2) \frac{M^{Born}}{(2\pi)^6 (2k_1^0 2k_2^0 2p_1^0 2p_2^0)^{1/2}}, \quad (\text{C.95})$$

and can straightforwardly derive the interference of the Born and box diagrams as contributions to the differential cross section:

$$d\sigma^{box} = \frac{1}{j} (2\pi)^4 \delta^{(4)}(k_1 + k_2 - p_1 - p_2) \frac{1}{4} \frac{\sum_{spin} 2 \Re (M^{box} \cdot M^{Born*})}{(2\pi)^6 (2k_1^0 2k_2^0 2p_1^0 2p_2^0)^{1/2}} d^3 \vec{p}_1 d^3 \vec{p}_2, \quad (C.96)$$

$$\text{with } j = \frac{\sqrt{(k_1 \cdot k_2)^2 - m_e^4}}{(2\pi)^6 k_1^0 k_2^0} = \frac{s\beta_0}{(2\pi)^6 2k_1^0 k_2^0}. \quad (C.97)$$

We sum over all final-state helicities and average over the initial-state polarizations (for the unpolarized cross section contribution).

$$d\sigma^{box} = (2\pi)^4 \delta^{(4)}(k_1 + k_2 - p_1 - p_2) \frac{1}{4} \frac{\sum_{spin} 2 \Re (M^{box} \cdot M^{Born*})}{2s \beta_0} \cdot \frac{d^3 \vec{p}_1}{(2\pi)^3 2p_1^0} \frac{d^3 \vec{p}_2}{(2\pi)^3 2p_2^0}. \quad (C.98)$$

The current structure of M^{Born} can be seen in Section A.1. The matrix element to the box diagrams contains one loop integration over the free momentum q .

$$M_{di}^{\gamma\gamma} = e^4 Q_e^2 Q_f^2 \int \frac{d^n q}{(2\pi)^n} \bar{u}(-k_2) \gamma^\mu \frac{-(\not{q} + \not{k}_2) + m_e}{(q + k_2)^2 - m_e^2 + i\bar{\varepsilon}} \gamma^\nu u(k_1) \cdot \bar{u}(p_1) \gamma_\beta \frac{-(\not{q} + \not{p}_2) + m_f}{(q + p_2)^2 - m_f^2 + i\bar{\varepsilon}} \gamma^\alpha u(-p_2) \cdot \frac{g_{\mu\alpha} g_{\nu\beta}}{q^2 Q^2}, \quad (C.99)$$

$$M_{cr}^{\gamma\gamma} = e^4 Q_e^2 Q_f^2 \int \frac{d^n q}{(2\pi)^n} \bar{u}(-k_2) \gamma^\mu \frac{-(\not{q} + \not{k}_2) + m_e}{(q + k_2)^2 - m_e^2 + i\bar{\varepsilon}} \gamma^\nu u(k_1) \cdot \bar{u}(p_1) \gamma_\beta \frac{\not{q} + \not{p}_1 + m_f}{(q + p_1)^2 - m_f^2 + i\bar{\varepsilon}} \gamma^\alpha u(-p_2) \cdot \frac{g_{\mu\beta} g_{\nu\alpha}}{q^2 Q^2}, \quad (C.100)$$

$$\begin{aligned}
M_{di}^{\gamma Z} &= e^2 Q_e Q_f \frac{g^2}{4 \cos^2 \theta_W} \int \frac{d^n q}{(2\pi)^n} \bar{u}(-k_2) \gamma^\mu \frac{-(\not{q} + \not{k}_2) + m_e}{(q + k_2)^2 - m_e^2 + i\bar{\varepsilon}} \\
&\quad \cdot \gamma^\nu (v_e + a_e \gamma_5) u(k_1) \bar{u}(p_1) \gamma_\beta (v_f + a_f \gamma_5) \frac{-(\not{q} + \not{p}_2) + m_f}{(q + p_2)^2 - m_f^2 + i\bar{\varepsilon}} \\
&\quad \cdot \gamma^\alpha u(-p_2) \frac{g_{\mu\alpha}}{q^2} \frac{g_{\nu\beta} - \frac{1}{m_Z^2} Q_\nu Q_\beta}{Q^2 - m_Z^2}, \tag{C.101}
\end{aligned}$$

$$\begin{aligned}
M_{cr}^{\gamma Z} &= e^2 Q_e Q_f \frac{g^2}{4 \cos^2 \theta_W} \int \frac{d^n q}{(2\pi)^n} \bar{u}(-k_2) \gamma^\mu \frac{-(\not{q} + \not{k}_2) + m_e}{(q + k_2)^2 - m_e^2 + i\bar{\varepsilon}} \\
&\quad \cdot \gamma^\nu (v_e + a_e \gamma_5) u(k_1) \bar{u}(p_1) \gamma_\beta \frac{\not{q} + \not{p}_1 + m_f}{(q + p_1)^2 - m_f^2 + i\bar{\varepsilon}} \\
&\quad \cdot \gamma^\alpha (v_f + a_f \gamma_5) u(-p_2) \frac{g_{\mu\beta}}{q^2} \frac{g_{\nu\alpha} - \frac{1}{m_Z^2} Q_\nu Q_\alpha}{Q^2 - m_Z^2}, \tag{C.102}
\end{aligned}$$

$$\begin{aligned}
M_{di}^{Z\gamma} &= e^2 Q_e Q_f \frac{g^2}{4 \cos^2 \theta_W} \int \frac{d^n q}{(2\pi)^n} \bar{u}(-k_2) \gamma^\mu (v_e + a_e \gamma_5) \frac{-(\not{q} + \not{k}_2) + m_e}{(q + k_2)^2 - m_e^2 + i\bar{\varepsilon}} \\
&\quad \cdot \gamma^\nu u(k_1) \bar{u}(p_1) \gamma_\beta \frac{-(\not{q} + \not{p}_2) + m_f}{(q + p_2)^2 - m_f^2 + i\bar{\varepsilon}} \gamma^\alpha (v_f + a_f \gamma_5) u(-p_2) \\
&\quad \cdot \frac{g_{\mu\alpha} - \frac{1}{m_Z^2} q_\mu q_\alpha}{q^2 - m_Z^2} \frac{g_{\nu\beta}}{Q^2}, \tag{C.103}
\end{aligned}$$

$$\begin{aligned}
M_{cr}^{Z\gamma} &= e^2 Q_e Q_f \frac{g^2}{4 \cos^2 \theta_W} \int \frac{d^n q}{(2\pi)^n} \bar{u}(-k_2) \gamma^\mu (v_e + a_e \gamma_5) \frac{-(\not{q} + \not{k}_2) + m_e}{(q + k_2)^2 - m_e^2 + i\bar{\varepsilon}} \\
&\quad \cdot \gamma^\nu u(k_1) \bar{u}(p_1) \gamma_\beta (v_f + a_f \gamma_5) \frac{\not{q} + \not{p}_1 + m_f}{(q + p_1)^2 - m_f^2 + i\bar{\varepsilon}} \gamma^\alpha u(-p_2) \\
&\quad \cdot \frac{g_{\mu\beta} - \frac{1}{m_Z^2} q_\mu q_\beta}{q^2 - m_Z^2} \frac{g_{\nu\alpha}}{Q^2}, \tag{C.104}
\end{aligned}$$

$$\text{with } Q \equiv q + k_1 + k_2, \tag{C.105}$$

$$v_e = -\frac{1}{2} + 2 \sin^2 \theta_W, \quad a_e = -\frac{1}{2}, \tag{C.106}$$

$$v_f = I_3^f - 2Q_f \sin^2 \theta_W, \quad a_f = I_3^f, \tag{C.107}$$

$$m_Z^2 = M_Z^2 - iM_Z \Gamma_Z. \tag{C.108}$$

The box terms have been calculated in [32, 34, 35] and they are shown below. One can show that the infrared singularities in the box contributions exactly cancel the divergences of the soft initial-final state interference terms, derived in Section C.1.

The integrated cross section contributions from the hard and soft initial-final interference terms $\bar{H}_A^{int}(v, c)$ and $\bar{S}_A^{int}(c)$ (see also Appendix B.2 and C.1.2) and its virtual box corrections $\bar{B}_A(c, m, n)$ presented in terms of the regularized, infrared-finite flux functions are given below (we use $\sigma_A^0(s, s'; m, n)$ from Section 2.2, see for example (2.41)):

$$\sigma_T^{int} = \sum_{m,n} \int_0^\Delta dv \Re \left[\sigma_{FB}^0(s, s'; m, n) R_T^{int}(v, c; m, n) \right], \quad (\text{C.109})$$

$$\sigma_{FB}^{int} = \sum_{m,n} \int_0^\Delta dv \Re \left[\sigma_T^0(s, s'; m, n) R_{FB}^{int}(v, c; m, n) \right], \quad (\text{C.110})$$

$$R_A^{int}(v, c, m, n) = \delta(v) \left[\bar{S}_A^{int}(c) + \bar{B}_A(c, m, n) \right] + \bar{H}_A^{int}(v, c), \quad (\text{C.111})$$

The γZ exchange box contribution can be derived from the $\gamma\gamma$ and ZZ exchange functions ($m, n = \gamma, Z, A = T, FB$):

$$\bar{B}_A(c; m, n) = \frac{1}{2} \left[\bar{B}_A(c; m, m) + \bar{B}_A(c; n, n)^* \right], \quad (\text{C.112})$$

$$\bar{B}_A(c; n, n) = \frac{\alpha}{\pi} Q_e Q_f \left\{ \bar{b}_A(c; n, n) \mp \bar{b}_A(-c; n, n) \right\}. \quad (\text{C.113})$$

The corresponding box terms contained in (C.113) finally are ($c_\pm = \frac{1}{2}(1 \pm \cos c)$):

$$\begin{aligned} \bar{b}_T(c; \gamma, \gamma) &= \frac{1}{2} (c^2 - 1) \ln^2 c_+ + (-c^2 + 2c - 3) \ln c_+ - 3c \\ &\quad - i\pi(c^2 - 1) \ln c_+, \end{aligned} \quad (\text{C.114})$$

$$\begin{aligned} \bar{b}_{FB}(c; \gamma, \gamma) &= -\frac{1}{2} (c^2 - 1) \ln^2 c_+ - (-c^2 + 2c - 3) \ln c_+ \\ &\quad - \frac{1}{2} (\ln^2 2 + 6 \ln 2 + c^2) \\ &\quad - \frac{i\pi}{3} \left[5 \ln 2 + (2c^3 + 3c^2 + 6c + 5) \ln c_+ - \frac{2}{3} c^2 \right], \end{aligned} \quad (\text{C.115})$$

$$\begin{aligned}
\bar{b}_T(c; Z, Z) = & -2 \left\{ -cR_Z(R_Z + 1) - 2cR_Z(1 - R_Z) \ln c_+ \right. \\
& - \left[-2R_Z^2 + R_Z(c^2 + 1) + c^2 - 1 \right] \ln c_+ \left. \right\} L_Z \\
& + 2R_Z c - 6c + 4cR_Z(R_Z - 1)l(1) - 2c \ln R_Z \\
& + (c^2 - 1) \ln^2 c_+ + 2 \left[R_Z(c^2 - 1) - c^2 + 2c + 3 \right] \ln c_+ \\
& - 2 \left[2R_Z^2 + 2cR_Z(R_Z - 1) - R_Z(c^2 + 1) \right] l(c_+),
\end{aligned} \tag{C.116}$$

$$\begin{aligned}
\bar{b}_{FB}(c; Z, Z) = & \left[C_T(c) + \frac{4}{3} \right] \ln^2 c_+ \\
& + \left\{ c^2 \left(-R_Z^2 + 3R_Z - \frac{4}{3} \right) + \left(4R_Z^2 - 2R_Z + \frac{10}{3} \right) \ln 2 \right. \\
& + \left[4R_Z^2 - 2R_Z(c^2 + 1) + 2c^2 + \frac{10}{3} \right] \ln c_+ \\
& + 4 \left[cR_Z(R_Z - 1) + C_T(c) \right] \ln c_+ \left. \right\} L_Z \\
& + c^2 \left(\frac{4}{3} R_Z - \frac{5}{3} \right) \ln R_Z + \left(\frac{16}{3} R_Z^3 - 4R_Z^2 + 2R_Z - \frac{2}{3} \right) l \left(\frac{1}{2} \right) \\
& + 2c^2(R_Z - 1)l(1) - \frac{4}{3} \ln^2 2 + \left(\frac{8}{3} R_Z^2 + \frac{8}{3} R_Z - 6 \right) \ln 2 \\
& + \left[\frac{8}{3} R_Z^2 + R_Z \left(-\frac{4}{3} c^2 + \frac{8}{3} \right) + 2(c^2 - 3) \right] \ln c_+ \\
& + \left(\frac{8}{3} R_Z^2 + \frac{4}{3} R_Z - 4 \right) c \ln c_+ \\
& + 2 \left[-\frac{8}{3} R_Z^3 + 2R_Z^2 - R_Z(c^2 + 1) + c^2 + \frac{1}{3} \right] l(c_+) \\
& + 2 \left[2c(R_Z^2 - R_Z) + C_T(c) \right] l(c_+) + \left(\frac{2}{3} R_Z - 1 \right) c^2,
\end{aligned} \tag{C.117}$$

with the following abbreviations:

$$l(a) = \text{Li}_2(1 - aR_Z^{-1}), \tag{C.118}$$

$$L_Z = \ln(1 - R_Z^{-1}), \tag{C.119}$$

$$R_Z = \frac{m_Z^2}{s}. \tag{C.120}$$

Bibliography

- [1] S. L. Glashow, *Nucl. Phys.* **22** (1961) 579.
- [2] S. Weinberg, *Phys. Rev. Lett.* **19** (1967) 1264.
- [3] A. Salam, “Weak and Electromagnetic Interactions”, in N. Svartholm (ed.), *Elementary Particle Theory*, Proceedings of the Nobel Symposium held 1968 at Lerum, Sweden, (Almqvist and Wiksell, Stockholm, 1968), p. 367.
- [4] H. Fritzsch, M. Gell-Mann, and H. Leutwyler, *Phys. Lett.* **B47** (1973) 365.
- [5] H. D. Politzer, *Phys. Rev. Lett.* **30** (1973) 1346.
- [6] D. J. Gross and F. Wilczek, *Phys. Rev. Lett.* **30** (1973) 1343.
- [7] S. Weinberg, *Phys. Rev. Lett.* **31** (1973) 494.
- [8] S. L. Glashow, J. Iliopoulos, and L. Maiani, *Phys. Rev.* **D2** (1970) 1285.
- [9] UA1 Collaboration, G. Arnison *et al.*, *Phys. Lett.* **B122** (1983) 103.
- [10] UA2 Collaboration, M. Banner *et al.*, *Phys. Lett.* **B122** (1983) 476.
- [11] UA1 Collaboration, G. Arnison *et al.*, *Phys. Lett.* **B126** (1983) 398.
- [12] UA2 Collaboration, P. Bagnaia *et al.*, *Phys. Lett.* **B129** (1983) 130.
- [13] P. W. Higgs, *Phys. Lett.* **12** (1964) 132.
- [14] T. W. Kibble, *Phys. Rev.* **155** (1967) 1154.
- [15] M. W. Grünewald, “Combined analysis of precision electroweak results”, preprint prepared for 29th International Conference on High-Energy Physics (ICHEP 98), Vancouver, British Columbia, Canada, 23-29 Jul 1998, HUB-EP-98/67.
- [16] M. W. Grünewald, *Phys. Rept.* **322** (1999) 125.

- [17] ALEPH Collaboration, R. Barate *et al.*, “Measurement of the Z resonance parameters at LEP”, preprint (1999), CERN-EP-99-104.
- [18] OPAL Collaboration, G. Abbiendi *et al.*, “Update to Precision Measurements of the Z0 Lineshape and Lepton Asymmetry”, preprint to be published in the proceedings of International Europhysics Conference on High-Energy Physics (EPS-HEP 99), Tampere, Finland, 15-21 Jul 1999, OPAL Physics Note PN404.
- [19] DELPHI Collaboration, P. Abreu *et al.*, “Cross sections and leptonic forward-backward asymmetries from the Z0 running of LEP”, preprint CERN-OPEN-2000-031.
- [20] L3 Collaboration, M. Acciarri *et al.*, “Measurements of cross sections and forward-backward asymmetries at the Z resonance and determination of electroweak parameters”, preprint subm. to Eur. Phys. J. C, [hep-ex/0002046](#).
- [21] LEP Collaboration, D. Abbaneo *et al.*, “A combination of preliminary electroweak measurements and constraints on the standard model”, preprint CERN-EP-2000-016.
- [22] SLD Collaboration, K. Abe *et al.*, “A high-precision measurement of the left-right Z boson cross-section asymmetry”, preprint SLAC-PUB-8401 (Apr 2000), subm. to Phys. Rev. Lett., [hep-ex/0004026](#).
- [23] SLD Collaboration, K. Abe *et al.*, “Measurements of Z0 electroweak couplings at SLD”, preprint SLAC-PUB-8444 (May 2000), [hep-ex/0005001](#).
- [24] M. Veltman, *Nucl. Phys.* **B7** (1968) 637.
- [25] G. 't Hooft, *Nucl. Phys.* **B35** (1971) 167.
- [26] G. 't Hooft and M. Veltman, *Nucl. Phys.* **B44** (1972) 189.
- [27] G. 't Hooft and M. Veltman, *Nucl. Phys.* **B50** (1972) 318.
- [28] CDF Collaboration, F. Abe *et al.*, *Phys. Rev. Lett.* **74** (1995) 2626.
- [29] D0 Collaboration, S. Abachi *et al.*, *Phys. Rev. Lett.* **74** (1995) 2632.
- [30] M. Veltman, *Nucl. Phys.* **B123** (1977) 89.
- [31] D. Bardin, M. Bilenky, O. Fedorenko, and T. Riemann, “The electromagnetic $O(\alpha^3)$ contributions to e^+e^- annihilation into fermions in the electroweak theory. Total cross-section σ_T and integrated asymmetry A_{FB} ”, Dubna preprint JINR E2-87-663 (1987), JINR E2-88-324 (1988).

- [32] D. Bardin, M. Bilenky, A. Chizhov, A. Sazonov, Y. Sedykh, T. Riemann, and M. Sachwitz, *Phys. Lett.* **B229** (1989) 405.
- [33] D. Bardin, M. S. Bilenky, G. Mitselmakher, T. Riemann, and M. Sachwitz, *Z. Phys.* **C44** (1989) 493.
- [34] D. Bardin, M. Bilenky, A. Sazonov, Y. Sedykh, T. Riemann, and M. Sachwitz, *Phys. Lett.* **B255** (1991) 290.
- [35] D. Bardin, M. Bilenky, A. Chizhov, A. Sazonov, O. Fedorenko, T. Riemann, and M. Sachwitz, *Nucl. Phys.* **B351** (1991) 1.
- [36] D. Bardin *et al.*, “ZFITTER v.4.5: An analytical program for fermion pair production in e^+e^- annihilation”, preprint CERN-TH. 6443/92 (May 1992), [hep-ph/9412201](#).
- [37] P. C. Christova, M. Jack, and T. Riemann, *Phys. Lett.* **B456** (1999) 264.
- [38] D. Bardin, P. Christova, M. Jack, L. Kalinovskaya, A. Olshevski, S. Riemann, and T. Riemann, “ZFITTER v.6.21: A semi-analytical program for fermion pair production in e^+e^- annihilation”, preprint DESY 99-070 (1999), subm. to *Comp. Phys. Comm.*, [hep-ph/9908433](#).
- [39] M. Greco and G. Rossi, *Nuovo Cim.* **50A** (1967) 168.
- [40] E. Etim, G. Pancheri, and B. Toushek, *Nuovo Cim.* **51B** (1967) 276.
- [41] W. Wetzel, *Nucl. Phys.* **B227** (1983) 1.
- [42] A. Akhundov, D. Bardin, and T. Riemann, *Nucl. Phys.* **B276** (1986) 1.
- [43] F. Jegerlehner, *Z. Phys.* **C32** (1986) 425; E: *ibid.*, **C38** (1988) 519.
- [44] W. Beenakker and W. Hollik, *Z. Phys.* **C40** (1988) 141.
- [45] J. Bernabéu, A. Pich, and A. Santamaria, *Phys. Lett.* **B200** (1988) 569.
- [46] B. W. Lynn and R. G. Stuart, *Phys. Lett.* **B252** (1990) 676.
- [47] R. N. Cahn, *Phys. Rev.* **D36** (1987) 2666, E: *ibid.*, **D40** (1989) 922.
- [48] A. Barroso *et al.*, “Electroweak radiative corrections at LEP energies”, in *Proc. of LEP200 ECFA Workshop, Aachen, West Germany, Sep 29 - Oct 1, 1986*, report CERN 87-08 (1987) (A. Böhm and W. Hoogland, eds.), p. 157.
- [49] F. A. Berends, G. Burgers, W. Hollik, and W. L. van Neerven, *Phys. Lett.* **B203** (1988) 177.

- [50] D. Bardin *et al.*, “Z line shape”, in *Proc. of Workshop on Z Physics at LEP, Geneva, Switzerland, Feb 20-21 and May 8-9, 1989*, report CERN 89-08 (1989) (G. Altarelli, R. Kleiss, and C. Verzegnassi, eds.), vol. 1, p. 89.
- [51] W. Beenakker, F. A. Berends, and S. C. van der Marck, *Z. Phys.* **C46** (1990) 687.
- [52] D. Bardin, A. Leike, T. Riemann, and M. Sachwitz, *Phys. Lett.* **B206** (1988) 539.
- [53] T. Riemann, *Acta Phys. Polon.* **B28** (1997) 2317.
- [54] T. Riemann, “The Z boson resonance parameters”, in *Irreversibility and Causality, Lecture Notes in Physics, vol. 504* (A. Bohm *et al.*, eds.), p. 157, Springer, Berlin, 1998, hep-ph/9709208.
- [55] D. Bardin *et al.*, “Forward - backward asymmetries”, in *Proc. of Workshop on Z Physics at LEP, Geneva, Switzerland, Feb 20-21 and May 8-9, 1989*, report CERN 89-08 (1989) (G. Altarelli, R. Kleiss, and C. Verzegnassi, eds.), vol. 1, p. 201.
- [56] T. Riemann, *Phys. Lett.* **B293** (1992) 451.
- [57] D. R. Yennie, S. C. Frautschi, and H. Suura, *Ann. Phys.* **13** (1961) 379.
- [58] M. Greco, G. Pancheri-Srivastava, and Y. Srivastava, *Nucl. Phys.* **B101** (1975) 234.
- [59] M. Greco, G. Pancheri-Srivastava, and Y. Srivastava, *Nucl. Phys.* **B171** (1980) 118; E: *Nucl. Phys.* **B197** (1982) 543.
- [60] A. Leike, T. Riemann, and J. Rose, *Phys. Lett.* **B273** (1991) 513.
- [61] A. Leike, S. Riemann, and T. Riemann, *Phys. Lett.* **B291** (1992) 187.
- [62] F. A. Berends, G. Burgers, and W. L. van Neerven, *Nucl. Phys.* **B297** (1988) 429; E: *ibid.*, **B304** (1988) 921.
- [63] G. Montagna, O. Nicrosini, and L. Trentadue, *Phys. Lett.* **B231** (1989) 492.
- [64] S. Willenbrock and G. Valencia, *Phys. Lett.* **B259** (1991) 373.
- [65] A. Sirlin, *Phys. Lett.* **B267** (1991) 240.
- [66] A. Sirlin, *Phys. Rev. Lett.* **67** (1991) 2127.
- [67] B. A. Kniehl and A. Sirlin, *Phys. Lett.* **B440** (1998) 136.

- [68] A. R. Bohm and N. L. Harshman, “On the mass and width of the Z-boson and other relativistic quasistable particles”, preprint **hep-ph/0001206**.
- [69] M. Bilenky and A. Sazonov, “QED corrections at Z^0 pole with realistic kinematical cuts”, Dubna preprint JINR-E2-89-792 (1989).
- [70] M. Bilenky and A. Sazonov, ZFITTER Fortran routines for photonic corrections with acollinearity and acceptance cuts, unpublished (1989).
- [71] J. Goldstone, *Nuovo Cim.* **19** (1961) 154.
- [72] Super-Kamiokande Collaboration, Y. Fukuda *et al.*, *Phys. Rev. Lett.* **81** (1998) 1562.
- [73] N. Cabibbo, *Phys. Rev. Lett.* **10** (1963) 531.
- [74] M. Kobayashi and T. Maskawa, *Prog. Th. Phys.* **49** (1973) 652.
- [75] S. L. Adler, *Phys. Rev.* **177** (1969) 2426.
- [76] J. S. Bell and R. Jackiw, *Nuovo Cim.* **60A** (1969) 47.
- [77] W. A. Bardeen, *Phys. Rev.* **184** (1969) 1848.
- [78] M. L. Swartz, “Precision electroweak physics at the Z”, preprint to be published in the proceedings of 19th International Symposium on Lepton and Photon Interactions at High-Energies (LP 99), Stanford, California, 9-14 Aug 1999, **hep-ex/9912026**.
- [79] Particle Data Group, C. Caso *et al.*, *Eur. Phys. J.* **C3** (1998) 1.
- [80] G. Källén and A. Sabry, *K. Dan. Vidensk. Selsk. Mat.-Fys. Medd.* **17** (1955) 29.
- [81] G. Källén, *Springer Tracts in Modern Physics* **46** (1968) 67.
- [82] A. Czarnecki and W. J. Marciano, “Lepton anomalous magnetic moments - a theory update”, preprint **hep-ph/9810512**.
- [83] S. M. Berman, *Phys. Rev.* **112** (1958) 267.
- [84] T. Kinoshita and A. Sirlin, *Phys. Rev.* **113** (1959) 1652.
- [85] T. van Ritbergen and R. G. Stuart, *Phys. Lett.* **B437** (1998) 201.
- [86] T. van Ritbergen and R. G. Stuart, *Phys. Rev. Lett.* **82** (1999) 488.

- [87] A. Freitas, “Exact Results for Fermionic Two-Loop Contributions to Muon Decay in the Standard Model”, preprint to be published in the proceedings of Loops and Legs 2000 WORKSHOP, Bastei/Königstein, Germany, 09 - 14 April, 2000.
- [88] F. A. Berends, G. J. H. Burgers, C. Mana, M. Martinez, and W. L. van Neerven, *Nucl. Phys.* **B301** (1988) 583.
- [89] Z. Kunszt, “Electroweak physics, theoretical aspects”, preprint hep-ph/0003057.
- [90] M. Steinhauser, *Phys. Lett.* **B429** (1998) 158.
- [91] S. Eidelman and F. Jegerlehner, *Z. Phys.* **C67** (1995) 585.
- [92] S. Eidelman, F. Jegerlehner, A. L. Kataev, and O. Veretin, *Phys. Lett.* **B454** (1999) 369.
- [93] A. Sirlin, “Ten years of precision electroweak physics”, preprint to be published in the proceedings of 19th International Symposium on Lepton and Photon Interactions at High-Energies (LP 99), Stanford, California, 9-14 Aug 1999, NYU-TH-99-12-01 (Aug 1999), hep-ph/9912227.
- [94] T. Appelquist and J. Carazzone, *Phys. Rev.* **D11** (1975) 2856.
- [95] M. Veltman, *Acta Phys. Polon.* **B8** (1977) 475.
- [96] G. Passarino and M. Veltman, *Nucl. Phys.* **B160** (1979) 151.
- [97] R. W. Brown, R. Decker, and E. A. Paschos, *Phys. Rev. Lett.* **52** (1984) 1192.
- [98] M. Böhm and W. Hollik, *Phys. Lett.* **B139** (1984) 213.
- [99] B. W. Lynn and R. G. Stuart, *Nucl. Phys.* **B253** (1985) 216.
- [100] R. Barbieri, M. Beccaria, P. Ciafaloni, G. Curci, and A. Vicere, *Nucl. Phys.* **B409** (1992) 105.
- [101] J. Fleischer, O. V. Tarasov, and F. Jegerlehner, *Phys. Lett.* **B319** (1993) 249.
- [102] G. Degrassi, P. Gambino, and A. Vicini, *Phys. Lett.* **B383** (1996) 219.
- [103] G. Degrassi, P. Gambino, and A. Sirlin, *Phys. Lett.* **B394** (1997) 188.
- [104] G. Degrassi, P. Gambino, M. Passera, and A. Sirlin, *Phys. Lett.* **B418** (1998) 209.

- [105] B. Kniehl, *Nucl. Phys.* **B347** (1990) 86.
- [106] A. Czarnecki and J. H. Kühn, *Phys. Rev. Lett.* **77** (1996) 3955.
- [107] A. Djouadi, *Nuovo Cim.* **100A** (1988) 357.
- [108] L. Avdeev, J. Fleischer, S. Mikhailov, and O. Tarasov, *Phys. Lett.* **B336** (1994) 560–566, E: *ibid.*, **B349** (1995) 597.
- [109] K. G. Chetyrkin, J. H. Kühn, and M. Steinhauser, *Phys. Rev. Lett.* **75** (1995) 3394.
- [110] R. Harlander, T. Seidensticker, and M. Steinhauser, *Phys. Lett.* **B426** (1998) 125.
- [111] A. L. Kataev, *Phys. Lett.* **B287** (1992) 209.
- [112] T. van Ritbergen, J. A. M. Vermaseren, and S. A. Larin, *Phys. Lett.* **B400** (1997) 379.
- [113] M. Consoli, W. Hollik, and F. Jegerlehner, *Phys. Lett.* **B227** (1989) 167.
- [114] M. Consoli, W. Hollik, and F. Jegerlehner, “Electroweak radiative corrections for Z physics”, in *Z Physics at LEP 1*, CERN 89–08 (1989) (G. Altarelli, R. Kleiss, and C. Verzegnassi, eds.), vol. 1, p. 7.
- [115] M. Veltman, *Phys. Lett.* **B70** (1977) 253.
- [116] W. F. L. Hollik, *Fortschr. Phys.* **38** (1990) 165.
- [117] F. Jegerlehner, *Prog. Part. Nucl. Phys.* **27** (1991) 1.
- [118] G. Montagna, O. Nicrosini, and F. Piccinini, *Riv. Nuovo Cim.* **21** (1998) 1.
- [119] M. Skrzypek, *Acta Phys. Polon.* **B23** (1992) 135.
- [120] G. Montagna, O. Nicrosini, and F. Piccinini, *Phys. Lett.* **B406** (1997) 243.
- [121] B. A. Kniehl, M. Krawczyk, J. H. Kühn, and R. G. Stuart, *Phys. Lett.* **B209** (1988) 337.
- [122] S. Jadach, M. Skrzypek, and M. Martinez, *Phys. Lett.* **B280** (1992) 129.
- [123] A. B. Arbuzov, “Light pair corrections to electron positron annihilation at LEP/SLC”, preprint hep-ph/9907500.
- [124] G. Quast, “Weak Boson Parameters at LEP”, preprint to be published in the proceedings of Loops and Legs 2000 WORKSHOP, Bastei/Königstein, Germany, 09 - 14 April, 2000.

- [125] J. J. van der Bij, *Nucl. Phys.* **B248** (1984) 141.
- [126] J. van der Bij and M. Veltman, *Nucl. Phys.* **B231** (1984) 205.
- [127] J. J. van der Bij and F. Hoogeveen, *Nucl. Phys.* **B283** (1987) 477.
- [128] R. Barbieri, P. Ciafaloni, and A. Strumia, *Phys. Lett.* **B317** (1993) 381.
- [129] J. Fleischer, O. V. Tarasov, and F. Jegerlehner, *Phys. Rev.* **D51** (1995) 3820.
- [130] G. Montagna, O. Nicrosini, G. Passarino, and F. Piccinini, *Comp. Phys. Comm.* **93** (1996) 120.
- [131] G. Montagna, O. Nicrosini, F. Piccinini, and G. Passarino, *Comp. Phys. Comm.* **117** (1999) 278.
- [132] W. Beenakker, F. Berends, and S. C. van der Marck, *Nucl. Phys.* **B349** (1991) 323.
- [133] S. Jadach, B. F. L. Ward, and Z. Was, *Comp. Phys. Comm.* **79** (1994) 503.
- [134] S. Jadach, B. F. L. Ward, and Z. Was, *Phys. Lett.* **B449** (1999) 97.
- [135] S. Jadach, B. F. L. Ward, and Z. Was, *Comp. Phys. Comm.* **124** (2000) 233.
- [136] S. Jadach, B. F. L. Ward, and Z. Was, “The precision Monte Carlo event generator KK for two-fermion final states in e^+e^- collisions”, preprint DESY-99-106, CERN-TH/99-235, UTHEP-99-08-01, subm. to *Comp. Phys. Comm.*, [hep-ph/9912214](#).
- [137] G. Bonneau and F. Martin, *Nucl. Phys.* **B27** (1971) 381.
- [138] F. Bloch and A. Nordsieck, *Phys. Rev.* **52** (1937) 54.
- [139] T. Kinoshita, *J. Math. Phys.* **3** (1962) 650.
- [140] T. D. Lee and M. Nauenberg, *Phys. Rev.* **133** (1964) B1549.
- [141] E. Kuraev and V. Fadin, *Sov. J. Nucl. Phys.* **41** (1985) 466.
- [142] O. Nicrosini and L. Trentadue, *Phys. Lett.* **B196** (1987) 551.
- [143] F. Aversa and M. Greco, *Phys. Lett.* **B228** (1989) 134.
- [144] M. Greco and O. Nicrosini, *Phys. Lett.* **B240** (1990) 219.

- [145] P. Christova, M. Jack, S. Riemann, and T. Riemann, “Predictions of ZFITTER v.6 for fermion-pair production with acollinearity cut”, preprint DESY 99-037, [hep-ph/9908289](#).
- [146] P. C. Christova, M. Jack, S. Riemann, and T. Riemann, “Predictions for fermion-pair production at LEP”, in *Proceedings of the Fourth Int. Symposium on Radiative Corrections, Barcelona, Spain, Sep 8-12, 1998* (J. Sola ed.), p. 392, World Scientific, Singapore, 1999, [hep-ph/9812412](#).
- [147] W. Placzek, S. Jadach, M. Melles, B. Ward, and S. Yost, “Precision calculation of Bhabha scattering at LEP”, in *Proceedings of the Fourth Int. Symposium on Radiative Corrections, Barcelona, Spain, Sep 8-12, 1998* (J. Sola ed.), p. 325, World Scientific, Singapore, 1999, preprint CERN-TH-99-07, [hep-ph/9903381](#).
- [148] W. Beenakker and G. Passarino, *Phys. Lett.* **B425** (1998) 199.
- [149] D. Bardin, G. Passarino, and W. Hollik (eds.), “Reports of the working group on precision calculations for the Z resonance”, report CERN 95-03 (1995).
- [150] G. Montagna, O. Nicrosini, and F. Piccinini, *Z. Phys.* **C76** (1997) 45.
- [151] D. Bardin and G. Passarino, “Upgrading of precision calculations for electroweak observables”, preprint CERN-TH/98-92 (1998), [hep-ph/9803425 v.2](#).
- [152] D. Bardin, M. Grünewald, and G. Passarino, “Precision calculation project report”, preprint [hep-ph/9902452](#).
- [153] S. Jadach, M. Skrzypek, and B. Pietrzyk, *Phys. Lett.* **B456** (1999) 77.
- [154] S. Jadach, B. Pietrzyk, E. Tournefier, B. Ward, and Z. Was, “Initial-final-state interference in the Z line-shape”, preprint CERN-TH. 99-217 (1999), [hep-ph/9907547](#).
- [155] G. Passarino, “The twofold way: A short disquisition of LEP physics”, preprint to be published in the proceedings of 14th International Workshop on High Energy Physics and Quantum Field Theory (QFTHEP 99), Moscow, Russia, 27 May - 2 June, 1999, [hep-ph/9911310](#).
- [156] E. Accomando *et al.*, “Standard model processes”, in *Physics at LEP2*, report CERN 96-01 (1996) (G. Altarelli, T. Sjöstrand, and F. Zwirner, eds.), p. 207, [hep-ph/9601224](#).
- [157] G. Montagna, O. Nicrosini, and G. Passarino, *Phys. Lett.* **B309** (1993) 436.

- [158] G. Passarino, *Nucl. Phys.* **B204** (1982) 237.
- [159] O. Nicrosini and L. Trentadue, *Z. Phys.* **C39** (1988) 479.
- [160] D. Bardin, P. Christova, M. Jack, L. Kalinovskaya, A. Olshevski, S. Riemann, and T. Riemann, Fortran program ZFITTER v.6.04 (21 April 1999), v.6.06 (13 May 1999) obtainable from <http://www.ifh.de/~riemann/Zfitter/zf.html>.
- [161] D. Bardin, P. Christova, L. Kalinovskaya, A. Olshevski, and S. Riemann, Fortran program ZFITTER v.5.20 (17 Feb 1999).
- [162] D. Bardin, P. Christova, M. Jack, L. Kalinovskaya, A. Olshevski, S. Riemann, and T. Riemann, Fortran program ZFITTER v.6.11 (23 June 1999).
- [163] D. Bardin, P. Christova, L. Kalinovskaya, A. Olshevski, and S. Riemann, Fortran program ZFITTER v.5.14 (Oct 1998).
- [164] M. Jack and T. Riemann, “Prospects and problems in fermion pair production”, preprint to be published in the proceedings of 4th International Workshop on Linear Colliders (LCWS 99), Sitges, Barcelona, Spain, 28 Apr - 5 May 1999, [hep-ph/9909401](#).
- [165] M. Jack, “QED radiative corrections to $e^+e^- \rightarrow \bar{f}f$ with realistic cuts at LEP energies and beyond”, preprint to be published in the proceedings of 14th International Workshop on High Energy Physics and Quantum Field Theory (QFTHEP 99), Moscow, Russia, 27 May - 2 June, 1999, DESY 99-166, [hep-ph/9911296](#).
- [166] P. Christova, M. Jack, S. Riemann, and T. Riemann, “Radiative corrections to $e^+e^- \rightarrow \bar{f}f$ ”, preprint to be published in the proceedings of the DESY-ECFA LC Workshop held at Oxford, U.K., March 20-23, 1999, preprint LC-TH-2000-008, [hep-ph/0002054](#).
- [167] S. Jadach, M. Skrzypek, and B. F. L. Ward, *Phys. Lett.* **B257** (1991) 173.
- [168] D. Bardin, P. Christova, M. Jack, L. Kalinovskaya, A. Olshevski, S. Riemann, and T. Riemann, Fortran program ZFITTER v.6.10 (27 May 1999).
- [169] M. Grünewald, private communication, May 2000.
- [170] ALEPH Collaboration, R. Barate *et al.*, *Eur. Phys. J.* **C12** (2000) 183.
- [171] L3 Collaboration, M. Acciarri *et al.*, *Phys. Lett.* **B479** (2000) 101.
- [172] OPAL Collaboration, G. Abbiendi *et al.*, *Eur. Phys. J.* **C13** (2000) 15.
- [173] OPAL Collaboration, G. Abbiendi *et al.*, *Eur. Phys. J.* **C13** (2000) 553.

- [174] DELPHI Collaboration, P. Abreu *et al.*, “Searches for neutral Higgs bosons in e^+e^- collisions around $\sqrt{s} = 189\text{-GeV}$ ”, preprint CERN-EP-2000-038, subm. to Eur. Phys. J. C.
- [175] D. Bardin, P. Christova, L. Kalinovskaya, A. Olshevski, and S. Riemann, Fortran program ZFITTER v.5.12 (Jun 1998).
- [176] M. Beccaria, P. Ciafaloni, D. Comelli, F. M. Renard, and C. Verzegnassi, *Phys. Rev.* **D61** (2000) 011301.
- [177] P. Ciafaloni, “Leading electroweak corrections at the TeV scale”, preprint to be published in the proceedings of 2nd ECFA - DESY Study on Physics and Detectors for a Linear Electron - Positron Collider, Obernai, France, 16-19 Oct, 1999, to appear as report DESY-123F, [hep-ph/9911508](#).
- [178] S. Riemann, unpublished comparisons.
- [179] G. Passarino, private communication, November 1998.
- [180] K. Moenig, “Electroweak measurements on the Z”, preprint to be published in the proceedings of 2nd ECFA - DESY Study on Physics and Detectors for a Linear Electron - Positron Collider, Oxford, U.K., March 20-23, 1999, to appear as report DESY-123F.
- [181] S. Heinemeyer, “Precision Observables in the Standard Model and the MSSM”, preprint to be published in the proceedings of 2nd ECFA - DESY Study on Physics and Detectors for a Linear Electron - Positron Collider, Oxford, U.K., March 20-23, 1999, to appear as report DESY-123F.
- [182] R. Brinkmann, G. Materlik, J. Rossbach, and A. Wagner, eds., *Conceptual design of a 500-GeV e^+e^- Linear Collider with integrated X-ray laser facility. Vol. 1, 2.* 1997. preprint DESY-97-048, ECFA 97-182.
- [183] R. Settles, ed., *e^+e^- Linear Colliders: Physics and Detector Studies - Part E*, DESY 97-123E. 1997.
- [184] A. Djouadi, A. Leike, T. Riemann, D. Schaile, and C. Verzegnassi, *Z. Phys.* **C56** (1992) 289.
- [185] J. Erler and P. Langacker, *Phys. Rev. Lett.* **84** (2000) 212.
- [186] M. Czakon, J. Gluza, F. Jegerlehner, and M. Zralek, *Eur. Phys. J.* **C13** (2000) 275.
- [187] M. Heyssler, R. Rückl, and H. Spiesberger, “Leptoquark and R-parity violating SUSY processes”, preprint to be published in the proceedings of 4th International Workshop on Linear Colliders (LCWS 99), Sitges, Barcelona, Spain, 28 Apr - 5 May 1999, [hep-ph/9908319](#).

- [188] J. L. Hewett, *Phys. Rev. Lett.* **82** (1999) 4765.
- [189] L3 Collaboration, M. Acciarri *et al.*, “Search for Extra Z bosons in Fermion-Pair Production at LEP”, preprint L3 Note 1425 (1999), to be published in the proceedings of International Europhysics Conference on High Energy Physics 99, Tampere, Finland, 15-21 July, 1999.
- [190] G. Mann and T. Riemann, *Annalen Phys.* **40** (1984) 334.
- [191] J. I. Illana, M. Jack, and T. Riemann, “Predictions for $Z \rightarrow \mu\tau$ and Related Reactions”, preprint to be published in the proceedings of 2nd ECFA - DESY Study on Physics and Detectors for a Linear Electron - Positron Collider, Oxford, U.K., March 20-23, 1999, to appear as report DESY-123F, report number LC-TH-2000-007 (Feb 2000), DESY 99-165, hep-ph/0001273.
- [192] ECFA/DESY LC Physics Working Group Collaboration, E. Accomando *et al.*, *Phys. Rept.* **299** (1998) 1.
- [193] D. Bardin and S. Jadach, private communication, March 2000.
- [194] D. Bardin, J. Biebel, D. Lehner, A. Leike, A. Olchevski, and T. Riemann, *Comp. Phys. Comm.* **104** (1997) 161.
- [195] A. H. Hoang *et al.*, “Top-antitop pair production close to threshold: Synopsis of recent NNLO results”, preprint to be published in the proceedings of 2nd ECFA - DESY Study on Physics and Detectors for a Linear Electron - Positron Collider, Oxford, U.K., March 20-23, 1999, to appear as report DESY-123F, hep-ph/0001286.
- [196] A. A. Akhundov, D. Y. Bardin, and A. Leike, *Phys. Lett.* **B261** (1991) 321.
- [197] W. Beenakker and W. Hollik, *Phys. Lett.* **B269** (1991) 425.
- [198] V. Ravindran and W. L. van Neerven, *Phys. Lett.* **B445** (1998) 214, and references therein.
- [199] D. Bardin, L. Kalinovskaya, G. Nanava, A. Leike, and T. Riemann, in preparation.
- [200] S. Riemann, Fortran program ZEFIT v. 5.0 (1997).
- [201] G. 't Hooft, *Nucl. Phys.* **B61** (1973) 455.
- [202] G. 't Hooft and M. Veltman, *Nucl. Phys.* **B153** (1979) 365.
- [203] D. Bardin, P. Christova, and O. Fedorenko, *Nucl. Phys.* **B175** (1980) 435.

Acknowledgements

First, I would very much like to thank my advisor Tord Riemann for giving me the opportunity to finally make a dream come true. I am indebted to him, his expertise, his professionalism and his constant support on any issue, on and off the job. If I've learnt one thing during this time, then that there is more to success than just reading books and doing calculations.

I also would like to express many thanks to Fred Jegerlehner, Rainer Sommer and the theory staff at DESY Zeuthen for letting me be a part of the group and for the support until the very end, even in hectic moments. Many thanks also to Sabine Riemann, Arnd Leike and Professor Fritzsche for all their support. I would especially like to thank Silvia Arkadova and Penka Christova for kindly reading through the manuscript and for the many helpful suggestions.

I thank my parents for their support, love and wisdom and I owe them the knowledge, strength and self-discipline to carry through the last twenty-one years, and especially the last three. Mick, Butz, Ayrin, and Amina – thank you for just being there for me.

I would like to thank you, Marta, Jenny and Jochen, Francesco, Axel, Ilaria and Alessandro, Andreas, Lisa and Kurt, Ravindran, Martin and Stefan, for your friendship, the fun and the many lovely moments spent at DESY or during our spare time. Silvia A. and Silvia N., Avto, Chris, and Oleg, I thank you guys just as much for your camaraderie. And Axel, I will never forget that late-night 'burgers-and-beer-phase' ...

Fany and José, I owe you more than you can imagine, your kindness and friendship I will always treasure.

Tanja – if it hadn't been for you I don't think that I would have been able to finish this. You are special and this I know from the bottom of my heart.